Performance Monitoring of Ships

Hansen, Søren Vinther; Petersen, Jakob Buus; Jensen, Jørgen Juncher; Lützen, Marie

Publication date:
2012

Document Version
Publisher's PDF, also known as Version of record

Performance Monitoring of Ships

Søren Vinther Hansen

TECHNICAL UNIVERSITY OF DENMARK

DEPARTMENT OF MECHANICAL ENGINEERING

SECTION OF COASTAL, MARITIME AND STRUCTURAL ENGINEERING

SEPTEMBER 2011

Preface

This thesis is prepared as a partial fulfilment of the requirements for acquiring a PhD degree at the Section of Coastal, Maritime and Structural Engineering under the Department of Mechanical Engineering at the Technical University of Denmark (DTU). The work has taken place during the period of September 2008 to September 2011 and has been supervised by Professor Jørgen Juncher Jensen (DTU), Associate Professor Marie Lützen (SDU) and Vessel Performance Manager Jacob Buus Petersen (A.P.Moller-Maersk).

It has been a great privilege to have had the chance of working with Professor Jørgen Juncher Jensen during the project period. I have very much appreciated his valuable advice and his positive attitude and good sense of humour in many inspiring discussions. I am grateful to have had the opportunity to work with Jacob Buus Petersen who has introduced the world of performance monitoring for me. By sharing his high professional knowledge he has been a great inspiration for me in this work. Also a special thanks to the good colleges in the Performance Section in A.P.Moller-Maersk who have been very helpful to me in many aspects during the project period. Many thanks to Marie Lützen for introducing me to the world of research. Thanks for valuable discussions and for always being available in giving me good advice.

The study has been financed by Svendborg International Maritime Academy (SIMAC) and A.P.Moller-Maersk and the support is gratefully acknowledged.

Many thanks to the good people on board “Clementine Maersk” and “Maersk Newton” in assisting me in the setup of auto logging and delivering valuable data for the project. Thanks to the developer of GES, Hans V. Vugt for the valuable assistance during this project work.

At DTU I have had the pleasure of sharing office with Zoran Lajic with whom I have had many valuable discussions about all aspects of life and he has been a great support for me in my work. Also a special thanks to Ingrid Marie Vincent Andersen who with her positive attitude to life and work has brought value to the office life - will miss both “hindbærsnitter” and “romkugler”. Also thanks to good colleges at SKK.

Finally a very warm thanks to my two girls at home, my wife Lene and my daughter Nanna. Without their patience, love and support I would not have been able to be where I am today.

Abstract

The purpose of the research project is to establish a reliable index in the performance evaluation of ships. During operation the ship will experience added resistance due to fouling of hull and propeller. The added resistance will lead to increased fuel consumption and thus increased emissions to the environment. The monitoring of the ship's performance can be used as decision support in determining when actions to improve performance should be taken. The performance evaluation is based on a model of the ship and the added resistance from wind and waves during operation. Logged data on board the ship is used as input to the system and by comparing model and ship behaviour, an index describing the ship's performance is generated.

The work in this thesis is based on data logged through the automation system on board a PostPanmax container ship where data have been logged through a year. A routine handling drift in time series, spikes and outliers have been suggested for the purpose of introducing an automatic logging system.

The performance system is modelled in software based on the Bond Graph method. The system is described by bond graph elements which describe the characteristics of each component and several ships are modelled in the system. A simple model is used as initial model and several elements are added to improve the estimate of the performance. Several resistance models are compared in order to determine which is giving the best estimate of the performance.

Constraints in the models have been identified. The models used in this work are based on empirical relations or based on regression analyses of model tests and full-scale trials. In order to achieve valid results the conditions where performance is estimated have to be inside the boundaries of the model. Filters have been determined to establish cases where the ship is in steady state conditions and where these conditions are inside the boundaries of the constraints of the model.

Several indexes have been used in the evaluation. Two indexes relate to the ship's logged speed and one relates to the measured torque on the propeller shaft. Further, an index based on the properties of the ship's propeller, is used. The different indexes are described in a case study where the performance of a container ship is evaluated over one year. The reliability of the performance index is measured from the scatter in results and the ability of identifying the events that improves performance e.g. propeller and hull clean.

Resumé

Under sejlads vil et skib mærke ekstra modstand på grund af begroning på skrog og propeller. Denne ekstra modstand vil lede til øget brændstofforbrug og dermed øgning af emissioner til omgivelserne. En performance evaluering er baseret på en model af skibet og den modstand skibet møder fra vind og bølger under sejlads. Formålet med forskningen udført i projektet er at etablere et pålideligt indeks til performance evaluering af skibe. Modellen bruger data, der er logges kontinuerligt om bord på skibet og ved at sammenligne model og skib fremkommer et indeks, der beskriver skibets øjeblikkelige tilstand, kaldet performance. Ved at overvåge skibets performance holdes der kontrol med denne udvikling i begroning og dermed dannes der et beslutningsgrundlag for, hvornår der skal iværksættes tiltag til at reducere denne.

Arbejdet er baseret på loggede data fra et PostPanmax container skib, hvor data er blevet logget over en periode på et år. En rutine, der håndterer drift i tidssignaler, herunder elimination af fejlagtige data, er udarbejdet med henblik på at opnå et system, der generer et performance indeks automatisk.

Performance systemet er modelleret i et softwaresystem, der baserer sig på Bond Graph metoden. Systemet er opbygget ved hjælp af bond graph elementer, der hver især karakteriserer de enkelte delelementer i systemet. Udgangspunktet har været en enkel model, hvorpå der er tilføjet flere elementer for at forbedre estimatet af performance. Flere skibe er modelleret i systemet. Forskellige modstandsmodeller er sammenlignet med henblik på at afgøre hvilke, der er i stand til at give det bedste estimat af performance for de enkelte skibe.

Modellerne i systemet har visse begrænsninger med henblik på at beskrive indflydelsen af et skibs bevægelser under sejlads på dels performance og derfor er performance evalueringen alene foretaget i de tilfælde, hvor skibet befinder sig i en quasi-stationær kondition og en filtreringsrutine er foreslået med henblik på at identificere disse konditioner.

Flere performance indeks er benyttet i evalueringen. To indeks relaterer sig til skibets loggede fart og et relaterer sig til det målte moment på skibets skrueaksel. Yderligere benyttes et indeks, der baserer sig på skibets propelleregenskaber. De forskellige indeks beskrives og sammenlignes for et konkret tilfælde, hvor et container skibs performance evalueres over et år. De forskellige indeks vurderes ud fra spredning i værdier og ud fra evne til at identificere forskellige tiltag (f.eks. rensning af propellerblade for begroning), der kan have indflydelse på skibets performance.

Nomenclature list

4.2 Performance Index

dC_F	Frictional resistance coefficient	$\frac{\Delta R}{R}$	fractional added resistance due to roughness
k_{S2}	average hull roughness (AHR2) under the actual condition	Speed Pct	speed loss due to fouling
k_{S1}	average hull roughness (AHR1) at a smooth surface	U_{Smodel}	ship's speed according to model
Lpp	length between perpendiculars	Power Pct	increase in shaft power due to fouling
R_T	ship's resistance	P_{Smodel}	ship's shaft power according to model
ρ_W	density of sea water	P_S	ship's shaft power
S	hull wetted surface	b	slope of the curve of the estimated linear relation between measured shaft torque and ship's logged speed
C_T	total resistance coefficient	C	torque constant at 100 % slip of the propeller
U_S	ship's speed	S_a	apparent slip of the propeller
		Q_C	torque constant at the actual slip of the propeller

5.2 Ship Model

R_{XA}	wind resistance force	R_{XP}	Propeller thrust force
R_{XH}	ship's resistance force	$\dot{U}_{SM}$	ship's model acceleration
R_{XFR}	rudder and fin stabiliser resistance force	M	ship's mass (displacement)
R_{XW}	added resistance due to waves	U_{SM}	ship's model speed

Nomenclature list

5.2 Ship Model

ρ_A	density of air	w	wake fraction
A_T	transverse projected area of the hull and cargo above water	t	thrust deduction fraction
C_X	wind force coefficient in surge direction	J	advance number
U_{RW}	relative wind speed	n, ω, RPM	propeller shaft revolutions
R_{XW}	wave resistance force	D	propeller diameter
U_a	ship advance speed	Q	shaft torque

5.3 The GES software

P_E	effective power	ρ_0	reference density of water in the model basin
R_T	ship's resistance found by model tests	ρ_W	actual density of sea water during service
C_T	total resistance coefficient	R_F	the frictional resistance under service conditions
C_F	frictional resistance coefficient	c_{F0}	frictional coefficient found in the model basin
C_A	allowance coefficient	c_F	actual frictional resistance coefficient under service conditions
C_R	residuary resistance coefficient	T_W	seawater temperature
T	propeller thrust	v	kinematic viscosity of seawater
k	form factor	H_S	wave height
R_{AS}	resistance correction due to changes in seawater temperature and density	U_{TW}	true wind speed

Nomenclature list

5.3 The GES software

T_e	wave encounter period	z	height of the anemometer
T_S	wave period	z_{ref}	reference height of anemometer used in the wind resistance model
ω_e	wave encounter frequency	μ	ship's speed loss
ω	wave frequency	U_S	design service speed
g	acceleration of gravity	$\frac{\Delta U_S}{U_S}$	weather direction reduction factor
λ	wave length	BN	wind force by the Beaufort scale
β_{180}	relative wave angle	F_n	Froude number
k	wave number	ς	correction factor for the block coefficient and Froude number
η_{3bow}	vertical bow motion	A_M	midships section area under water
Φ_w	RAO for the heave motion	h	water depth
Φ_θ	RAO for the pitch motion	R_{XR}	rudder induced resistance
ξ	phase difference	δ	rudder angle
x_{bow}	distance from the sensor to the centre of gravity	F_N	rudder normal force
s_R^2	variance of calculated bow motion	t_R	resistance deduction fraction due to steering
s_{Rm}^2	variance of measured bow motion	Λ	aspect ratio of the rudder or foil
$S(\omega)$	wave spectrum	A_R	rudder area
L_{WL}	length of waterline	U_R	effective rudder inflow speed
C_B	block coefficient	δ^*	effective rudder inflow angle
U_W	measured wind speed	X	distance between rudder and propeller

Nomenclature list

5.3 The GES software

k_T	the thrust coefficient	C_D	drag coefficient
r	yaw rate	d_m	ship's mean draught
Ψ	ship's heading angle	A_{SF}	area of the stabiliser fin
F_L	foil lift force	b_f	span length
F_D	foil drag force	c_{mean}	mean chord length
α	lift angle	η_S	shaft efficiency
C_L	lift coefficient		

6.3 Data logging sensors

η_0	propeller efficiency	β_{RW}	relative wind direction
U_{TW}	true wind speed	β_{TW}	true wind direction

8 Performance analysis

df	ship's forward draught	Trim	ship's trim (negative forward)
da	ship's aft draught		

9 Improvements to the Performance Model

$U_{TW\_19.4}$	True wind at 19.4m height	R	turning radius
F_{nh}	Froude depth number	L_{pp}	length between perpendiculars
h	water depth	α	drift angle
ROT	rate of turn		

11 Propeller Performance Index

Q_C	torque constant	C	torque constant (100 % slip cond.)
p	propeller pitch	z	number of propeller blades
S_a	apparent propeller slip	α	propeller disc area coefficient

Contents

1 Background and Motivation

The basic purpose of a propulsive performance system on board a ship is to provide feedback of how the ship performs during a voyage or a period in the ship's life. By use of a performance system the goal of making the most efficient voyage may be achieved. It not only indicates how the ship performs at the moment of measurement, but also, on the basis of data collected over a period, monitors the condition of the ship while in service. The overall purpose will normally be to gain information on how to make the most economical or environmentally efficient voyage. An evaluation of the ship's performance must comprise a comparison of two or more conditions. As the sailing conditions, e.g. the environmental and loading conditions might be of great importance during the time of operation, a performance index taking this into account must be used. A suggestion is to compare the present condition with a model condition defined by some given standard circumstances.

Monitoring data during a period can be used to estimate the amount of fouling on the ship for deciding intervals of hull and propeller cleanings or dry-docking intervals. The engine efficiency due to wear and tear can be estimated and, finally, the monitored data can be used for estimating the most efficient way of operating the ship, optimal engine settings, navigation and loading conditions of the ship. The index of performance is defined by the performance system and is dictated by the purpose.

Various indexes can be chosen, e.g.:

- Added resistance of hull and propeller
- Propulsive efficiency
- Loss in speed
- Increase in power consumption

The model in the performance system is compared to logged data on board the ship. In most shipping companies these data is sent to shore regularly for analyses. The logging interval can vary depending on the system and so can the source, i.e. some data is logged manually by the crew on board the ship and some is logged automatically by sensors.

1.1 The Fouling Problem

During service the ship will experience fouling on hull and propeller. The degree of fouling depends on many factors; the length of port stay and the service speed at sea; the nature of water in different areas of the world, e.g. salinity, temperature, pH, salts and oxygen concentration. The ship also experiences different fouling grades on different parts of the hull. Those parts of the hull exposed to light (usually the sides of the hull) are more exposed to fouling. Finally, the treatment of the hull in between dry docking-periods has importance. Polishing of the propeller and underwater cleaning of the hull will remove the fouling on these parts, Almeida et al. (2007).

To prevent fouling of the hull it is painted with antifouling paint. In the second half of the 20th century these paints were primarily based on the dispersion of biocides over time. The most known biocide in paints is copper. It is toxic to a large number of marine organisms and has been – and still is - widely used in antifouling paints. Another type of paint from this period is TBT (tributylin) based and this paint is considered highly efficient. During a boom in the use of this paint it was discovered that it had a disastrous effect on marine life. Large concentrations around ports and dry docks affected mammal life in these areas, and in 2001 it was banned by IMO with a stop of manufacturing in 2003 and a stop of presence on ship's hulls in 2008, Anderson et al. (2003). Since then other paint types have been developed and the two most commonly used types are self-polishing and foul release paints, International Paints (2010).

1.2 Performance Prediction

Various methods and systems have been developed to estimate the performance of a ship. A procedure for predicting the power performance of a ship is presented by ITTC (1999). As a first estimation of the power required to operate the ship, the calm water resistance is used. General methods for estimating this are developed on the basis of the results of a large number of model and full-scale tests which are collected and described statistically in graphs and empirical formulas.

A commonly used method is the one by Holtrop & Mennen (1982), Holtrop (1984). It is developed in a regression analysis of random model experiments and full-scale data obtained by the Netherlands Ship Model Basin. A newer method is described by Hollenbach (1998). This method

is based on analysed model tank tests for 433 ships performed by the Vienna Ship Model Basin during the period from 1980 to 1995. For both methods a general power prediction is obtained and the result is valid for ships at no trim and under design draught conditions.

To obtain a more accurate power prediction for a specific ship, self-propulsion tests and resistance tests in model basins are carried out. A model of the ship is tested to find the influence on the propeller power as a function of the mean draught and also, if desired, under various trim conditions, Force Technology (2009).

During operation the ship is influenced by wind forces. Isherwood (1973) has described a wind resistance model by empirical formulas determining two horizontal components of the wind force and the wind-induced yawing moment. The model is based on wind resistance analyses from various laboratories with models covering a wide range of merchant ships. Blendermann's model (1994) is based on the same principles as that of Isherwood but with data of more recent ship models. Fujiwara et al. (2001) (2006) has described a semi-empirical model which takes into account the hydrodynamic forces in calm seas and in waves. These forces are coordinated with the wind effects in a steady state solution and the longitudinal and lateral forces and the roll and yaw moments are dealt with using the contributions from hull, propeller, waves and wind.

The wave forces acting on the ship during operation can be treated by several methods including both empirical and analytical solutions, Pérez (2007). A simple method developed by Kreitner (1939) is presented in ITTC (2005_1) and it can be used for describing the wave forces on the ship, especially for head seas. Another simple model combing the effect of added resistance in waves and wind is developed by Townsin & Kwon (1993), Kwon (2008). A method by Boese (1970) is based on the pressure integration method which integrates the linear pressure in the undisturbed wave over the ship's hull to obtain the mean force in the direction of the ship's heading. The method by Gerritsma & Beukelmann (1972) is based on the relation between the radiated energy of the damping waves and the added resistance and can be used for describing the energy the ship transmits to the water by maintaining a constant speed obtained by the ship's propulsion plant. The asymptotic method presented by Sverre Sten et al. (1998) is based on diffraction of induced resistance and neglects the ship motions. Marin has analysed various wave resistance models and made a comparison of each model, Bom et al. (2008).

The forces induced by the rudder movement can be described as in the model by Kijima (1990) combined with the work by Molland & Turnock (2007). Stabiliser-induced forces are dealt with by Larsen (2008). The added resistance due to shallow water effects is described by Lackenby (1963) and another approach to these effects is that by Vugt (2005). The effect of differences in sea water temperature and salt content can be corrected by the method described in ISO 15016 (2002).

In cases where towing tank ship models are not available performance prediction can be estimated by using the propeller characteristics and the logged speed on board. For analysis of the ships speed on a sea trial, a linear relationship between the shaft power and the ships speed is proposed by Jourdain (1964). A method developed by Telfer (1964) can be used to monitor the hull fouling by a torque constant and a propeller slip function.

1.3 Performance Systems

There are a vast number of performance evaluation systems on the market and there are different approaches to logging of data to evaluate the performance of a ship. A.P. Moller-Maersk has a very extensive system, A.P. Moller-Maersk (2010), in a large amount of ships (250+) and the performance evaluation is based on noon reports given by the ship's crews. Force Technology has developed a similar system, Force Technology (2010), with noon reports and Propulsion Dynamics has developed a system with weekly reports, Munk (2005). These systems are using manually logged data in the analysis of performance.

Other systems are developed which combine manually and automatically logged data. BMT SeaTech (2009) has developed such a system and Marorka (2006) has developed an energy analysis and performance evaluation system which logs data from a ship's automation system. SeaSense is a system developed for decision support in heavy weather but is also used to log performance parameters, Nielsen et al. (2006). The system is currently used as a performance evaluation tool in combination with the system provided by A.P. Moller-Maersk, Hansen et al. (2010). There are several other minor systems which will not be mentioned here. Moreover, some systems combine performance evaluation with route planning, but these are also omitted in this thesis work.

1.4 Logging of Data

Performance evaluation of ships has existed for several years. Drinkwater (1967) has described the need for developing instruments for the logging of parameters during service. Journée (2003) has made some extensive full-scale experiments on ships in service and contributed to the development of logging systems. A Joint Industry Project led by Marin (2008) has covered many aspects of performance monitoring on board ships. Pedersen et al. (2009) has described the logging of data on board a tanker and the challenges of getting valuable data.

This work also includes an analysis of filtering of data to exclude bad/missing data points. Further filters are used to identify periods where the ship is in steady state conditions. To the knowledge of the author, no other systems use continuous auto logging of all parameters.

2 Objective and Scope of the Thesis

The work in this thesis has been done in collaboration with a large shipping company with several hundred ships in the fleet. The logging of the fleet's performance have been incorporated as a daily routine for the crews on board the ships for several years and the data is collected in the system as "noon data" which is data values averaged over one day. The data sensors are typically installed on board as part of the operational equipment e.g. the speed log, the torque meter and the wind anemometer. In many cases the data also is logged continuously either by the ship's automation system, the Voyage Data Recorder (VDR) or a combination of both. The data have not previously been used in the performance evaluation of a ship and the scope of the thesis work is aimed at the following:

- Automatic logging of data.

Setting up a system where the continuously logged data are collected on disks or in a data base and transferred to shore for analysis and used in the performance evaluation. Several systems have been tested and the setup of the logging method has been defined by the available equipment on board the ship.

- Automation of data handling.

A shipping company with a large number of vessels in the fleet would try to establish some sort of automation in the evaluation of the different ship's performances to avoid time consuming manual analysis work. Data handling routines to avoid drift in timing of the signals, eliminating noisy signals and setting up boundaries for valid performance evaluation results are suggested.

- Data filtering.

The models used in the performance system are designed to handle the data logged on board the ship i.e. to handle the limitations in the number of data and the various logging intervals. This requires more or less simplicity in the models depending on the available signals. The models used are often not able to handle events where the ship is in manoeuvring situations or operations in heavy weather. In cases where these situations are included the model fails and this will lead to large scatter in the performance evaluation results. Continuously logged data with a short logging interval will contain data with all kind of operational conditions. A filtering routine to reduce scatter and improve the reliability of the performance evaluation result is suggested.

- Performance evaluation results

The performance of the ship is determined by a performance index. Over time this index will change with a certain rate depending on the operational conditions of the ship. Three indexes have been suggested in this work: One relating to the ships speed, one to the torque measurement on the propeller shaft and a third describing the added roughness of propeller and hull. A method qualifying the results by the measurement of scatter and the reliability of the model is suggested.

3 Methodology

A system based on modelling of the ship and the environment has been established. The models in the system focus on the following elements:

- Propeller shaft including shaft power measurement

- Propeller
- Hull including wake and thrust deduction varying by speed, draught and trim
- Ship's resistance including varying speed, draught and trim
- Wind resistance
- Wave resistance

These are the basic elements in the initial performance system. The various elements are described in the modelling section. In cases where it is relevant the model is extended with additional elements to be able to handle additional signals e.g. where rudder movements or bow motions are logged.

The ship is modelled in the GES software, TNO (2010), on the basis of the bond graph system, and the elements in the model are based on the particulars of the ship and the results from model tests.

Several systems and ships have been tested in order to establish a systematic auto logging system on board. A series of Panmax container ships equipped with auto logging systems have been setup and tested. The work has been described in a conference paper, Hansen et al (2010) and can be found in Appendix B. Another system has been setup based on logging through a ship's automation system. A PostPanmax container ship and a VLCC have been used in the work and the results from the container ship are used as a background for this thesis. The VLCC is only briefly described in Appendix A because of lack of consistent data at the end of this project period.

The main part of the data used in this thesis is logged on board a PostPanmax container vessel sailing on a route from Europe to the Far East. The data is collected over a period of approximately one year (2010) by the ship's automation system. The main part of the data is logged by sensors where the logging interval is 10 seconds. The draught information is logged manually every 24 hours (taken from the existing fleet performance system).

In cases where there are more than 300 ships in the fleet using the performance system, the evaluation of the performance index has to include some sort of automation i.e. the system will generate an index and in cases where the index is off the expected value or exceeds some user defined boundaries, an alert will generated which will lead to a further investigation by the performance evaluation dept. To avoid "false alarms" the data fed to the system have to be free of

noise and outliers generating off limit indexes. Drift in timing of the signals also have to be avoided in order to have all parameters logged at the same timestamp. A routine handling these issues are suggested in this work.

It is the intention to use the data to give an overview of the ship's operational profile during the logging period. The data will be subject to a time series analysis in order to give an input to the performance system.

By implementing data from auto logging systems on board and by using a proper filtering method the index reliability is intended to be improved. The filtering methods are based on identifying data periods in which the behaviour of the ship is captured by the model. Constraints in the model are linked to the elements describing the resistance during service and also linked to lack of ability to describe the dynamics of the ship

By establishing an initial filter used on the logged speed on board the ship it is the intention to extend the parameters used to filter the data in order to achieve a reliable index.

By improvement of the model the range of data being excluded by the filtering can be reduced. This will lead to a larger amount of data to be used to evaluate the performance index reliability. It is intended to improve the model by introducing models for rudder/stabiliser movements, variance in sea water temperature and sailing in shallow waters. Various resistance models will be analysed and compared to find the most suitable model to describe the performance of the ship.

The wave height is estimated from the wind force. By including the data logged by the motion sensor placed in the bow section it is the intention to use this data to estimate the wave height and thus get a more accurate estimate of the sea state.

The reliability of the system is given by an analysis of the trend in the performance index development and analysis of the scatter in index compared to a model. The performance index is in this work given by the average hull roughness, the increase in power consumption and the speed loss compared to model values.

Another approach to estimate performance of a ship is to use the propeller as performance index. The index is based upon characteristics of the propeller and the measured shaft torque and logged speed on board.

By introducing the same data filtering as mentioned above the reliability of this index is improved to a level where it can be used to estimate the performance of the ship in cases where towing tank models are not available.

4 Ship Modelling

4.1 Fouling of hull and propeller

An increase of underwater hull surface roughness will increase the hull frictional resistance of the ship while sailing. This will result in additional power requirements with increased fuel consumption leading to increased costs to maintain the ship's service speed. Hull surface roughness is divided into two types - physical and biological (fouling) - each with their own micro- and macro characteristics, King (1982).

Macrophysical roughness:	plate waviness, plate laps, welds and weld quality, mechanical damage and corrosion
Macrobiological roughness:	animal and weed fouling
Microphysical roughness:	steel profile, minor corrosion and coatings condition.
Microbiological roughness:	slime fouling

The initial hull roughness when the ship is delivered from dry dock is therefore dependent on the quality of work on building the ship and the quality of the bottom paint. Townsin (1986) has analysed the increase of average hull roughness (*AHR*) on ships over a period (1976 -1986) and Schultz (2007) has published an analysis of fouling influence on the added resistance.

During service the ship will experience an increase in hull fouling dependent on the operational conditions. Factors which influence the increase in fouling:

- Length of port stay
- Service speed at sea
- Sea water nature, i.e. salinity, temperature, pH, salts and oxygen concentration

The ship also experiences different grades of fouling on different parts of the hull. Those parts of the hull exposed to light (usually the sides of the hull) are more exposed to fouling. Finally, the treatment of the hull in between dry-docking periods has importance. Polishing of the propeller and underwater cleaning of the hull will remove the fouling on these parts.

Examples of fouling on hull and propeller and other hull conditions are shown in the following section. The tables and pictures are extracts from hull and propeller survey reports. First a container ship (#1) sailing feeder trade in the Caribbean and Central America area. The ship had a hull and propeller inspection which was performed one year after the ship had a complete hull and propeller cleaning. Hull conditions were as shown in Table 1:

LOCATION	TYPE	% AREA			SEVERITY	LENGTH / HEIGHT
		Bow	Mid	Stern		
Port	4 & 5	100%	100%	100%	C	50mm
Starboard	4 & 5	100%	100%	100%	C	50mm
Flat Bottom	1 & 5	90%			B	4mm
Rudder	1 & 5	100%			C	50mm
Gratings	1 & 5	80%			C	4mm
Propeller	1, 5 & 7	90%			B	2 & 3mm
Bow Thruster/s	1 & 5	70%			B	2 & 3mm

Table 1 Hull and propeller conditions for container ship #1 (from internal report, A.P.Moller-Maersk). Severity grades: A (light), B (moderate) and C (heavy). Type (1) acorn barnacle, (2) tubeworm, (3) gooseneck, (4) algae, (5) slime, (6) mussels, (7) calcareous/others. Length / height of fouling.

The survey shows heavy fouling on port and starboard sides, on gratings and rudder. Propeller, bow thrusters and flat bottom had moderate fouling.

Examples of heavy fouling on the hull, Figure 1.

The starboard vertical side at first turn of shoulder.

The starboard vertical side at midship.

Figure 1 Hull condition.

The ship had a propeller polish, Figure 2.

The root of propeller blade #4 before polishing.

The root of propeller blade #4 after polishing.

Figure 2 Propeller condition.

Another container ship (#2) sailing liner trade from Europe to the Far East (PostPanmax size) had a hull and propeller inspection. Hull conditions were as in Table 2:

LOCATION	TYPE	% AREA			SEVERITY	LENGTH / HEIGHT
		Bow	Mid	Stern		
Port	Clean					
Starboard	Clean					
Flat Bottom	Clean					
Rudder	Clean					
Gratings	1	10%			A	5mm
Propeller	1, 4 & 7	(1) 5%, (4) 20% & (7) 60%			A	5mm
Bow Thruster/s	No access					

Table 2 Hull and propeller condition, container ship #2 (from internal report, A.P.Moller-Maersk).

The report shows only light fouling on gratings and propeller.

The ship had a propeller polish, Figure 3.

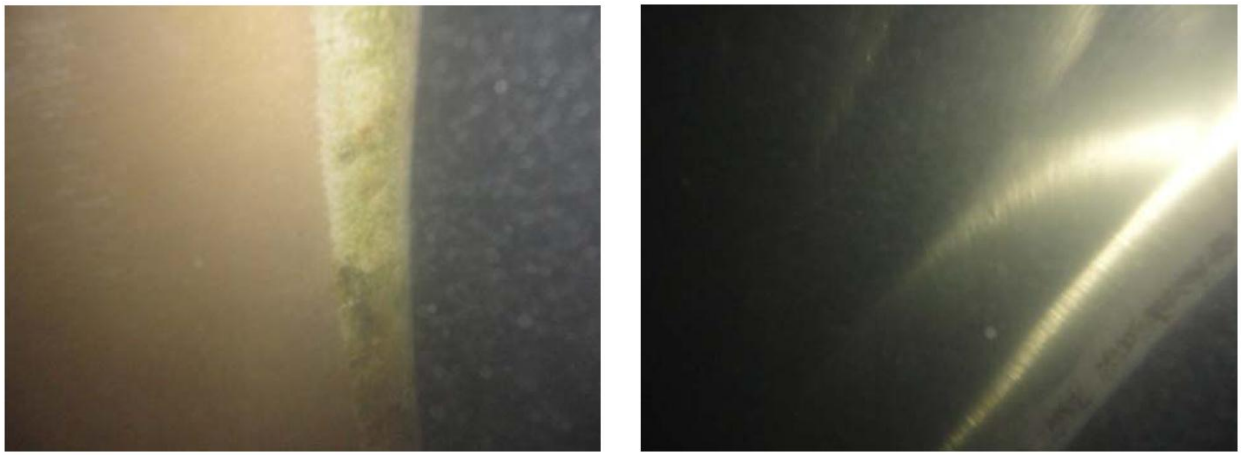

The pressure side of propeller blade #4 before polishing.

The pressure side of propeller blade #4 after polishing.

Figure 3 Propeller condition.

Condition of gratings and damages to paint, Figure 4.

The starboard vertical side at 4 m bow mark. The starboard vertical side of bow.

Figure 4 Hull condition.

The ship had a full blast on the bottom and a full primer and antifouling paint in dry dock three years before this inspection. Since the dry-docking the ship has had a propeller cleaning once every year.

The inspections for ships #1 and #2 shows a difference in the amount and type of fouling as well as a difference in how fast the fouling grows. The operational profile of the two ships is different with respect to speed, trade area and lay time in port and the antifouling paint on the ships is different with respect to type and manufacturer.

4.2 Performance index

The ships performance can be expressed by various indexes. The previously described fouling will lead to increased resistance while the ship is sailing and thereby increase the power consumption or reduce the ship's speed. One way to express the ship's degrading of performance is by the added roughness to the hull and propeller due to fouling.

The surface roughness can be measured on the ship while it is in dry dock. The hull roughness is defined as the maximum peak to the lowest trough height Rt_{50} in any given length of 50 mm along the ship's hull ISO1302 (2000), Figure 5.

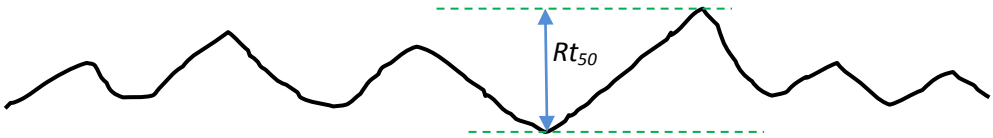

Figure 5 Hull roughness.

In various locations along the hull Rt_{50} is measured over distances of 750 – 1000 mm and an average for that location is calculated. At least 100 locations are measured and an *AHR* for the hull is found.

To monitor and to predict the increase of hull roughness during operation, a system using the frictional resistance coefficient dC_F can be utilised. This is found from Townsin (2003):

$$dC_F = 0.044\left[\sqrt[3]{\frac{k_{S2}}{L_{pp}}} - \sqrt[3]{\frac{k_{S1}}{L_{pp}}}\right] \quad (1)$$

where k_{S2} is the average hull roughness (*AHR2*) under the actual condition, k_{S1} is the average hull roughness (*AHR1*) at a smooth surface and *Lpp* is the length between perpendiculars.

The value of the ship's resistance R_T is given as

$$R_T = ½\rho_W S C_T U_S^2 \quad (2)$$

where ρ_W is the density of sea water, S is the hull wetted surface, C_T is the total resistance coefficient and U_S is the ship's speed.

Over time the resistance will increase due to added hull roughness and the ship's actual resistance is given as

$$R_{TS} = ½\rho_W S(C_T + dC_F)U_S^2 \quad (3)$$

The fractional added resistance due to roughness, $\frac{\Delta R}{R}$, is given in accordance with International(2004):

$$\frac{\Delta R}{R_T} = \frac{dC_F}{C_T} = \frac{0.044\left[\sqrt[3]{\frac{k_{s2}}{L_{pp}}} - \sqrt[3]{\frac{k_{s1}}{L_{pp}}}\right]}{C_T} \quad (4)$$

Besides having the hull roughness as a performance index, the ship's development in speed is also calculated. A speed percent indicates the speed loss due to fouling and found by

$$Speed\ Pct = \frac{U_{Smodel} - U_S}{U_{Smodel}} \cdot 100\% \quad (5)$$

where U_{Smodel} is the model predicted speed and U_S is the ship's actual speed. The previously mentioned indexes are dependent on the ship's speed and the measurements from the speed log.

The propeller shaft torque is measured by a torque meter and the shaft power is found by multiplying the torque by the revolutions of the shaft. By comparing the measured power with the modelled power, a power percent can be used to indicate the ship's performance:

$$Power\ Pct = \frac{P_{Smodel} - P_S}{P_{Smodel}} \quad (6)$$

Where P_{Smodel} is the model predicted power and P_S is the ship's actual power consumption. Finally the slope of the curve of the estimated linear relation between measured shaft torque and ship's logged speed is used to indicate the ship's performance, see Section 11:

$$b = \frac{(C - \overline{Q_C})}{1 - S_a} \quad (7)$$

where b is the slope, C is the torque constant at 100 % slip of the propeller, Q_C is the average torque constant at the actual slip and S_a is the apparent slip.

5 Bond Graph Modelling

5.1 The Bond Graph Method

The physical model describing a performance system is complex with power interactions in between multiple elements. To be able to model a valid system it is imperative to have a full understanding of the relation in between the different elements that form the system.

The language of the modeling system has to be transparent and a relation between the physical and the mathematical model has to be established in a way where the connection in between the two models is easily comprehended by the user. Such characteristics can be found in the Bond Graph language.

The method was developed in 1960 by H. Paynter, MIT, and is used to describe dynamic systems, Broenink (2000). The bond graph approach is useful when it comes to physical modelling of systems where power interactions are important. It is a transparent graphical language where a library of elements can be constructed and it is useful for systems where different energy domains are combined in a complete system. In addition, the bond graph method is an efficient method to find dependencies between different components in a system. By using causal analysis any problems in the model, e.g. algebraic constraints or dependent system variables will be detected, and identify where necessary remodelling may be performed to handle such problems. A short description of the method and the most common interactions are explained in the following section.

The power flow between two interacting systems results in interdependence between the energetic states of the two systems: it bonds the two systems together in one. Consequently, the basic symbol of the bond graph notation is a line called a bond. It depicts the exchange of power between the two systems or subsystems or elements at each end of the bond.

In the method a special notation is used to show the relation between the two systems A and B, Figure 6:

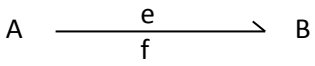

Figure 6 Bond Graph notation

The half arrow indicates the direction of the power flow (from system A to system B), and the effort (e) and the flow (f) are the variables which give the power when multiplied. As an example this could be a motor where the effort is the torque and the flow is the revolutions or the shaft speed and the power is the two variables multiplied.

The bond graphs represent the energetic coupling between the elements. This implies interaction between the systems and therefore the output of the one is input to the other and vice versa.

Because energetic interaction is a function of two variables when it comes to describe a system in terms of mathematical operations on numbers (i.e. signals), there are two possible choices for the input and output of each element (or subsystem). In making these choices one variable is assigned to the role of cause (or input) and the other to the role of effect (or output), so this choice is referred to as causality assignment. To represent this choice on a bond graph a causal stroke is added at one end of the bond, Figure 7:

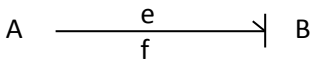

Figure 7 Causal element.

This graphical symbol means that the system nearest the causal stroke has effort impressed on it as input and produces flow as output. Of necessity, the system at the other end of the bond has flow imposed on it as input and produces effort as output.

Several systems can be described by bond graphs, Table 3:

Domain	Effort	Unit	Flow	Unit
Mechanical translation	Force F	[N]	Velocity v	[m/s]
Mechanical rotation	Torque M	[Nm]	Angular velocity ω	[rad/s]
Hydraulic	Pressure Δp	[N/m2]	Volume flow rate $\dot{V}$	[m^3/s]
Electric	Voltage U	[V]	Current I	[A]
Chemical	Chemical Potential μ	[J/mol]	Molar flow $\dot{N}$	[mol/s]
Thermodynamic	Temperature T	[K]	Entropy flow $\dot{S}$	[W/K]
Thermodynamic (stationary)	Specific enthalpy Δh	[J/kg]	Mass flow $\dot{m}$	[kg/s]

Table 3 Systems described by the bond graph method.

To connect more elements to a flow, two types of junctions can be used. The 1–junction where the flow is common and the sum of efforts equals zero, Figure 8:

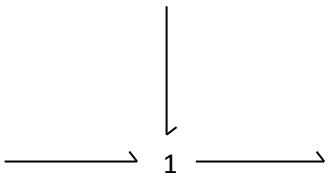

Figure 8 1-junction.

The 0-junction where the effort is common and the sum of flow equals zero, Figure 9:

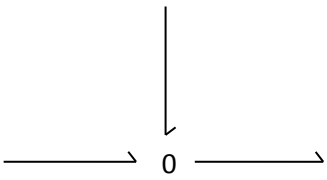

Figure 9 0-junction.

5.2 Ship Model

A container ship drawing with elements describing the elements in the performance system is shown in Figure 10. Based on this system a bond graph model will be described.

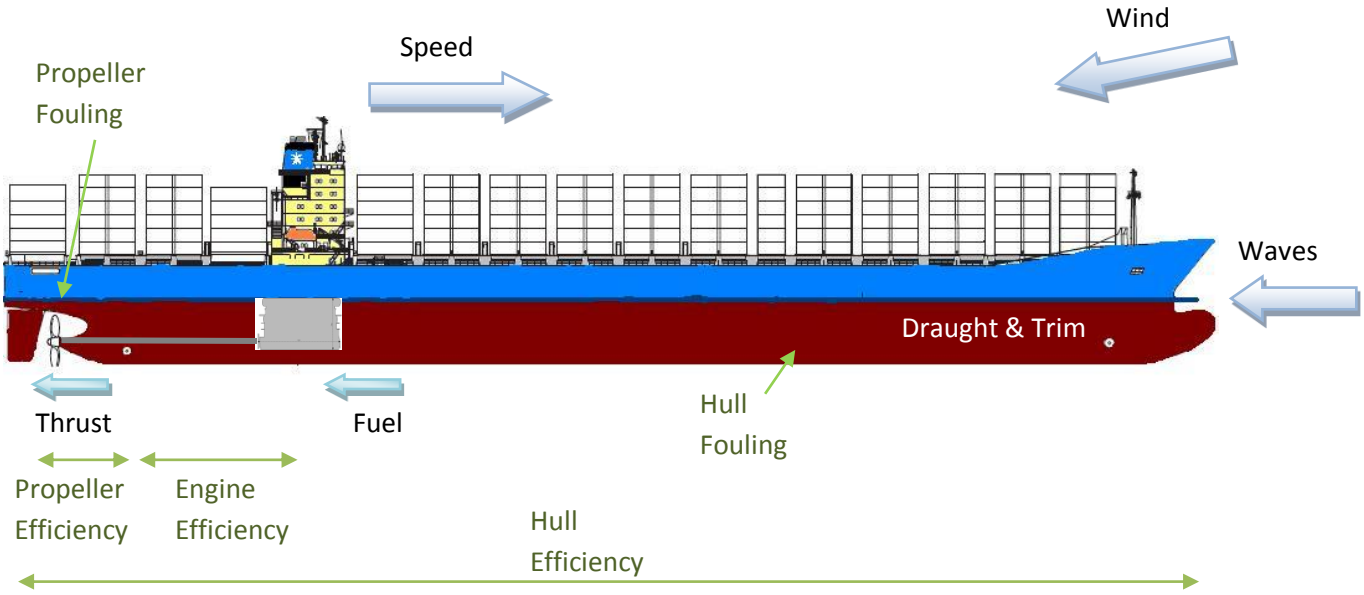

Figure 10 Performance System description

The system consists of a ship sailing at operational conditions defined by the loading of the ship, the ships speed and the environmental conditions. During operation the hull and propeller is exposed to a certain degree of fouling which affects the hull and propeller efficiency. The engine efficiency is affected by the wear and tear over the period of operation. All these factors affect the fuel consumption which will increase. To establish the forces acting in the system the following approach can be taken.

As a ship is moving forward through water, the forces acting on the ship should be balanced. The forces along the surge (R_X) and the sway (R_Y) axis, the yawing (N_Y) and the heeling (M_L) moments around the centre of gravity are composed of

$$R_{XA} + R_{XH} + R_{XFR} + R_{XW} + R_{XP} = 0 \quad (8)$$

$$R_{YA} + R_{YH} + R_{YFR} = 0 \quad (9)$$

$$N_{YA} + N_{YH} + N_{YR} = 0 \quad (10)$$

$$M_{LA} + M_{LH} + M_{LR} + M_{LB} = 0 \qquad (11)$$

The indices of the components represent the following contributions: *A* aerodynamic forces and moments from hull, deck cargo and superstructure, *H* hydrodynamic forces and moments from hull, *FR* hydrodynamic forces and moments from rudder and fin stabilisers, *W* added resistance due to waves, *P* propeller thrust and *B* hydrostatic righting moment due to heel.

When the ship's heading, propeller revolutions, load condition (draught and trim) and the environmental conditions are known, the equilibrium equations, Equations (8) – (11) are a function of the ship's speed through water (U_S), the drift angle (α), the rudder angle (δ) and the heeling angle (ε), Figure 11. This applies when inertia forces are neglected, i.e. in steady state conditions.

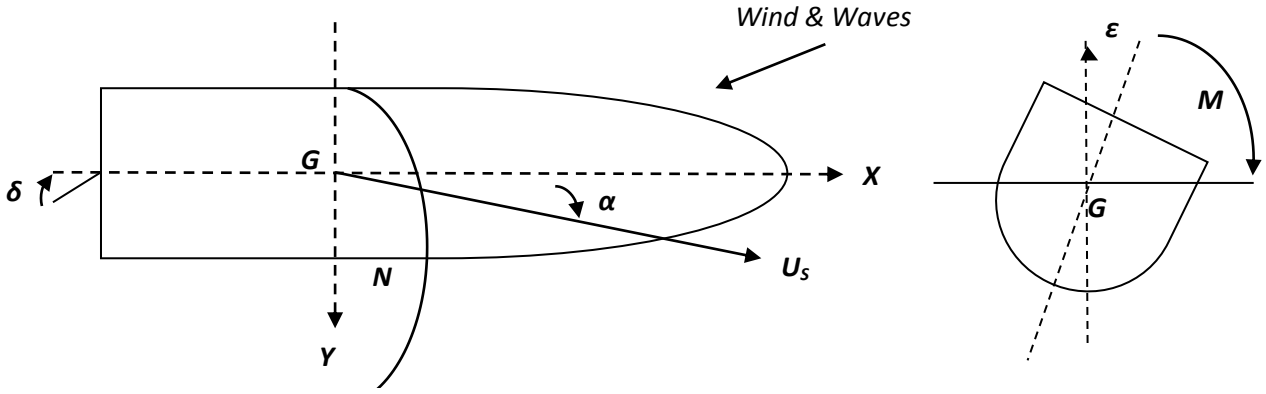

Figure 11 Definitions of forces and moments.

The forces along the surge axis are relevant to the performance calculations. The system can now be described by a simplified bond graph model, Figure 12.

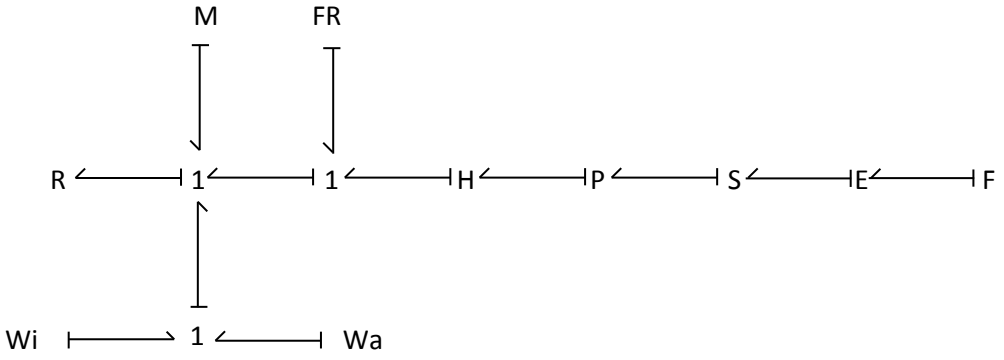

Figure 12 Bond Graph Performance System

The detail of the bond graph model is depending number of elements included and what the different elements will include. The bond graph model in Figure 12 is shown with causality and power directions on all the bonds. The models describes the ship's resistance element (R) connected to the rest of the system by a 1- junction. The element described the R_{XH} force in (8) and can be expressed by

$$R_{XH} = ½\rho_W C_T S U_S^2 \tag{12}$$

where ρ_W is the sea water density, C_T is the resistance coefficient, S is the hull wetted surface area and U_S is the ship's speed.

The velocity of the ship can be found by two methods. One is to insert a causal element in between the hull and the resistance element. The model velocity is then found by iteration until there is equilibrium in the system. Another way is to insert a mass model in the system (M). The model speed now comes from the flow in the system and is described by

$$M\dot{U}_{SM} = R \Longrightarrow U_{SM} = \frac{1}{M}\int R dt \tag{13}$$

where M is the ship's mass, $\dot{U}_{SM}$ is the ship's model acceleration, R is the total force in the system and U_{SM} is the ship's model speed. The resistance force R_{XA} for the wind (Wi) can be estimated by

$$R_{XA} = ½\rho_A C_X A_T U_{RW}^2 \tag{14}$$

where ρ_A is the density of air, C_X is the wind force coefficient in surge direction, A_T is the transverse projected area of the hull and cargo above water and U_{RW} is the relative wind speed.

The resistance force R_{XW} for the waves (W_a) will be estimated by several methods as described in Section 1.2. The additional data necessary to estimate the added resistance in waves i.e. wave height, direction and period are often not logged on board the ship and therefore other more simple approaches in estimating the added resistance in waves have to be used and description of these can be found in the wave element section.

Both wind and wave elements are connected by a 1-junction. The hull element (H) is described by the transformation of the ship speed U_S to the advance speed U_a through

$$U_a = (1 - w)U_S \tag{15}$$

where w is the wake fraction and the transformation of the hydrodynamic force R_{XH} to the thrust force, R_{XP}

$$R_{XH} = (1 - t)R_{XP} \quad (16)$$

where t is the thrust deduction fraction. The resistance force from rudder and stabiliser fins are further described in Sections 5.3.9 and 5.3.10.The propeller element (P) is described by the advance number J

$$J = \frac{U_a}{nD} \quad (17)$$

where n is the propeller revolutions, D is the propeller diameter and U_a is the advance speed. With J and the open water propeller curve, the torque coefficient k_Q and the thrust coefficient k_T is found. The shaft element (S) describes the power loss over the shaft, the engine element (E) delivers the shaft speed and thereby the shaft power P_S by

$$P_S = \omega Q \quad (18)$$

where ω is revolutions of propeller shaft and Q is shaft torque. The fuel tank element (F) is described by the fuel quality and the flow to the main engine.

The structure of the model follows more or less the structure of the drawing in Figure 10 (container ship) which is convenient in keeping the physical understanding of the developed mathematical model through the modeling and analysis process.

The model can be extended to include more elements, depending on the purpose of the model and of the available data to feed the model. The models developed in this work have been adjusted to fit to the logged signals with respect to number of elements.

In this work, the modeling has been done in special developed software based on the bond graph method.

5.3 The GES Software

The GES (General Energy System) software is developed by TNO (2010) and is based on the bond graph method. It is developed for describing the energy system and flows in a dynamic system, e.g.

a ship or a power plant. The elements created in the software are stored in libraries and are easily connected to complete energy systems. The software is used in the modelling of the ship and several models have been developed during this work. Each model consists of elements which are connected to a complete system. Each element is described by a set of input parameters, a set of equations and a bond to and from other objects in the system. An example of an element – a ship's propeller - is shown in Figure 13.

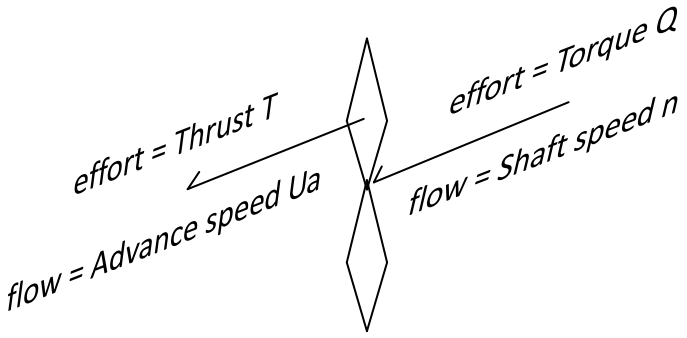

Figure 13 GES element

The equations - .equ files - defining the objects are stored in file folders and can be called on from commands in the equation writer in GES. In the following chapter, the objects used in the modeling are described in detail.

The input parameters to the models are defined by global variables. They can be defined in the system by matrixes or they can be loaded into the system by various tools, i.e. Matlab, Excel or other software systems. As an example, the logged speed is loaded into the system from Excel by a macro. The variable "!SpeedLog", which is defined by the macro, is inserted in an object defined as in Figure 14.

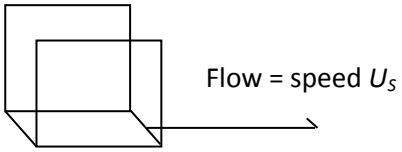

Figure 14 Global variable SpeedLog.

The global variable "!Speed" is now defined as flow in the object. The other input parameters are defined in the same way. The global variables are not connected by bonds to the model but can be called on in any equation used in the system. A model based on the PostPanmax container ship m/v "Clementine Maersk" is developed in the bond graph system and the full model with GES / Bond Graph notation is shown in Figure 15.

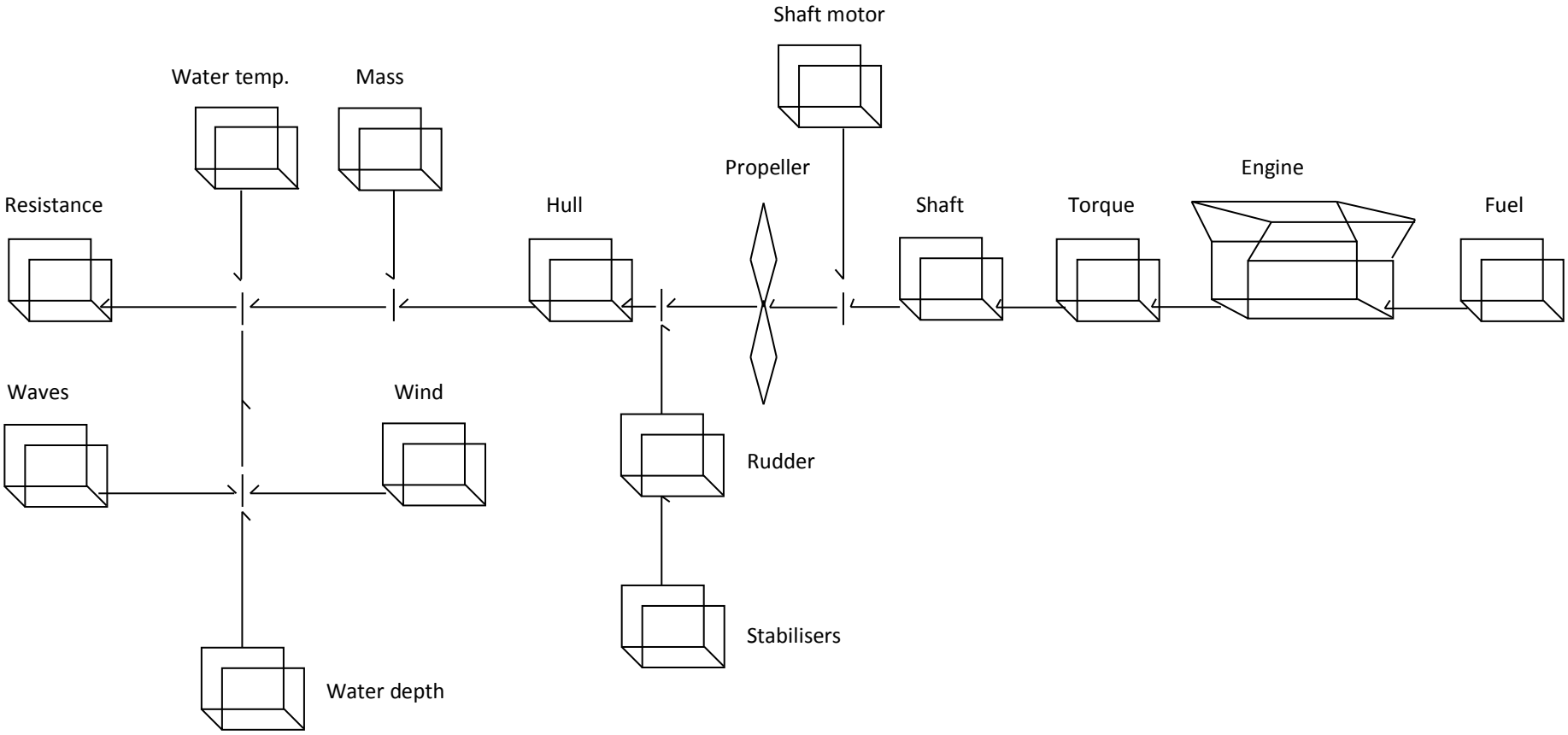

Figure 15 The ship model in GES.

5.3.1 **The Resistance Element**

The element includes ship's resistance and two of the performance indexes, Figure 16.

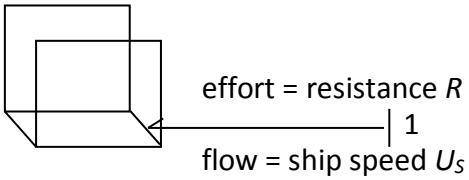

Figure 16 Resistance element.

The ship's resistance is based on results from model tests. Previous normal procedures regarding the model tests have shown to be insufficient with regard to describing the resistance of the ship. A series of tests with varying speed and draught – normally a number of conditions from ballast to full load around service speed – has been extended to a number of tests with varying speed, draught and trim in order to give a more detailed description of the ship's resistance under all load conditions and speeds.

To find the variation in thrust deduction fraction *t*, a series of tests were carried out at mean draughts and with no trim variation. The form factor *k* was found under the same conditions. These results were used in the subsequent trimmed resistance tests.

The total resistance coefficient C_T is found for the conditions. It is assumed that only the frictional resistance coefficient C_F is dependent on the scale. It is calculated according to Eq. D18 and subtracted from C_T, giving the residuary resistance coefficient C_R, which is assumed to be the same for the model and the ship. C_F for the ship is calculated and added to C_R together with the allowance coefficient C_A, which allows for the resistance of deck houses, bilge keels, hull roughness and steering loss, ITTC (1999).

The model tests have resulted in a set of power curves for each condition and from these a set of matrixes is imported to the model. The resistance R_T is then found by the relation

$$P_E = R_T U_S \tag{19}$$

where P_E is the effective power extracted from the power matrix by 3D interpolation with the arguments of speed, draught and trim.

C_T is found by Eq. D17 and the wetted surface area S is found by interpolation with the arguments of draught and trim.

In the resistance element the performance indexes Speed Pct and k_{S2} are included. The Speed Pct is found by Eq. 5 where the model speed – with no fouling - is compared to the actual ship's speed – with actual fouling k_{S2} is found by Eq. 4 where k_{S1} is the initial *AHR* and k_{S2} is the *AHR* after a certain period. Change in resistance due to change in dC_F is found by

$$\Delta R = \frac{dC_F}{C_T} R_T \tag{20}$$

where k_{S2} is optimized with reference to the ship's logged speed, Figure 17.

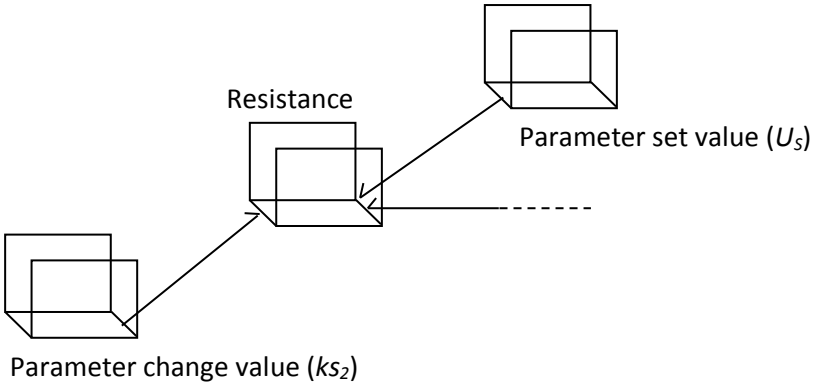

Figure 17 Optimising ks_2.

Equation (8) can be expressed as

$$R_{XH} + R_{XA} + R_{XR} + R_{XW} = (1 - t)T \tag{21}$$

where $R_{XH} = R_{Ta}$ is the actual hydrodynamic resistance and T is the thrust force (R_{XP}). R_{Ta} can be expressed as in Eq. 3:

$$R_{Ta} = ½\rho S(C_T + dC_F)U_{SM}^2 \tag{22}$$

Where dC_F is as in Eq. 1:

$$dC_F = 0.044\left[\sqrt[3]{\frac{k_{S2}}{L_{pp}}} - \sqrt[3]{\frac{k_{S1}}{L_{pp}}}\right] \tag{23}$$

The initial roughness value k_{S1} is set to 130μm and the Newton Raphson method is used for the optimization. The ship's logged speed is now used instead of the model speed and the final equation used in the optimization can then be expressed as

$$½\rho S\left(C_T + 0.044\left[\sqrt[3]{\frac{k_{S2}}{L_{pp}}} - \sqrt[3]{\frac{k_{S1}}{L_{pp}}}\right]\right)U_S^2 + R_{XA} + R_{XR} + R_{XW} - (1-t)T = 0 \qquad (24)$$

When Eq. (24) equals 0, i.e. when the model resistance equals the actual resistance of the ship, k_{S2} has a value which is used as an expression for the added roughness of hull and propeller due to fouling. The optimization is exemplified by Figure 18 where the difference between the model and the logged speed is shown. After the optimization the resulting k_{S2} roughness value is as shown on Figure 19.

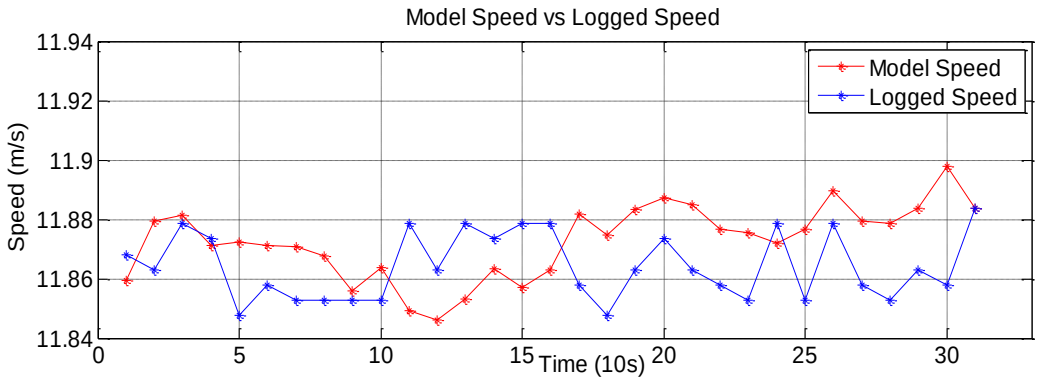

Figure 18 Model speed vs. logged speed

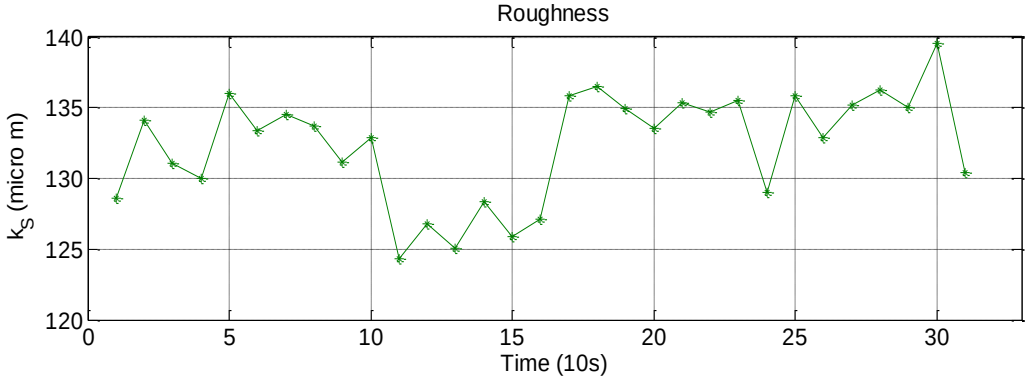

Figure 19 Roughness k_{S2} after optimization

5.3.2 **Sea Water Temperature**

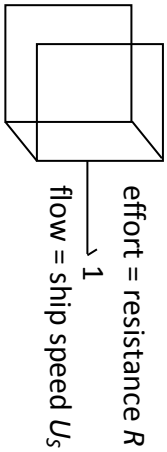

Figure 20 Sea water temperature element.

The resistance tests in the model basin are performed under conditions with reference to a specific basin water temperature and salt content. During service these factors may vary and the resistance correction due to these effects is found by ISO 15016 (2002):

$$R_{AS} = R_{T0}\left(1 - \frac{\rho_W}{\rho_0}\right) - R_F\left(1 - \frac{C_{F0}}{C_F}\right) \quad (25)$$

where R_{T0} is the total resistance found by model tests, ρ_W is the actual density of sea water during service, ρ_0 is the density of water in the model basin, R_F is the frictional resistance under service conditions, c_{F0} is the frictional coefficient found in the model basin and c_F is the actual frictional resistance coefficient under service conditions.

The variation in density due to variation in temperature is estimated by ISO 15016 (2002):

$$\rho(T_W) = g(a + bT_W + cT_W^2 + dT_W^3) \quad (26)$$

where a = 104.83004

b = -6.210858 x 10-3

c = -5.976822 x 10-4

d = 2.5797397 x 10-6

The kinematic viscosity ν in sea water is estimated by ISO 15016 (2002):

$$\nu(T_W) = a + bT_W + cT_W^2 + dT_W^3 + eT_W^4 \quad (27)$$

where a = 1.8277885 x 10-6

b = -6.0200312 x 10-8

c = 1.528715 x 10-9

d = -2.741868 x 10-11

e = 2.3718711 x 10-13

R_{T0}, C_{F0} and ρ_0 are found by model tests. The element containing the sea water temperature correction is connected to the model, Figure 20.

The sea water temperature is measured during service. The element is added to the initial performance model and is further described in Section 9.

5.3.3 **The Wave Element**

The wave element is divided in two. One element is used to find the estimated wave height and one is used to estimate the added resistance due to waves.

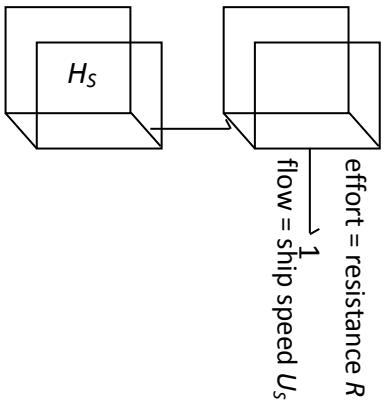

Figure 21 Wave resistance element.

The wave height is estimated by using the true wind speed or by using the measured bow motions.

The wave height can be found by the following relation, Fossen (1994):

$$H_S = \frac{2.06}{g^2} U_{TW\_19.4}^2 \tag{28}$$

where $U_{TW\_19.4}$ is the true wind speed measured at a height of 19.4 m above sea level.

The wave height can also be found by using the response measurements from an accelerometer in the bow. The encounter period T_e is measured and it relates to the encounter frequency ω_e as

$$\omega_e = \frac{2\pi}{T_e} \tag{29}$$

ω_e relates to the wave frequency ω as

$$\omega_e = \omega - \omega^2 \frac{U_s}{g} cos\beta_{180} \tag{30}$$

where β_{180} is the relative wave angle (180° is head seas). The direction of the waves is assumed to be the same as the direction of the true wind. The wave number k relates to the wave frequency (in deep water) as

$$k = \frac{\omega^2}{g} \tag{31}$$

and the wave length λ relates to k as

$$\lambda = \frac{2\pi}{k} \tag{32}$$

The vertical motion in the bow η_{3bow} is measured by the sensor and it relates to the wave height H_s as

$$\eta_{3bow} = ½H_S\Phi_w \, cos(\omega_e t + \xi) - ½H_S x_{bow}\Phi_\theta \, sin(\omega_e t + \xi) \tag{33}$$

where Φ_w is the RAO for the heave motion, Φ_θ is the RAO for the pitch motion, ξ is the phase difference and x_{bow} is the distance from the sensor to the centre of gravity.

The RAOs for heave Φ_w and pitch Φ_θ can be found by using closed-form expressions, Jensen et al. (2003), see Appendix D.

The variance of the bow motion s_R^2 is given as:

$$s_R^2 = \int_0^\infty \Phi_R^2(\omega) S(\omega) d\omega \quad (34)$$

where Φ_R is the frequency response function given as:

$$\Phi_R^2 = \Phi_w^2 + (x_{bow} \Phi_\theta)^2 \quad (35)$$

It is assumed the heave and pitch motion are 90° out of phase.

The wave spectrum $S(\omega)$ is a Pierson-Moskowitch spectrum given as:

$$S(\omega; H_S; T_S) = 173 H_S^2 T_S (\omega T_S)^{-5} e^{-692(\omega T_S)^{-4}} \quad (36)$$

The frequency response functions for heave and pitch are calculated by closed form expressions and they are used in Eq. 34 to find a calculated value for s_R^2 at wave height $H_S = 1$, by:

$$s_w^2 = \int_0^\infty \Phi_w^2(\omega) S(\omega) d\omega \quad (37)$$

$$s_\theta^2 = \int_0^\infty \Phi_\theta^2(\omega) S(\omega) d\omega \quad (38)$$

The final expression for the calculated wave height is then:

$$H_S^2 = \frac{s_{Rm}^2}{s_R^2} \quad (39)$$

where s_{Rm}^2 is the variance of the measured bow motion.

As mentioned earlier the logged data used in the performance calculation are most often based the equipment already installed on board the ships. Where ship motions are not measured and logged the wave height will have to come from estimations based on the true wind speed or estimates from the crew on board the ships. When it comes to estimating the added resistance in waves it will be necessary use relations based on the data that are available and in cases where it is not possible to have detailed ship motion and wave data, a more universal wave resistance model will have to be used. The model used in this work is based on the model used in the performance system in which this work is based upon.

The wave-induced force R_{XW} is estimated by the relation of Kreitner, ITTC (2005_1):

$$R_{XW} = 0.64 H_S^2 B^2 C_B \rho_W \frac{1}{L_{WL}} g \quad (40)$$

where H_S is the wave height, ρ is the density of the sea water, g is the acceleration of gravity and L_{WL} is the length of the waterline. The relation can be used in significant wave heights of 1.5 to 2m. A correction for the wave direction is given by

$$R_{XWC} = F_{XW}(0.667 + 0.333 cos\beta_{180}) \quad (41)$$

where β_{180} is the angle between ship's heading and the incoming wave.

5.3.4 **The Wind Element**

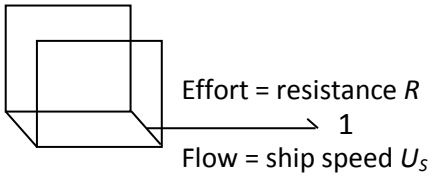

Figure 22 Wind resistance element.

The element is based on the relation Eq. 14.

The wind force coefficient C_X can be found by wind tunnel tests on a particular ship model or by various models. Two models have been chosen in this work:

#1 Isherwood

#2 Fujiwara

The models are both semi empirical models and they are described in details in Appendix D. Model #1 is chosen because it is already used in the performance system used as background for this work. Model #2 is chosen because it is based on more extensive data from wind tunnel tests, towing tank tests and full scale data, Fujiwara (2006).

The exposed wind area varies depending on the ship type e.g. if it is a tanker or a container ship. For container ships the deck load varies and in order to estimate the wind load, the load

configuration of containers on the weather deck has to be known. Especially the load configuration on the deck forward of the accommodation has a significant importance on the longitudal force, where a randomly stacked load will induce a larger force than a full load, Blendermann (1997).

The relative wind directions are dependent on the ships course and speed relative to the true wind direction and speed and will vary during operation. The service speed of a container ship is normally high and the relative wind will normally come from forward of amidships and it will be seen in this work that this will always be the case after the filtering of data. The cross sectional area is not as sensitive to the load configuration of the containers since the area covered by containers already is covered by the superstructure and other parts of the ship. The longitudal projected area and the position of centre of dynamic pressure will change with varying load configuration and this will affect the wind induced resistance force a soon as the relative wind comes from other directions than the bow.

The wind force input to models is the relative wind speed. The wind force input to model #1 is originally set to a mean square wind, but results have shown that better results are achieved by using the measured wind, Isherwood (1973). The wind force input to model #2 is given by Eq. D14, Appendix D.

The measured wind will have to be corrected for the height of the anemometer placement on board the ship. The wind is varying in strength with height and the wind resistance models used are to a certain reference height. The wind velocity variance with height can be corrected by, Bom et al (2008):

$$U_W(z_{ref}) = U_W(z)\left(\frac{z_{ref}}{z}\right)^{1/7} \tag{42}$$

Where U_W is the measured wind velocity, z is the height of the anemometer and z_{ref} is the reference height used in the wind resistance model.

The wind areas are found as described in Appendix D. The two models are used in the "Performance analysis" in Section 10 and results are compared and analysed in this section.

5.3.5 **The combined wind and wave model**

An approximate relation describing the combined wind and wave resistance is developed for practical usage by Townsin and Kwon, Kwon (2008). The relation is based on the wind speed by the Beaufort scale, a block coefficient and Froude number correction and a weather direction correction factor. An element estimating the combined wind and wave resistance is developed in GES and also used in the final performance analysis, see section 10.

A percentage of speed loss is given by

$$Speedloss = \varsigma \cdot \mu \frac{\Delta U_S}{U_S} 100\% \tag{43}$$

where ς is the correction factor for the block coefficient (C_B) and Froude number (F_n), μ is the weather direction reduction factor, U_S is the design service speed and $\frac{\Delta U_S}{U_S}$ is the speed loss in head seas and wind. See Table 4 for the correction factor block coefficient and Froude number for container ships.

CB	Condition	ς
0.55	Loaded	$1.7 - 1.4\mathrm{F_n} - 7.4\mathrm{F_n^2}$
0.60	Loaded	$2.2 - 2.5\mathrm{F_n} - 9.7\mathrm{F_n^2}$
0.65	Loaded	$2.6 - 3.7\mathrm{F_n} - 11.6\mathrm{F_n^2}$
0.70	Loaded	$3.1 - 5.3\mathrm{F_n} - 12.4\mathrm{F_n^2}$

Table 4 Correction factors.

The Froude number is given by

$$F_n = \frac{U_S}{\sqrt{gL}} \tag{44}$$

For container ships (C_B = 0.55, 0.60 and 0.65) the speed loss in head weather is given as

$$\frac{\Delta U_S}{U_S} 100\% = 0.7BN + \frac{BN^{6.5}}{2.2\nabla^{2/3}} \tag{45}$$

where *BN* is the wind force given by the Beaufort scale. For other ships than container ships, the correction values for block coefficient/Froude number and speed loss in heavy weather are tabulated in Kwon (2008).

The weather direction reduction factor is given in Table 5.

Correction factor	Relative wind direction (0° head seas)
$\mu_{\text{bow}} = 1$	0° - 30°
$\mu_{\text{bow}} = 1.7 - 0.03(\text{BN} - 4)$	30° - 60°
$\mu_{\text{bow}} = 0.9 - 0.06(\text{BN} - 6)^2$	60° - 150°
$\mu_{\text{bow}} = 0.4 - 0.03(\text{BN} - 8)^2$	150° - 180°

Table 5 Weather reduction factors.

5.3.6 **The Water Depth Element**

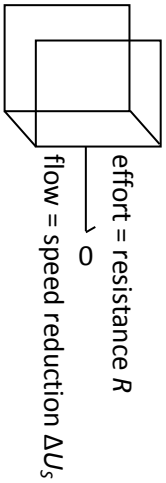

Figure 23 Water depth element.

The shallow water effect can be divided into two parts.

1. Added resistance due to increase in water velocity along the ship's hull. This effect will cause an added sinkage (squat) of the hull and thereby an increased wetted surface which will lead to changed frictional resistance and wave making resistance.
2. Added resistance due to change of the wave pattern. In deep waters the wave velocity for the ship induced diverging waves is dependent on the wave length only where as in shallow

waters the wave velocity is dependent on the water depth. The changed wave velocity will change the wave pattern and thereby the wave resistance.

The element used in the model estimates the speed reduction due to sailing in shallow waters as described in the work of Lackenby (1963):

$$\frac{\Delta U_S}{U_S} = 0.1242\left(\frac{A_M}{h^2} - 0.05\right) + 1 - \left(tanh\frac{gh}{U_S^2}\right)^{1/2} \text{ for } \frac{A_M}{h^2} \geq 0.05 \quad (46)$$

where ΔU_S is the speed loss due to shallow water, U_S is the ship's speed, A_M is the midships section area under water and h is the water depth.

The estimated speed reduction affects the flow in the system and the element is therefore connected to the system with a 0-junction, Figure 23. The shallow water effect is further described in the Case Study in Section 9.3.

5.3.7 **The Mass Element**

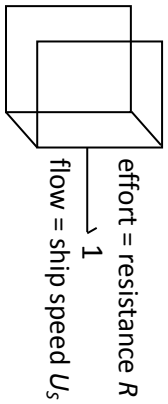

Figure 24 Mass element.

The model speed is found from the flow in the system and is described by

$$M\dot{U}_{SM} = R \Longrightarrow U_{SM} = \frac{1}{M}\int R dt \quad (47)$$

where M is the ship's mass, $\dot{U}_{SM}$ is the ship's model acceleration, R is the force in the system and U_{SM} is the ship's model speed. The mass input is found by a matrix with draught forward and aft as

input. The added mass in surge is assumed to have a value of 5% of the ship's mass, Lützen (2001), and is included in *M*.

5.3.8 **The Hull Element**

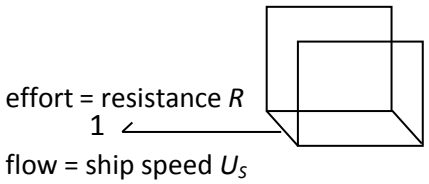

Figure 25 Hull element.

The hull element is describing the thrust deduction fraction *t* and the wave fraction *w*. The advance speed U_a, the ship's speed U_S and *w* are related as in Eq. 15. The resistance R_T, the propeller thrust *T* and *t* are related as in Eq. 16.

Parameters *w* and *t* are found by model tests; *w* is found by a matrix with speed, draught and trim as arguments and *t* is found by a matrix with draught and speed as arguments.

5.3.9 **The Rudder and Steering Element**

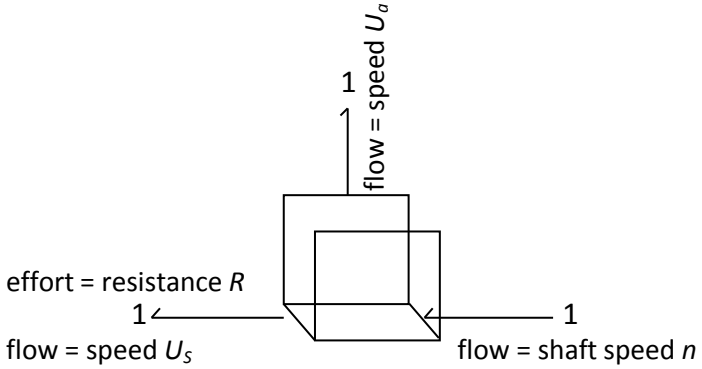

Figure 26 Rudder element in GES

The rudder induced resistance and is given by Kijima et al. (1990):

$$R_{XR} = F_N sin\delta \tag{48}$$

where δ is the rudder angle and F_N is the rudder normal force. The rudder normal force can be approximated as suggested by Kijima et al. (1990):

$$F_N = ½\rho_W(1-t_R)\frac{6.13\Lambda}{\Lambda+2.25}A_R U_R^2 sin\delta^* \quad (49)$$

where ρ_w is the density of the sea water, t_R is the resistance deduction fraction due to steering, Λ is the aspect ratio of the rudder, A_R is the rudder area, U_R is the effective rudder inflow speed and δ^* is the effective rudder inflow angle (assumed to be equal to the rudder angle δ).

The effective rudder inflow speed U_R can be approximated as defined by Molland & Turnock (2007):

$$U_R = U_a\left[1+k_R\left\{\left(1+\frac{8k_T}{\pi J^2}\right)^2-1\right\}\right] \quad (50)$$

where U_a is the average inflow speed to the propeller, k_T is the thrust coefficient, J is the advance ratio. k_R can be expressed as in Molland & Turnock (2007):

$$k_R = ½ + ½\left[\frac{1}{1+\frac{0.15}{X/D}}\right] \quad (51)$$

where X is the distance between rudder and propeller and D is the diameter of the propeller.

The fraction t_R can be found by model tests or by a relation between the block coefficient of the ship and t_R, Aoki et al (2006):

$$t_R = -0.626C_B^2 + 0.605C_B + 0.129 \quad (52)$$

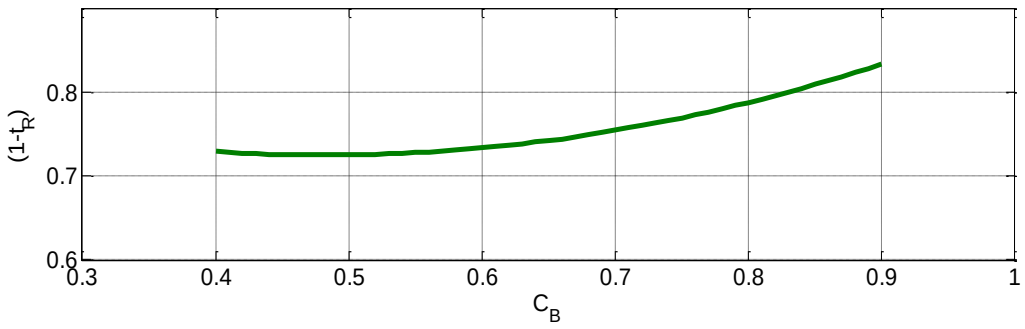

Figure 27 Resistance thrust deduction fraction

This leads to the final expression for the added resistance due to rudder movements:

$$R_{XR} = ½\rho_W(1 - t_R)\frac{6.13\Lambda}{\Lambda+2.25}A_R U_R^2 \delta^2 \quad (53)$$

The element is connected with three 1-junctions. Two junctions are using the shaft speed n and the advance speed U_a in order to find k_t. The third junction delivers the rudder resistance to the system.

During sailing or during a turn the ship will experience a drift angle α which will expose a part of the side of the ship's hull towards the direction of motion, Figure 28.

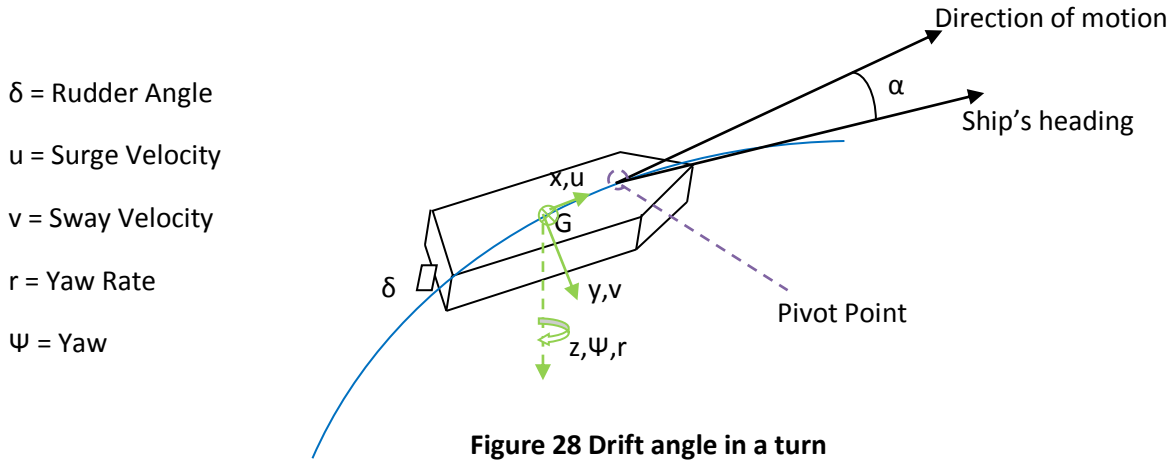

Figure 28 Drift angle in a turn

The yaw rate can be found by

$$r = \frac{d\Psi}{dt} \quad (54)$$

where Ψ is the ship's heading angle. When the ship is in a constant turn, the rudder holds the hull of the ship at a constant angle of attack or constant drift angle. This creates a hydrodynamic lift from the hull in order to accelerate towards the centre of the turn. The lift will create a drag (resistance) force and this force will cause the ship to experience reduced speed. The ship will decelerate and eventually reach constant (reduced) speed sometime during the turn.

It is not only through a ship's turn that the ship will experience a drift angle. When sailing the ship might experience a lift force exited either from wind forces or from unsymmetrical properties of underwater part of the hull. Further can the propeller to some extent induce a side force with the largest effect at slow speed. The ship will counteract the side force by activating the rudder at a

usually small rudder angle and this will keep the hull a steady drift angle. This angle is usually also small – in the order of 1 to 2°, PNA (1988).

Ref. Section 6.3 it seems like the case study ship m/v "Clementine Maersk" is operating with a constant rudder angle, which might be caused by the above mentioned phenomenon. By considering the ship's hull like a foil it is known that the induced lift force F_L will act at a right angle towards the direction of motion. The inflow angle – in this case α – will relate to the lift coefficient C_L and the aspect ratio of the foil Λ as

$$\alpha = \frac{C_L}{\pi\Lambda} \tag{55}$$

The drag coefficient C_D will relate to C_L as

$$C_D = C_L \tan\alpha \tag{56}$$

For small angles $C_D = C_L\alpha$ and inserted in Eq. 55, C_D can be expressed as

$$C_D = \frac{C_L^2}{\pi\Lambda} \tag{57}$$

The drag force due to a drift angle can be expressed as

$$R_D = ½\rho U_S^2 C_D A_{HULL} \tag{58}$$

where A_{HULL} is the underwater area of the hull. By using Eq. 55 and Eq. 57 in Eq. 58 the drag force would then be

$$R_D = ½\rho U_S^2 \pi d_m^2 \alpha^2 \tag{59}$$

where d_m is the ship's mean draught. This expression would be valid if the foil – the ship's hull in this case – was elliptical. Since this is not the case, an efficiency factor ε will have to be used on Eq. 58. For a ship's hull this can be estimated to ε = 0.5, Hooft (1987) and then Eq. 58 will be transformed to

$$R_\alpha = 0.25\pi\rho_W d_m^2 U_S^2 \alpha^2 \tag{60}$$

which is the expression as given in ISO 15016 (2002).

5.3.10 **The Fin Stabiliser Element**

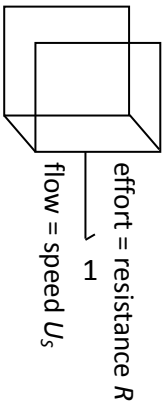

Figure 29 Fin Stabiliser element.

The fin stabiliser-induced force R_{SF} is found in accordance with Larsen (2008):

$$R_{SF} = ½\rho C_D A_{SF} U_S^2 \tag{61}$$

where A_{SF} is the area of the stabiliser fin and C_D is the drag coefficient.

C_D is found by using the aspect ratio of the fin. An average value of the drag induced by the fin can be found by integrating the drag over one oscillation of the fin movement and dividing by the time of one oscillation. The effective aspect ratio of the fin Λ_{SF} is then found by

$$\Lambda_{\mathrm{SF}} = 2\frac{b_f}{c_{mean}} \tag{62}$$

where b_f is the span length and c_{mean} is the mean chord length.

The slope of the lift curve is found by

$$\frac{dC_L}{d\alpha} = \frac{1.95\pi}{57.3(1+\frac{3}{\Lambda_{\mathrm{SF}}})} \tag{63}$$

where α is the lift angle and C_L is the lift coefficient. C_L is found by

$$C_L = \frac{dC_L}{d\alpha}\alpha + \frac{1.7}{\Lambda_{\mathrm{SF}}}\left[\frac{\alpha}{57.3}\right]^2 \tag{64}$$

C_D is then found by

$$C_D = 0.015 + 0.37\frac{C_L}{\Lambda_{\mathrm{SF}}} \tag{65}$$

5.3.11 **The Propeller Element**

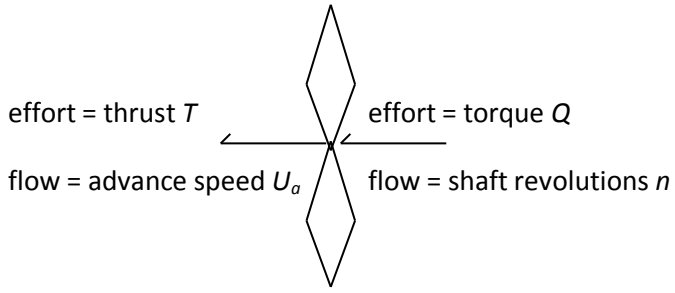

Figure 30 Propeller element.

The propeller revolutions n are added to the system from data. The propeller characteristics are from the open water propeller curves, Appendix D, Figure D5 and the torque and thrust coefficient are found in a matrix with the advance number J as argument.

5.3.12 **The Shaft Element**

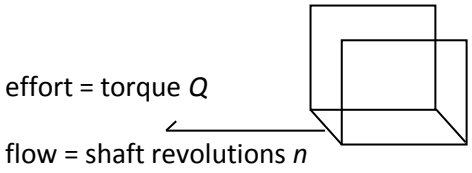

Figure 31 Shaft element.

The element is used to find the power loss from engine to propeller, Figure 31. The shaft efficiency η_S is found by

$$\eta_S = \frac{P_D}{P_B} \tag{66}$$

where P_D is the power delivered to the propeller and P_B is the brake power delivered by the main engine. The power loss is dependent on the efficiency in gearboxes (if any), number of bearings

along the shaft etc. In the literature η_S is estimated to have values around 0.96 to 0.995, Friis et al. (2002). Since there are no gearboxes in this model the value is set to 0.99.

5.3.13 **The Torque Meter Element**

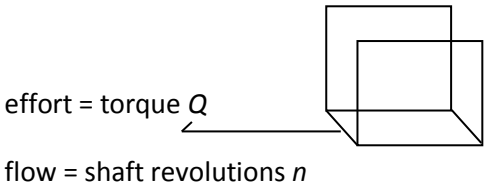

Figure 32 Torque meter element.

The element is used to find the model shaft power P_{SM} and thereby estimate the performance index Power pct by comparing model power with measured power logged on board.

5.3.14 **The Engine Element**

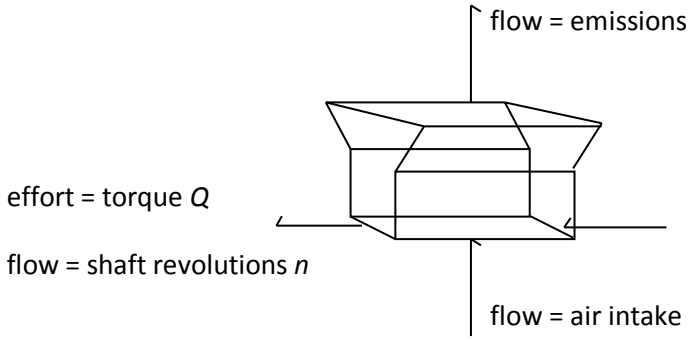

Figure 33 Engine element.

The main engine model, Figure 33 is defined from the following parameters:

- The characteristics of the ship's main engine with reference to minimum/nominal speed (revolutions) and nominal power
- The fuel quality with regard to percentage of carbon C, hydrogen H_2 and sulphur S
- The aspect values of the engine with regard to nominal fuel consumption and nominal emissions ratio for nitrogen oxides (NO_X), methane (CH) and carbon oxides (CO).

- Emissions ratio for oxygen (O_2), nitrogen (N_2), water (H_20), NO_X, HC, CO, sulphur dioxide (SO_2) and carbon dioxide (CO_2)
- The power to weight ratio of the engine, energy density of the fuel and specific fuel oil consumption per produced effect

The shaft revolutions, the mass flow of fuel and the air intake are used to generate the output from the engine model. Output is emissions and power to the propeller shaft.

5.3.15 **The Fuel Tank**

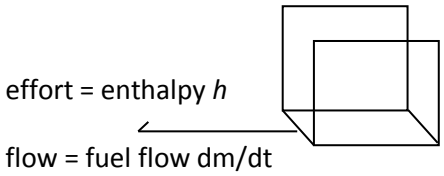

Figure 34 Fuel tank element.

The fuel tank is described by physical properties and the fuel, which is described by specific enthalpy and mass flow to the engine.

6 Case Study

The models described in the previous section can be used to describe the performance of a particular type of ship. A series of Panmax container ships have been used in the initial stage of the modelling process (see Appendix B) and a VLCC have been modelled (see Appendix A).

In the process of establishing an auto logging system based on the data collected by a ship's automation system, a model of a PostPanmax containership have been developed and it is this particular ship and the data logged on board the ship that the following case study is based upon. The data is logged through the year 2010 and the ship's particulars and an overview of the operational profile for 2010 will be described. The logging of data is based on the sensors that already are installed on board and a description of each sensor will follow in Section 6.3.

6.1 The Ship

Figure 35 m/v"Clementine Maersk"

The ship used for the case studies in this thesis is m/v "Clementine Maersk", Figure 35. The ship is a PostPanmax container ship and particulars are as in Table 6.

Length between particulars	332	m
Breadth moulded	42.8	m
Scantling draught extreme	15.02	m
Engine type	WARTSILA Diesel 12RTA96C	-
Number and type of propellers	1 Fixed	-
Available engine power at MCR	63000	kW
Propeller rotation rate	100	RPM

Table 6 Ship particulars

The ship was equipped with logging software ultimo 2009 and data has continuously been logged through 2010. Logging interval of all parameters has been set to 10 seconds per default and all parameters have been logged through the ship's automation system (ABB). The data have been stored on discs by the crew and transferred to shore by mail. During the logging period various modifications have been made to the system e.g. in autumn 2010 a thrust meter was installed on the propeller shaft. The ship and the data is the background for the analyses made in this thesis.

6.2 Operational Profile – 2010

The operational analysis is based on data logged on board in the year 2010, for data logging see the section "Data Analysis". The ship is in service on the Europe – Far East route, Figure 36.

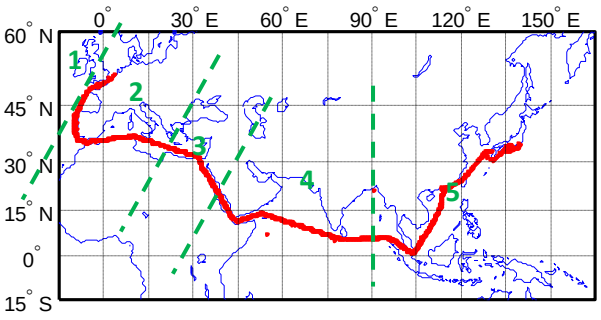

Figure 36 Operational area for m/v "Clementine Maersk"

The ship is sailing through areas with different characteristic environmental conditions:

1. The North Sea, the English Channel and the North Atlantic Ocean
2. The Mediterranean Sea
3. The Suez Canal and the Red Sea
4. The Arabian Sea, the Indian Ocean and the Strait of Malacca
5. The South China Sea and the East China Sea and the North Pacific Ocean

The areas are described with reference to predominant weather and currents.

Area 1:

In northern Europe the ship is operating with loading/discharging cargo in ports with short sea voyages between ports. The weather is dominated by a passage of depressions in eastern and north-eastern directions, which gives varying winds in both direction and strength – with a westerly wind as the dominant direction. Gales are frequent in the winter period. Around Ile d'Ouessant currents are dominated by tidal currents from the English Channel, along the Iberian Coast, the Portugal Current, which is south-going, is dominating and at the entrance to the Strait of Gibraltar an east-going current is dominating.

Area 2:

The weather in the Mediterranean Sea is characterised by hot dry summers with mainly moderate to light winds and mild wet winters with a high frequency of strong winds and gales. Due to the land masses surrounding the sea, many local wind phenomena dominate the area and some of these may cause extreme weather conditions. In the western part currents are dominated by the easterly flow of water from the Atlantic, which loses strength as it passes east. In the eastern part the flow of current is varying and of little strength.

Area 3:

The weather in the Red Sea is hot and dry in the summer and remains very warm in the winter. The winds are mainly light but may be strong in the southern part during the Southwest Monsoon. Currents are generally weak and directions follow the coast and the directions of the predominant monsoon winds.

Area 4:

The weather in the Indian Ocean and adjacent waters is dominated by the monsoons. From June to September the Southwest Monsoon sends south-westerly winds over the area with highest wind strengths in the height of the season (up to gale forces). From November to March the Northeast Monsoon sends north-easterly winds over the area with moderate wind strengths. The inter-monsoon periods – April, May and October – are characterised by varying moderate weather conditions.The currents are dominated by the monsoon wind directions and reversed during the inter-monsoon periods.

Area 5:

The weather in the China Sea is dominated by the monsoons as in Area 4. The area is also affected by typhoons where 90 % of these occur between May and December with September as the month with the highest frequency.

Currents are in the southern part of the area dominated by the monsoon wind direction and in the northern part the Japan Current is the dominating north-easterly current.

Distances between cardinal points, Table 7 and Figure 37.

From	To	Distance (nautical miles)
Ile d'Ouessant	The Strait of Gibraltar	930
The Strait of Gibraltar	The Suez Canal	1910
The Suez Canal		99
The Suez Canal	Bab el Mandeb	1300
Bab el Mandeb	The Strait of Malacca	3650
The Strait of Malacca		500
Singapore	Hong Kong	1460
Singapore	Yokohama	2970
Hong Kong	Shanghai	825
Hong Kong	Yokohama	1660
Shanghai	Yokohama	1030

Table 7 Distances between cardinal points

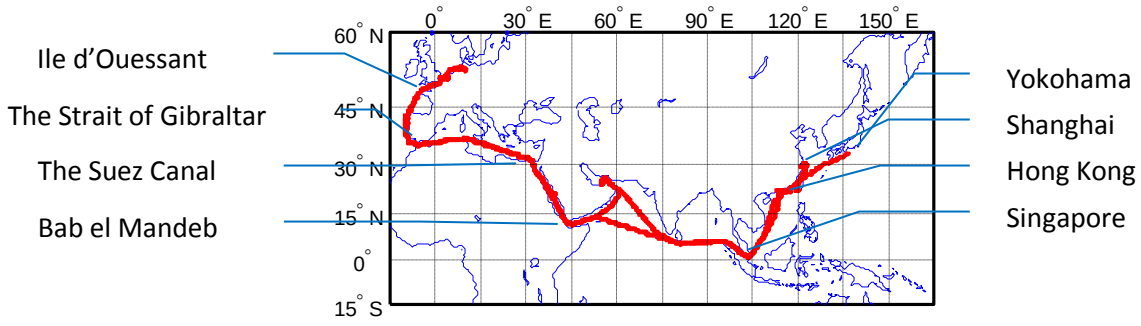

Figure 37 Route with cardinal points.

The distributions of operational and environmental data including all conditions – in port and at sea - during 2010 are plotted in figures. The figures give an overview of the most common conditions during the logging period and the information can be used for selecting the data which should be used in the performance analysis. In Section 10, data filters are introduced to identify conditions where the ship is in steady state conditions. The filters are based on auto-logged data from different

sensors on board. In cases where auto-logging is not possible and the performance analysis is based on manually reported data, e.g. through daily reporting, the operational analysis can be used to find most common conditions, i.e. the performance analysis will be based on these conditions in order to obtain an index based on identical conditions. This approach can also be used in the case where model tests are not available and the propeller is used to create a performance index, see Section 11.

The distribution of data is not included in this report as it is considered confidential information for the Owner of the ship.

6.3 Data Logging Sensors on Board the Ship

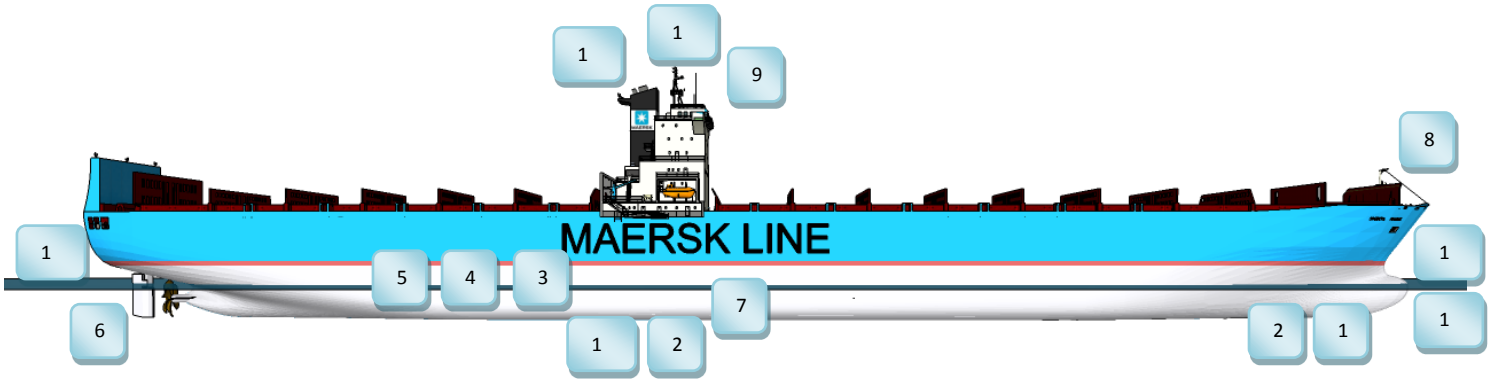

Figure 38 Ship data logging sensors.

Figure 38 shows a drawing of the ship with positions of data logging sensors as on the following list:

1. Speed log
2. Echo sounder
3. RPM and torque meter
4. Shaft motor
5. Thrust meter
6. Rudder indicator
7. Stabiliser fins
8. Wind anemometer
9. GPS
10. Air temperature
11. Gyrocompass
12. Accelerometer
13. Sea water temperature
14. Draught aft
15. Draught forward

The sensors are of the type which could be commonly seen in a cargo ship and the data quality therefore as could be expected without installing specialized logging sensors on board. In the following section the sensors are described and examples of use are analysed. Examples are taken from the operational analysis 2010 and to avoid manoeuvring conditions, only incidents with ME Power loads > 30% are taken into consideration.

6.3.1 **Speed Log**

The speed log is a crucial source for data in the performance calculation. The accuracy of the sensor depends on the calibration and on the manufacture. An offset between speed log readings and the actual speed will indicate the need for calibration.

With regard to accuracy, various manufactures of speed logs give various information. Once calibrated the speed log measurements may have an accuracy of 0.1%, Griffiths et al. (1998), but series of factors influences the measurements.

Environmental factors influencing the speed log measurements, Litton (1998):

Water clarity	Measurement of the speed through water depends on acoustic reflection from solid particles in the water such as microorganisms or suspended dirt. In extremely clear water the quantity of scatters may be insufficient for adequate signal return.
Aeration	Aerated water under the transducer may reflect sound energy which could erroneously be interpreted as sea bottom returns. Sailing in heavy weather may be the source of this effect and so could non-laminar flow around the transducer. By placing the transducer near the bow the effect of non-laminar flow is reduced considerably.
Ship’s trim and list	Changes in the trim (affects fore/aft speed) and list (affects transverse speed) of the ship will affect the measured speed. (Example: 5° trim change gives 0.4% speed change, (Litton (1998)).

Current profile	Speed through water is measured relative to a water layer beneath the ship (> 3m). Sailing in strong tides and current, the direction and magnitude of the surface current can be different from the measured layer, which may lead to errors in the measured speed.
Eddy currents	Sailing in eddies in boundaries of ocean currents where the flow can be opposite or normal to the direction of the primary current and will affect the speed measurement.
Sea state	Following seas result in a variable change in the vessel's speed. This produces a fluctuation in the measured speed.
Fouling of sensor	To the author's knowledge, no effect of fouling of the sensor has affected the speed measurements.

For an analysis of the relation between speed over ground and log speed, see the section "GPS".

6.3.2 **Echo Sounder**

Two sensors are installed on the ship – one in the forward section and one approx. below the accommodation. The frequency ranges for the sensor are in the interval from 28 to 210 kHz and the measuring accuracy is in the order of 2.5% of the measured depth, Litton (1998).

Environmental factors which may influence the measurements:

Sea state	Violent pitching in bad weather.
Sea water temperature	Rising cold water in several sea areas. Hot water discharges from power plants.
Noise	From bow thrusters, main engine vibrations and propeller running reversely.

The echo sounder is used in confined waters for navigational purposes, for which the echo sounder frequency is set to 50 kHz. At this frequency the sea bed detection level is around 90-150 m depending on sea water salinity and temperature. Therefore, no water depths are detected above this level.

6.3.3 **RPM and Torque Meter**

Propeller torque is most commonly measured by strain gauge techniques. The strain gauges are placed on the propeller shaft and measure the shaft elongation due to forces and moments. The deformations are transferred into voltages which determine the strain on the shaft. The typical torque measurements on a propeller shaft are in the order of 330 micro strains and the strain gauges are able to detect changes in the order of 1.5 micro strains, Wärtsila (2009).

The Maihak torque meter is measuring torque by strings (strain gauges) and RPM by laser, SICK/Maihak (2010). Shaft rings are mounted and they are placed as close as possible to the main engine. The measuring accuracy is in the order of 0.5 % and the update period of the measurements can be varied. The RPM / Torque meter is calibrated at installation and depending on manufacture and type, various calibration intervals and methods are suggested.

The torque meter and RPM measurements are used to find the shaft power.

6.3.4 **Shaft Motor**

The shaft motor is an electric motor delivering power to the shaft. The specific motor is in the 6 MW power range and the power to the shaft is delivered in the following speed range, Siemens (2000):

34 - 85 rpm with 2.3 MW linear up to 6 MW with constant torque

85 - 99 rpm with a constant power of 6 MW

The shaft motor is supplied with electrical power generated from the ship's waste heat recovery system, which has an optimal working function when the ship is operating at a high engine load. This operating condition is seldom the case in 2010, which has resulted in little use during the year, Figure 39.

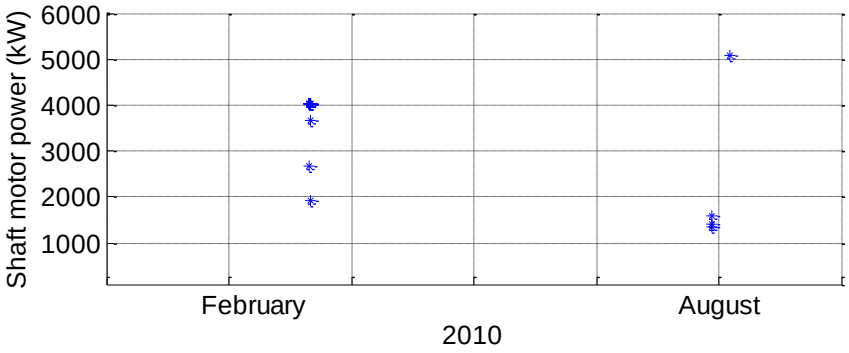

Figure 39 Shaft motor operation incidents 2010.

6.3.5 **Thrust Meter**

If thrust were to be measured by strain gauges the thrust measurements would be in the order of 35 micro strains which would lead to a far too large inaccuracy and therefore alternative methods are to be used. High definition sensors are therefore developed and used in the thrust meter.

The thrust meter measures the RPM, torque and thrust on the shaft, Figure 40. The measuring accuracy is in the range of 0.1 % and the update period of measurements can be varied, TxMarine (2010).

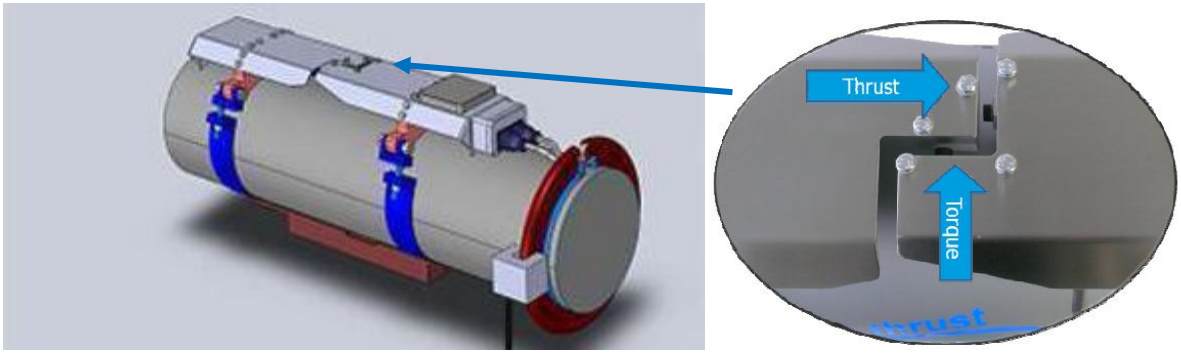

Figure 40 EVOThrust installation.

There have been some problems with the installation on board m/v "Clementine Maersk". The intention with the installation is to separate the propeller fouling from the hull fouling. By measuring thrust and torque it is possible to indicate the propeller efficiency

$$\eta_0 = \frac{U_S(1-w)T}{Q\omega} \tag{67}$$

where T is the measured thrust, Q is the measured torque, w is the wake fraction and U_S is the ship's logged speed.

An example of data from the thrust/torque meter, Figure 41.

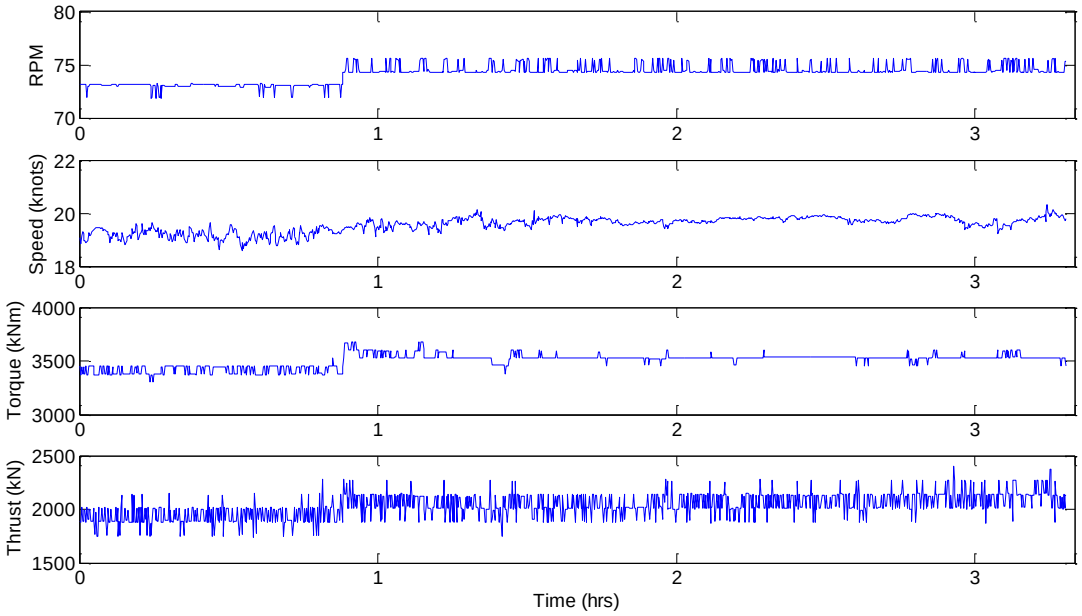

Figure 41 Thrust/ torque meter data

Data from Figure 41 is then used in finding the actual propeller efficiency and to compare this with the model propeller efficiency. An example is shown on Figure 42.The installation has shown some instability in function and therefore it has not yet been able to produce any long term analysis of η_0.

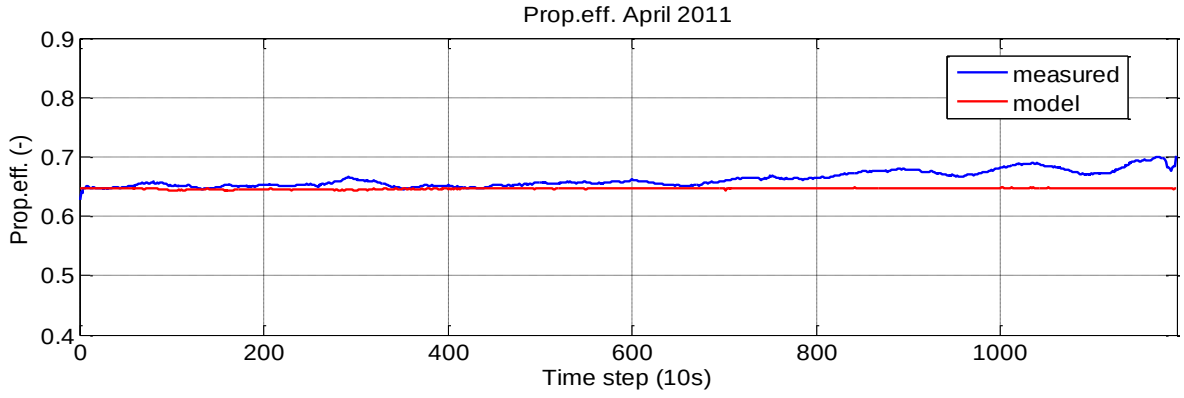

Figure 42 Propeller efficiency comparison

6.3.6 **Rudder Indicator**

The rudder indicator measures the rudder angle continuously and the measuring accuracy in the range of +/- 0.5° at angles near midships and +/- 1.5° at hard over rudder, Sperry (1995).The rudder movements are shown under operating conditions (ME Power pct. > 30%), Figure 43.

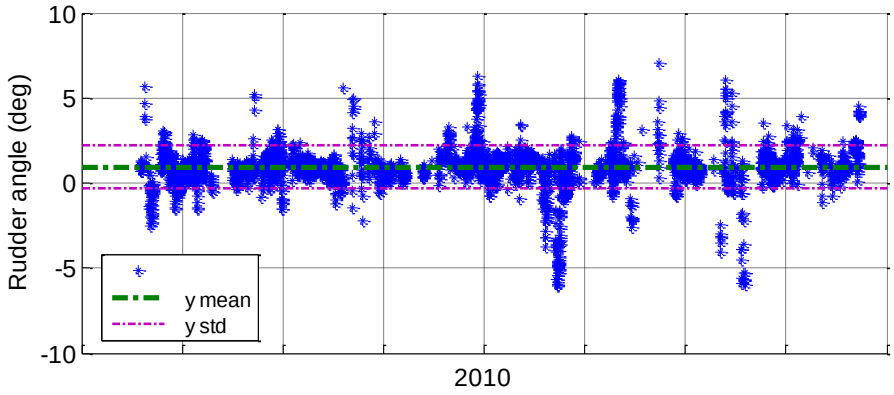

Figure 43 Rudder angles 2010.

μ	σ
0.9475°	1.244°

Table 8 μ and σ for rudder angles

The rudder seems to have a permanent offset during service, Table 8. Reasons for this could be:

- An index error in the rudder angle measurement device.
- A permanent rudder angle counteracting the turning effect of the right-hand propeller.
- A permanent yawing effect induced by the ship's hull or by the wind effect on the superstructure and container cargo during sailing.

6.3.7 **Stabiliser Fins**

The stabiliser fins counteract the roll movements of the ship when sailing. They are fitted on both sides of the ship at the turn of the bilge approx. 3.5 m above the keel and at the aft end of hold no. 15 (m/v "Clementine Maersk"). They are mounted at an angle of 25° with horizontal and when not

in use, they are retracted into the ship's hull. In use, the angle of attack of the fins is varied and this variation is measured continuously.

The fin stabilisers are not often used. During 2010, there were only four incidents where the stabilisers were used, Figure 44.

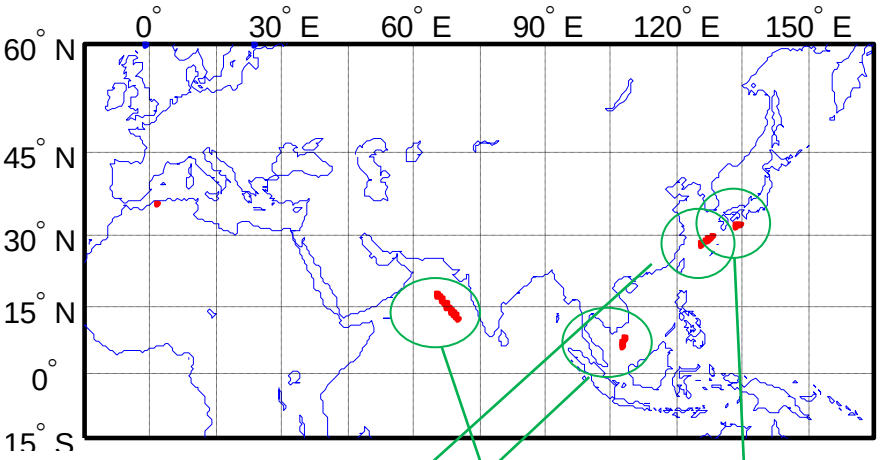

Figure 44 Map with stabiliser incidents 2010.

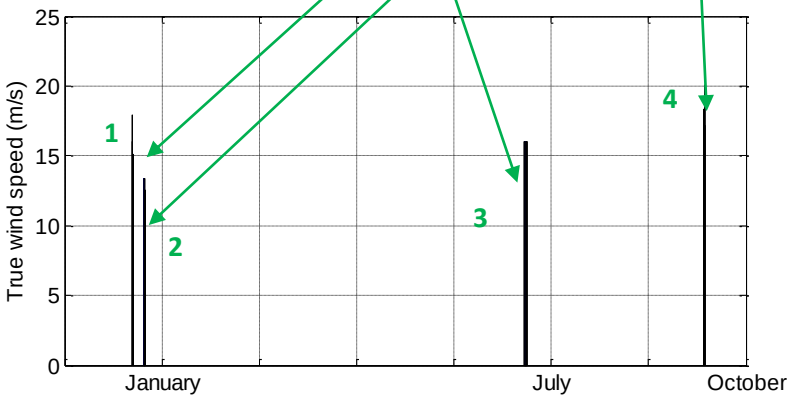

Figure 45 True wind speed.

In the four incidents, the ship is experiencing hard weather, true wind speeds over 13 m/s, Figure 45, large bow motions, Figure 46 (for cases 3 and 4), which indicates high sea state and probable beam to aft sea direction, Figure 47, which would cause large roll angles.

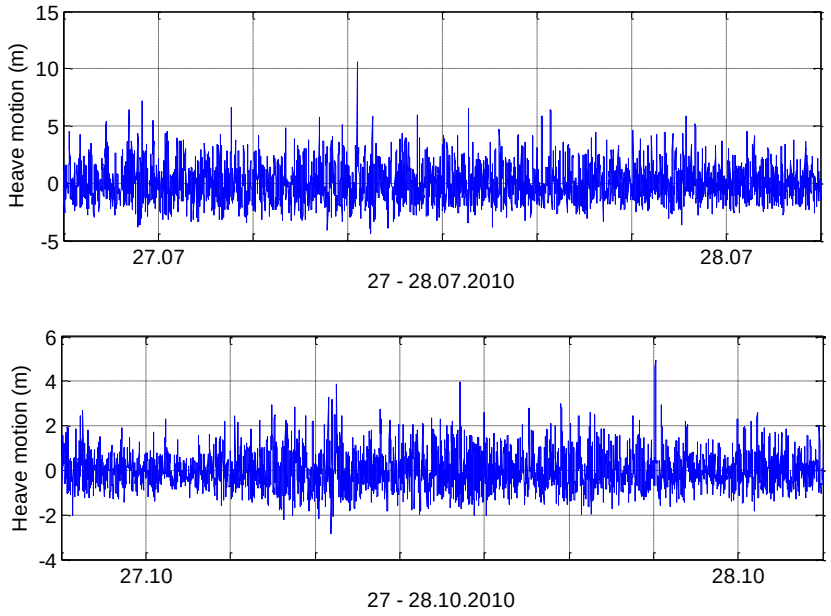

Figure 46 Bow motion examples during stabilizer incidents.

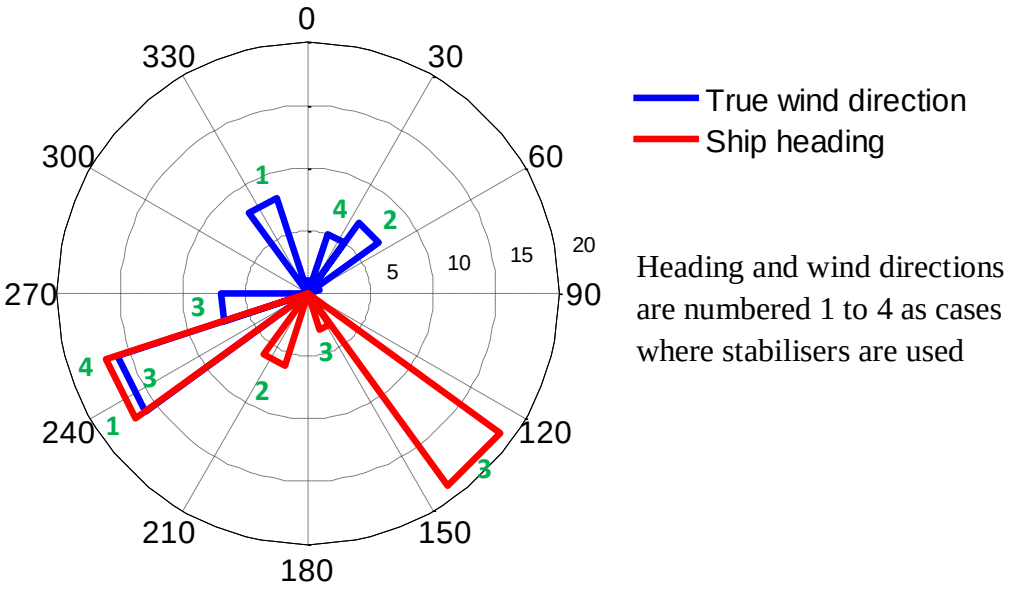

Figure 47 True wind vs. heading.

6.3.8 **Wind Anemometer**

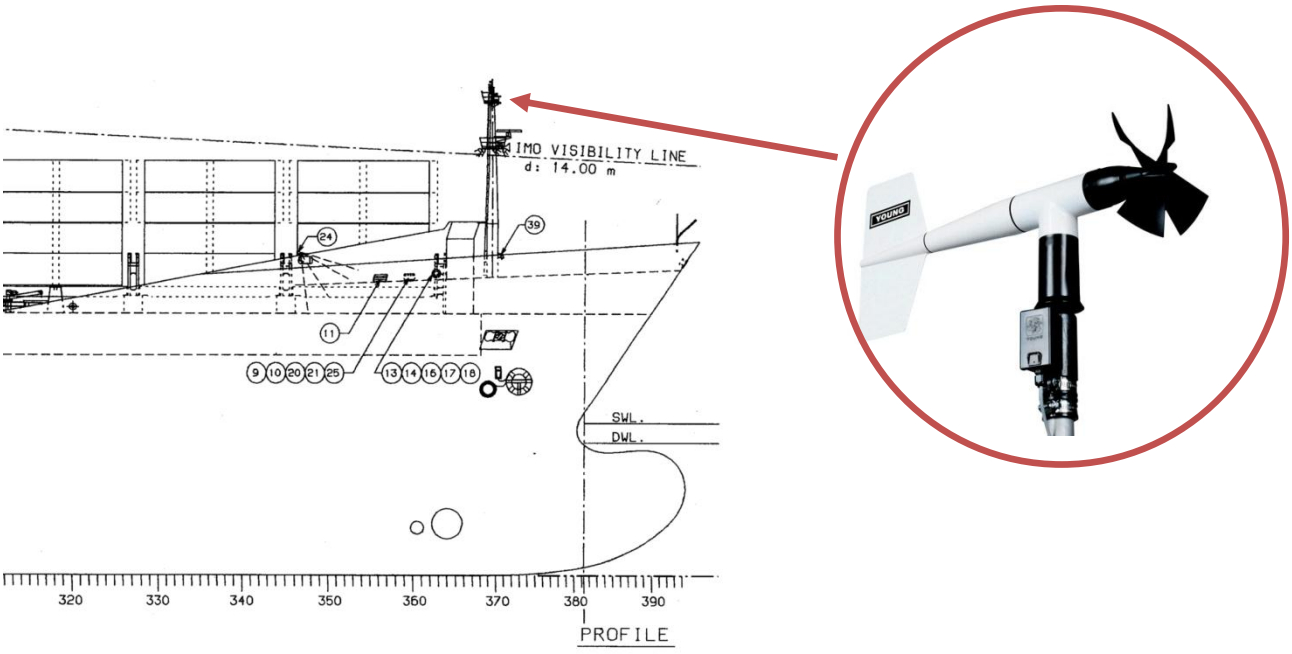

Figure 48 Wind anemometer position on board.

The wind anemometer is a helicoid propeller type with a vane for direction measurement. It is mounted in the forward mast (m/v "Clementine Maersk"), Figure 48, which follows the general rule that anemometers should be placed as high and far ahead as possible in the ship, Yelland et al. (2002), to be free of distortion of the airflow to the anemometer.

The measuring accuracy is in the order of +/- 0.3 m/s or 1% of the wind speed and +/- 3° of the wind direction, Young (2010). The accuracy is given to the range in which the anemometer is calibrated.

The relative wind speeds are as shown in Figure 49 with the predominant distribution in the interval 8 to 16 m/s.

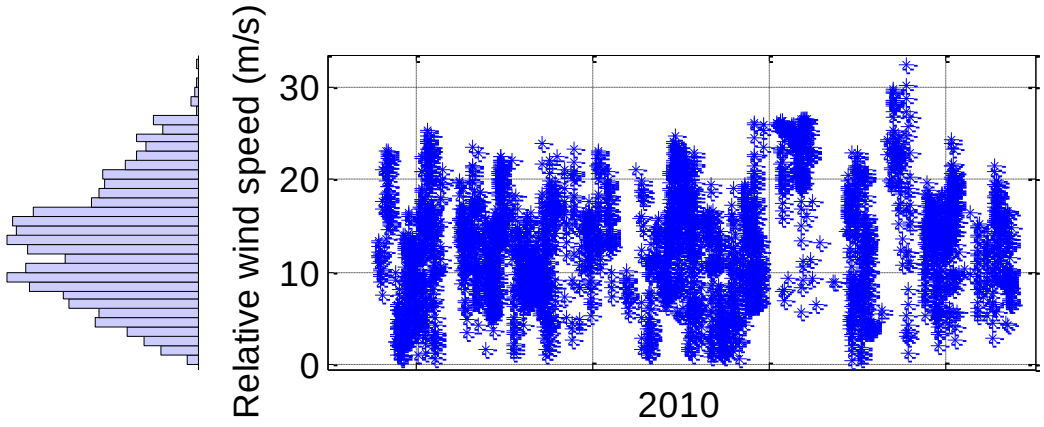

Figure 49 Relative wind speeds 2010.

The relative wind directions are as shown in Figure 50 and predominantly distributed in the area "head winds", which covers 0° to 30° on each side of the bow with a slight overweight of incidents to starboard.

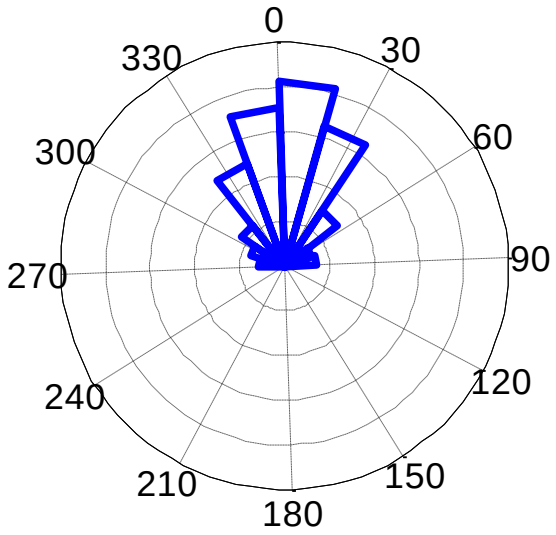

Figure 50 Relative wind directions 2010.

Considering an overweight of head winds and the placement of the sensor in the forward mast, the wind measurements are subject to little distortion of airflow, which should lead to reliable measurements, Yelland et al. (2002).

The anemometer measures the relative wind speed and direction. In the logging system on board the ship, this is converted to a true wind speed and direction.

To convert from true to relative measurements, the following relations are used, Figure 51:

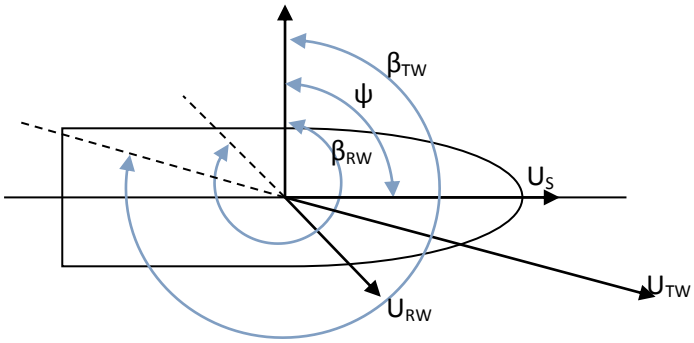

Figure 51 Wind conversion.

$$U_{RW} = \sqrt{[U_{TW}\cos(\beta_{TW} - \psi) + U_S]^2 + [U_{TW}\sin(\beta_{TW} - \psi)]^2} \quad (68)$$

(83)

$$\beta_{RW} = arctan\left[\frac{U_{TW}\sin(\beta_{TW}-\psi)}{U_{TW}\cos(\beta_{TW}-\psi)+U_S}\right] \quad (69)$$

where U_{RW} is the relative wind speed, U_{TW} is the true wind speed, U_S is the ship's speed, β_{RW} is the relative wind direction, β_{TW} is the true wind direction and ψ is the ship's heading.

6.3.9 **GPS**

The GPS gives information about the speed of the ship. The speed is measured above ground whereas the speed measured by the ship's log is speed through water. In cases where the ship is not subject to any set and drift caused by current, the two measured speeds should be alike. The difference in measured speed in 2010 is seen in Figure 52.

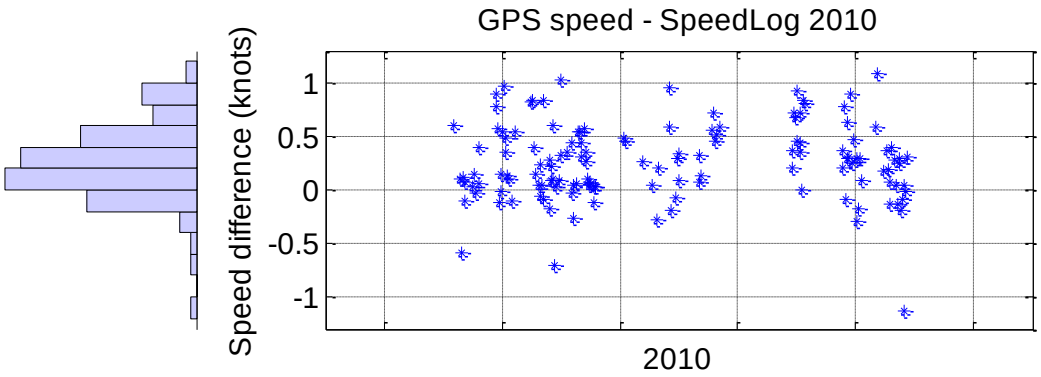

Figure 52 Difference in speed, GPS vs speed log.

μ	σ
0.26	0.35

Table 9 μ and σ for differences in speed

The difference in speed has an overweight of incidents with positive figures which could be caused by

- An overweight of incidents where the ship experiences a positive effect on the ship's speed caused by the current
- A constant offset on the speed log resulting in a lower measured speed

Fouling of the speed log sensor could cause an error or a drift in the measured speed from the speed log. By analysing incidents over one year (2010) in specific areas the comparison of the GPS speed and the speed from the log is used to indicate if there is any drift in the measured speed by the log and to find a bias in the speed measurements from the speed log. The case study areas are chosen to be in the Mediterranean Sea. Current variations are well documented during a year, Mediterranean Pilot, British Admiralty (2010), and the magnitude of current and variation is rather small, e.g. Table 10.

Case Study 1 is from the eastern part of the Mediterranean, Figure 53. In this area the ship's heading is either towards the Suez Canal or towards the Strait of Gibraltar and the set of the dominant current is either against or with the ship's heading.

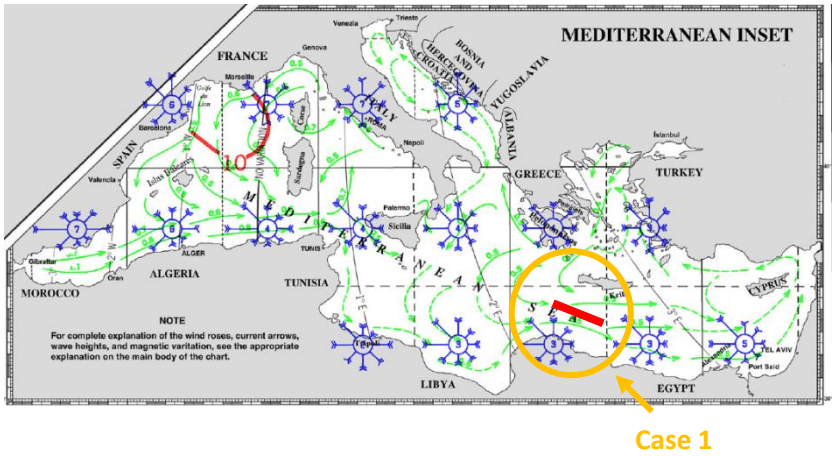

Figure 53 Pilot chart extract.

Jan	Feb	Mar	Apr	May	Jun	Jul	Aug	Sep	Oct	Nov	Dec
0.5	0.5	0.5	0.4	0.4	0.4	0.5	0.4	0.5	0.5	0.4	-weak

Table 10 Average current set in the case study area.

Table 10 shows dominant current variations during 2010 in Case Study area 1, Mediterranean Pilot (2010). The current magnitude is more or less constant except for December where it is weakened.

Figure 54 shows the difference between GPS and speed log measurements in the case study area. Red circles are eastbound voyages and green circles are westbound voyages. The figures are based on mean values for the ship while it was in the area concerned.

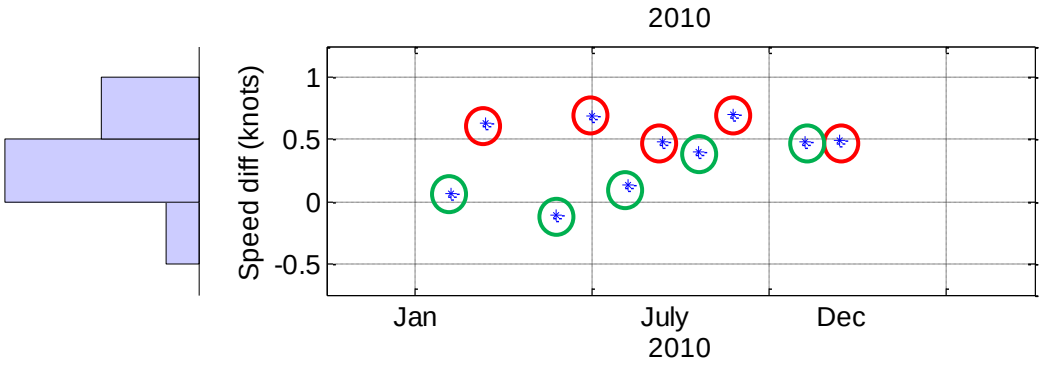

Figure 54 Difference in speed case study 1.

Voyage	μ	σ
Eastbound	0.60	0.11
Westbound	0.19	0.24

Table 11 μ and σ for speed differences Case study 1

The eastbound cases show a more or less constant speed difference. The current is in the order of 0.45 knots (mean current value) in the same direction of the ship's heading. This indicates a bias in speed log measurements in the order of 0.15 knots, which is less than the yearly average as in Table 9.The westbound cases show a constant speed difference in the first half of 2010. Towards the second half of the year, the speed difference is increasing to the eastbound level. This is not expected if the currents are as seen from Table 10. These currents are based on statistical information and cannot always be considered as the actual current. Surface currents are also affected by the wind speed and direction, which could cause the anomalies for the westbound cases.

The Case Study 2 speed analysis is based on data from the area marked in Figure 55.

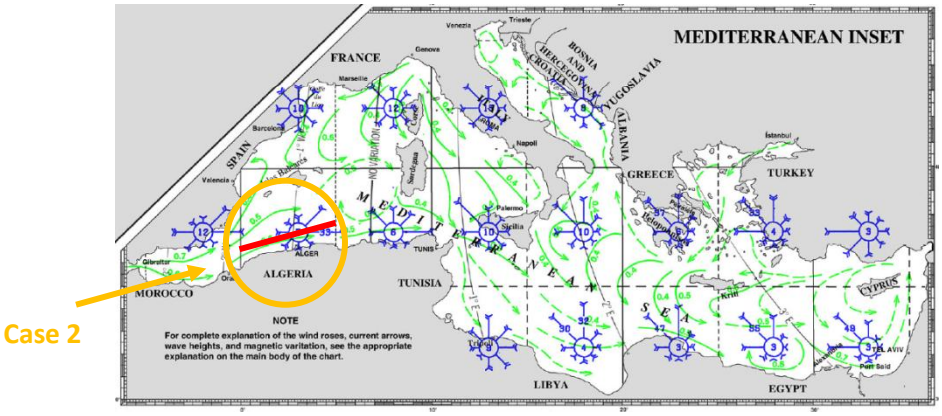

Figure 55 Case study area.

West and eastbound cases are compared for 2010 and results are as shown in Figure 56 and in Table 13.The current speed values for Case Study area 2, Table 12, Mediterranean Pilot (2010):

Jan	Feb	Mar	Apr	May	Jun	Jul	Aug	Sep	Oct	Nov	Dec
0.9	0.8	0.6	0.8	0.6	0.7	0.6	0.6	0.6	0.6	0.7	0.7

Table 12 Average current set in the case study area

The speed difference values from m/v "Clementine Maersk", Table 15:

Jan	Feb	Mar	Apr	May	Jun	Jul	Aug	Sep	Oct	Nov	Dec
	1.23			0.7		0.24		0.55			0.94
0.38			-0.16		0.36				0.26	0.12	

Table 13 Speed differences in Case study 2, Red = East bound, Green = West bound

The results are shown in Figure 56 where green dots mark westbound voyages, red dots mark eastbound voyages and blue dots mark current values.

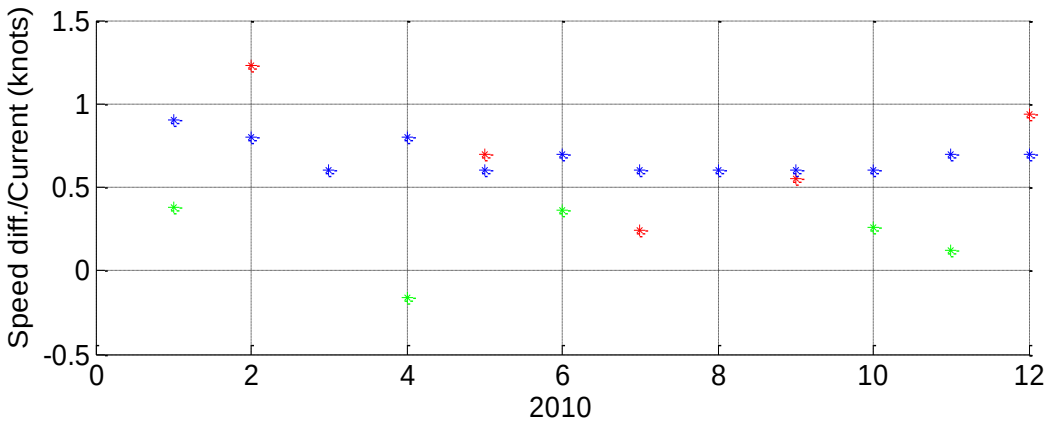

Figure 56 Speed difference and current set in the case study area.

Voyage	μ	σ
Eastbound	0.73	0.37
Westbound	0.19	0.22

Table 14 μ and σ for speed differences Case study 2

The bias in the speed log measurements are less than 0.1 knots with regards to the east bound values. The westbound values are more scattered (as in Case 1). The results of the two case studies can only indicate the bias in the measurements as the ship values are compared to statistical values for the areas. The local variation in currents may be large, see for example Figure 57 for Case Study area 2.

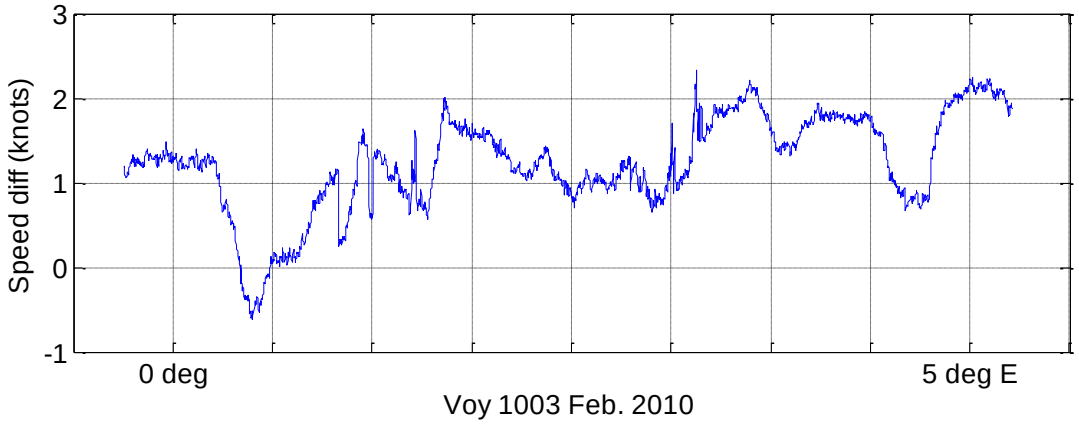

Figure 57 Speed difference, Voyage 1003.

μ	σ
1.23	0.57

Table 15 μ and σ for speed differences Voyage 1003

The two case studies indicate no drift in the speed log measurements. The speed log values are therefore considered to be accurate as regards estimation of a trend in the performance for the ship.

6.3.10 **Air Temperature and Pressure**

The air temperature is measured by a thermometer and the air pressure is measured by a barometer, both placed outside on the aft part of the navigation bridge. The temperature changes during day and night, during change of the seasons and during passage of areas with different climates. The air pressure changes with temperature and with various weather conditions. An example of daily changes in temperature/pressure is seen in Figure 58.

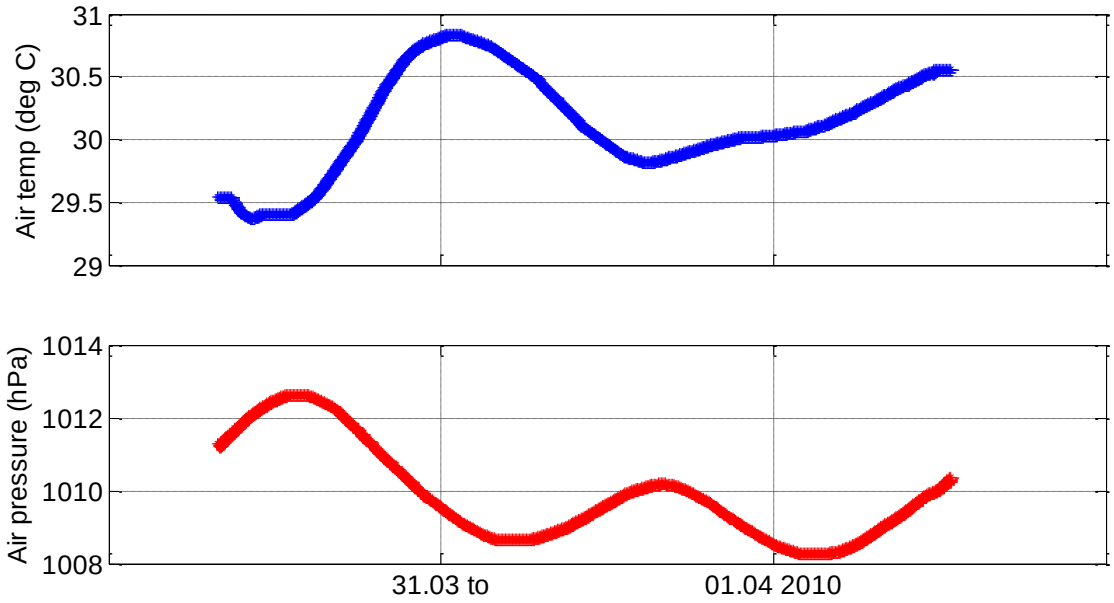

Figure 58 Air temperature and pressure.

Temperature/pressure measurements are not corrected for height variations.

6.3.11 **Gyrocompass**

The gyrocompass measures the ship's heading with reference to true north. The heading is used to calculate true wind speed and directions based on relative measurements from the wind anemometer in the foremast.

The compass gets its input from the speed log (for correction of speed error) and the GPS (for correction of latitude error).

The compass is connected to the autopilot which steers the ship when it is not in manoeuvring conditions. The autopilot keeps the ship's course as set by the navigator by taking into account environmental disturbances from waves, wind and currents, as well as the ship's sailing conditions such as speed, loading conditions and trim. Rudder commands from the autopilot are partly based on setting applied by the navigator and partly by a mathematical model of the ship programmed in the autopilot. To achieve the most economical steering for the ship it is essential that settings given

to the autopilot are in accordance with weather and load conditions. Examples of rudder movements in rough weather conditions are given in Figure 59.

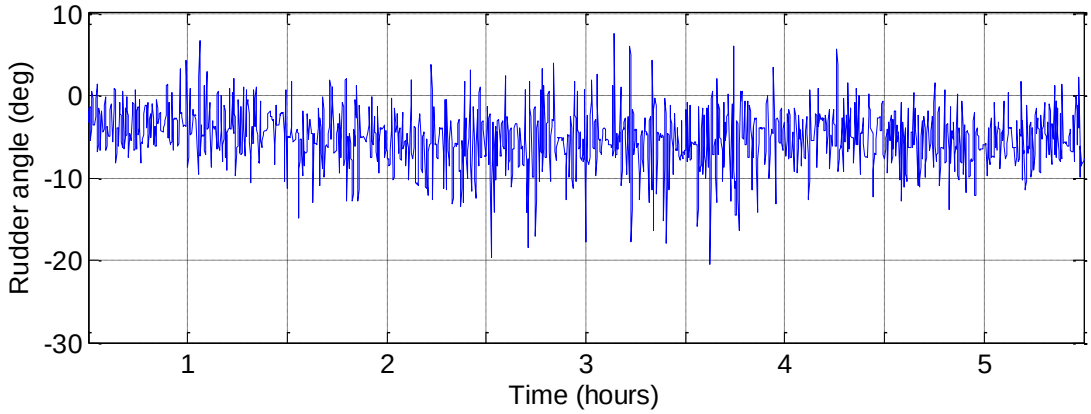

Figure 59 Rudder movements in heavy weather.

Environmental conditions: True wind speed 22 m/s and wind direction N; ship's heading west-southwest and speed 16 knots.

6.3.12 **Motion Sensor**

The bow motions are measured by an accelerometer which is of the low-frequency type and placed in the bow section. It measures the vertical acceleration and velocity is calculated from acceleration by integration. The vertical motion is found from velocity by a second integration.

The logging and the calculations are performed continuously by the software connected to the automation system. In order to compensate for low frequency drift, two first order filters calculates and subtracts the mean value continuously. The best compensation was found with filter constants at 24 seconds and 60 seconds.

The data from the accelerometer is shown in Figure 60, a case study where the ship is sailing from open sea into calm water. There is very little motion in the bow section when entering calm waters, which affects the encounter period values, Figure 61.

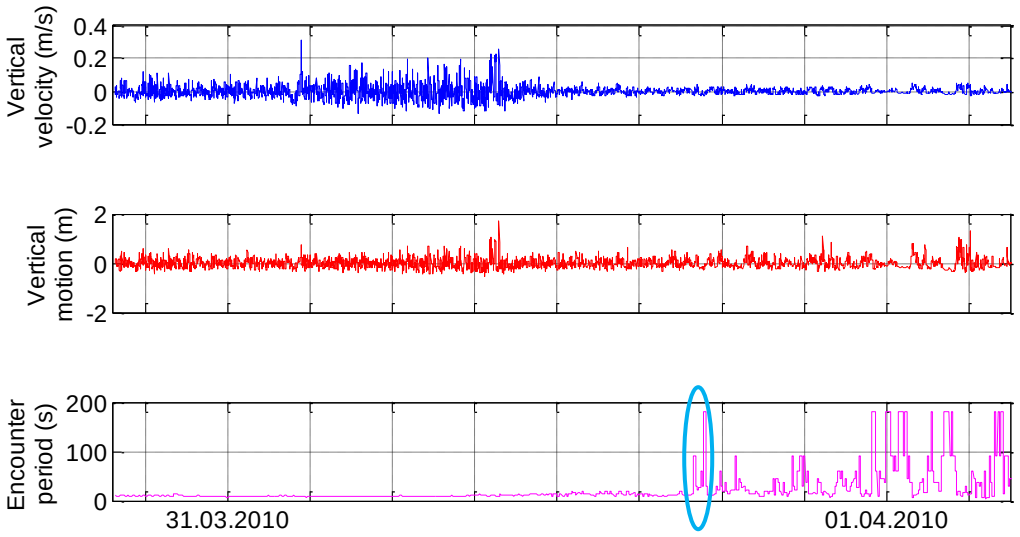

Figure 60 Accelerometer data.

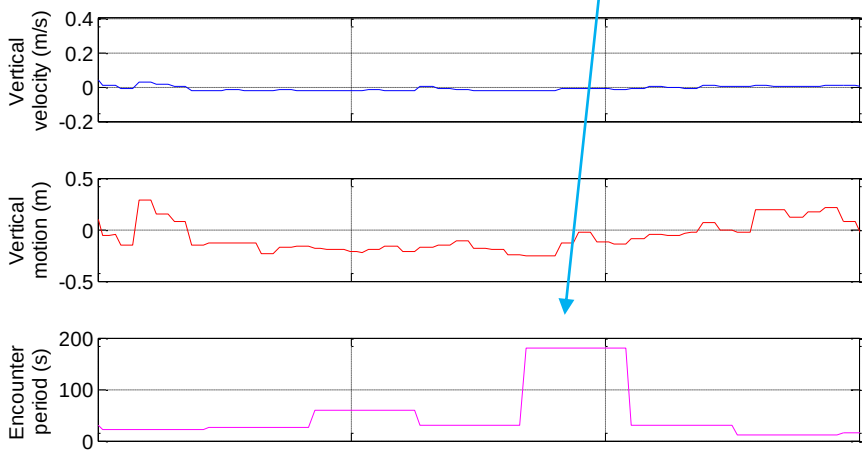

Figure 61 Accelerometer data close-up.

The encounter period T_e is found from the vertical motion as specified in Figure 62.

The measured T_e is defined as the time in between two troughs and in the special case where the ship is entering calm waters and there is little bow movement, the values of T_e are unreasonably high. This is caused by the sampling period of the signals which is 10 seconds for this ship. In order to capture the motions correctly the sampling period is normally considered to have a value as low as 0.2 seconds (Marin 2011).

The off values of the T_e affects the wave height calculations as specified in Section 9.2.

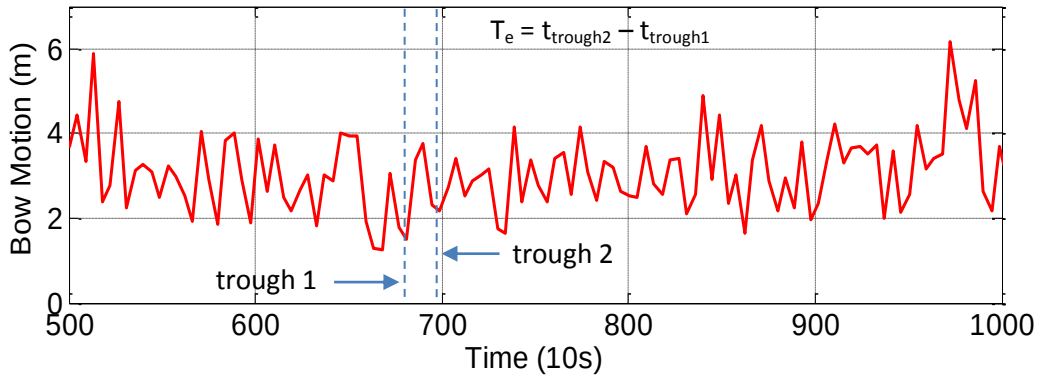

Figure 62 Estimating T_e from bow motions

6.3.13 **Sea Water Temperature**

The sea water temperature is measured at the sea chest suction on the starboard side. The water temperature at this level more or less follows the air temperature, except on occasions at high latitudes in the winter period where cold winds have not affected the sea. Figure 63 shows sea temperature vs. air temperature, except at low temperatures and at sea temperatures around 20° C, where colder winds do not affect the sea temperature.

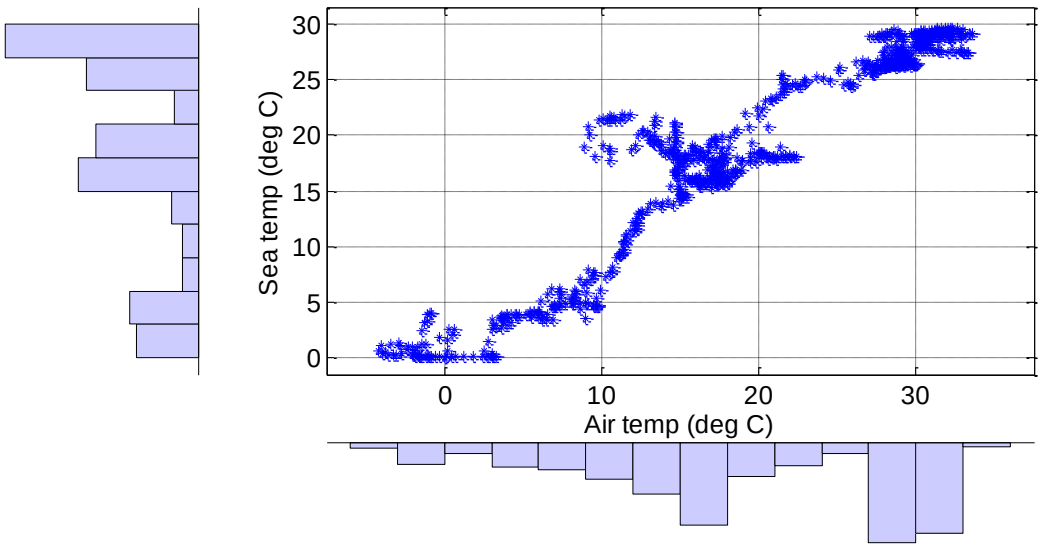

Figure 63 Sea water temperature vs. air temperature.

6.3.14 **Draught**

Draught information is given as manual input. At departure from port the draught forward and aft is taken from draught marks on the side of the ship. During sailing the draught information is updated daily and updates are based on daily consumption of fuel, oil and water.

7 Data Logging

The logged data from the sensors on board the ship is picked up by software designed for the purpose. The ship will normally be equipped with an automation system which is used to monitor all input from sensors on the ship during operation. The data logging software is connected to the automation systems and will pick up the relevant data for the performance system. The data is logged on disks and sent to shore for analysis. To develop the system further to an auto logging system, the logged data can be accessed on board by an online performance system or from shore via a satellite link. The data can be stored in a database on board. By request from the user selected data can be withdrawn from the system for analysis or exported to a performance reporting tool. An overview of data logged to the performance system is given in Table 16:

Conditions	**Logged data**	
Loading conditions	Draught – trim Loading – wind area	Position of point of gravity
Operational conditions	Heading Speed through water (speed log) Speed over ground (GPS) Rudder angle Stabilisers in/out Bow vertical movements	Engine shaft torque Engine shaft trust Engine RPM ME fuel consumption ME power Shaft engine power Position – Latitude/longitude
Environmental conditions	Wind speed and direction Wave height and direction Water depth Sea water temp	Sea water density Air temperature Air pressure

Table 16 Performance parameters.

Settings up a data acquisition system on board, a number of concerns have to be dealt with. A flow diagram as in Figure 64 can be established as an initial work flow in handling the data.

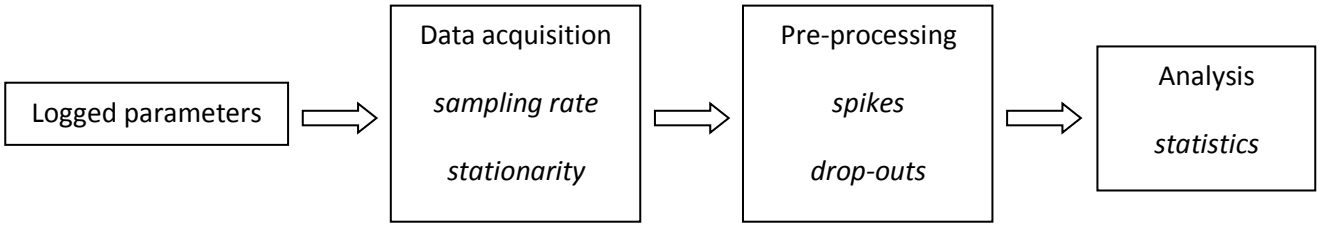

Figure 64 Data handling steps.

7.1 Data Acquisition

7.1.1 **Sampling Rate**

The data is sampled at an interval given by the software system. According to the Nyquist sampling theorem, Jerri (1977), if, to retain the information that a continuous signal contains, the sampling rate must be greater than twice the highest frequency component in the original signal to avoid frequency aliasing (= confusion between low- and high-frequency components in the original data), the Nyquist frequency is half of the sampling rate of the discrete time series. Frequency aliasing can be removed by introducing a low-pass bandwidth filter. At least two sample values per cycle are required to define the highest frequency in the signal. If the sampling rate is larger than the pulse period of the signal there is a risk of losing information about the frequency of the signal.

When determining the sample rate it is therefore necessary to have information about expected frequencies in the measured data, e.g. expected bow motion measured by an accelerometer or expected cycles from the ship's rudder.

An example of movements from a ship's rudder is as follows: The m/v "Tor Magnolia's" rudder movements – resistance due to movements of rudder – comparison between 1 second updates and 10 seconds updates, Figure 65.

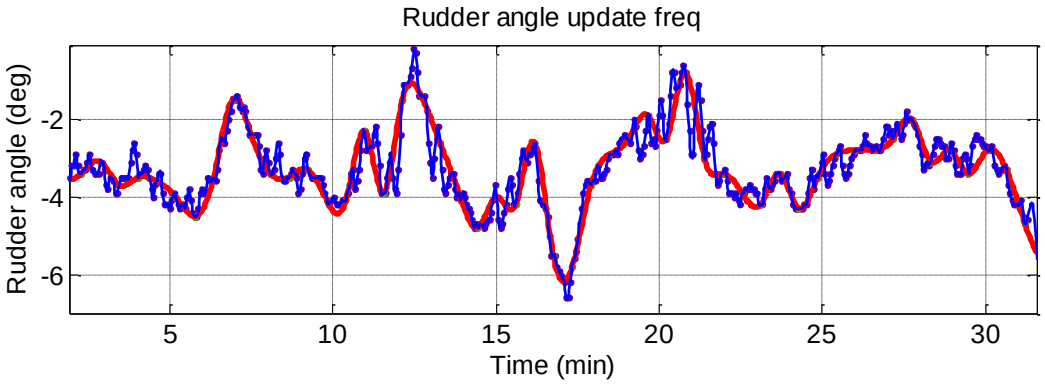

Figure 65 Rudder movements over 30 min interval.

Blue line Cubic spline interpolant of rudder values updated at a freq of 1 Hz

Red line Cubic spline interpolant of rudder values updated at a freq of 0.1 Hz

Not all peaks are captured by the 0.1 Hz signal and the rudder cycling frequencies are different as well. The interpolant values of the rudder movements are extracted and applied to a rudder of the same dimensions as the one on m/v "Clementine Maersk" and added resistance due to rudder movements is calculated, Table 17.

Update frequency [Hz]	Average rudder resistance over logging period [kN]
1	19.2
0.1	19.4

Table 17 Rudder resistance.

By using the larger sampling period, the full dynamics of the rudder movements is not captured, which will lead to a difference in rudder movement induced resistance. The difference is negligent in the previous mentioned example and thus to identify the resistance and to implement a rudder resistance model as described in the "Rudder element" section, it is considered sufficient with a 10 seconds update on the rudder movements.

With reference to case studies for the m/v "Clementine Maersk", the logging period of all parameters is per default set to 10 seconds.

7.1.2 **Stationary Data**

When measuring and analysing the data it is desirable that the data has statistical properties that are invariant over time, i.e. stationary data. In practice, this is not the case and the data will often be non-stationary seen over the whole period, e.g. the ship will vary its RPM and speed as it will change course depending on the area of operation. It is possible though to find cases where the ship is in a steady state condition, i.e. conditions where mean and variance are more or less constant. The conditions can be processed in the model and thus a piecewise analysis of the performance of the ship can be made.

7.2 Preprocessing

7.2.1 **Synchronisation of Parameters**

More than 20 parameters are logged through the ship's automation system. The timestamp for the logging has to be the same for each parameter in order to have the data logged at the same time. The logging interval has also to be consistent or synchronised to the same level, e.g. 10 seconds as in the m/v "Clementine Maersk" case. In this case study it has been shown that over time there has been some drift in time due to drift in the time interval for some of the parameters. The drift in time interval is only a few seconds but over time this will lead to larger drift in timestamps. The data format is an Excel sheet with approximately one weeks' data in each sheet. Each parameter has its own individual timestamp. To neutralise drift and to achieve consistent logging intervals the following steps are taken:

- Consolidate identical start time for all parameters
- Identify timestamp interval by choosing one timestamp as default
- Run routine with synchronisation of parameters to default timestamp. In cases where values are off sync, a linear interpolation is performed between data points.

The routine will ensure that all parameters now have the same timestamp and the same logging interval.

7.2.2 **Spikes in Data**

If the ship's performance has to be simulated under all conditions it is necessary to find a method for running the series from point A to point B including series with variations over time. It is needed to find a way to handle data which varies, e.g. it is not the intention to treat a change in RPM as a spike in the data. To handle the data as "steady state" in a time frame t it will be necessary to investigate the assumed variation of the ship's movements, e.g. if the RPM are changed, which response time of the vessel is then the result. As an example, Case 1 where an engine order from 92 to 97 RPM is shown, Figure 66.

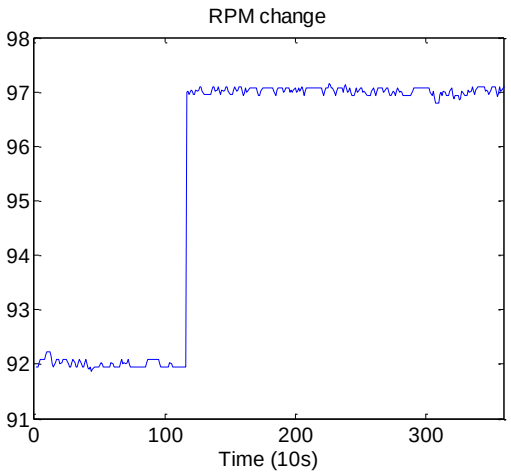

Figure 66 RPM change.

Another example, Case 2 has the same increase in RPM, this time only momentarily. After another 10 seconds the RPM value is back to the same level as before, Figure 67.

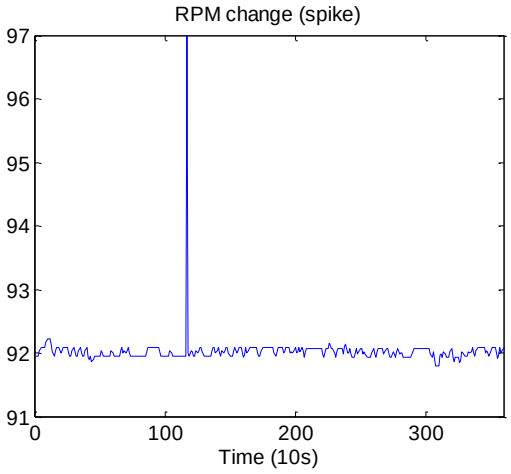

Figure 67 Momentary RPM change.

This can be treated as a spike in data, which will create distortion in the resulting output from the model. It is the intention to create a function to detect and remove disturbances in signals in order to create a consistent output from the system.

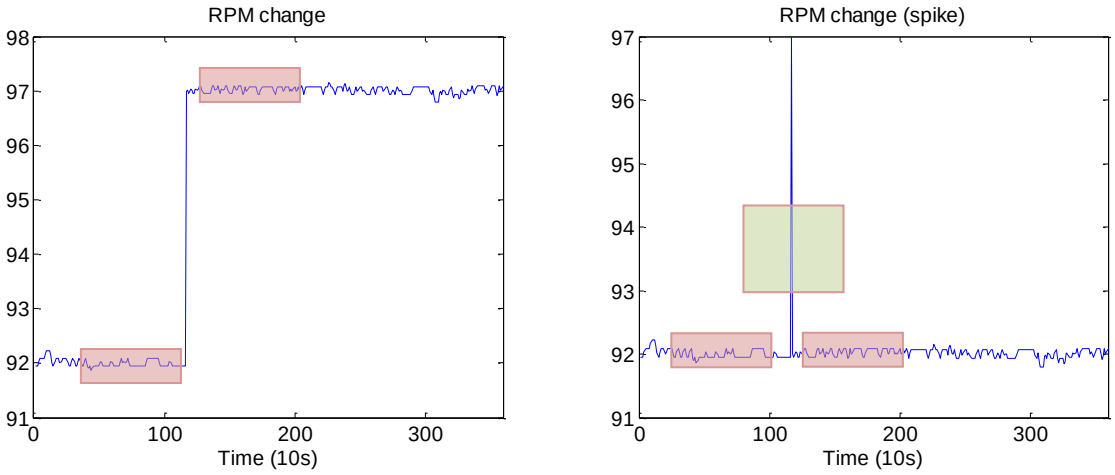

Figure 68 RPM change – constant and momentary.

Case 1 is characterised by a change in mean of data before and after the RPM change.

Case 2 is characterised by a change in variance of data.

7.2.2.1 Mean and variance

When setting up rules for removal of spikes it will be necessary to evaluate the mean and variance in a certain time frame. If a spike is detected, it can be replaced by an interpolated value. To identify a spike, a threshold value and a window size have to be identified for each parameter.

A detection rule can be set up based on evaluating the mean and the standard deviation in a defined time frame. Given X_i as an instant value at time i, a running mean μ_{rt} in a time frame dt combined with a running standard deviation σ_{rt} in the same time frame is used to identify the cases. The trigger value is as defined in the flow diagram in Figure 69.

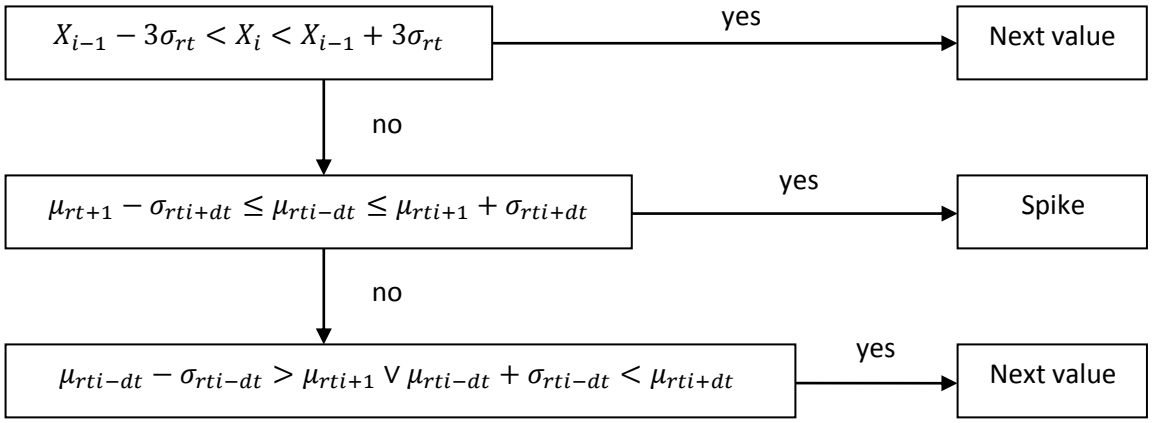

Figure 69 Flow diagram identifying spikes and voluntary changes.

The value at time *i* is compared to values at time *i-1*. If the value is inside the boundaries (3 σ_{rt}) then the next value is examined. If it is not, then the running mean of the previous values (in time frame *dt*) is compared to the running mean of the next values (in time frame *dt*). If the mean is inside the boundaries then the value is a spike, if it is outside the boundaries (over or under) then it is a voluntary change. Spike values are replaced by linear interpolated as shown in flow diagram (page 83) for the CUSUM values.

The limit for the allowed variation in the signal is set to $3\sigma_{rt}$. This limit would not under all conditions be sufficient, i.e. in hard weather conditions the variation in e.g. the ship's speed could be more than $3\sigma_{rt}$ without being a faulty signal. In the performance system one of the data filters is True wind speed < 10 m/s, which will allow us to use $3\sigma_{rt}$. The rule can also be used for detection of drop-outs in signals. If the drop-outs are temporary they will be treated as spikes, otherwise they will be treated as voluntary changes. The drop-out will have a zero value, and a rule with regard to the time frame where a zero value is allowed will have to be set up for each parameter.

7.2.2.2 CUSUM function

Another method for detecting changes in a signal is based on change detection algorithms. An expected behaviour of a system is compared to the actual behaviour and a change or a fault is detected by the algorithm. In a noisy system it can be difficult to detect small changes and therefore it can be useful to introduce a statistical test based on the log-likelihood ratio. The test is a

hypothesis test where a probability density function is attached to each hypothesis. The following test is based on a CUSUM test, Gustafsson (2000). A hypothesis test is used to detect a change in either mean or variance of a signal. Two hypotheses recognising:

1. There is no change in signals hypothesis $\mathcal{H}_0$
2. There is a change in signals hypothesis $\mathcal{H}_1$

Each hypothesis is characterised by normal distributed probability density functions (pdf) characterised by

$$p_\mu(z) = \frac{1}{\sqrt{2\pi\sigma}} exp\left(-\frac{(z-\mu)^2}{2\sigma^2}\right) \quad (70)$$

where z is the signal value. For each data sample a pdf for $\mathcal{H}_0$ and $\mathcal{H}_1$ is calculated. The log-likelihood for a change in mean can be expressed as:

$$s(k) = ln\left(\frac{p_{\mu_1}(z_k)}{p_{\mu_0}(z_k)}\right) \quad (71)$$

This function has its maxima in $z_k = \mu_1$, which means that it has its maxima in a specific change in mean. The cumulative sum can be expressed as

$$S(k) = \sum_{i=1}^{k} s(z_i) = \sum_{i=1}^{k} ln\left(\frac{p_{\mu_1}(z_i)}{p_{\mu_0}(z_i)}\right) \quad (72)$$

where index k is the signal at an actual timestamp k. By inserting Eq. 70 in Eq. 72:

$$S(k) = \sum_{i=1}^{k} \frac{\mu_1-\mu_0}{\sigma^2}\left(z_i - \frac{\mu_1+\mu_0}{2}\right) \quad (73)$$

The cumulative sum will decrease when data is closer to hypothesis $\mathcal{H}_0$ and increase when data is closer to hypothesis $\mathcal{H}_1$. An example is the voluntary RPM change, Case 1. The development of the cumulative sum is as in Figure 70.

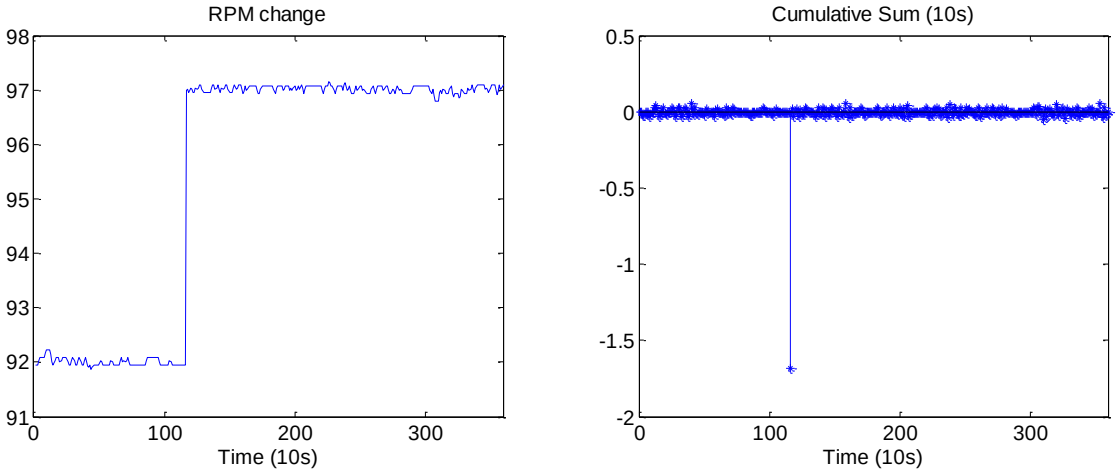

Figure 70 Voluntary change in RPM (left) and corresponding CUSUM values (right).

In order to detect changes as they arise, μ_r is set to a two-step value only. The change in RPM arises at time step 116 and it is detected as a negative value by the CUSUM function as it should be, Figure 70 right.

Another example is Case 2 where there is a sudden change in RPM due to a spike in data. Here the development of the cumulative sum is as in Figure 71.

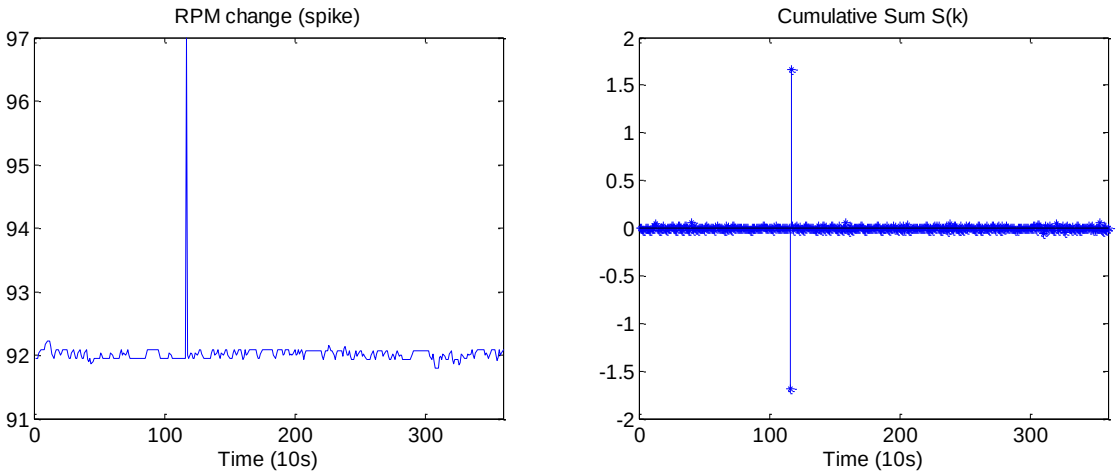

Figure 71 Spike in RPM value (left) with corresponding CUSUM values (right).

The CUSUM function detects the spike first as a negative response (when the RPM value increases) and then as a positive response (when the RPM value decreases). The spike occurs at timestamp 117, which is detected by the CUSUM function. The case study shows that a CUSUM algorithm is capable of detecting both voluntary changes in signal as well as to detect spikes.

The RPM data used in the previous example are compared to a threshold value *h* where an alarm would be triggered as soon as the limit is exceeded. The limit has to be chosen to a level so the detection will not be delayed (too high threshold value) or there will too many false alarms (too low threshold value). The threshold value is traditionally set as a constant value where the level of alarms will depend on fluctuations of the test statistics in the fault free case.

In previous cases the data is sampled under steady state conditions. The CUSUM function will have to work under all conditions and as an example another case study is shown in Figures 72 and 73. The data is sampled under heavy weather conditions and this affects the logged RPM data i.e. heavy scattered data.

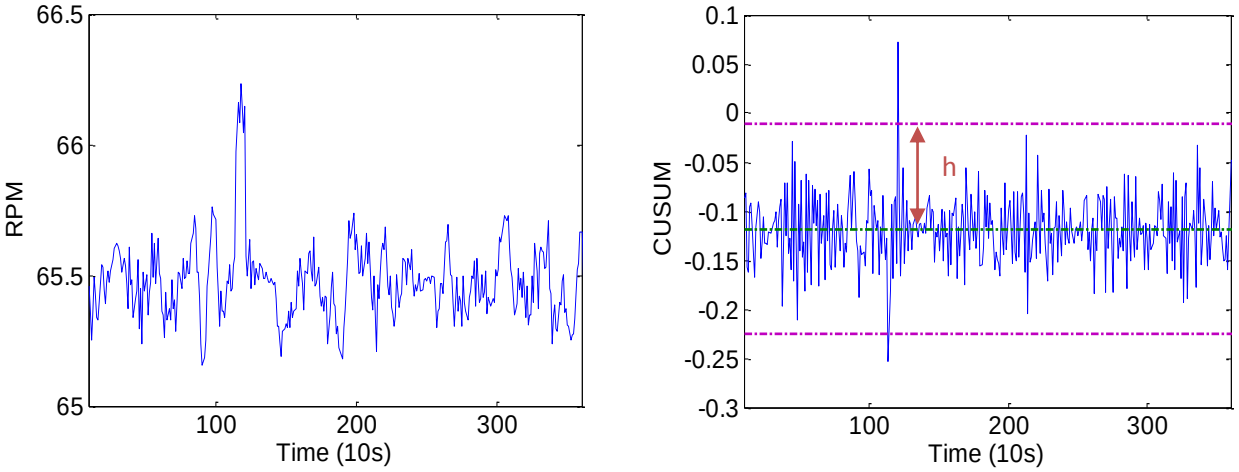

Figure 72 Spike in data (left) and CUSUM with threshold value (right)

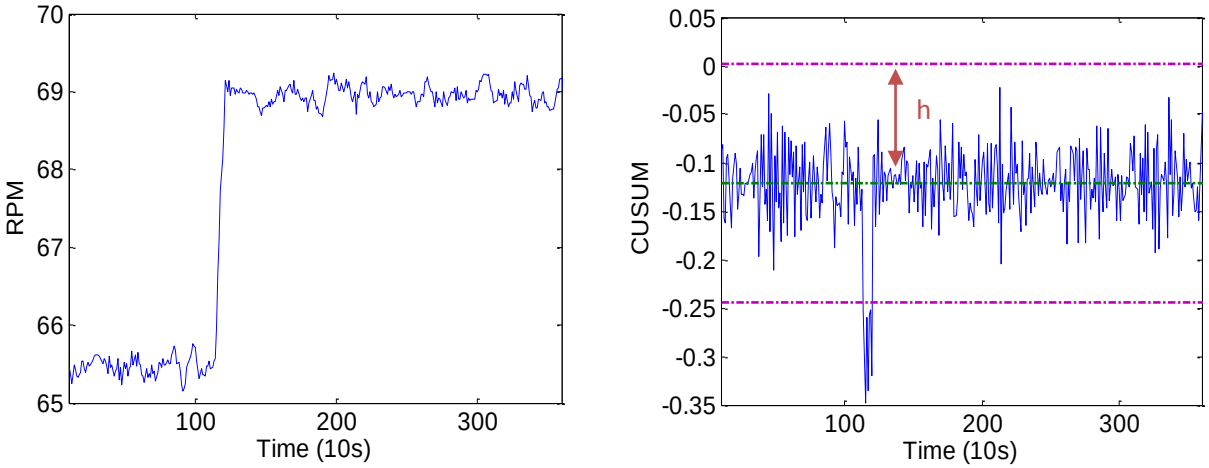

Figure 73 Voluntary change in data (left) and CUSUM with threshold value (right)

The run length in this case is set to 1 hour and the CUSUM function is used on 1 minute averaged data in order to be able still trigger an alarm without being too sensitive to large variations in the data.

The CUSUM mean μ and the alarm limit h are shown on CUSUM plots, Figure 72 and 73 right.

The CUSUM algorithm can now be used to clear signals from noise and spikes:

$$if\ X_{CUSUMis} > \mu_{CUSUM} + h\ \vee X_{CUSUMis} < \mu_{CUSUM} - h$$

$$\Downarrow$$

The index point where the change occurs is found from a function f_{cs} that estimates the slope of the CUSUM

$$if\ f_{CS} < 0, index = find(CUSUM == \min(CUSUM))$$

$$else\ index = find(CUSUM == \max(CUSUM)$$

$$\Downarrow$$

In case of a spike, the CUSUM value is either first negative and following positive or the opposite:

$$X_{CUSUMis} < \mu_{CUSUM} - h\ \wedge X_{CUSUMis+1} > \mu_{CUSUM} + h\ or$$

$$X_{CUSUMis} > \mu_{CUSUM} + h\ \wedge X_{CUSUMis+1} < \mu_{CUSUM} - h$$

$$\Downarrow$$

The CUSUM value at the index point is now substituted by a point found by linear interpolation

$$X_{CUSUMis} = \frac{X_{CUSUMis-1} + X_{CUSUMis+1}}{2}$$

The new index value is now used in the forward calculations. The test cases are shown with RPM data but can be used with other logged data as well.

7.3 Analysis of Data

The data used for the performance analysis in the present work is as previously mentioned with an interval of 10 seconds. It has also been mentioned that this interval is not sufficient to describe the full dynamics of all logged parameters in the system, and it therefore gives a pointwise description of the conditions during sailing. Further the logged data is only used in conditions where the main engine load is larger than 30%. This is so to comply with the ship model, which is not performing well at low speeds and to avoid manoeuvring conditions.

With regard to further analysis of the data, there are analyses in following sections:

- Daily reporting Distribution and correlation of data with performance parameters
- Operational profile Distribution of main operational parameters
- Data logging sensors Correlation of log/GPS speed and correlation of temperatures

With reference to GPS speed, engine load, fuel consumption and engine RPM vs. logged speed the correlation is as in Figure 74.

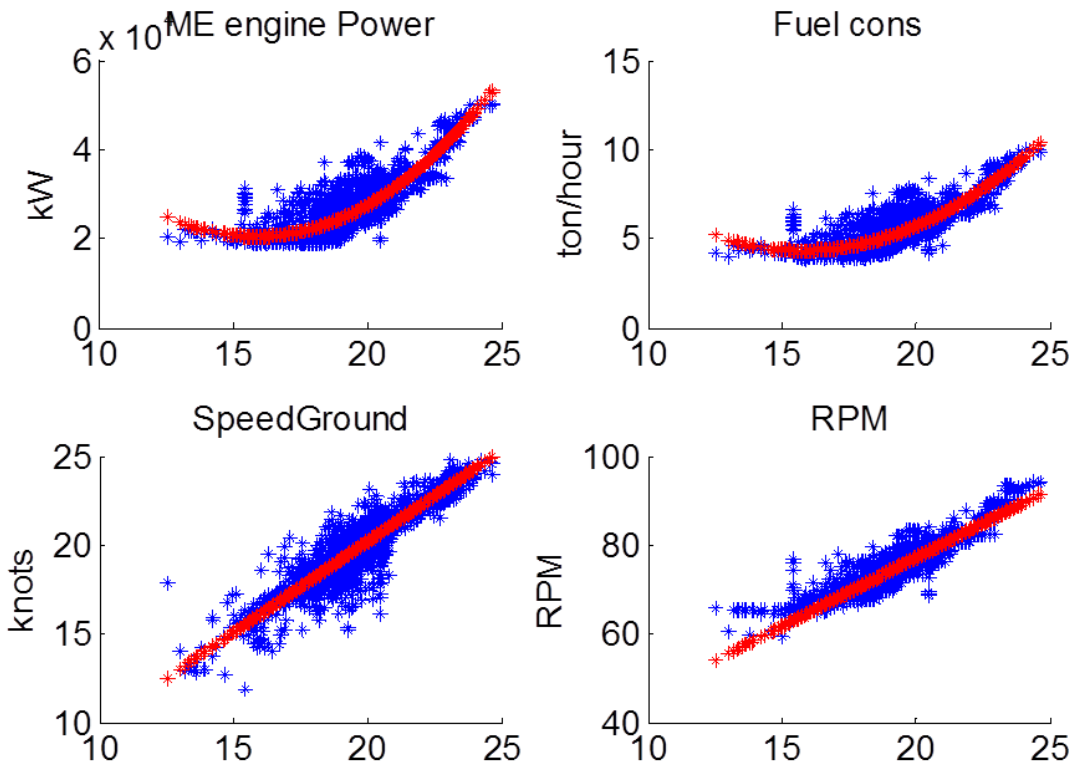

Figure 74 SpeedLog (knots) vs. torque, fuel consumption, SpeedGround and engine RPM.

SpeedLog vs. shaft power follows more or less the relation of an expected polynomial p(x) with a third degree order. SpeedLog vs. fuel consumption follows more or less the relation of an expected polynomial p(x) with a second degree order. SpeedLog vs. SpeedGround and engine RPM follows more or less an expected linear relation. All with the scattered image caused by environmental disturbances.

7.3.1 **Uncertainty and Sensitivity**

With relation to uncertainty in measurements of data it is necessary to analyse each sensor with respect to manufacture and type. The manufacturer of the sensor provides information about the expected accuracy of measurements by the sensor, ref Section 6.3, and this information can be used as an indicator when evaluating the data. Several uncertainty analyses have been published in the literature. With regard to the ITTC Powering Prediction Method an analysis of the uncertainty assessment in performance parameters during sea trials is performed by ITTC (2002) and ITTC (2005_2). Research work performed by Insel (2008) contains full-scale measurements including environmental factors and Marin has analysed data from several ships with regard to uncertainty in a Joint Industry Project, Marin (2008). A number of results from these reports have been available for the author and used in this work. The reports are considered confidential and therefore results are not included in this work.

Several sea trials form the background for an uncertainty analysis in ITTC (2005_2). Every input parameter used in the performance analysis is evaluated on each sea trial. Total bias and precision errors are evaluated and results are as shown on Figure 75.

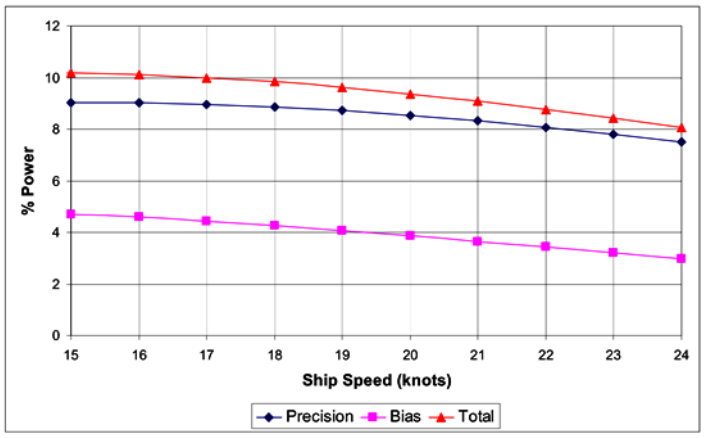

Figure 75 Errors in sea trials (ITTC 2005)

The total errors are in a range from approximately 10% at low speed (15 knots) to approximately 8% at high speed (24 knots). These results are confirmed in Insel (2008) where results show that low speed induces larger sensitivity to parameters than high speed..

The models used in this work are based on towing tank tests and several studies with regards to uncertainty in model–ship correlations and propulsion parameters are summarized in ITTC (2011). Generally it is found that from regression of the model-ship correlation factors obtained, standard deviations of estimated power and propeller revolutions were found to be around 5% and 1.5% respectively, ITTC (2005_2).

Sensitivity analyses with relation to performance parameters (PI) show the relative variation in PI to a change in the given parameter. The various models used in this work are used to show where the model is sensitive to input parameters, ref Section 8 and Section 10. Depending on the performance evaluation method it varies how significant the variation in PI is, e.g. estimation of ship's speed could either be obtained by the ship's log, the DGPS or by the propeller inflow method. The three methods show the largest sensitivity to different parameters, which has to been taken into consideration in the modelling of the ship and thus the choice of performance parameter.

8 Performance Analysis - Daily Reporting

A performance system can be based on daily reporting by the ship's crew (noon data). The intention of the reporting system is that the crew sends in average values of parameters over a certain period, normally 24 hours when the time at sea is of that length. The values are put into the model and the outcome is performance indexes for each day at sea. A similar procedure with average values for each day is now set up with auto logged parameters. A case study for m/v "Clementine Maersk" is described in the following paragraph. The model used is as on Figure 76, for detailed model descriptions, see Section 5.

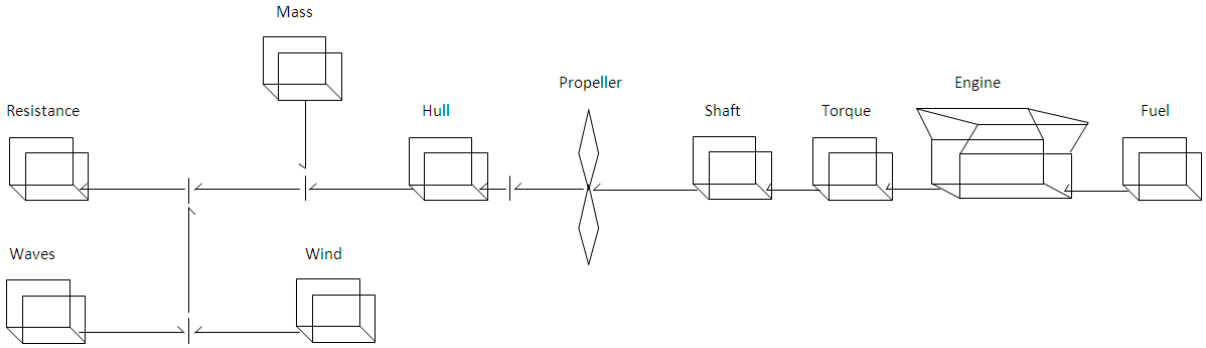

Figure 76 Model for daily reporting values

The data is initially filtered as in Table 18.

Parameter	Filter
ME Power percentage	> 30%
True wind speed	< 10 m/s
Water depth	> 80 m

Table 18 Initial filter values

A set of data from the performance system based on noon-data is now used in the model. The data are logged through 2010 and the filters as described in Table 18 are used on the data. When running the data through the model the results are highly scattered and does not give a reasonable view of

the ship's performance. Outliers are removed from the data by using only the data that are inside +/- 2.7σ of the mean of the data.

Assuming linear regression can be used in estimating the trend of the performance, a set of values describing the goodness of fit are generated for each model. The RMSE values to indicate the scatter in the results and the line slope with 95 % confidence bounds, see Appendix C. The values are used as standards of reference when comparing the performance of the different models, see Section 10. Performance indexes Power Pct, Speed Pct and roughness k_S (as described in Section 4.2) are used in the analysis.

The ship has had a propeller polish after 175 days. The incident is taken in consideration and the performance index plots are split into 2 sections - one before the cleaning and one after. The results are as in Figures 77, 78 and 79.

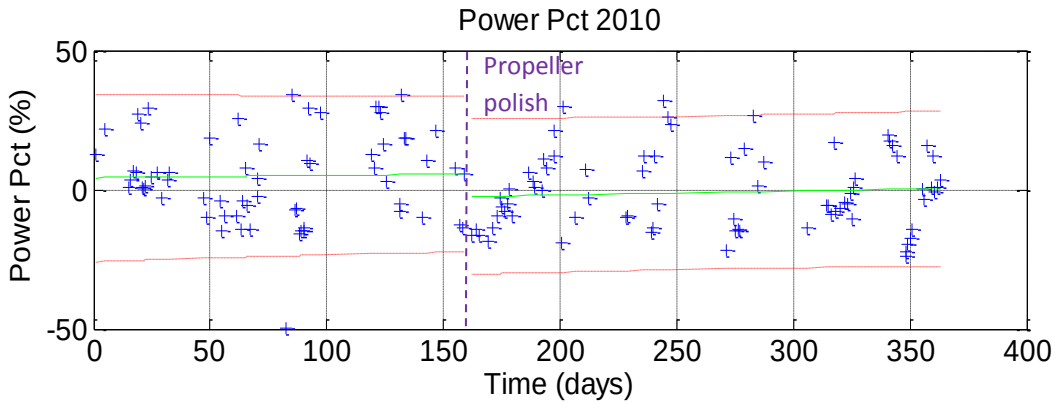

Figure 77 Power Pct vs. time inc. 95% confidence interval

Parameter	Before prop clean	After prop clean
RMSE	16.21	13.68
Line slope with 95% conf.bounds	0.1256 (-0.03998, 0.012911)	0.01421 (-0.03171, 0.06012)

Table 19 Goodness of fit for Power Pct regression

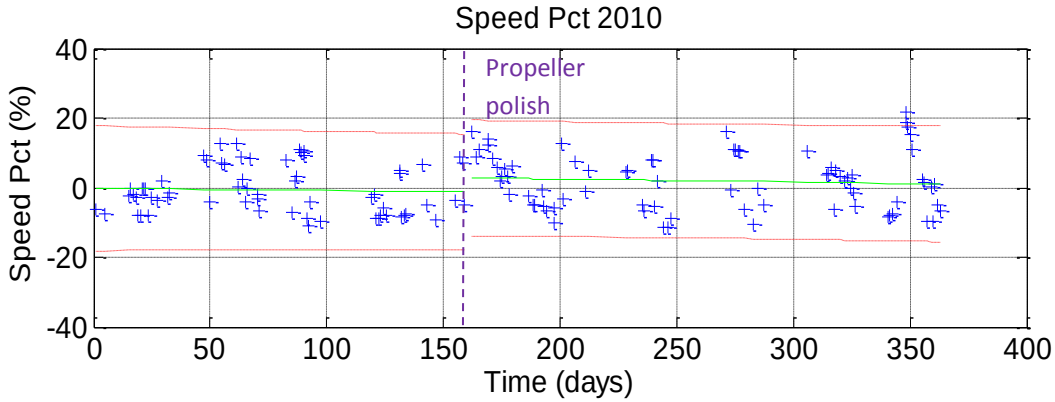

Figure 78 Speed Pct vs. time inc. 95% confidence interval

Parameter	Before prop clean	After prop clean
RMSE	6.763	8.15
Line slope with 95% conf.bounds	-0.006631 (-0.04387, 0.03061)	-0.008625 (-0.03598, 0.01873)

Table 20 Goodness of fit for Speed Pct regression

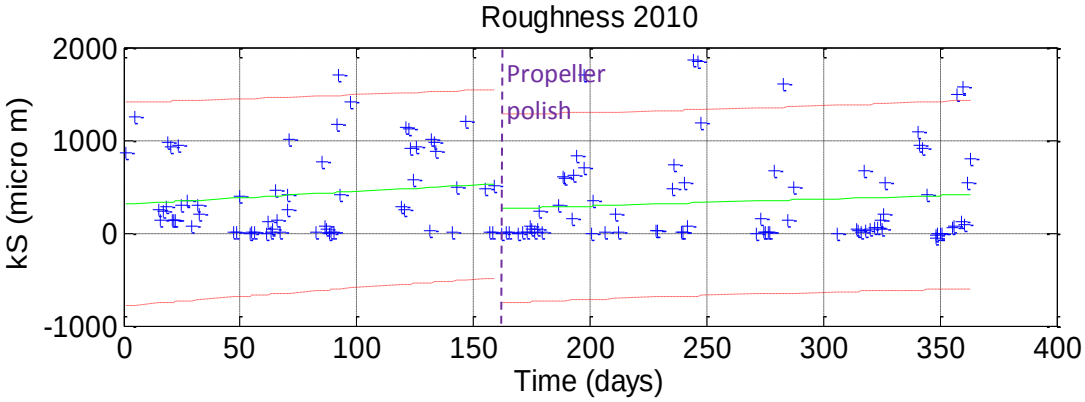

Figure 79 Roughness vs. time inc. 95% confidence interval

Parameter	Before prop clean	After prop clean
RMSE	449	498
Line slope with 95% conf.bounds	1.396 (-1.076, 3.868)	0.7498 (-0.9209, 2.42)

Table 21 Goodness of fit for Roughness regression

The scatter is high and many values are unreasonable high or low for all indexes. The trend in the development of indexes is as expected – slightly rising (Power Pct and k_S) and slightly descending (Speed Pct) before the propeller clean and a shift in indexes after. The results are unreliable in indicating the effect of a propeller polish and the data far too scattered to indicate the development of the ship's performance.

The auto logged data are now used in the same analysis. The input data to the model are averaged values from the available time series and the series are split into daily averages. The time series are of various lengths – from 2 hours to 24 hours depending on number of data points in a 24 hour split period. The variation in data is also different depending on the operational conditions in the 24 hour period. The split time series are now processed in the model. The model generates performance indexes and they are exported to the time series files. The time series files are filtered with respect to outliers in performance indexes. Outliers are caused by errors in data measurements, fall out and spikes in signals and missing data points. Filters are removing faulty signals and averaging for missing data points, for detailed time series analysis, see Section 7.

Average values and standard deviations are generated for each parameter. Average daily values for the performance index Power Pct is shown on Figure 80.

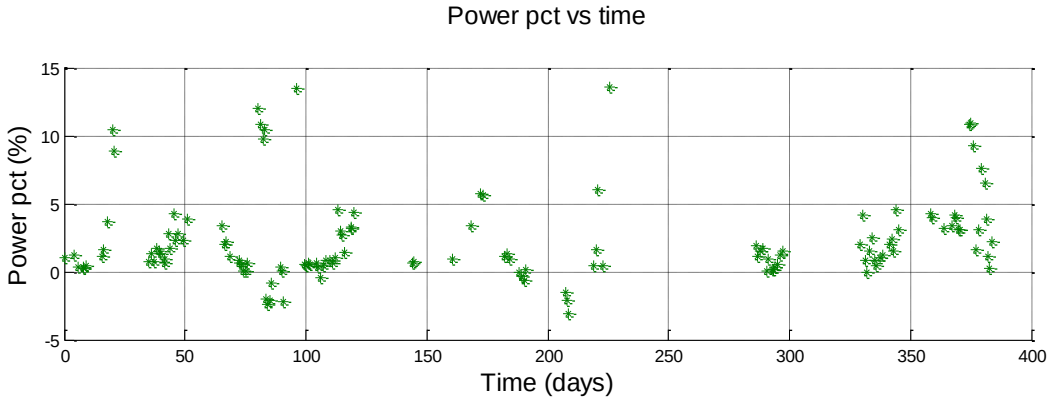

Figure 80 Power Pct vs. time

The power model used in this analysis is detailed with reference to speed, draught and trim of the ship. The results from this detailed model test should give a good estimation of the ships performance under all load conditions. To verify the model with actual results, the Power Pct is now plotted with respect to the forward draught, Figure 81.

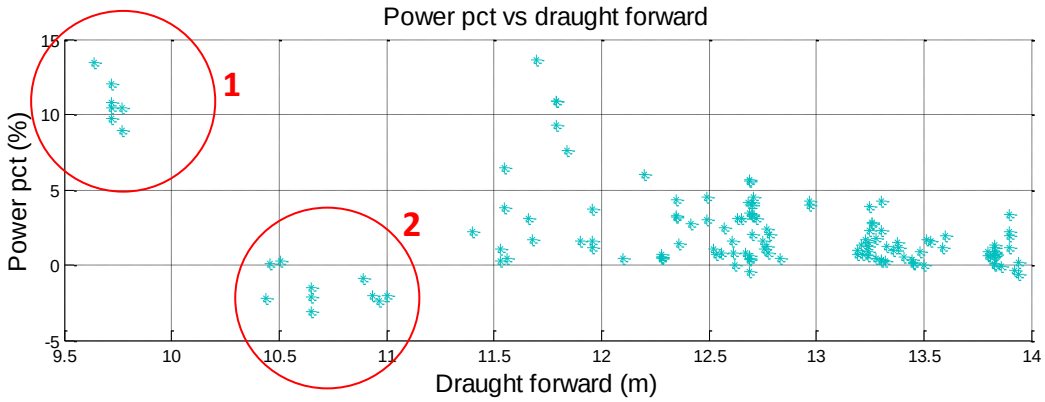

Figure 81 Power Pct vs draught forward

On the figure is marked two areas (1 & 2) where there could be a trend with respect to errors in the performance model.

Area 1	Low draught and aft trim (0.3 to 1.2m)
Area 2	Low draught and forward trim (~ -0.85m)

Areas 1 and 2 show a trend of either error in power model or conditions that are not covered by the GES ship model. The areas are low draught conditions where the bulbous bow is partly out of the water. In area 1 the trim is aft and this gives (too) high power consumption compared to model. In area 2 the trim is forward and this gives (too) low power consumption compared to model. With regards to these observations an additional filter is added to the initial filtering (df > 11 m) and values are removed from the plot. There are still areas where the Power Pct shows large values and to identify these, the Power Pct is plotted with regards to the ships trim, Figure 82.

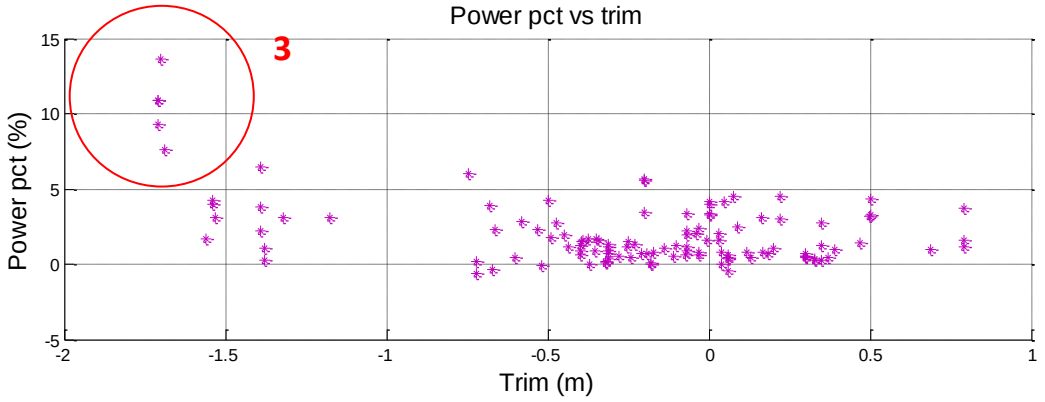

Figure 82 Power Pct vs. trim

On the figure an area (3) is marked where the Power Pct shows large values which also could be caused by an error / limitation in the modelling.

Area 3 High forward trim values > 1.7 m

An additional filter is added (trim > -1.7m) and values are removed from the plot, Figure 83.

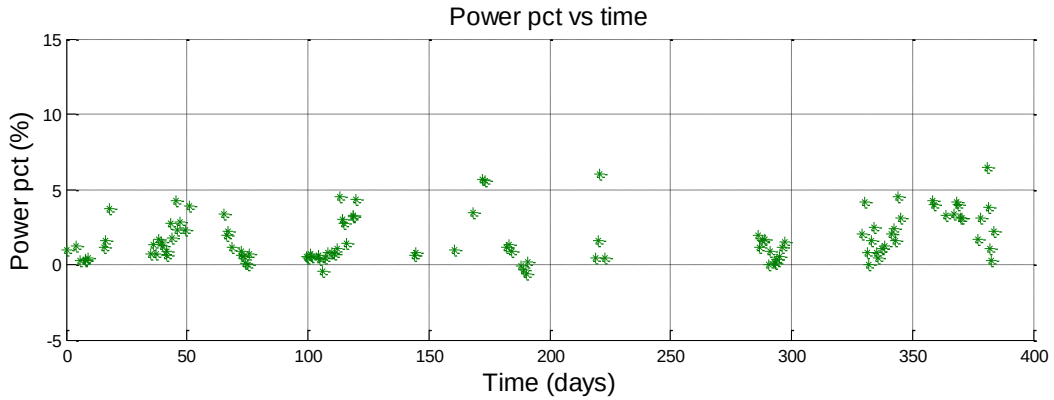

Figure 83 Power Pct vs time

Other performance indexes used in this work are the Speed Pct and the Roughness values and they are plotted on Figures 84 and 85.

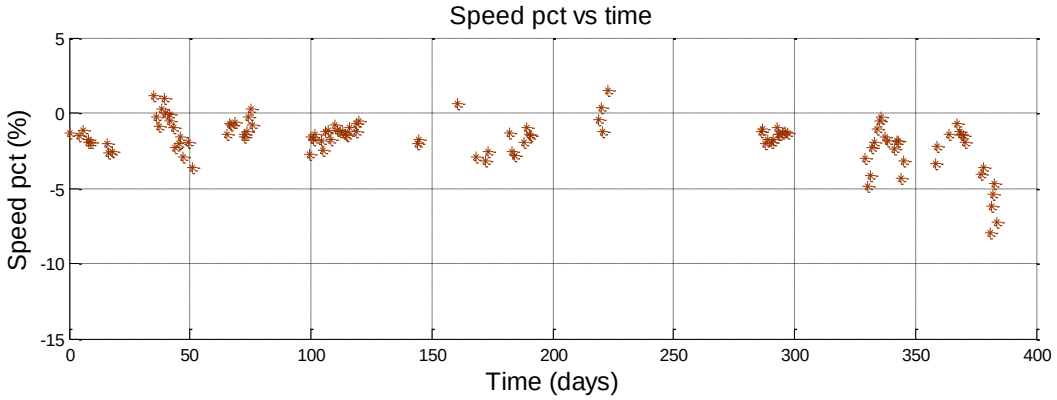

Figure 84 Speed Pct vs time

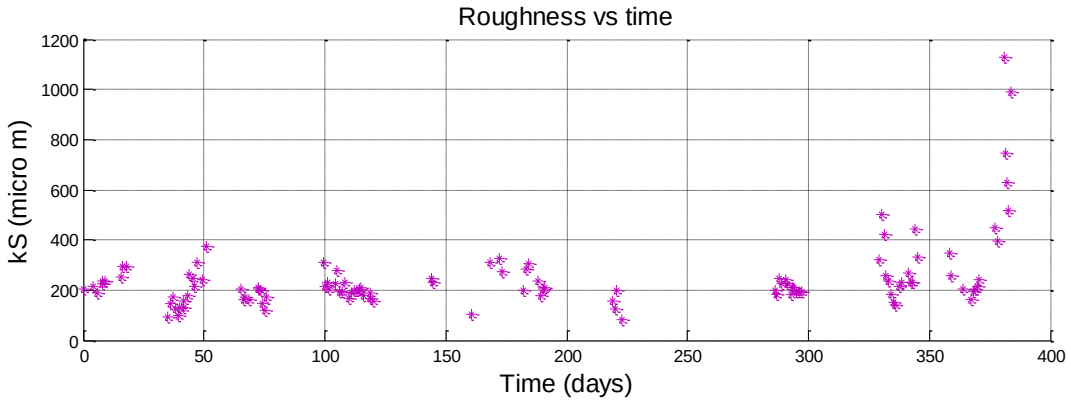

Figure 85 Roughness vs. time

Figures shows rather large scattered values in the last period of the observations and to identify the cause of scatter the Roughness values are plotted with respect to the ships trim, Figure 86.

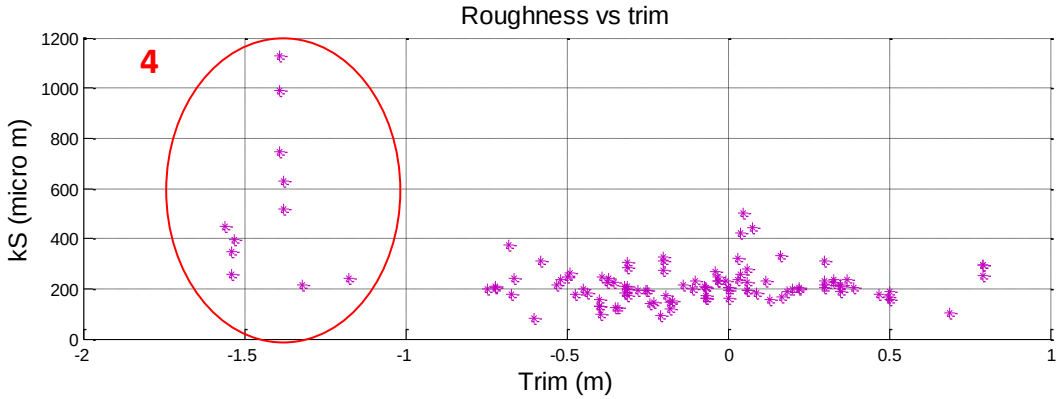

Figure 86 Roughness vs. trim

An area (4) is identified where there are large scatter in results. There is not a clear indication on what causes the scatter by analysing the averaged data and therefore another filter is introduced to the analysis (trim > -1). For a more detailed analysis of the individual time series, see Section 10. In this section time series are analysed with respect to improvement of the model and also to introduce other filters in selecting data for the performance analysis.

The data are now filtered with respect to filters in Table 18 and filters introduced in this analysis. All filters are listed in Table 22.

Parameter	Filter
ME Power percentage	> 30%
True wind speed	< 10 m/s
Water depth	> 80 m
df	> 11 m
Trim	> -1 m

Table 22 Filter values

The result is shown on Figures 87, 88 and 89 where linear regression lines are plotted with each interval.

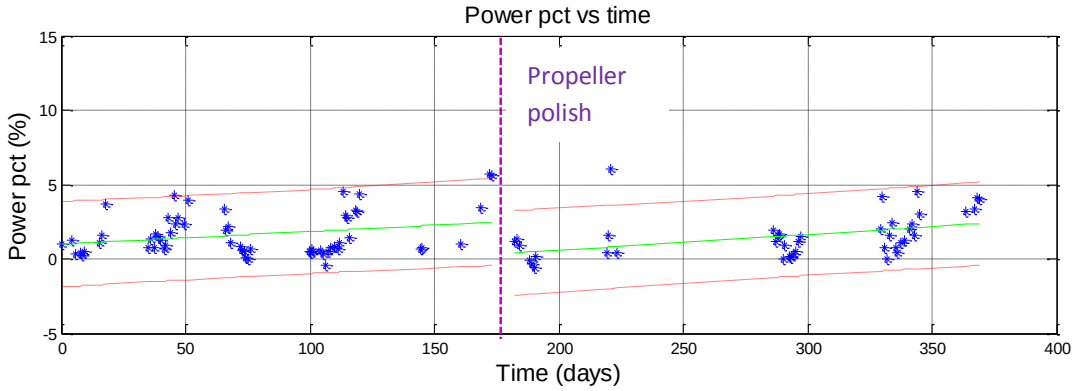

Figure 87 Power Pct vs. time inc. 95% confidence interval

Parameter	Before prop clean	After prop clean
RMSE	1.396	1.356
Line slope with 95% conf.bounds	0.0086 (0.00066, 0.0165)	0.0105 (0.0035, 0.0176)

Table 23 Goodness of fit for Power Pct regression

The Power Pct as performance index shows good results in indicating the ships performance. Underwater surveys of m/v "Clementine Maersk" show almost no increase in fouling over time and the power consumption is therefore not expected to rise considerably due to this factor. The trend of power consumption is slightly increasing during the period and the propeller polish incident is

clearly shown by a fall in index after the incident. Goodness of fit values show slightly less scatter in data after the propeller polish – RMSE have lower values and there is less variance in confidence bounds. The slope has a higher value after the propeller polish than before – this is general for all three performance indexes – and could be explained by the fact that the shift in index value is caused by a propeller polish only.

According to hull surveys, the hull is not experiencing any significant fouling and therefore the value of the performance index is primarily linked to the effect of the propeller polish. The higher slope is due to the degrading effect of the propeller polish which is levelled after approximately 6 months, see Section 10.

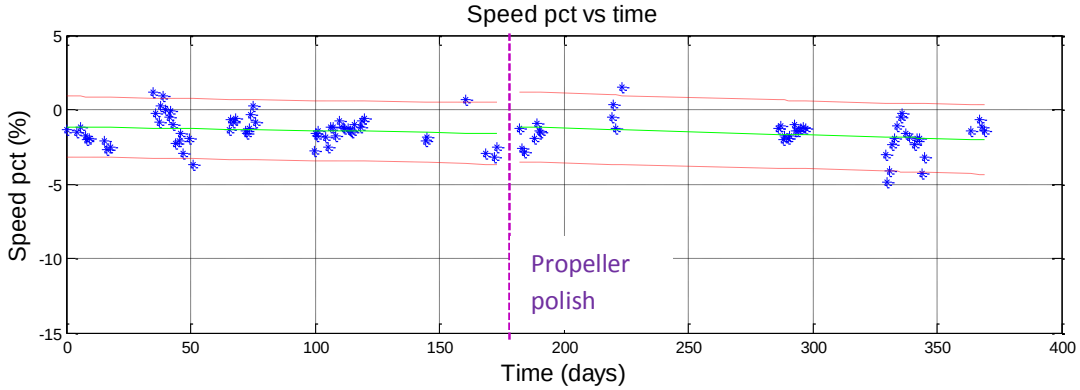

Figure 88 Speed Pct vs. time inc. 95% confidence interval

Parameter	Before prop clean	After prop clean
RMSE	0.993	1.129
Line slope with 95% conf.bounds	-0.0026 (-0.0083, 0.0030)	-0.0045 (-0.0104, 0.0013)

Table 24 Goodness of fit for Speed Pct regression

The trend in the speed Pct values is slightly decreasing which is expected. The propeller polish incident is not quite clearly indicated by a change in index. Goodness of fit parameters shows slightly less scatter in index before the propeller polish.

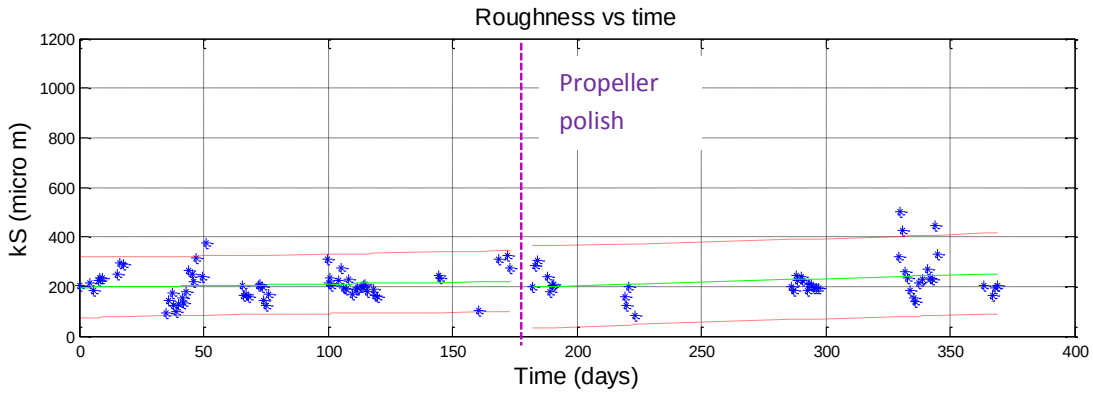

Figure 89 Roughness vs. Time inc. 95% confidence interval

Parameter	Before prop clean	After prop clean
RMSE	59.21	79.61
Line slope with 95% conf.bounds	0.1434 (-0.1934, 0.4803)	0.2914 (-0.1228, 0.7057)

Table 25 Goodness of fit for Roughness regression

The trend is that the roughness values is slightly increasing which is expected. The propeller clean incident is not quite clearly indicated by a change in index. Goodness of fit parameters shows slightly less scatter in index before the propeller cleaning.

The logged data in this case study is now analysed with respect to correlation with performance indexes. For each data set the distribution and the values over the period is plotted and correlation plots with linear regression lines are made for each data set / performance index. The analysis will indicate where the model could be improved with regards to implementing data e.g. sea water temperature or rudder movements.

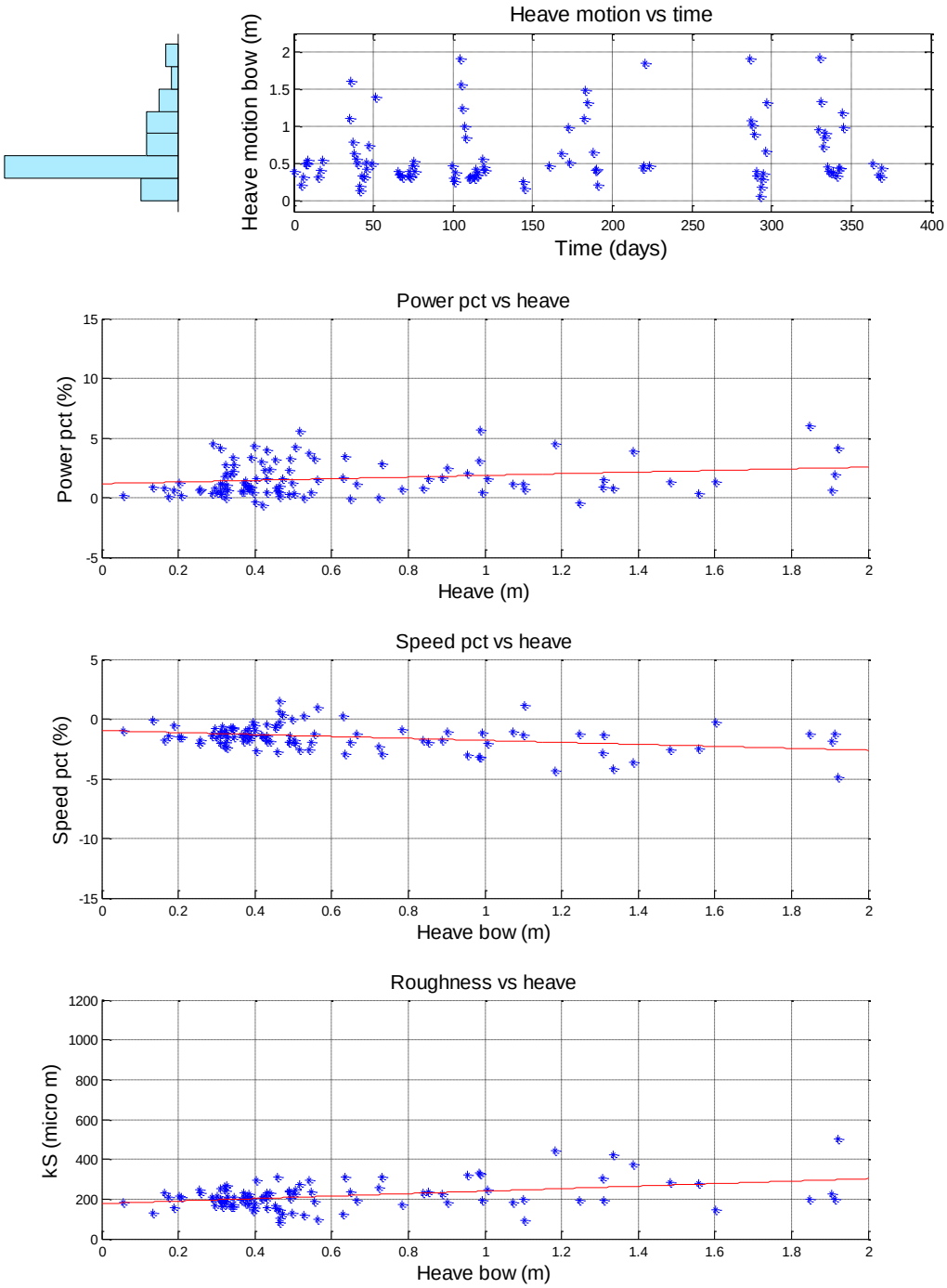

Figure 90 Bow motion distribution and correlation

Bow motion is measured by a sensor in the bow. The motions of the ship are not taken in consideration in this model. There seems to be some sensitivity in indexes towards motions in the bow, Figure 90.

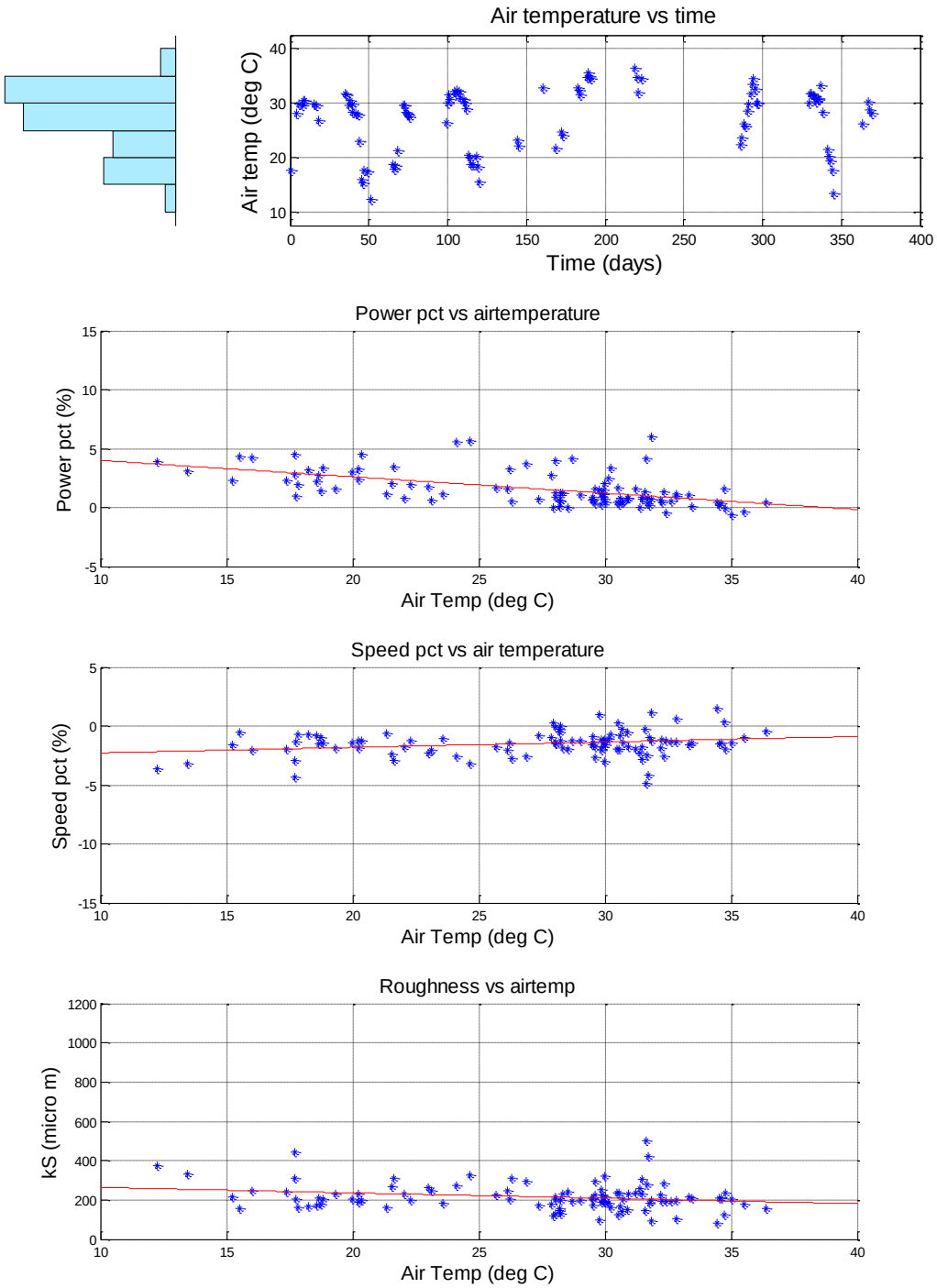

Figure 91 Air temperature and correlation

Air temperature is not considered in this model. It seems to have an effect on the indexes, Figure 91. The majority of the data sets are distributed around 20 to 30 °C. The air temperature follows the seawater temperature and it is reasonable to consider the seawater temperature as the parameter which has the largest effect on the indexes, see Section 9.1.

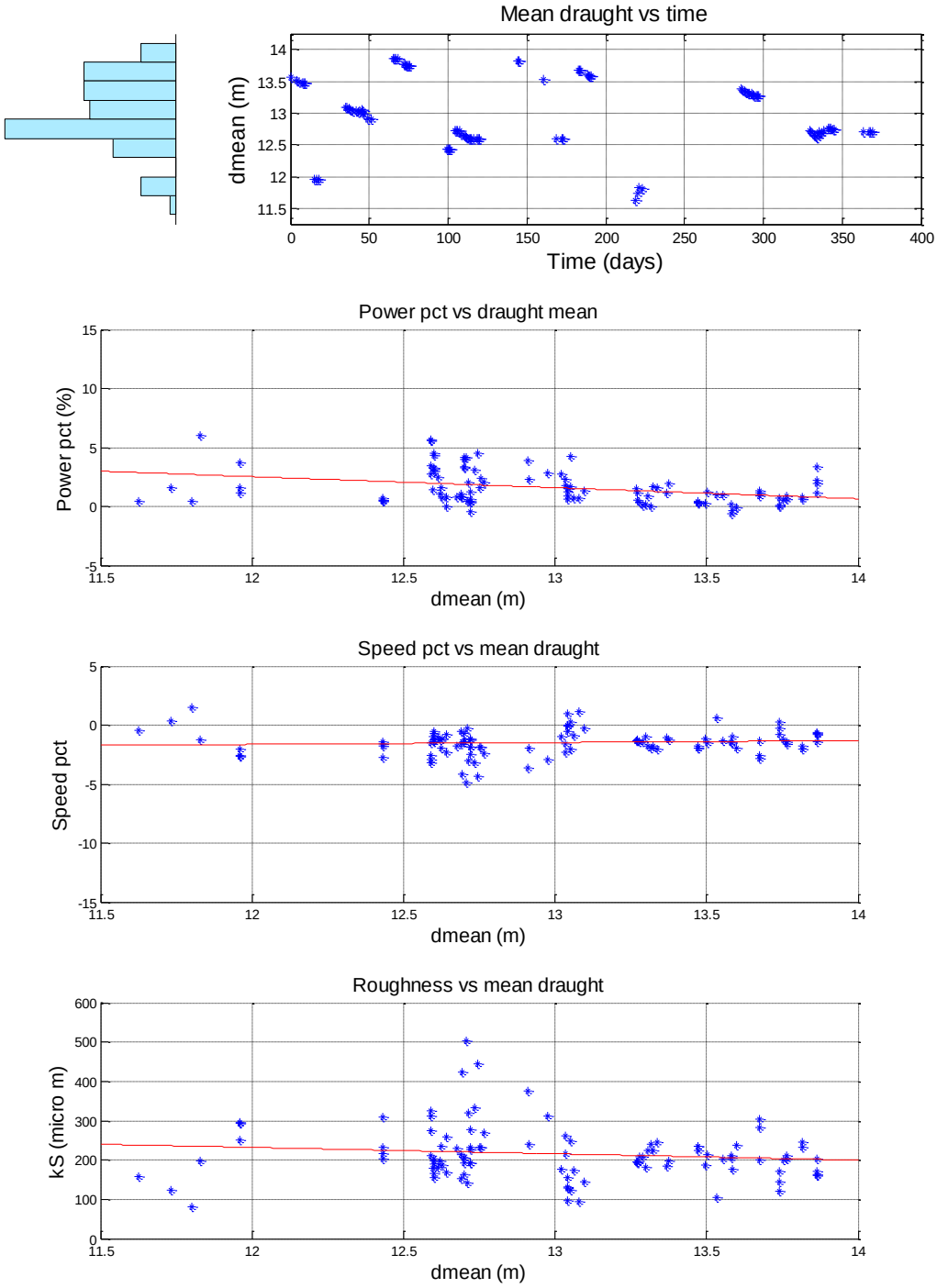

Figure 92 Mean draught distribution and correlation

The mean draught is included in the model and it has no further effect on the indexes, Figure 92. The low draught areas create some scatter in the indexes which is causing interference in the results.

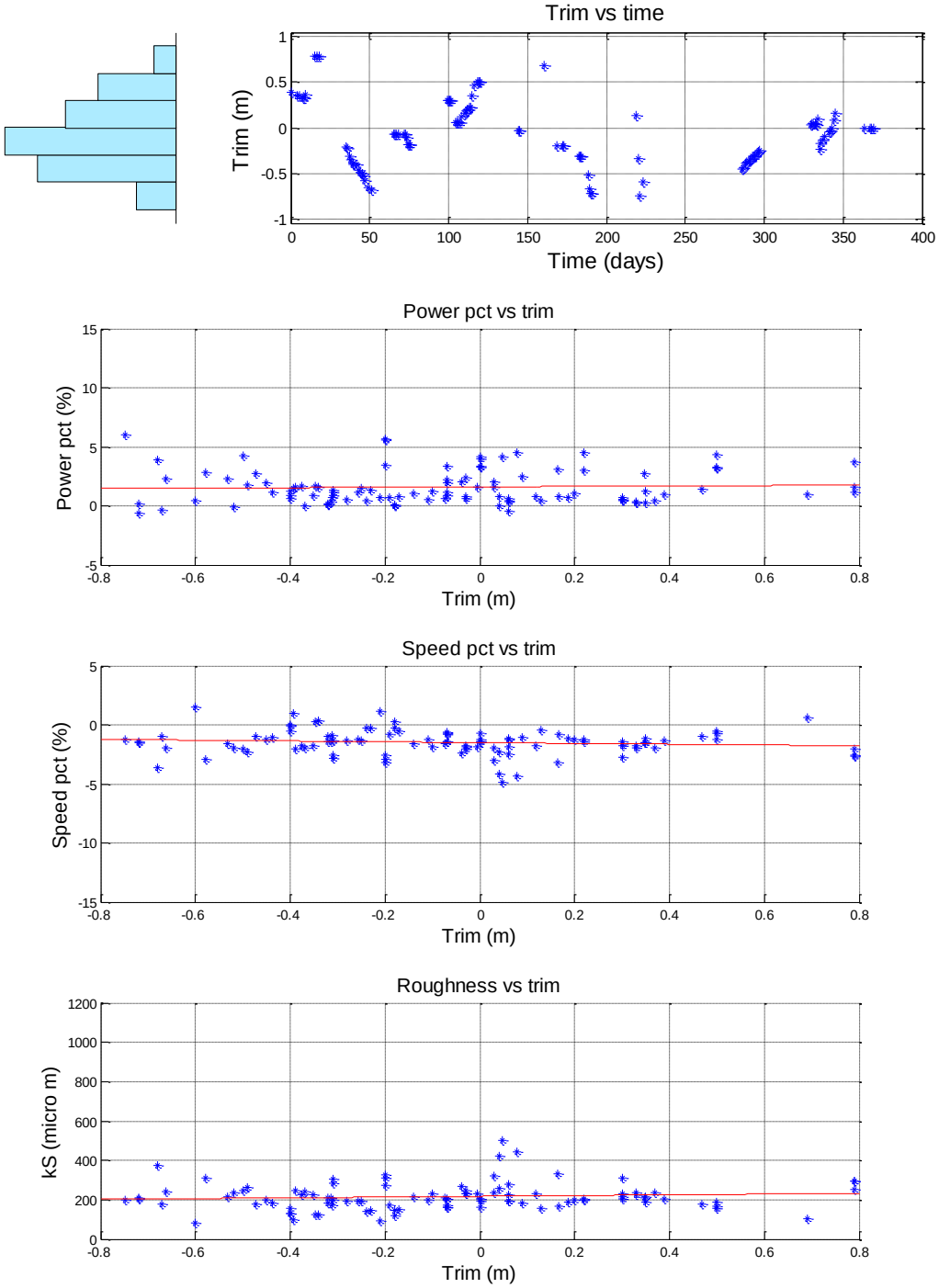

Figure 93 Trim distribution and correlation

Trim is included in the model. The lowest negative trim values have been filtered out and the remaining values do not affect the indexes further, Figure 93.

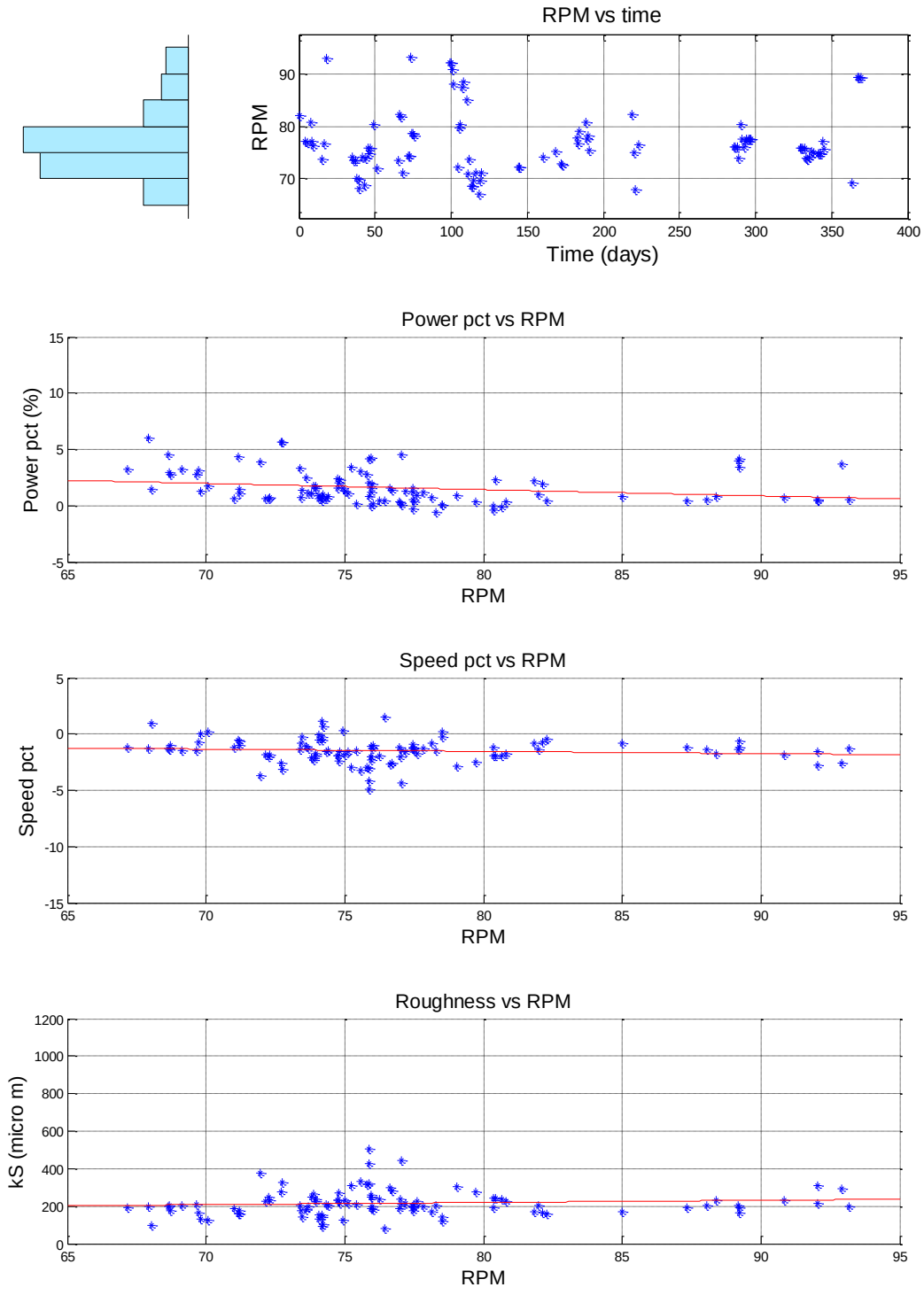

Figure 94 RPM distribution and correlation

RPM is included in the model. The main distribution of data sets is around values 70 to 80 RPM and the data does not affect the indexes further, Figure 94.

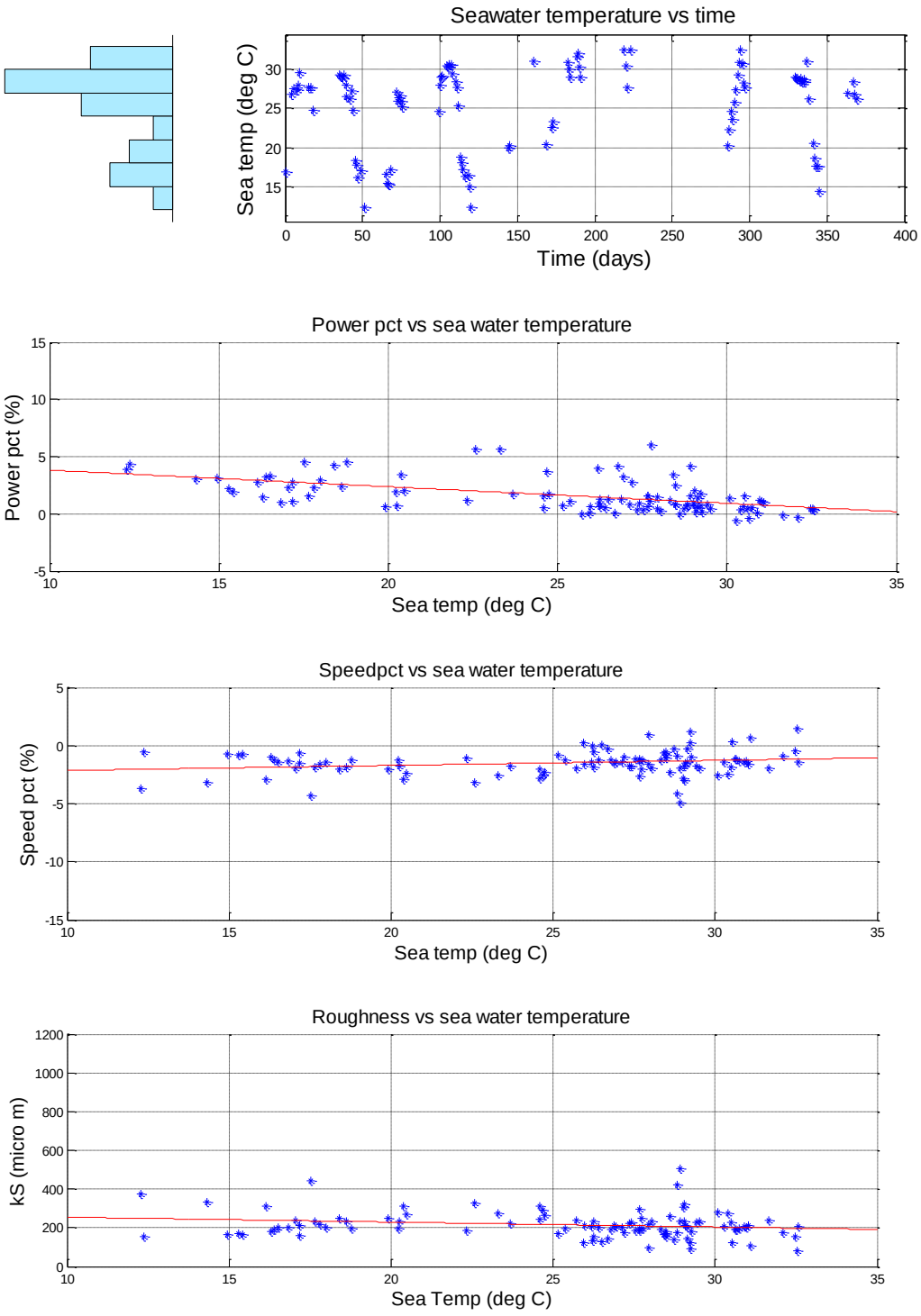

Figure 95 Sea water distribution and correlation

The sea water temperature seems to have some effect on the Power Pct index, Figure 95. The power model is based on model tests in a model tank with water temperature of 15°C and a seawater temperature correction will be implemented in the improved model, see the section "Improvements to the Performance Model ".

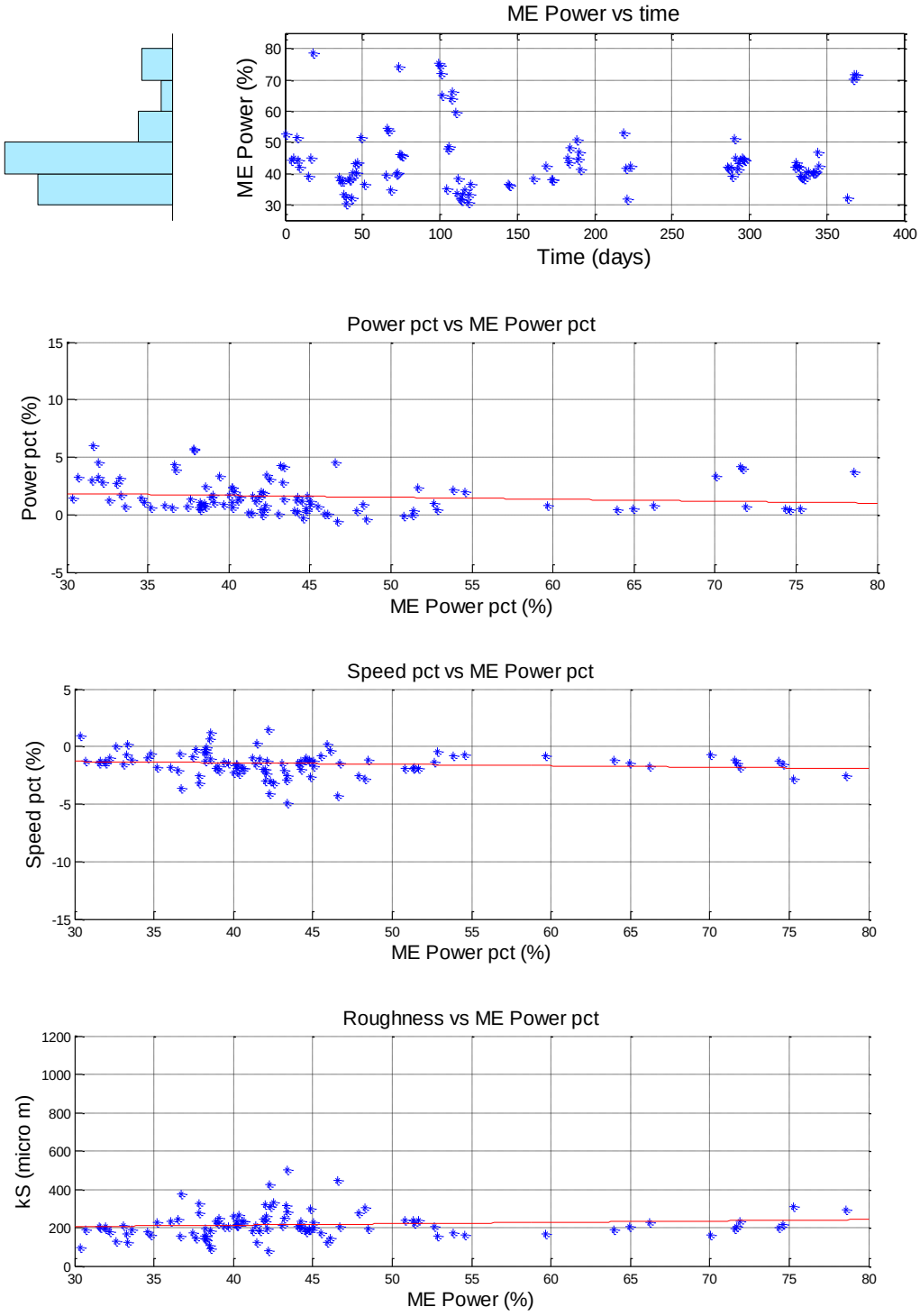

Figure 96 ME Power % distribution and correlation

Main engine power (% of MCR) is distributed around 30 – 40 % and has now further effect on the indexes, Figure 96.

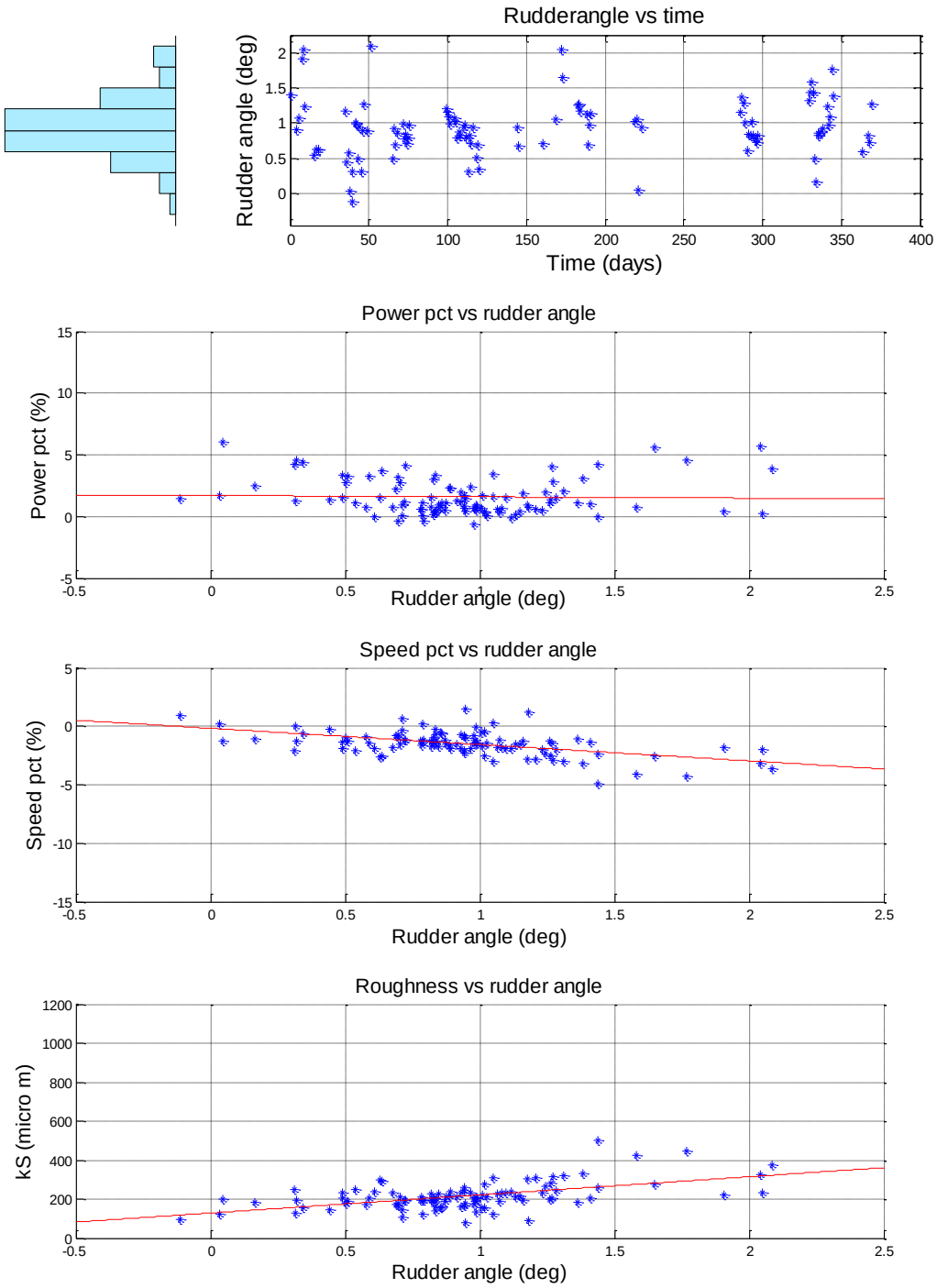

Figure 97 Rudder angle distribution and correlation

There seems to be some effect of rudder positions on indexes Speed Pct and Roughness, Figure 97. From rudder angles > 1° there are some scatter in results which could cause some interference in results. The rudder angle is a mean angle over the time series period and it would make more sense to investigate the rudder effect by implementing fluctuations in rudder angles over a period. A further analysis of rudder effects can be seen in Section 9.4.

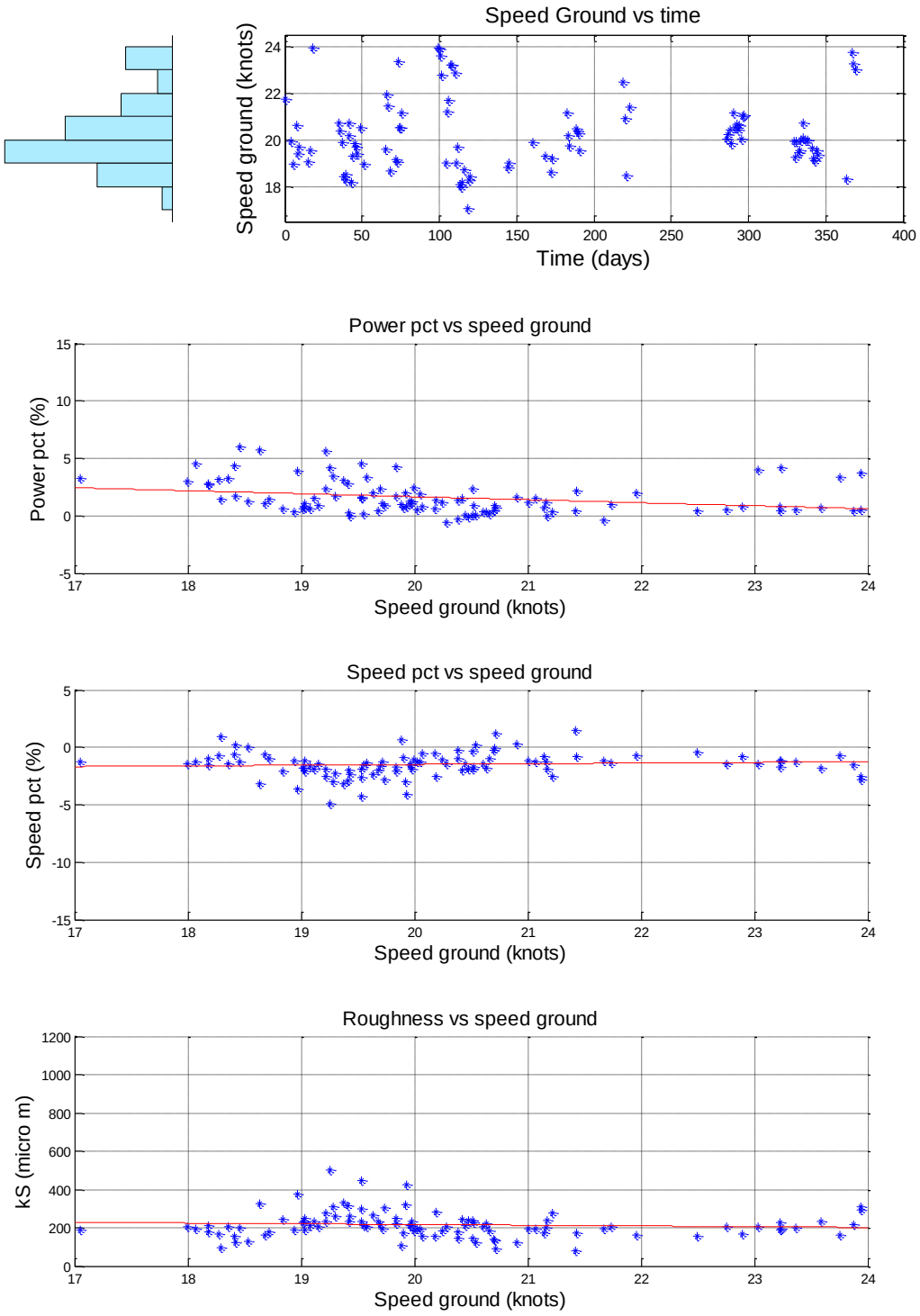

Figure 98 Speed ground distribution and correlation

The ground speed is logged by the GPS and has no effect on the indexes, Figure 98. A comparison of ground speed and logged speed can be found in Section 6.3.9.

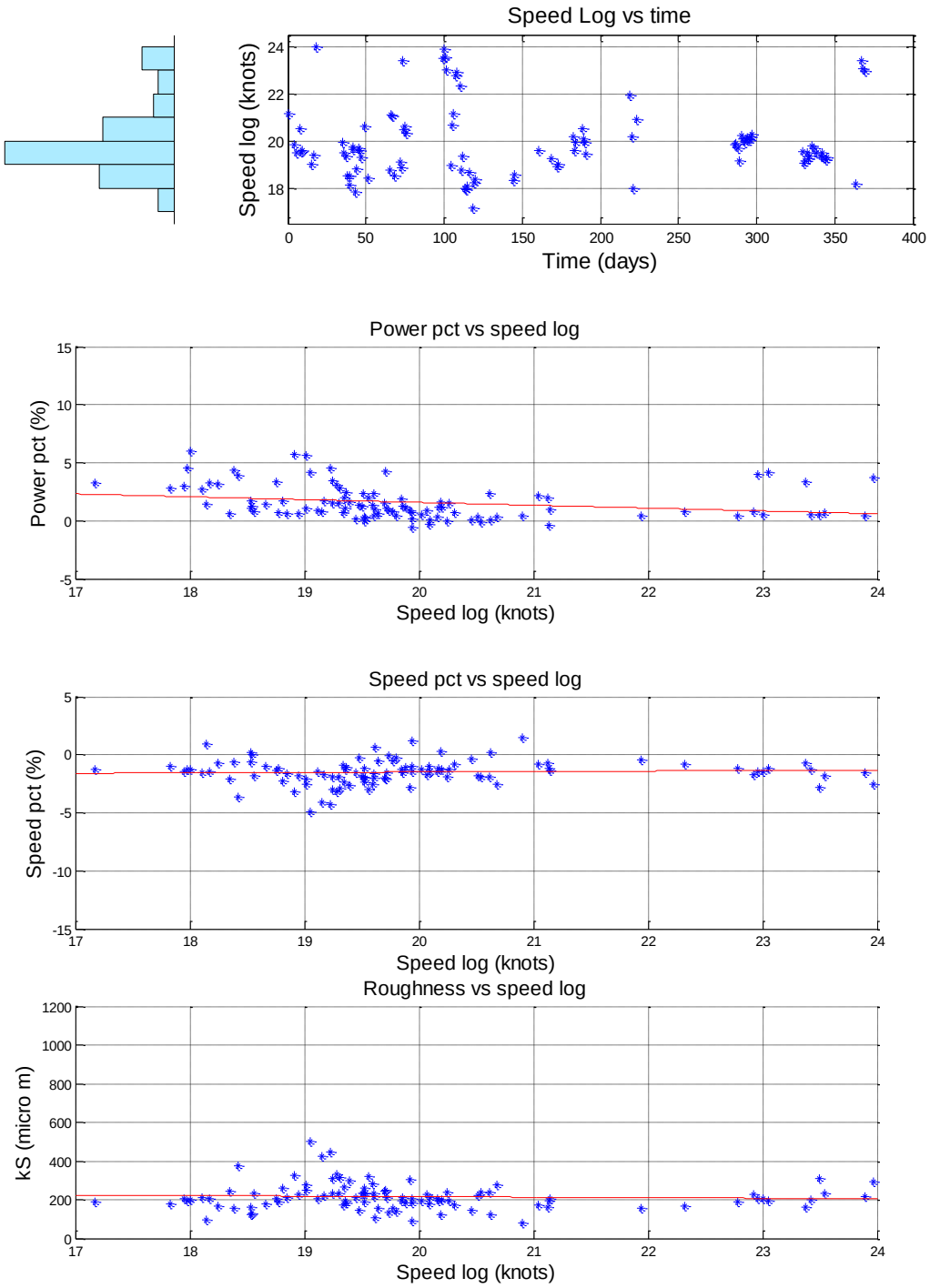

Figure 99 Speed log distribution and correlation

The speed log is used to estimate the indexes Speed Pct and Roughness see Section 4.2. There is no further effect on indexes, Figure 99.

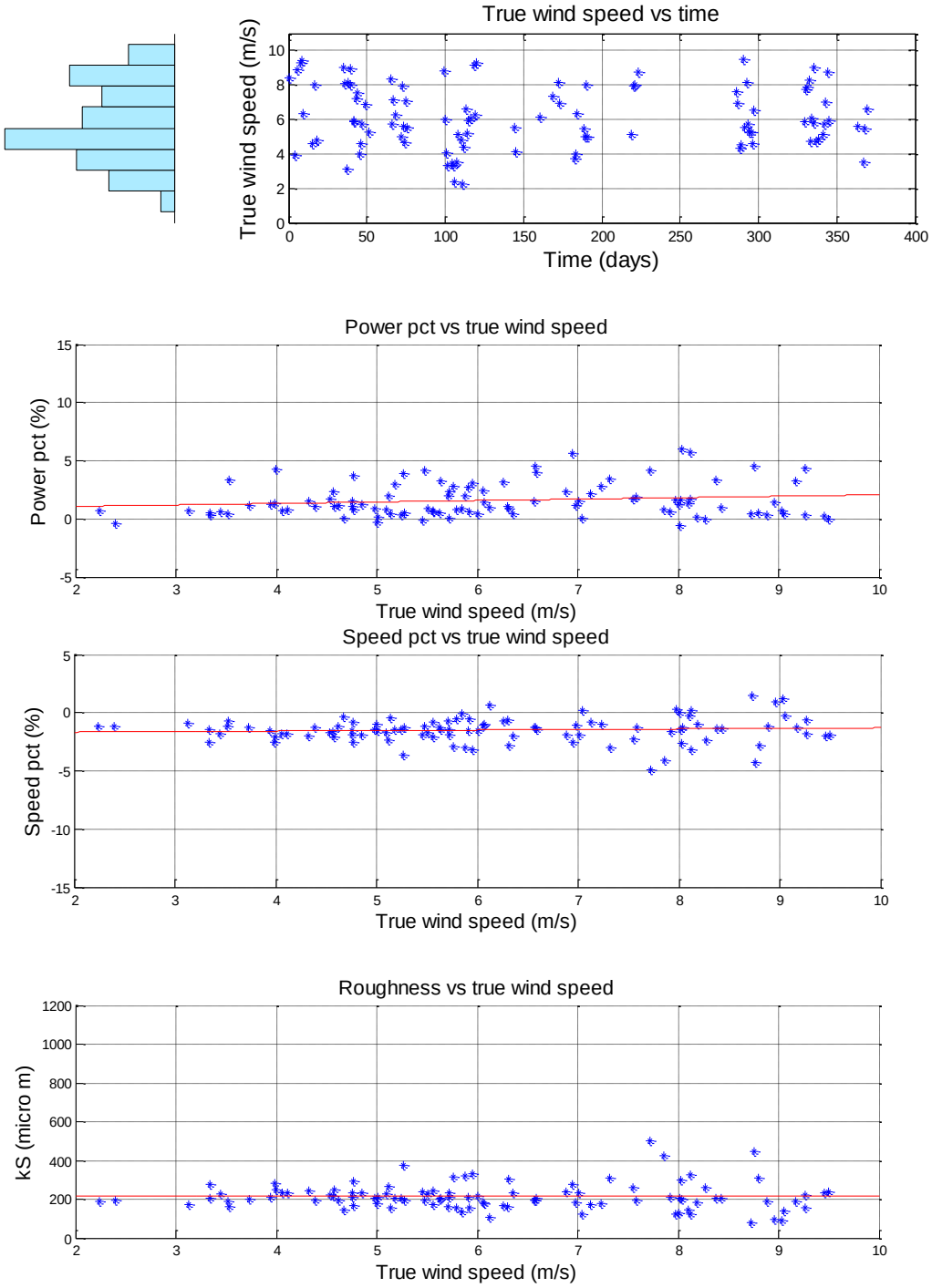

Figure 100 true wind speed distribution and correlation

The true wind speed is filtered to values < 10 m/s and is implemented in the model. There is no further effect on indexes by this parameter, Figure 100.

8.1.1 **Conclusion**

Two sets of data are used in the Performance Analysis – one set collected by the ship's crew and sent to shore daily and one set based on daily averages of values logged in the automation system. The data are used to indicate the ships performance over a period of 380 days. The data are filtered with respect to shaft power, true wind speed and water depth. The ship model is based on towing tank tests where speed, draught and trim are taken in consideration.

Three performance indexes are used to indicate the ships performance in the logging period.

The results from the performance system based on noon data are highly scattered and unable to show the effect of a propeller cleaning event. The auto logged data reduces the scatter considerably and the effect of the propeller cleaning is visible.

With regards to the auto logged data, the results in this section show that the model still is sensitive to draught and trim, especially at low draughts and high forward trim values and additional filters are introduced based on this knowledge.

To establish a relation between input parameters and performance indexes a set of correlation plots are used to identify where the performance model could be improved. The improvements are described in the following case study, Section 9.

9 Improvements to the Performance Model

The analysis in the previous section is based on the performance model shown on Figure 74. Based on correlation plots in the previous section it is the intention to improve the Performance Model by adding elements to the model. The improvements are measured by the reduced scatter in the performance index results i.e. less scatter = better model.

The variation in seawater temperature, the wave height, the shallow water effect and the rudder movements are modelled in this section. The data used are from the m/v "Clementine Maersk" case study.

9.1 Sea Water Temperature

The resistance element in the Performance Model is based upon towing tests from model tanks. The model tests are performed with reference to water with the properties as shown in Table 26.

Water temperature	Water density	Water viscosity
15°C	1025.88 kg/m^3	1.188×10^{-6} m^2/s

Table 26 Model tank water properties

During operation the ship is sailing under various environmental changes, including changes in the properties of the sea water.

These changes and their effect on ρ, *dCt* and added resistance *R* are exemplified by input parameters in Table 27 and the results in Figure 101.

d_m	S	Cf	Us
12.65 m	17195 m^2	0.001499	22 knots

Table 27 Input parameters to the sea water temperature element where d_m is mean draught, S is area of wetted surface, Cf is the frictional coefficient and Us is the ship's speed.

The input parameters are from a case study incident from m/v “Clementine Maersk” and seawater temperature properties are experienced during the case study period (2010).

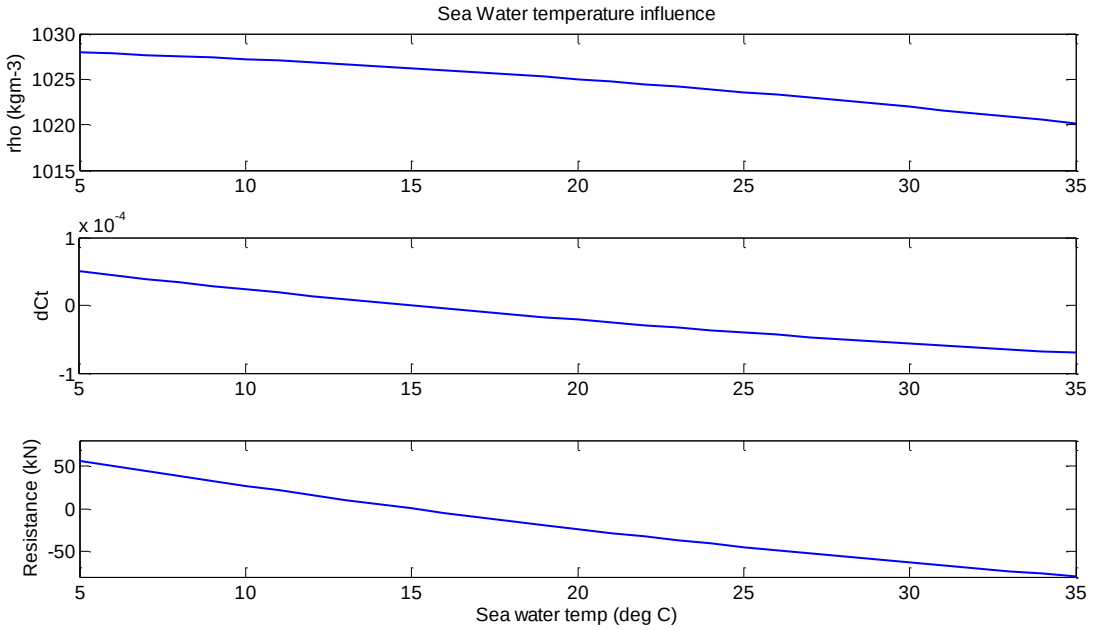

Figure 101 Sea water temperature influence on ρ, dCt and R

The varying temperature affects the variables as

- $1020 < \rho < 1028$
- $-0.8e\text{-}4 < dCt < 0.6e\text{-}4$
- $-80\ kN < R < 55kN$

It is not possible to take the variance in seawater density due to other factors e.g. varying salinity into consideration in this study.

By implementing the element in the GES performance model the variances in sea water temperature during the performance evaluation period and thus the influence on the ship’s resistance will be captured. This will have an effect on the performance index by reduced scatter over the period.

9.2 Wave Height

The parameters logged by the motion sensors are Encounter Period T_e, Bow Vertical Velocity V_b and Bow Vertical Motion η_R, see Section 6.3.12.

The true wind speed wave height and the wave height based on Closed Form expressions are compared to hind cast data for the specific areas. The areas are from the m/v "Clementine Maersk" case study. The input data (T_e, U_s, η_R) for the calculations are averaged over a 20 minute window.

9.2.1.1 *True Wind Speed Formula*

The wave heading angle β, Figure 102, is estimated from the true wind direction and the ship's heading – with 180° as head seas.

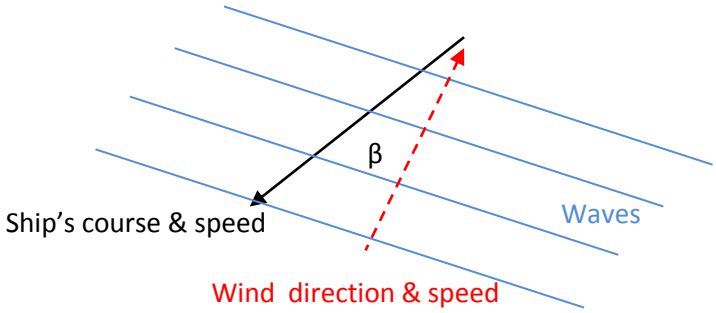

Figure 102 Wave heading angle.

The measured wind speed is averaged over 10 minutes and is used in Eq. 74 to calculate H_S:

$$H_S = \frac{2.06}{g^2} U_{TW\_19.4}^2 \qquad (74)$$

9.2.1.2 *Hind-cast Data*

The hind cast data used in this thesis is obtained through a subscription of data from Buoyweather Inc. The data is based on NOAA's WAVEWATCH III global model (http://polar.ncep.noaa.gov

/waves/) with a 1.0 x 1.25 degrees grid resolution. The data is provided at three hour intervals and can be retrieved for any model latitude/longitude grid point.

9.2.1.3 *Case Study 1*

The ship was experiencing hard weather on the 27 October 2010 in the Northwest Pacific Ocean. The measured wind speed on board was as given in Figure 103.

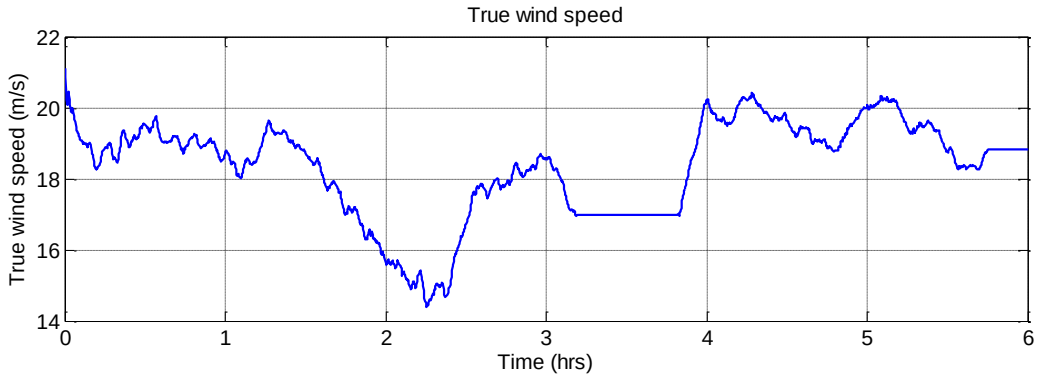

Figure 103 True wind speed Case 1

The wind speed is around Beaufort gale force 8 varying to force 7 after 2 hours and then intensifying to force 8. Between 3 and 4 hours the wind speed is constant for a period, which could be interpreted as a faulty signal.

β and the logged encounter period T_e is used to find the wave period by

$$T_S^2 - T_S T_e - \frac{T_e 2\pi U_S}{g}\cos\beta = 0 \qquad (75)$$

and the result is shown in Figure 104.

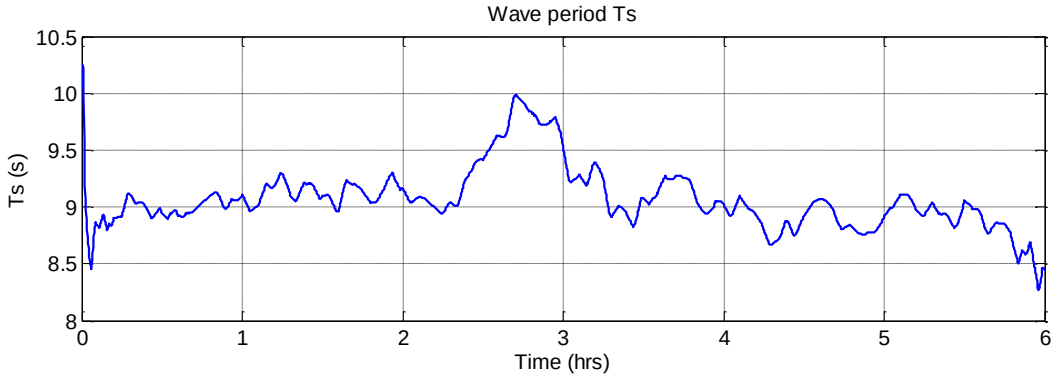

Figure 104 Calculated wave period, Case 1.

The value of the wave period is around 9 seconds with a peak (10 seconds) around 2½ hours. The hind cast data from the day and the area where the ship is positioned is shown in Table 28. The corresponding wave period is around 9 seconds and the direction of the waves is more or less as the direction of the wind.

		Wind			Seas		
Date	**Time**	**Dir**	**Deg**	**Range (m/s)**	**Dir**	**Period**	**Range (m)**
27.10.2010	00Z	NNE	014	13 - 18	NNE	10	5.5 – 8.5
27.10.2010	06Z	NNE	015	13 - 18	NNE	9	5.0 – 7.5
27.10.2010	12Z	N	007	15 - 20	NNE	9	5.0 – 8.0
27.10.2010	18Z	N	001	16 - 22	NNE	9	5.0 – 8.0

Table 28 Hind cast data Case 1

An overview of the area with wind data and ship's position at the end of red arrow is presented in Figure 105.

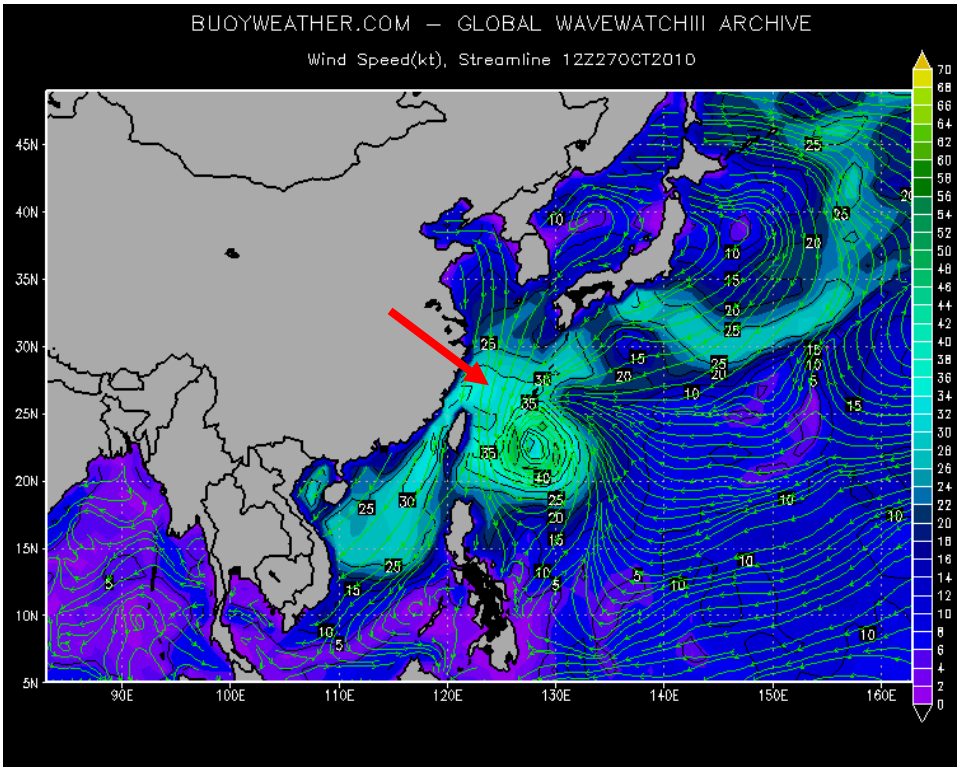

Figure 105 Case study area, Case 1 (Wind speed streamlines).

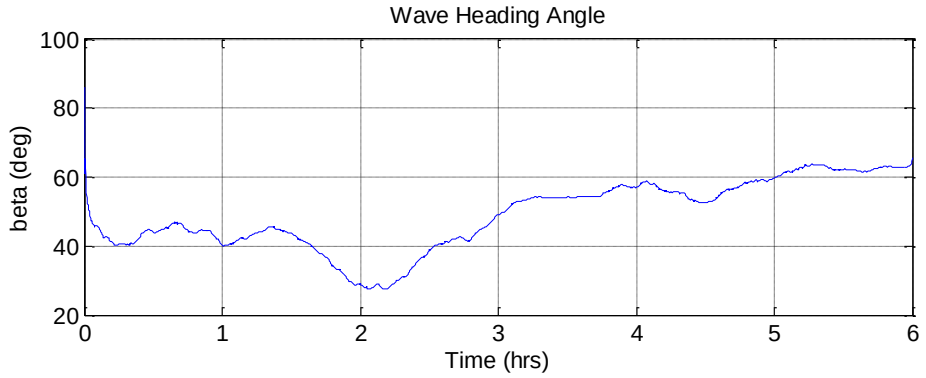

Figure 106 Calculated wave heading angle Case 1.

The wave heading angle is shown in Figure 106.The estimated relative wave direction is on the aft quarter of the ship. The measured bow motions are as in Figure 107.

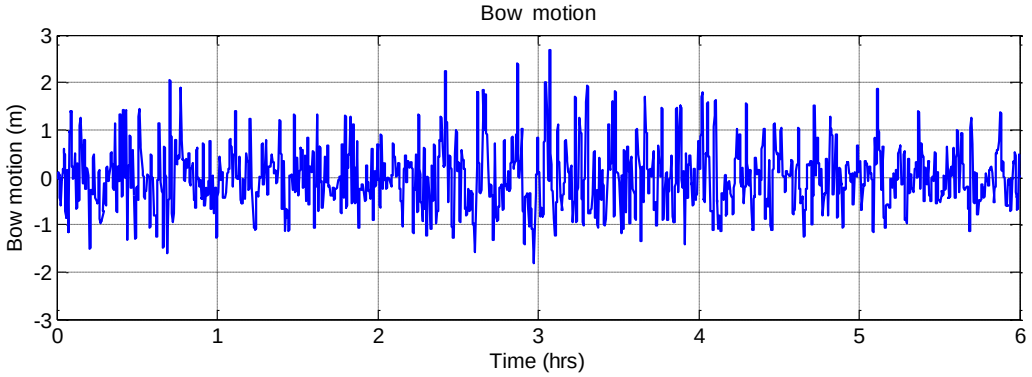

Figure 107 Measured bow motions Case 1

The measured motions are in the area of 0 to 3 m and the data are used in the wave height calculations Eq. 39 and compared by the wind speed calculations Eq. 74 and the result is shown in Figure 108.

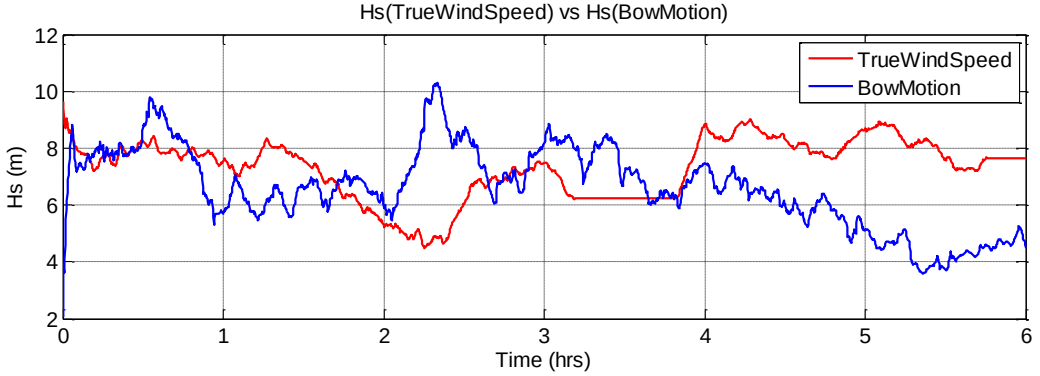

Figure 108 H_S values for two methods, Case 1.

H_S values found by bow motions show partial agreement with results from true wind calculations and with hind cast data from the area. Between 2 and 3 hours there is discrepancy between the results – the H_S(BowMotion) has a peak due to large motions in the bow and the H_S(TrueWindSpeed) has a drop in value due to a drop in measured wind speed. From 4 to 6 hours the H_S(BowMotion) drops in value due to less motions in the bow and the H_S(TrueWindSpeed) follows the wind speed and rises to a steady (high) value.

9.2.1.4 *Case Study 2*

The ship was en route eastward on 3. October 2010 through the Bay of Aden.

The measured wind speed on board was as in Figure 109.

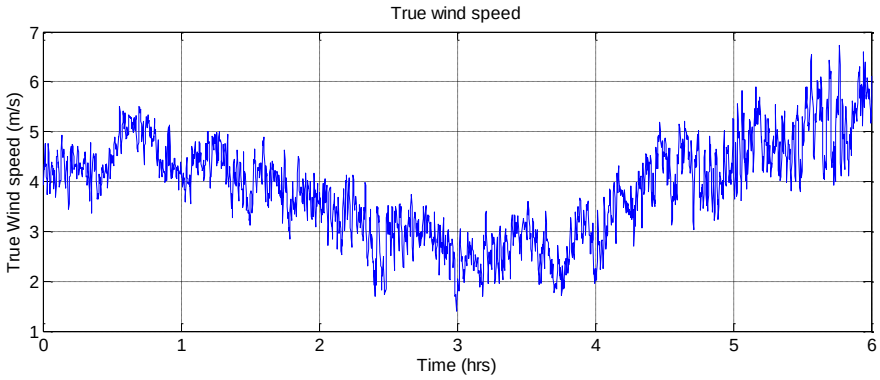

Figure 109 True wind speed Case 2

The wind speed is around Beaufort force 2 to 3. Using β and T_e, the wave period is calculated and the result is shown in Figure 110.

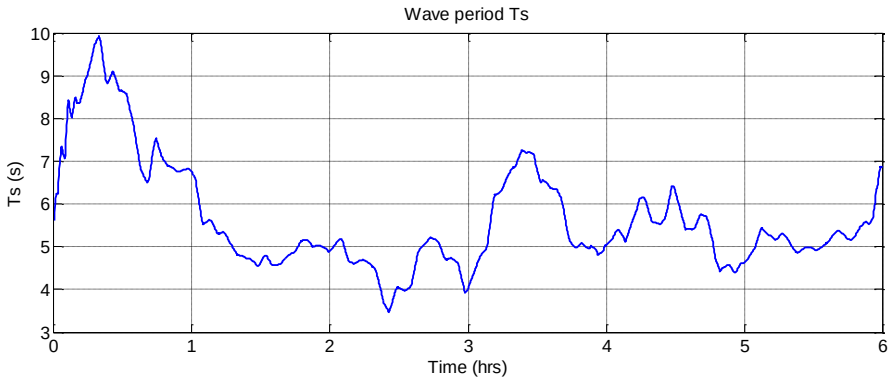

Figure 110 Calculated wave period, Case 2.

The wave period varies from a value > 6 seconds in hour 0 to 1 to a value 4 to 5 in hour 1 to 6. Between hour 3 and 4 there is a small peak where T_S reaches a value of 7.2 seconds. The hind cast data from the day and the area where the ship is positioned is shown in Table 29. The wave period is around 4 seconds and the direction of the waves is more or less as the direction of the wind. The data shows no values larger than 4 seconds, which disagrees with results from calculations in time 0 to 1 hour and time 3 to 4 hours.

		Wind			Seas		
Date	**Time**	**Dir**	**Deg**	**Range (m/s)**	**Dir**	**Period**	**Range (m)**
03.10.2010	00Z	ENE	050	2 - 3	E	4	0.3 – 1
03.10.2010	06Z	ENE	074	3 - 5	E	4	0.3 – 1
03.10.2010	12Z	ENE	074	1- 2	ENE	4	0.3 – 1
03.10.2010	18Z	ENE	066	2 - 4	ENE	4	0.3 – 0.6

Table 29 Hind cast data, Case 2.

An overview of the area with wind data and ship's position at the end of the red arrow as given in Figure 111.

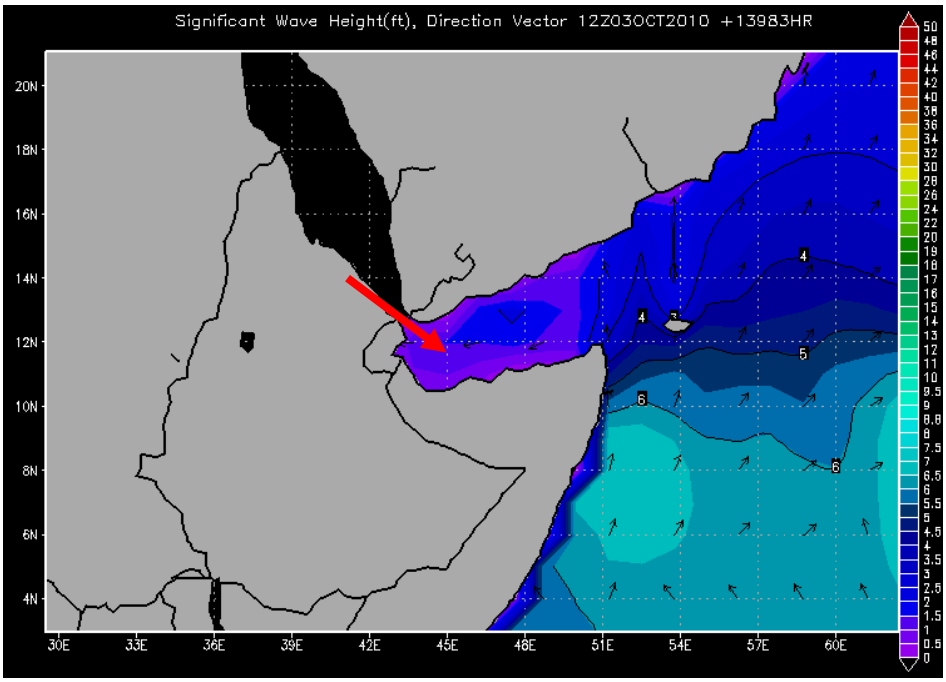

Figure 111 Case study area, Case 2 (Significant wave height with direction vector).

The wave heading angle is shown in Figure 112. The angle gives beam to head seas.

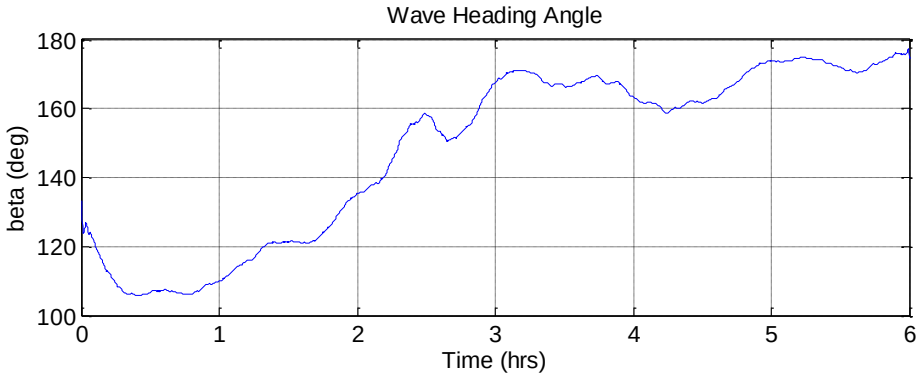

Figure 112 Estimated θ_{180} Case 2

The measured bow motions are as in Figure 113.

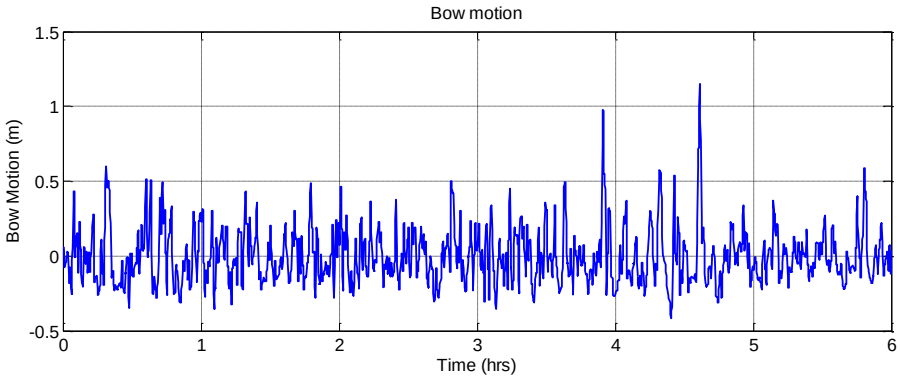

Figure 113 Measured bow motions, Case 2.

The measured motions are in the area of 0 to 0.5 m with two peak incidents up to 1 m. By using these data in the wave height calculations and comparing them with the wind speed calculations, results are obtained as depicted in Figure 114. Wave heights up to 10 m are included in the plot.

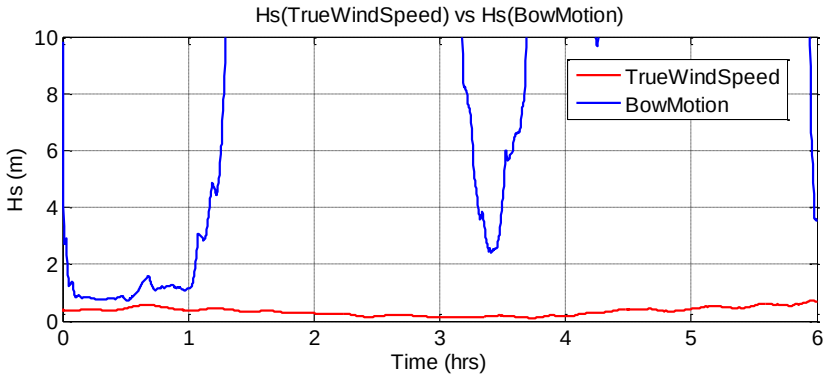

Figure 114 *Hs* values for two methods, Case 2.

In hour 0 to 1 there is agreement in H_S calculations by the two methods. The rest of the period the H_S(BowMotions) shows results with too large values. The hind cast values shows wave height values in the area of 0.3 to 1 m, which is in area of the calculated values when there is agreement between values.

In Figure 115 the calculated H_S values are plotted (up to 10m) vs. the calculated wave period. There is agreement between values from the two methods starting around T_S = 7.2 seconds and upwards. For discussion of this result, see "Conclusion" in Section 9.2.16.

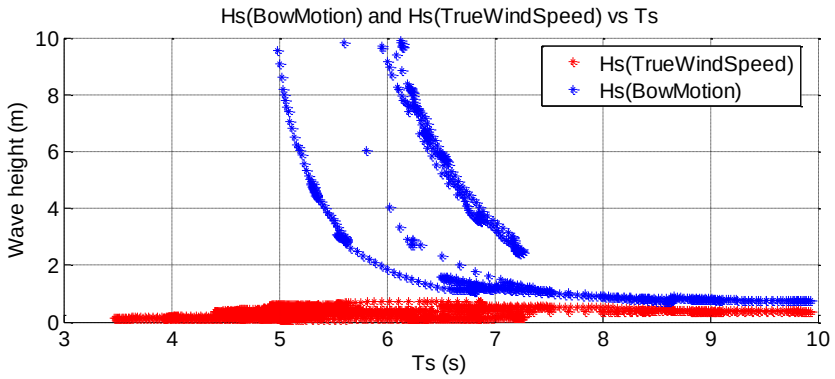

Figure 115 Calculated wave heights vs. calculated wave period.

9.2.1.5 *Case Study 3*

The ship was en route westward on 31. October 2010 through the Bay of Aden. The measured wind speed on board was as in Figure 116.

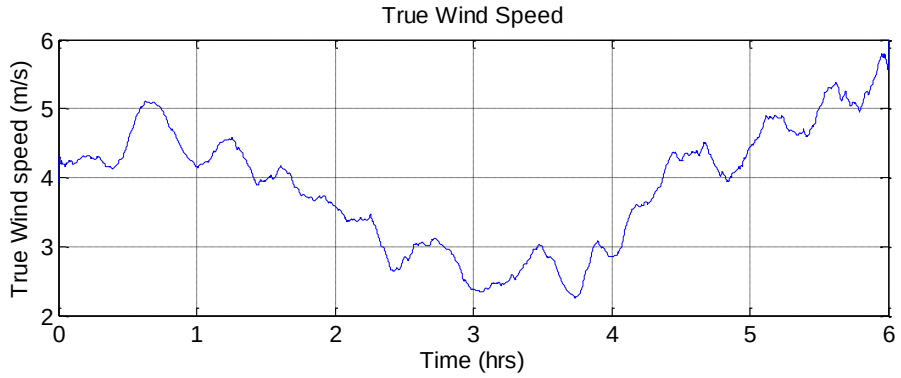

Figure 116 True wind speed, Case 3.

The wind speed is around Beaufort force 2 to 4. Using β and T_e, the wave period is calculated and the result is shown in Figure 117.

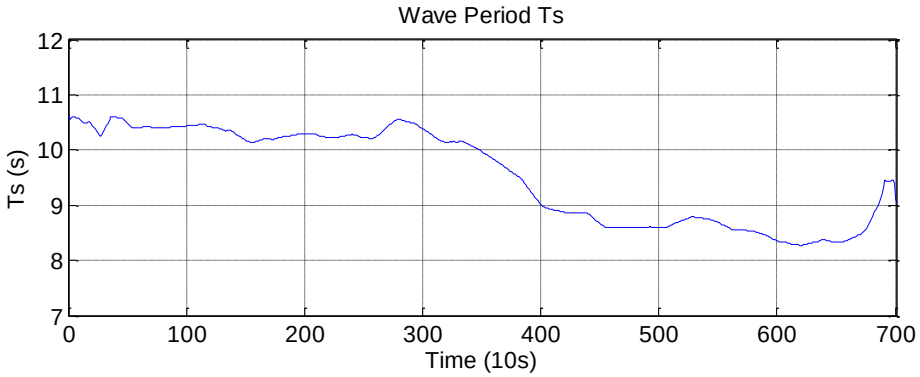

Figure 117 Wave period, Case 3.

The wave period is varies from a value of 8.5 to 10.5 seconds. The hind cast data from the day and the area where the ship is positioned is shown in Table 30. The wave period is around 3 seconds and the direction of the waves is easterly. The data shows no any values larger than 3 seconds which disagrees with results from calculations.

		Wind			Seas		
Date	**Time**	**Dir**	**Deg**	**Range (m/s)**	**Dir**	**Period**	**Range (m)**
31.10.2010	00Z	E	080	2 - 3	ENE	3	0.3 – 0.6
31.10.2010	06Z	ENE	052	3 - 4	ENE	3	0.3 – 0.6
31.10.2010	12Z	NE	038	4- 5	ENE	3	0.3 – 0.6
31.10.2010	18Z	ESE	106	5 - 6	ENE	3	0.3 – 0.6

Table 30 Hind cast data, Case 3.

The wave heading angle is seen in Figure 118. The angle gives following to beam seas.

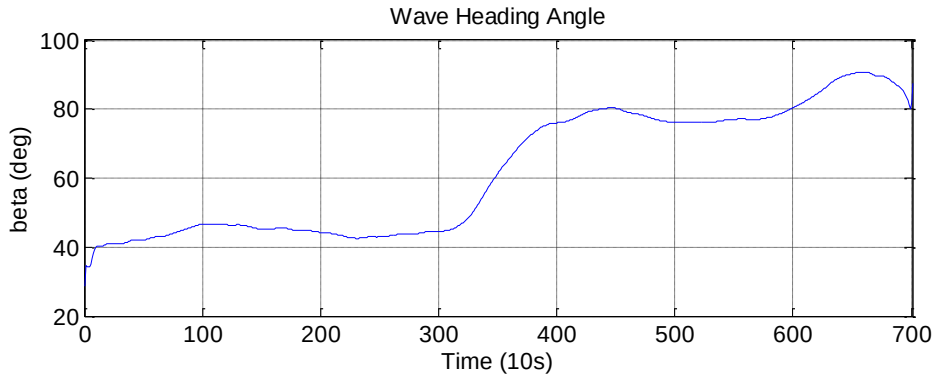

Figure 118 Wave heading angle, Case 3.

The measured bow motions are as in Figure 119.

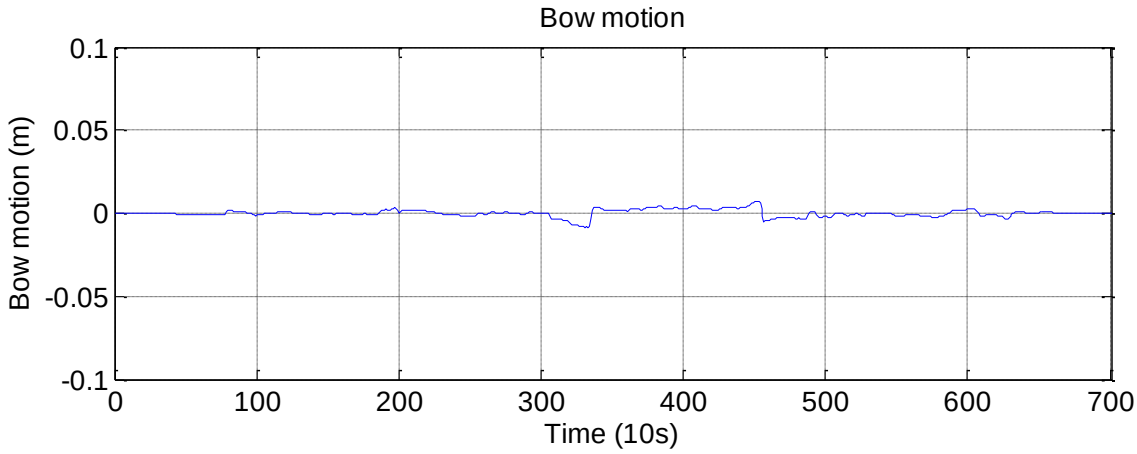

Figure 119 Bow motions, Case 3.

The measured motions are in the area around 0 m with two disturbances in the area of 300 to 500 seconds. By using these data in the wave height calculations and comparing them with the wind speed calculations, results are obtained as in Figure 120.

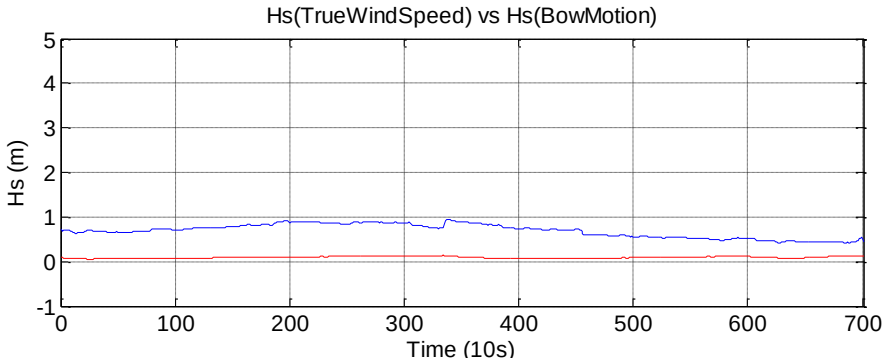

Figure 120 Hs values for two methods, Case 3.

There is reasonable accordance with results from motion and wind calculated H_S with values below 1 m. The H_S values from bow motions capture the two disturbances which were seen in Figure 119.

The calculated wave period does not agree with the hind cast data. The values are in the order of 3 x the hindcast values and they are in the region where the H_S values should be valid, see Figure 115.

Even though recorded motions are very weak, the result for Hs is a valid estimation for the wave height.

9.2.1.6 ***Conclusion***

The three case studies show that H_S(BowMotion) calculations are sensitive to the calculated wave period. When Ts < 7.2 seconds there is discrepancy in results achieved by bow motions vs. results from wind calculations / hind cast data. Case studies 2 and 3 are from the same area with more or less the same environmental conditions. In Case Study 2 there are head seas and in 3 there are following seas and the recorded bow motions are very different, as 2 has larger bow motions than 3. In the head seas case the estimated H_S fails where Ts is below 7.2 seconds.

H_S(BowMotion) is found by only one measured signal, i.e. the motion sensor in the bow and therefore it cannot be compared to relative motions measured by other devices, e.g. pitch motions or vertical bending moments. By comparing two or more signals and implementing sensor fusion it would be possible to identify the most suitable sensor for the wave estimation, Lajic 2010.

The direction of the wave is found by comparing wind direction with ships heading. If the dominant wave direction is different from the wind direction, the calculation of the wave period will be erroneous, which would again lead to erroneous H_S calculations. A method for establishing the wave direction and wave height by using the ship as a wave buoy has been developed by U.D. Nielsen, Nielsen (2005), and by implementing logged signals from more motion sensors on board it will be possible to implement this method in the system.

The wave spectrum is a Pierson Moskowitz spectrum and it can be questioned if this spectrum is appropriate in the area. The spectrum is developed for fully developed sea, based on spectra for the North Atlantic Ocean and the case study area (Case 2) is with limited fetch and not comparable to open sea. The element could be analysed with respect to other spectra, e.g. the JONSWAP spectrum, Fossen (2002).

In Case 2 the responses are very small and therefore non-measureable by the motion sensor in the bow. H_S(BowMotion) is found by Eq. 39 where the variance of the measured bow motion is used with the variance of the calculated motion. The frequency response functions for heave and pitch are based on closed form expressions, see Appendix D, and dependant on the relation between wavelength, λ and ship length, L and further on wave number, *k*.

For $\lambda/L \rightarrow 0$, the wave number $k \rightarrow \infty$ and this will affect frequency response functions will tend to zero, $\Phi_w \rightarrow 0$ and $\Phi_\theta \rightarrow 0$. As the functions are in the denominator in Eq. 39, the calculated wave height will tend towards infinity, H_S(BowMotion) $\rightarrow \infty$ which is shown in Figure 115. Hind cast wave heights are less than 1 m, the value of the period is in the area of 4 seconds and wave length in the area of 25 m.

In Case 3 the wave height is less than 1 m, the value of the period is 3 seconds (hind cast) and the wave length is in the area of 15 m. The calculated T_s shows values considerably higher than values from the hind cast and above 7.2s which results from Case 2 estimates as a valid limit for the H_s calculation. Even though the estimated H_S(BowMotion) is in a valid area, it can be discussed if it is possible to estimate wave heights from bow motions with values around 0.

As the analysis shows, the method used in this section has some limitations in use, which will be considered when the data filtering process is described in Section 10.

9.3 Shallow Water

Entering shallow water the ship encounters added resistance, Carlton (2007)

- when the Froude depth number exceeds 0.7. This number is defined by

$$\mathrm{F_{nh}} = \frac{\mathrm{U_S}}{\sqrt{\mathrm{gh}}} \tag{76}$$

- when the depth to draught (h/T) ratio is less than 4 (independent of F_{nh} effect).

Another approach is given by Barras (2009) where the depth of influence is given as

$$\mathrm{h_i} = \frac{4.44}{\mathrm{C_B^{1.3}}}\mathrm{d}_m \tag{77}$$

The water depth element is based on the following relation, Lackenby (1963):

$$\frac{\Delta U_S}{U_S} = 0.1242\left(\frac{A_M}{h^2} - 0.05\right) + 1 - \left(\tanh\frac{gh}{U_S^2}\right)^{1/2} \text{ for } \frac{A_M}{h^2} \geq 0.05 \qquad (78)$$

The area of the midship section under water is found by a matrix with draught forward and aft used as argument. The element is connected to the system with a 0-junction.

When sailing in shallow waters the Speed Log is still able to measure the speed through water all though there could be disturbances affecting the measured speed i.e. changed water speed below the ship or changes in trim, see Section 6.3.1.The question whether the GPS speed should be used instead in shallow waters could be discussed and it is considered (by the author) that there are too large variations in ground speed due to current - especially in shallow waters – and therefore the Speed Log will also be used as reference here in estimating the Performance Index. This could be exemplified by Figure 121 where the ship is sailing in shallow waters.

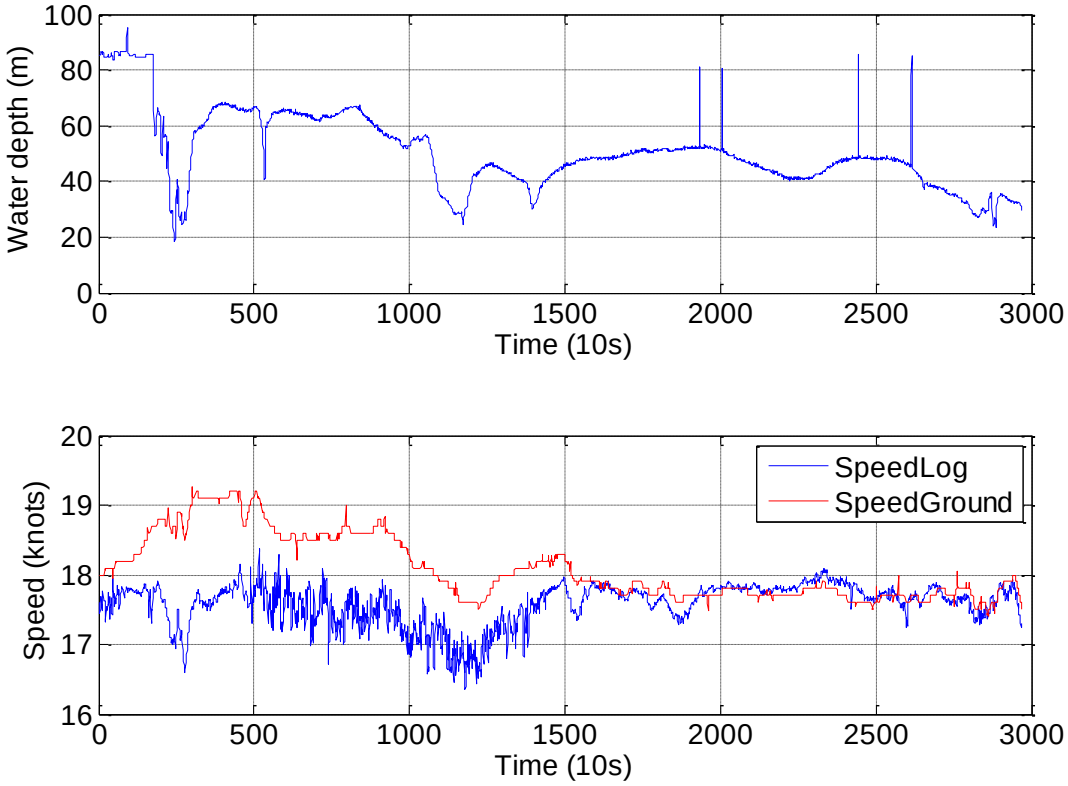

Figure 121 Speed variations in shallow water

From timestamp 0 to 1500 there are the ground speed are higher than the water speed due to current. After timestamp 1500 the two speeds are almost equal. At timestamp 200 the water depth

falls from 85 m to approximately 25 m and the change affects both the ground and water speed by reduced speed. The effect is larger on the water speed than on the ground speed. At timestamp 1100 there is another drop in water depth and in this case the two speeds are affected by the same drop in speed.

A case study is now used to exemplify the effect of the water depth module. The ship is sailing with a mean draught of 13.65 m. According to Eq. 78 the water depth will affect the ship's speed until

$$h \leq \sqrt{\frac{A_M}{0.05}} \leq 108 \text{ m} \tag{79}$$

and by the Barras relationship

$$h_i = \frac{4.44}{C_B^{1.3}} d_m = 101 \text{ m} \tag{80}$$

The influence of water depth on speed reduction is shown in Figure 122. The draught is as mentioned above and the ship's speed is 13 m/s. The speed reduction becomes negative at the value h = 93.85 m (Limit 1).

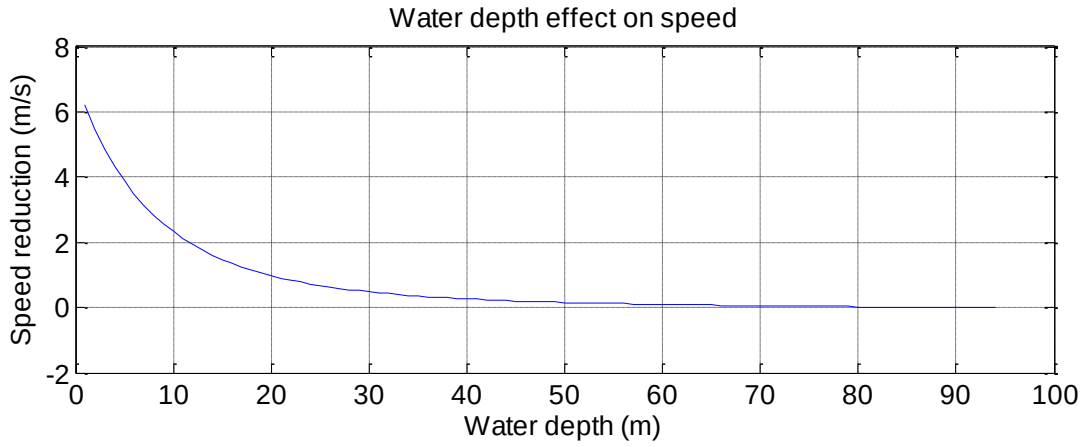

Figure 122 Water depth speed reduction

A case study is used to show the effect of the water depth element on the performance model and indexes. The water depth, the ship's speed and the model speed is shown on Figure 123.

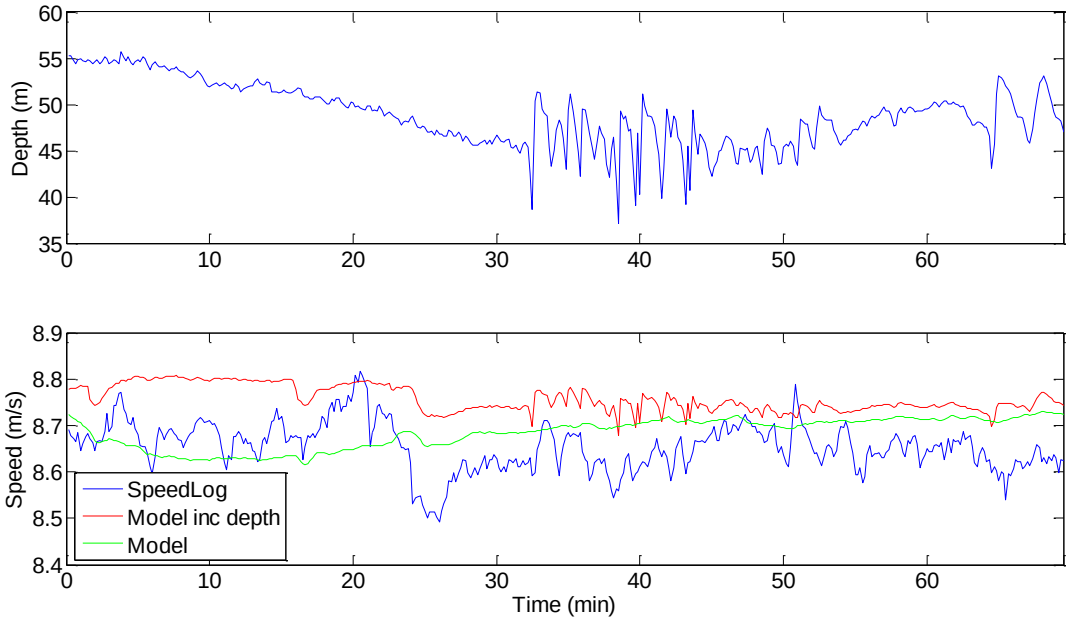

Figure 123 Water depth and speed from ship and models

The water depth is slowly decreasing and between timestamp 30 and 50 minutes there are some fluctuations in water depth which affects the logged and the modelled speed. The model without the water depth element does not capture the variations in water depth. The effect on the performance indexes is shown in Figure 124 and table 31.

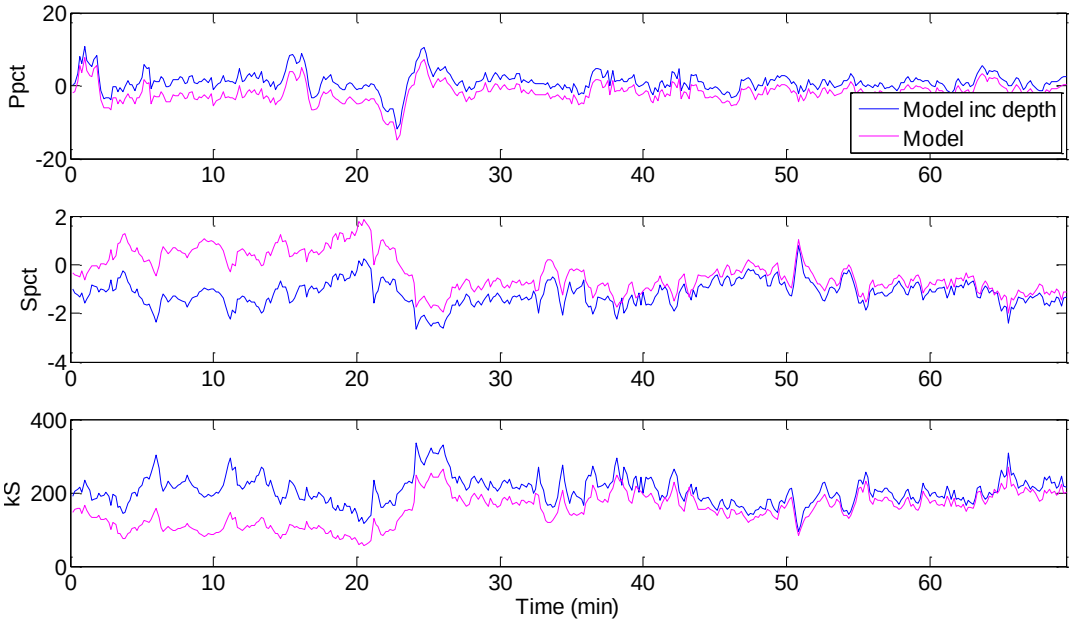

Figure 124 Performance indexes with and without water depth element.

Performance index	Power pct	Model	Model inc depth corr.
Power pct	μ	-1.91	1.03
	σ	2.69	2.67
	Scatter reduction		1%
Speed pct	μ	-0.33	-1.18
	σ	0.78	0.51
	Scatter reduction		35%
kS	μ	153	206
	σ	44	38
	Scatter reduction		14%

Table 31 Water depth influence on performance indexes.

The depth element has a significant effect on the scatter of the speed related indexes where-as on the effect on the torque related index is negligent. The model without the depth element does not capture the increased power consumption when sailing in areas with a low water depth. The model shows a power gain, almost no speed loss and a low roughness value.

Results from this particular case study indicate that the water depth element does to some extent capture

- the speed variation due to variations in water depth.
- the increased power consumption due to sailing in shallow water areas.

There are other issues that should be taken into consideration when sailing in shallow water areas. Entering such areas the effects on the operation of the ship could be as follows, Barras (2009)

- Reduced engine RPM.
- Increased resistance which affects the power consumption, the manoeuvring ability and the ship's speed.
- Change of trim and sinkage

It would be a challenging task to include all effects in a performance model and the available data in this study would not be sufficient to do so. The water depth element is then limited to be used with the following restrictions

- If ΔUS < 0 then ΔUS = 0 (Limit 1)
- If $h < 4T$ then the data are discarded and not used in performance calculations (Limit2)

These limits are inserted in the element in the GES performance model.

9.4 Rudder and Steering

This case study is performed to give an overview of the influence of the rudder movements on the resistance during sailing. A period of approx. two hours from the Bay of Aden on a westerly course is considered with ship's speed as shown in Figure 125 and rudder movements as in Figure 126.

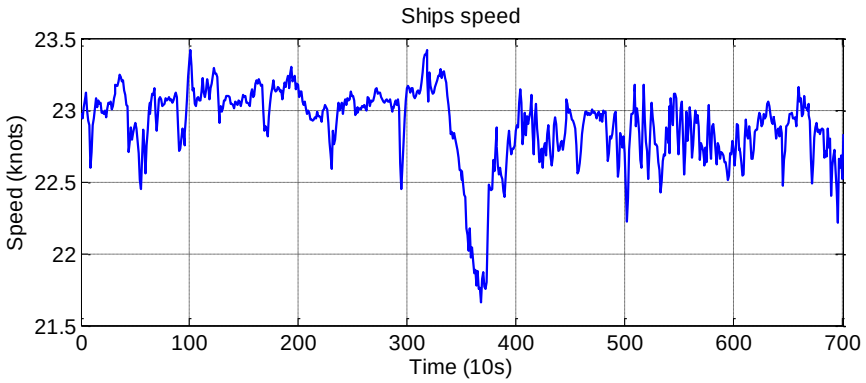

Figure 125 Logged speed

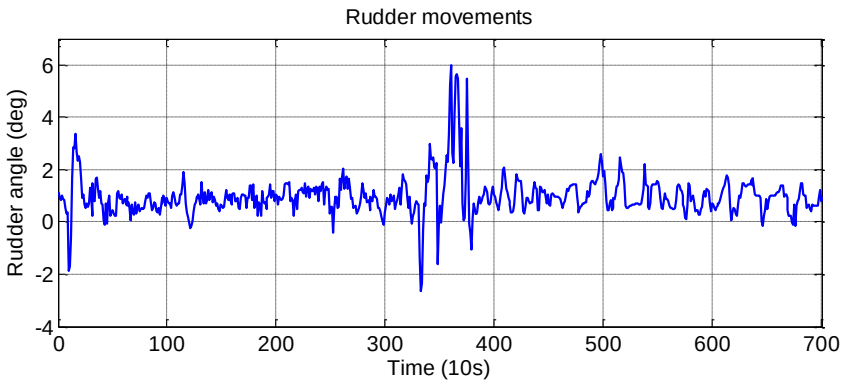

Figure 126 Rudder movements.

Between timestamp 300 and 400 the ship alters course which can be seen on rudder movements and ship's heading, Figure 127.

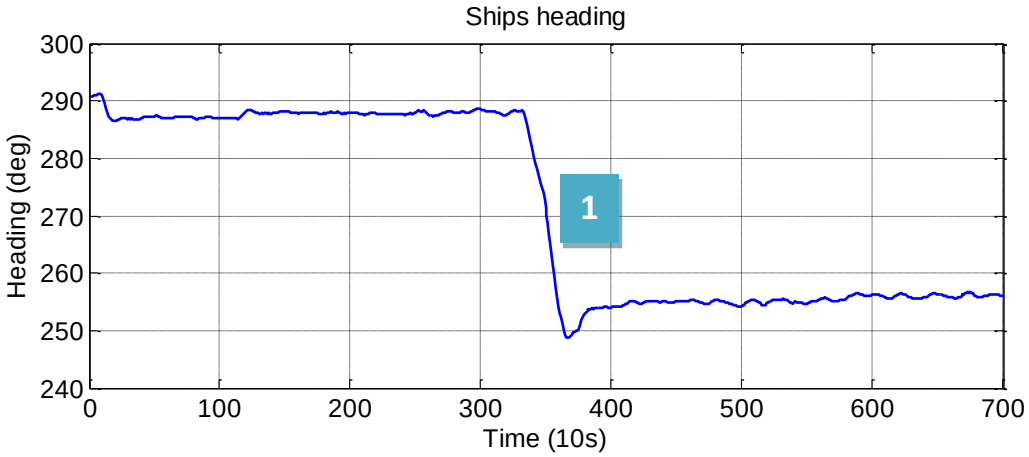

Figure 127 Heading (by gyro compass).

The marked turn (1) is significant and has a significant effect on the ships speed. The change of heading as in Figure 126 is a turn of 38 degrees in a period of 5½ minutes. The turn rate is constant during the turn and has a rate of turn (ROT) value = 6.9° / min. The speed loss due to the turn is 1.6 knots ≈ 0.82 m/s.

According to the GES model including the rudder the speed loss due to these rudder movements is only 0.1 m/s. The correction methods proposed by ISO 15016, see Section 5.3.9, only include constant drift and constant rudder offset and should not be used to determine added resistance due to cyclic rudder movements used in a turn or for course keeping in a seaway. Finding the drift angle in a turn is possible by assuming that the previously mentioned turn can be approximated as a steady turn where the ship is taking a circular movement. The rate of turn, *ROT*, can be found by

$$ROT = \frac{d(\Psi)}{dt}\frac{\pi}{180}\left[\frac{rad}{s}\right] = \frac{U_S}{R} \tag{81}$$

where Ψ is the ship's course, U_S is the ships speed and R is the turning radius. The turning radius can be used to find the drift angle

$$\alpha = \text{asin}\left(\frac{½Lpp}{R}\right) \tag{82}$$

here assuming the pivot point to lie in the bow.

The turn in Figure 3 will induce a drift angle of approx. 1°5 when the turn has a steady value. The R_α function is plotted with the R_δ function as shown in Figure 128.

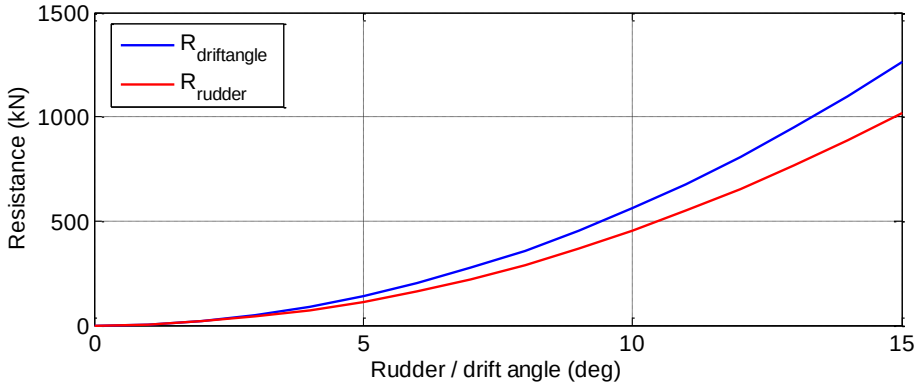

Figure 128 Resistance induced by rudder movements and drift angle.

The angles are rudder angle and drift angle respectively and the resistance is given in kN. The angle limit is set to 15°, which is the maximum drift angle for most merchant ships at full helm, Clark (2005). For the rudder the maximum rudder angle is in the order of 35 - 40° for most merchant ships. In the present case the ship's draught is 12.65 m and the speed is 23 knots. It is assumed that the speed is constant during the turn.

The effect of the rudder movements is implemented as an element in the GES model. Results from the case study with for speed are shown in Figure 129.

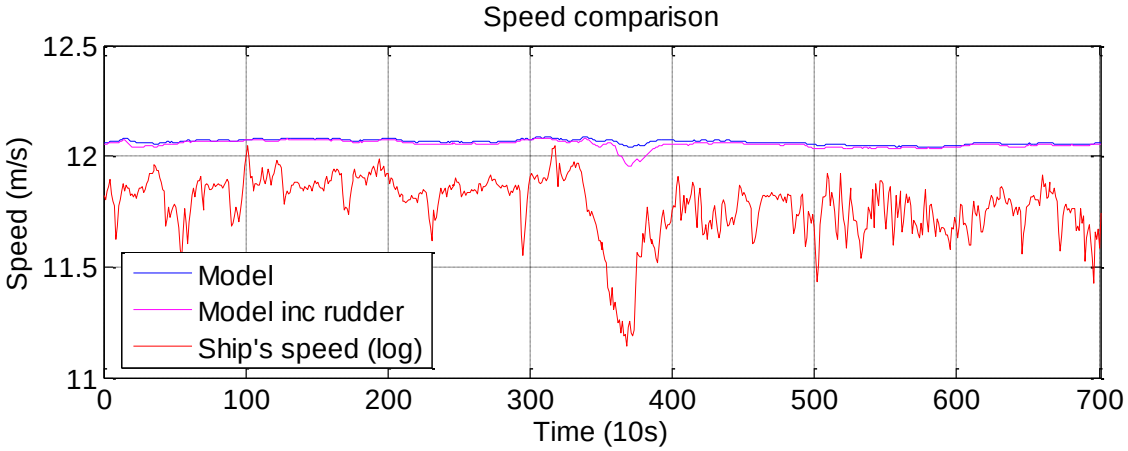

Figure 129 Ship's logged speed vs model speed.

The rudder movements are identifiable in the results from the model including rudder, the turning incident is clearly marked and the constant rudder offset is indicated by the added resistance and hence lower speed in the results from the model including rudder. The influence on the performance indexes is shown in Figures 130, 131 and 132 and in Tables 32, 33 and 34.

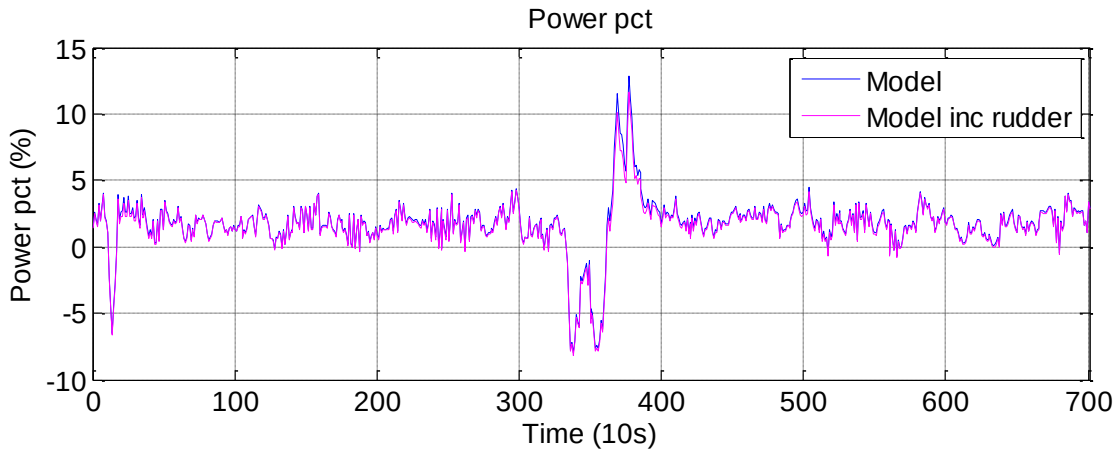

Figure 130 Power pct comparison.

Power pct	Model	Model inc rudder
Mean	1.738	1.581
Std deviation	2.06	1.983
Scatter reduction		4%

Table 32 Power pct comparison.

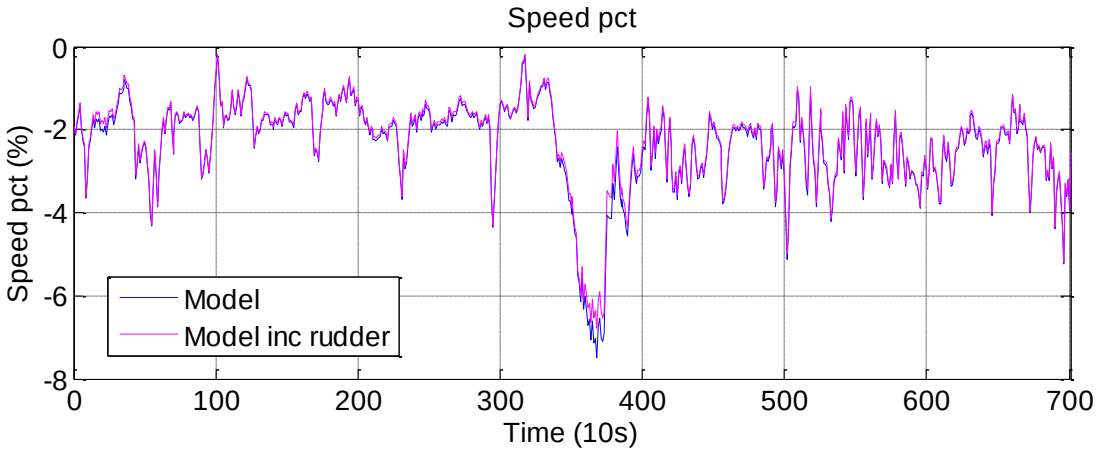

Figure 131 Speed pct comparison

Speed pct	Model	Model inc rudder
Mean	-2.366	-2.283
Std deviation	1.085	1.033
Scatter reduction		5%

Table 33 Speed pct comparison.

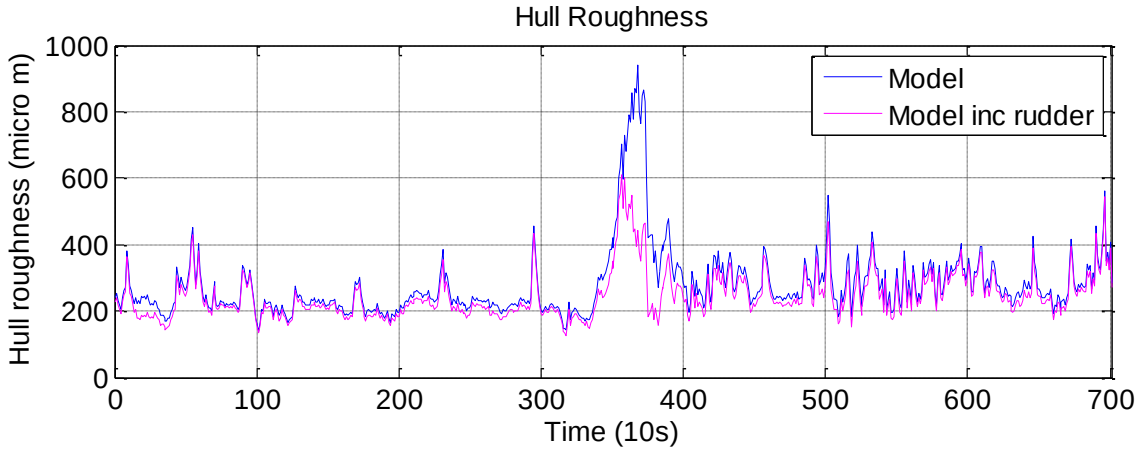

Figure 132 Hull roughness comparison

kS	Model	Model inc rudder
Mean	278.8	246.4
Std deviation	106.3	70.42
Scatter reduction		34%

Table 34 Hull roughness comparison.

The results show that when the rudder is modelled and implemented in the GES performance model there is an effect on the performance indexes. Mean values are reduced and so is scatter in the results. Especially as regards the hull roughness values there is a large reduction in scatter (34%).

The study also shows that to be able to capture the resistance caused by steering it is necessary to include the motions of the vessels. By measuring yaw and sway motions and by knowledge of the hydrodynamic coefficients, the resistance terms including the dynamics of the ship could be found. This would lead to a more accurate ship model which would be able to capture the dynamics of the ship not only during manoeuvring situations but also during normal operation.

The hydrodynamic coefficients are normally found by towing tank tests, CFD calculations or empirical formulas. These data are not very often available or accurate enough and would have to be found another way e.g. by

- introducing data with a shorter sampling time, see Section 7.1.
- introducing neural network techniques, as Yoon & Rhee (2003)
- selecting data with little environmental disturbances and feeding these to the network

This method has shown good results and would be valid to introduce to the estimation of hydrodynamic coefficients.

10 Performance Analysis – Filtered Values

The following performance analysis and subsequent data filter identification are based on the data from m/v "Clementine Maersk" through 2010. The logged data are first processed before given as input in the GES performance system, Table 35.

The routines in the initial data handling step are described in Section 7. First spikes and outliers are removed and the drift in timestamp is identified and removed. Then a conversion of some of the data is initiated to fit the data to the element where it should be used as input e.g. wave height element or wind resistance element. The routines are described with reference to the logged data on board m/v "Clementine Maersk" but can be used in general to prepare the data as input to a Performance System.

GES Parameter	Logging interval	Initial step	Conversion
Ship Time	10 s	Remove spikes and outliers Consolidate data to uniform time stamp	Logging interval
Latitude	10 s		
Longitude	10 s		
Air temperature	10 s		
Air pressure	10 s		
Sea water temperature	10 s		
Water depth	10 s		
True wind speed	10 s		10 min average
True wind direction	10 s		10 min average
Encounter period	10 s		20 min average
Bow velocity	10 s		Value – running mean
Bow movement	10 s		
Draught mean	24 hrs		
Draught fore	24 hrs		
Draught aft	24 hrs		
Heading	10s		
Rudder angle	10s		
Stabilisers port	10s		
Stabilisers starboard	10s		
Speed ground	10s		
Speed log	10s		None / 20 min average
ME power pct	10s		
ME power	10s		
Shaft torque	10s		
ME RPM	10s		
Shaft motor	10s		

Table 35 Parameters logged on board Clementine Maersk.

10.1.1 **Data Filtering**

After the first data handlings steps, the data are sorted in weekly log files. The data are then filtered as in Table 36.

Coarse filtering	Effect on system
ME Power pct > 30 %	Avoid manoeuvring conditions. Stay inside the limitations of the power curve. Minimise environmental influence.
True wind speed < 10 m/s	To avoid heavy seas.
Water depth > 60 m	To avoid significant water depth effects

Table 36 Coarse filtering of data

The limitations in the modelling and the data quality would require additional filtering in order to achieve reliable performance indexes. In order to identify the periods where the ship can be considered to be close to a quasi-static condition a test case is chosen in the Bay of Aden. The period has a length of one day and the ship's (westbound) track is shown in Figure 133.

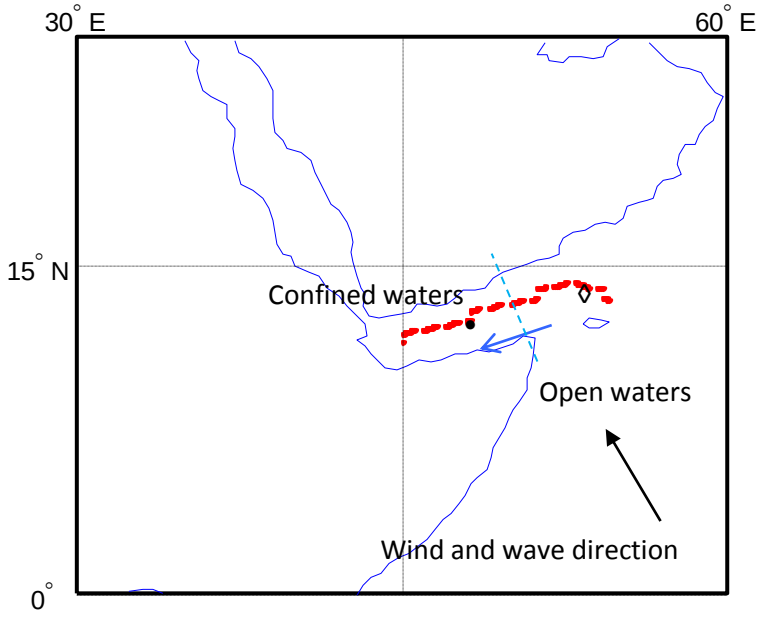

Figure 133 Bay of Aden case study.

The ship comes from open waters (the Indian Ocean) into confined waters (the Bay of Aden). Two incidents are chosen to exemplify the filtering to steady conditions. A period with little variations in

data (stable period, mark • in Figure 133) and a period with larger variations in data (an unstable period, mark ◊ in Figure 133) of five minutes are identified in the one day time series. The two periods are chosen to examine the relation in between all parameters used in the performance evaluation. The governing parameters with reference to the two conditions are shown in Figures 134 – 136.

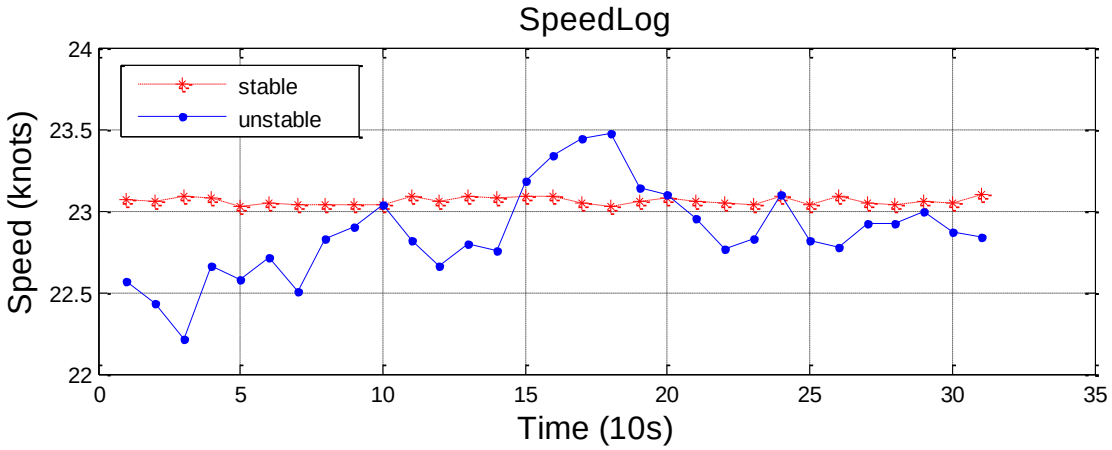

	Stable	Unstable
μ	23.06	22.87
σ	0.02	0.28

Figure 134 Stable / Unstable conditions for logged speed.

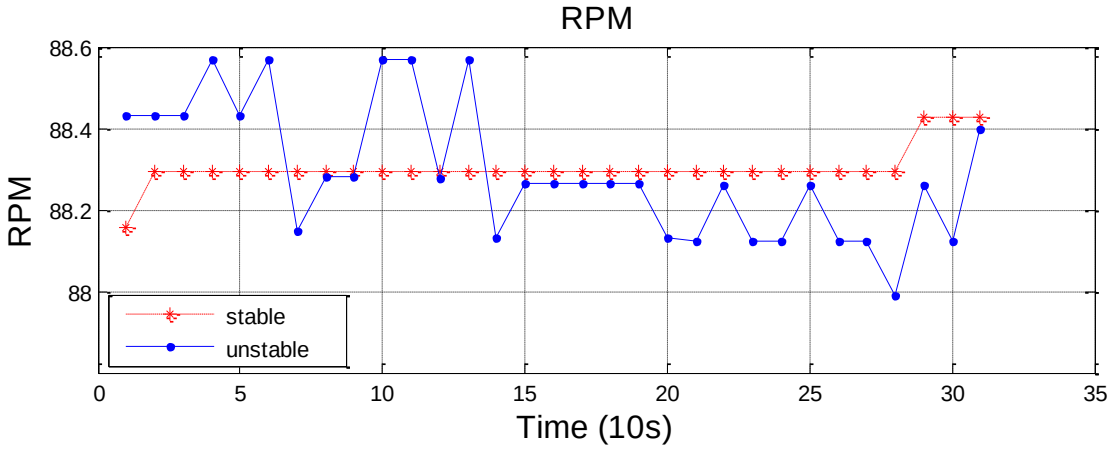

	Stable	Unstable
μ	88.3	88.3
σ	0.05	0.16

Figure 135 Stable / Unstable conditions for engine RPM.

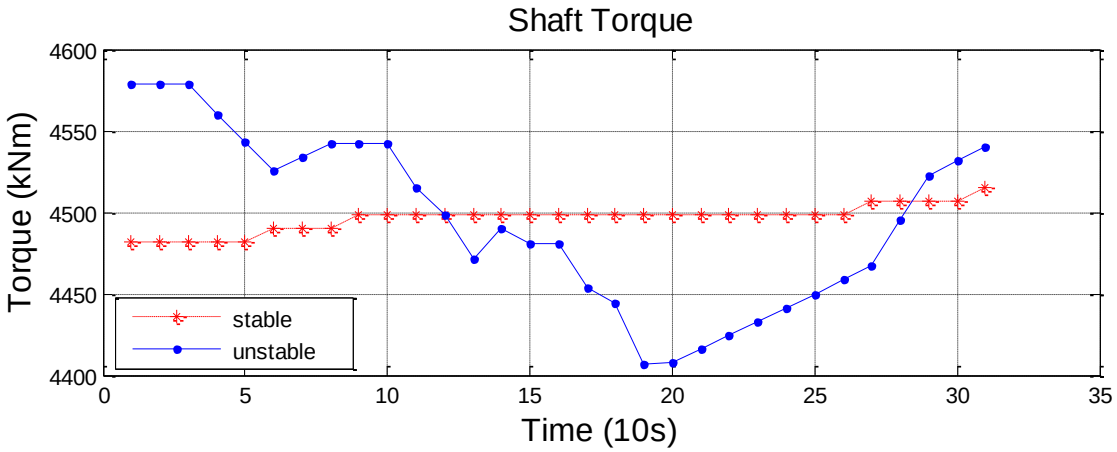

	Stable	Unstable
μ	4497	4495
σ	8	53

Figure 136 Stable / Unstable conditions for shaft torque.

When these three parameters have a steady value, the rest of the input parameters are also stable. The effect on the performance indexes is shown in Figures 137 to 139.

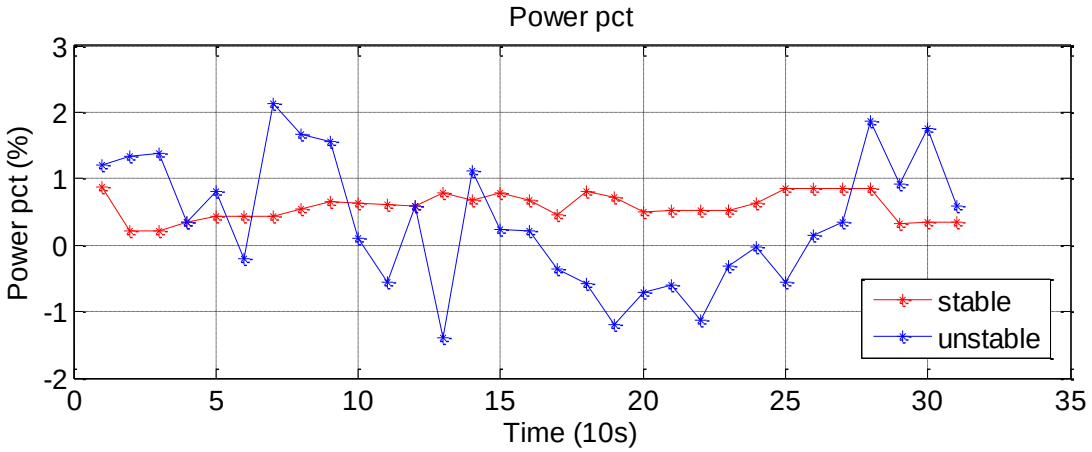

	Stable	Unstable
μ	0.58	0.35
σ	0.2	1.0

Figure 137 Conditions effect on Power pct index.

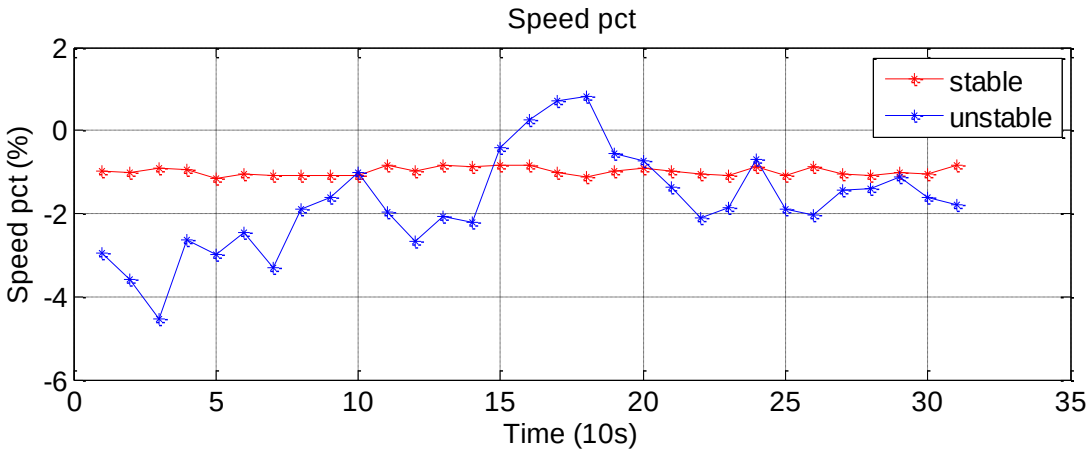

	Stable	Unstable
μ	-0.99	-1.71
σ	0.1	1.2

Figure 138 Conditions effect on Speed pct index.

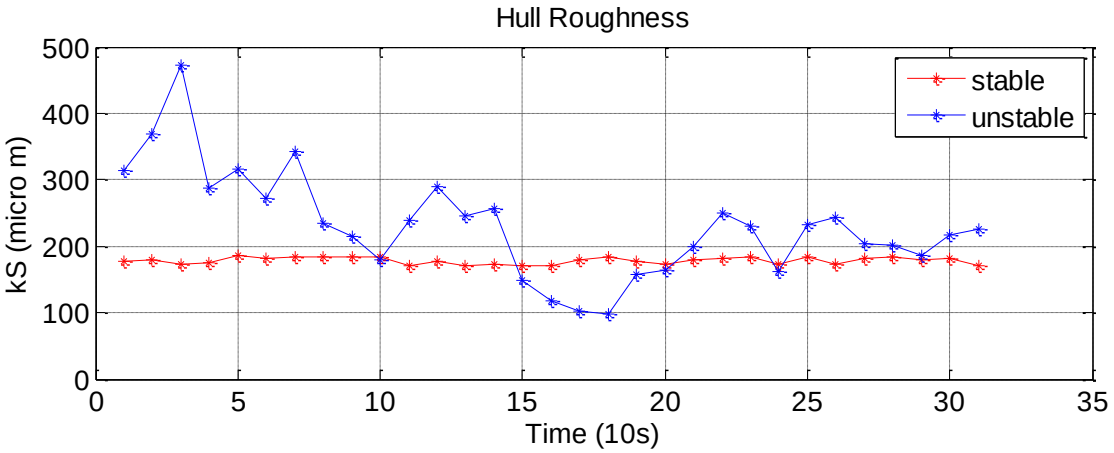

	Stable	Unstable
μ	178	231
σ	5	98

Figure 139 Conditions effect on Hull roughness index.

The variation in performance index follows the variation in input parameters i.e. large scatter in input parameters will lead to large scatter in performance indexes. Concerning a reliable result for a

performance index, this analysis proves that stable periods will give the best result when it comes to variation in index. Another approach could be to investigate the slope of the data curve plot. The data which are used for the filtering are the speed log and the torque data.

The logging interval of the data is set to 10 seconds in this case study and does not fully describe the dynamics of the vessel but the variations in data will to some extent capture these effects. A function describing the slope of the data curve plot ($\frac{dF}{dx}$) can be established where the function describes the slope over a moving window. The slope of the stable / unstable data is plotted in Figure 140 and the result shows that the slope is affected by the variation in data.

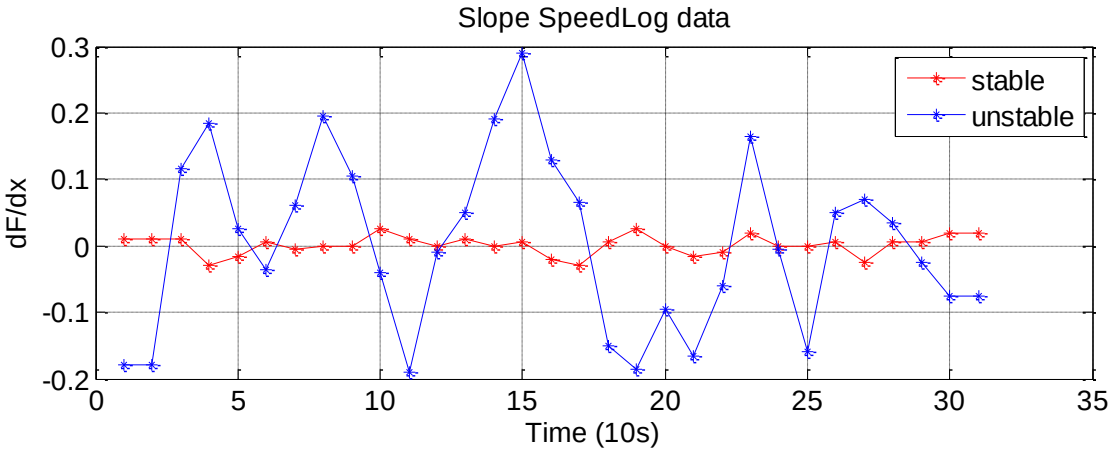

Figure 140 Conditions effect on slope of speed log curve.

A filtering function can now be established based on the previous definitions:

- Filter 1 stable period
- Filter 2 slope filter

With regard to Filter 1 the stable periods are found by evaluating the σ of the ship's log and torque meter. The conditions shown in the stable period described in the previous section are not often to occur and if the five minutes period is to be extended to longer intervals, it becomes impossible to find matching conditions.

The logging period is tested with filter values as in Table 37.

	ShaftTorque	SpeedLog
σ	<=0.5 % of logged torque	<=0.4 % of logged speed
dF/dx		-0.08 <= dF/dx <= 0.08

Table 37 Filter values referring to shaft torque and speed log

The filter period is varied in intervals of 5, 10, 20 and 30 minutes.

The former test case is used to show the effects on the performance indexes. For simplification the k_S value is the performance index that is used to indicate the effect of the filter.

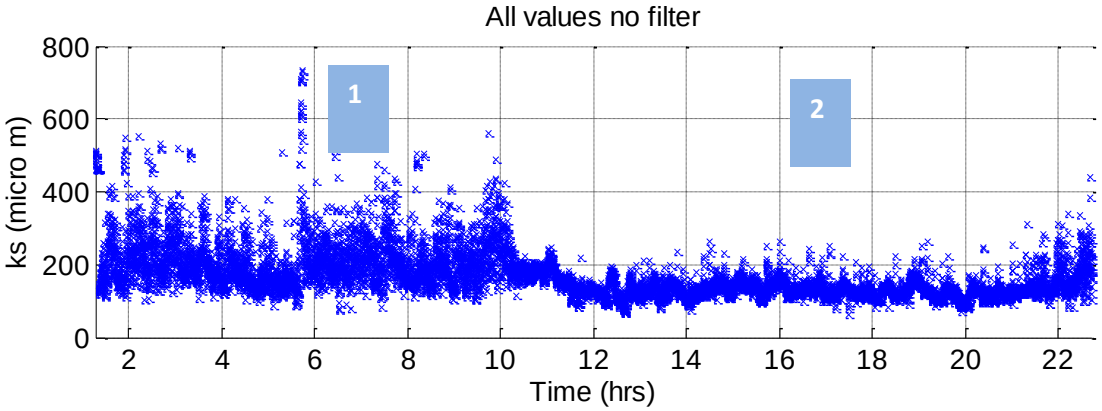

	k_S
μ	174
σ	70

Figure 141 Hull roughness index unfiltered data.

Figure 141 shows the k_S index over the test case period. The scatter in the index is high when the ship is sailing in open waters (marked 1 in Figure 141) and it falls to a steady value when entering confined waters (marked 2 in Figure 141). When applying the filters over various periods the results are as seen from Figure 142.

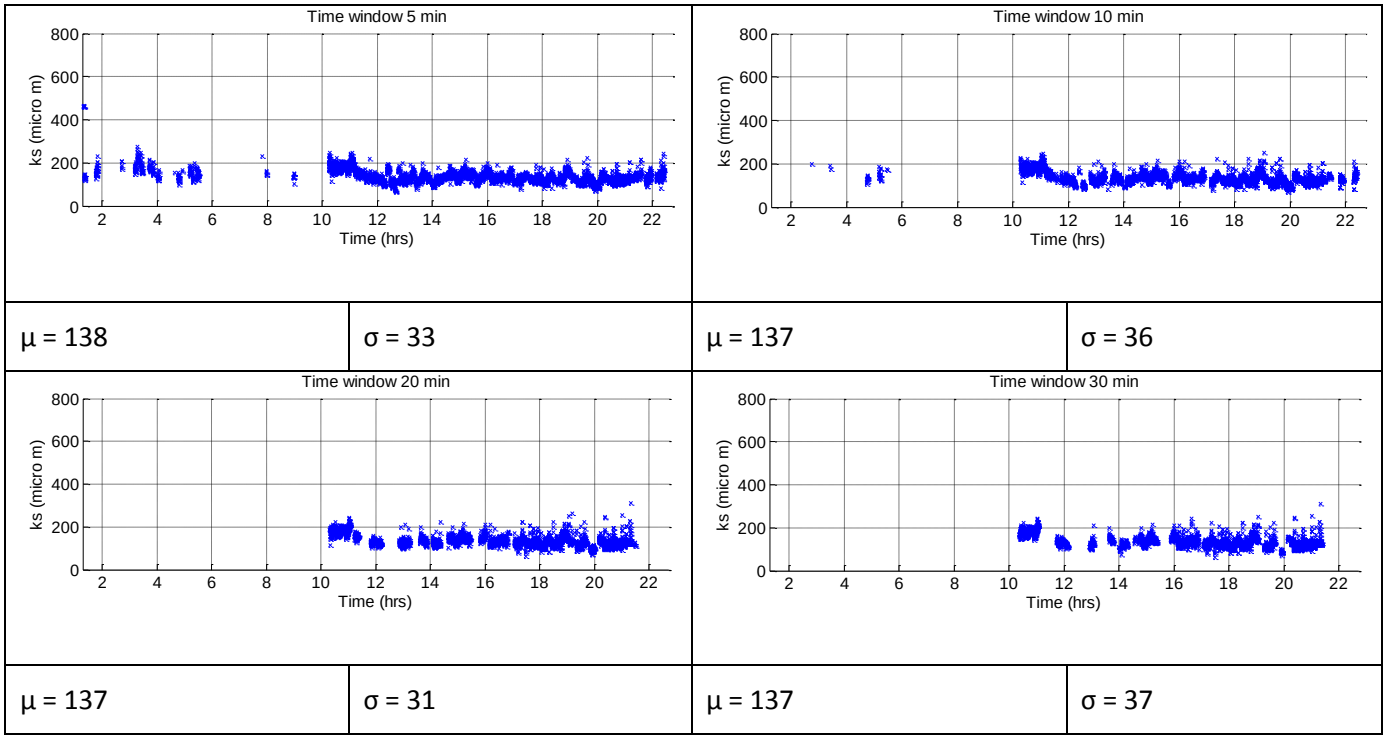

μ = 138	σ = 33	μ = 137	σ = 36
μ = 137	σ = 31	μ = 137	σ = 37

Figure 142 Filter effect on hull roughness index with various time windows.

In this case the mean values are not affected by the period length and the standard deviation is more or less unaffected, with a tendency towards being better at 5 and 20 minutes. The number of data point is decreasing when the period is extended, which is expected. This has to be taken into consideration when choosing filter values.

10.2 2010 Case study m/v "Clementine Maersk"

An analysis of the data received through 2010 from m/v "Clementine Maersk" will now be used to examine the effects of the improvements on the model and the effect of using filters on the data. The model including elements described in Section 9 is as in Figure 143.

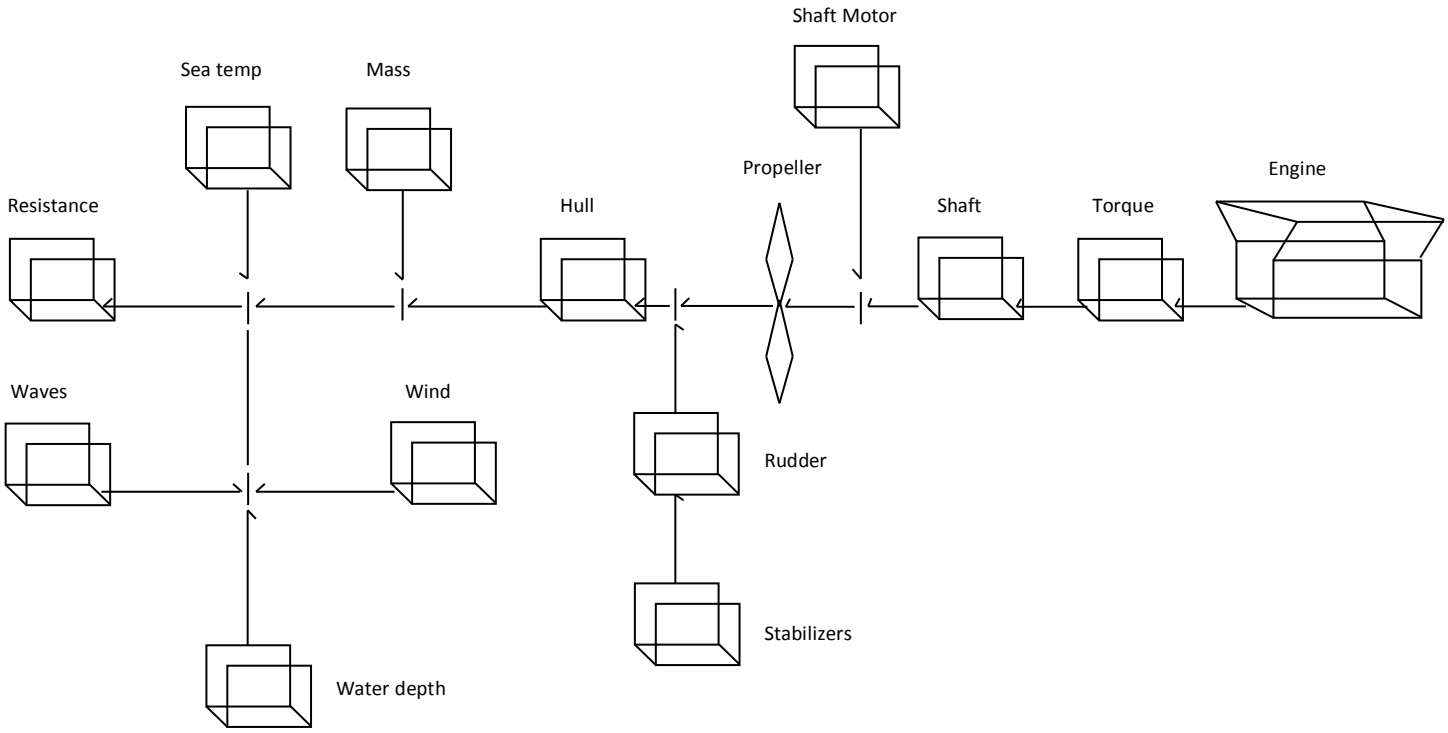

Figure 143 GES Performance Model

Four models are used in the analysis

1. Extended model – as in Figure 143.
2. Extended model – Waves and Wind element substituted by Townsin/Kwon combined Wind & Waves element.
3. Basic model – used in Section 8.
4. Extended model – Wind element substituted by the Fujiwara Wind element.

Initial filter values are

- Window length 30 minutes
- Boundaries $\sigma < 0.2\%$ of Speed Log values

The data are separated in two parts – one part before a propeller polish (blue) and one after a propeller polish (red).

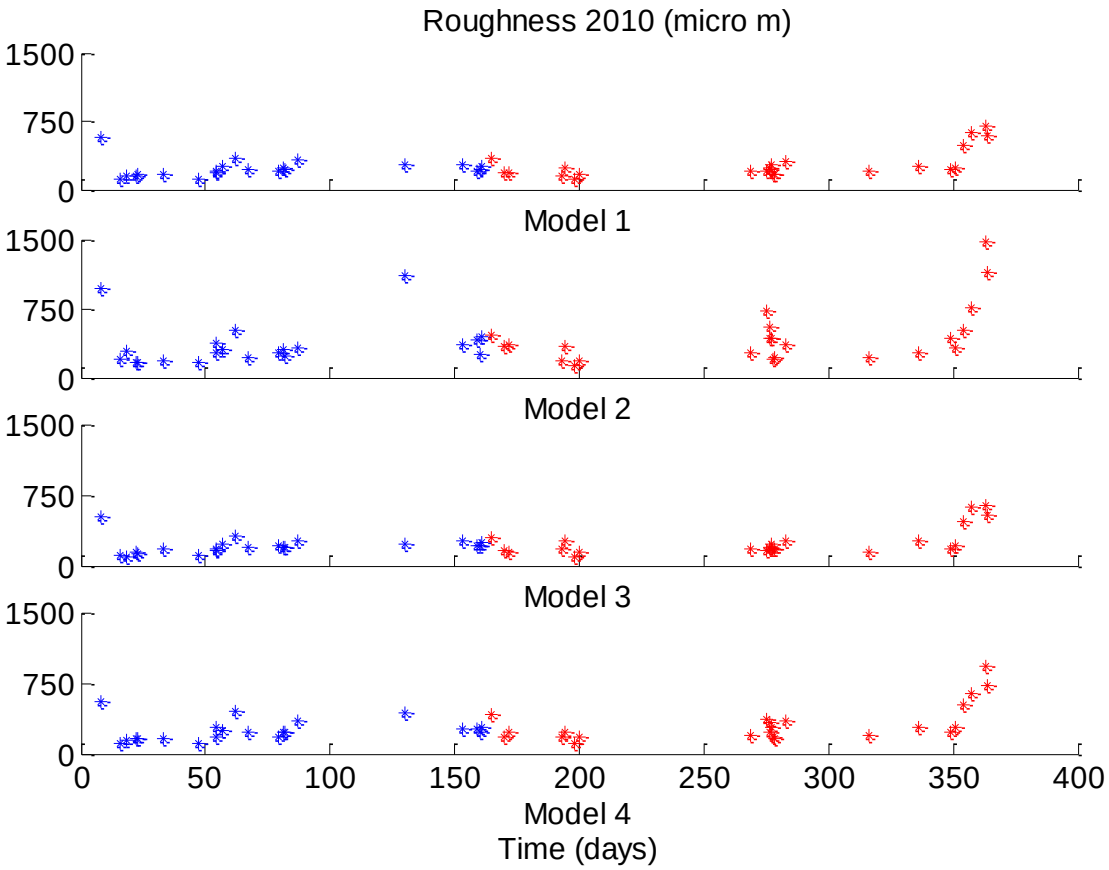

Model	μ1	μ2	σ1	σ2
1	230	280	97	160
2	360	446	246	320
3	211	258	89	155
4	250	324	113	203

Figure 144 Roughness values 2010.

Comments on

μ The values are lower before the polish than after, which is due to the rather large values in the last part of the period.

σ As for the mean, the σ values are larger after the polish than before. With reference to the scatter around the mean, model no. 3 is the best performing model.

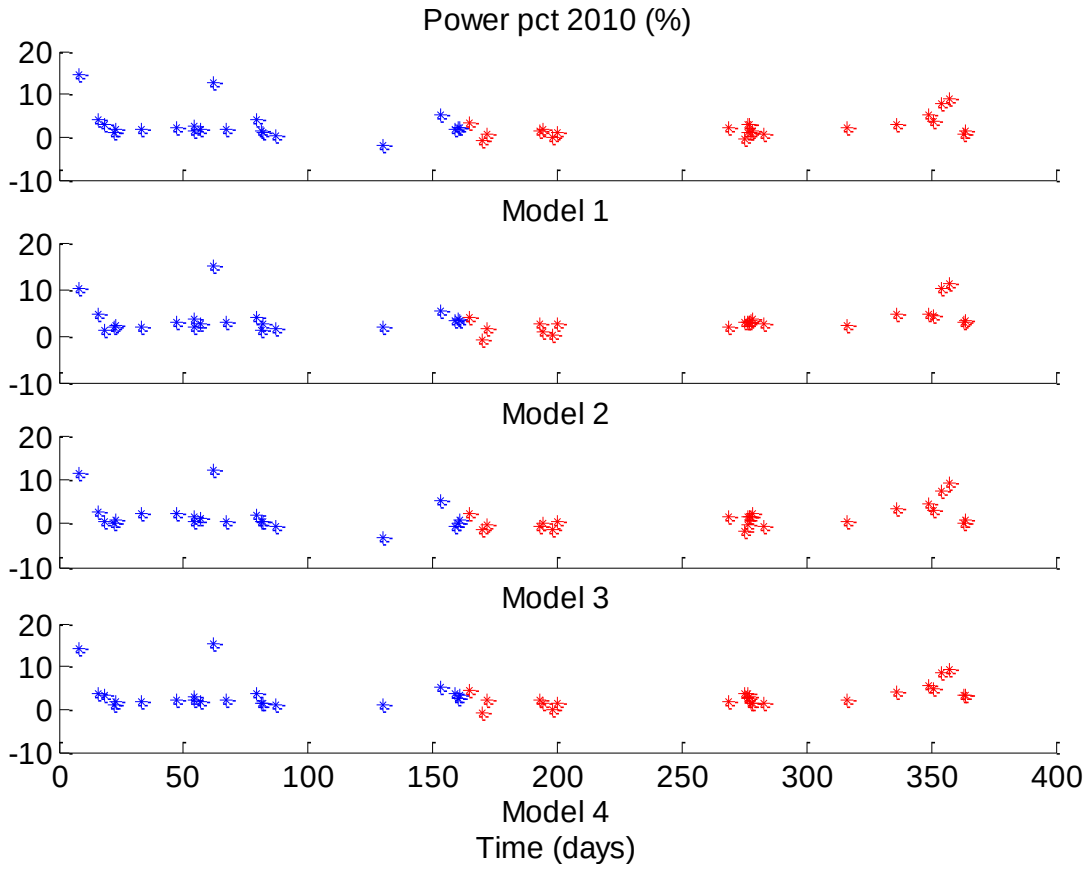

Model	μ1	μ2	σ1	σ2
1	3.11	2.24	3.82	2.38
2	3.72	3.37	3.22	2.64
3	1.90	1.40	3.61	2.68
4	3.57	3.08	3.88	2.38

Figure 145 Power pct values 2010.

Comments on

μ The values are higher before the polish than after. This would be expected if the propeller clean has a visible effect on the shaft torque measurements. A few outliers with very high Power pct values is also the reason in this case.

σ As for the mean, the σ values are larger before the polish than after. With reference to the scatter around the mean, Model no. 2 is the best performing model.

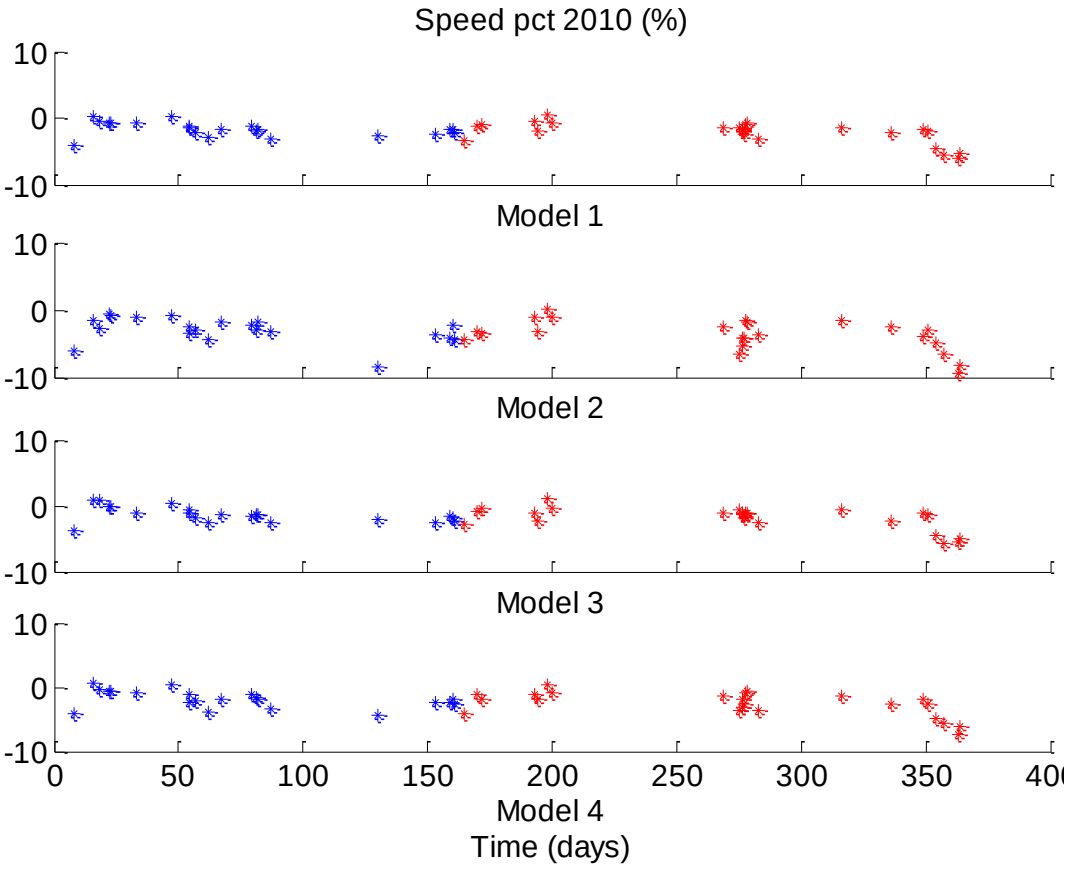

Model	μ1	μ2	σ1	σ2
1	-1.62	-2.20	1.11	1.70
2	-2.96	-3.72	1.87	2.31
3	-1.31	-1.87	1.19	1.76
4	-1.85	-2.65	1.37	1.92

Figure 146 Speed pct values 2010

Comments on

μ the values are higher after the polish than after. As for the k_S values this is due to a large scattered area with high values at the end of the period.

σ as for the mean, the σ values are larger before the polish than before. With reference to the scatter around the mean, Model no. 2 is the best performing model.

To verify and to eliminate some of the scatter in the results it will be necessary to determine the correlation between input parameters and the performance indexes. Figures 147 to 149 show the correlation between the indexes and the input parameters of draught, trim, bow velocity and rudder angle (mean values).

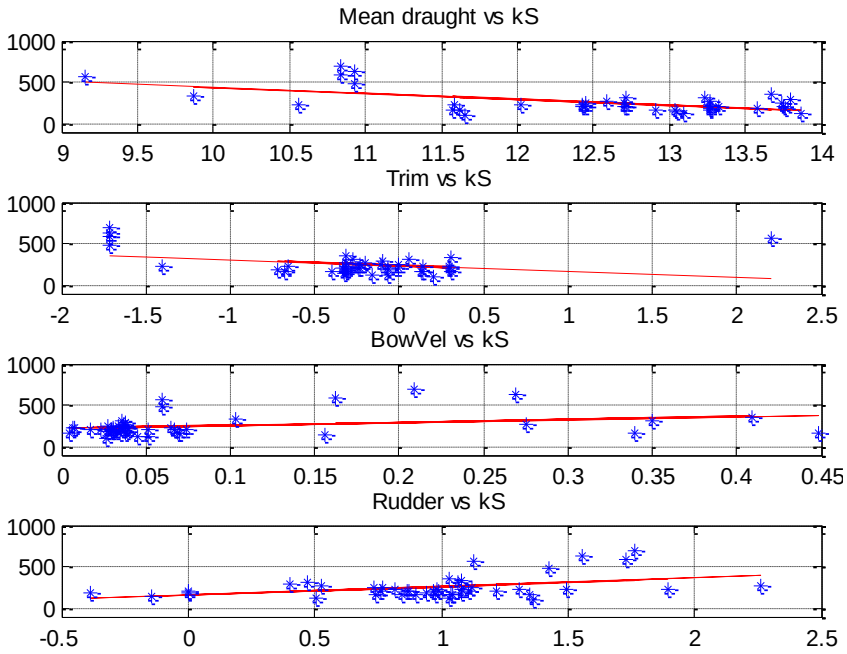

Figure 147 Roughness correlation

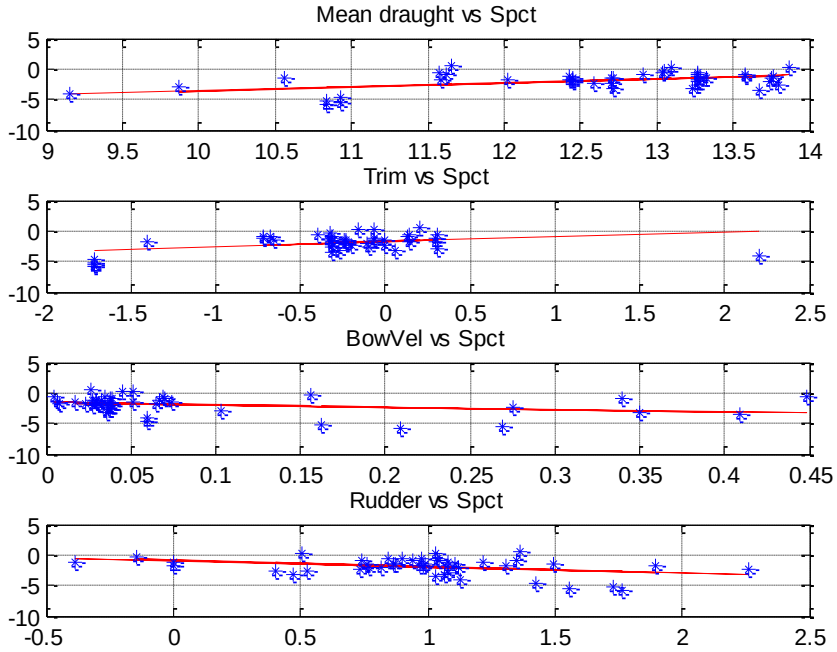

Figure 148 Speed Pct correlation

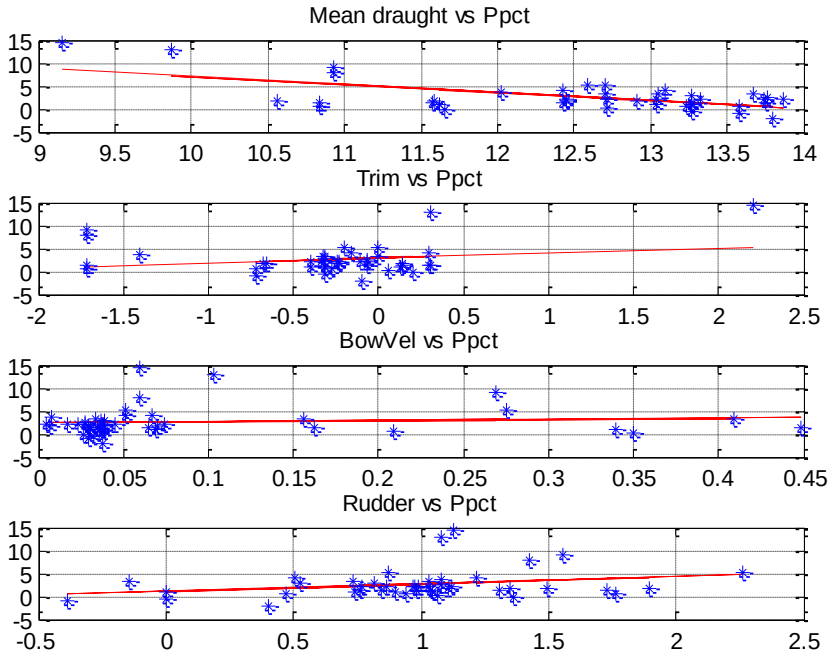

Figure 149 Power Pct correlation.

The indexes correlate with parameters as

- Low draught values create higher index values
- Larger negative trim creates higher index values
- Higher bow velocity creates higher index values
- Larger rudder angles create higher index values

This will lead to a further analysis of the specific cases to verify the above mentioned correlation. The cases are analysed with respect to k_S values (with reference to the speed log) and Power Pct values (with reference to the shaft torque meter). It is considered that the index Speed Pct will correlate to the same parameters as k_S.

9 incidents are chosen for identification, Figure 150. The incidents are marked with different colours depending on characteristics of the correlation.

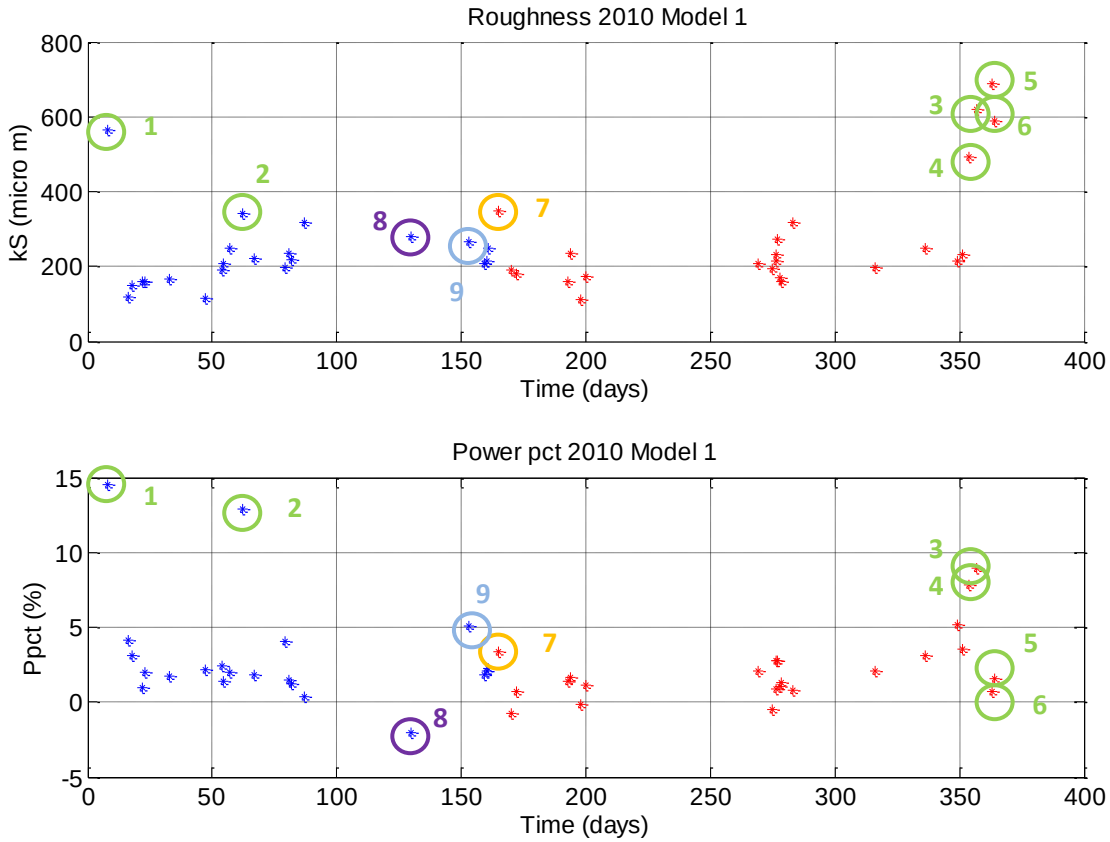

Figure 150 Incidents which cause large scatter in index.

10.2.1.1.1 Cases 1 to 6

In an earlier analysis (Section 8) it was established that operational conditions where the draught mean (d_m) is low would create outliers in the performance index. Figure 149 shows that there are some incidents where this is the case. Incidents 1 to 6 are obvious when considering the k_S values and 2 is obvious when considering the Power Pct value. The operational values and indexes for the six cases are as in Table 38.

	dm	trim	k_S	Power Pct	Speed Pct
1	9.15	2.2	565	14.6	-4.2
2	9.9	0.3	342	14.9	-2.8
3	10.9	-1.7	492	7.8	-4.6
4	10.9	-1.7	620	8.9	-5.6
5	10.9	-1.7	689	0.7	-5.9
6	10.9	-1.7	590	1.5	-5.3

Table 38 Incidents with low draught and large negative trim values.

In Cases 1 and 2 the draught is below 10m and in Cases 3 to 6 the draught is around 11 m but the trim is negative with a high value. The index related to the shaft torque (Power Pct) and the indexes related to the logged speed (k_S and Speed Pct) are not consistently sensitive to the same conditions in the various cases. In Case 2 the Power Pct has a very high value where k_S and Speed Pct have not and in Case 5 & 6 the opposite is the case.

In case 3 & 4 and case 5 & 6 the load condition is the same. The power consumption varies though and to look for parameters that could justify the difference in Power Pct a series of values are listed in Table 39.

	β_0 (0° head seas)	β_{RW}	U_{RW}	Hs_{wind}	ubow	Rwind	Rwave	Rtotal
Case 3&4	155°	10°	7m/s	0.2m	0.06m/s	35 kN	12 kN	1.1e3 kN
Case 5&6	18°	5°	18m/s	1.1m	0.21m/s	135 kN	30 kN	1.6e3 kN

Table 39 Environmental and resistance parameters.

Cases 3 and 4 have estimated following seas and wind, negligent wave height and bow movements.

Cases 5 and 6 have estimated head seas and wind, approx. 1 m wave height and larger bow movements.

With regards to Power Pct: In Cases 5 and 6 the model compensates for the (head sea) environmental effects until a reasonable level of power consumption.

In Cases 3 and 4 the model over compensates for the environmental effect i.e. the ship uses too much power compared to the model prediction.

With regards to k_S and Speed Pct:

In all four cases the speed of the ship is too low compared to model prediction.

Cases 1 and 2 are also analysed and results are as indicated with regards to the above mentioned. In the analysis in Section 8 one of the results was that all low draught cases were filtered out. Even though the model tests also cover this area of the draught scale the results here in this analysis indicates that performance analyses from this area of operation should be used with caution.

10.2.1.1.2 Case 7

Case 7 is the first reported incident after the propeller polish. The index values are higher than expected as regards the subsequent values and as regards expected performance with a polished propeller. The model indicates higher power consumption and lower speed than expected and by analysing the parameters the following results are achieved.

In Section 5.3.3 a filter for the estimated H_S was established:

Ts < 7.2 s Estimated H_S from wind speed

Ts > 7.2 s Estimated H_S from closed-form expressions

In this case the conditions were as presented in Table 40.

	B_{TW}	U_{TW}	Ψ
	263°	1.5m/s	288°
	Ts [s]	**Hs** [m]	β_0
Wind generated		0.1	25°
Closed Form	7.1	3.0	
Hind Cast	9 - 13	3.0	85°

Table 40 Wave information Case 7.

The calculated wave period is just below the H_S filter value and therefore Hs_{wind} is used to calculate the wave resistance. The Hs_{CF} value agrees with the hind-cast swell values and if this value is inserted in the performance calculations the index values would be as in Table 41.

	k_S	Power Pct	Speed Pct
Hs_{wind}	347	3.4	-3.4
Hs_{CF}	219	0.4	-1.72

Table 41 Performance indexes with two different wave heights, Case 7.

10.2.1.1.3 Case 8

Case 8 is the only incident in May. The Power pct value is rather low compared to expectations and in this case the conditions were as presented in Table 42.

	β_{TW}	U_{TW}	Ψ
	148°	10.5m/s	161°
	Ts [s]	**Hs** [m]	β_0
Wind generated		2.5	013°
Closed Form	3	-	-
Hind Cast	No data for this area		

Table 42 Wave information, Case 8.

The wind speed indicates a wave height of 2 to 3 m but by comparing the ships motions in the bow with case 7 where the H_S is estimated to be around 3 m and as well as head seas it is seen that the motions in the bow do not justify the estimated Hs_{wind}, Table 43.

$\mu_{ubow\ 10.05.2010}$	$\mu_{ubow\ 14.06.2010}$
0.04	0.41

Table 43 Vertical velocity bow, Case 8.

The ship is sailing within a confined area (the Red Sea), Figure 151 where the waves are short (approximately λ = 15 m according to estimated T_S) and heights are not as high as the wind speed would justify.

Figure 151 Ship's position (white circle), Case 8.

By inserting wave height of an estimated 0.5 m the index values will now be as in Table 44.

	k_S	Power Pct	Speed Pct
Hs_{wind}	281	-2.1	-2.7
Hs estimated	336	0.9	-3.4

Table 44 Performance indexes with two different wave heights, Case 8.

10.2.1.1.4 Case 9

Case 9 is one of the incidents in June just before the propeller polish. The k_S value and Speed Pct values are at an expected level where the Power Pct is rather high. The operating conditions are as in Table 44.

	β_{TW}	U_{TW}	Ψ
	096°	8.3m/s	246°
	Ts [s]	**Hs** [m]	β_0
Wind generated		1.5	150°
Closed Form	8.7	2.0	
Hind Cast	No data for this area		

Table 45 Wave information, Case 9.

The ship is sailing with waves coming from aft and a rather large wind speed compared to ship's speed. The ship maintains speed as expected – indicated by the k_S and Speed Pct indexes – but in order to maintain course the ship has to use more rudder than normal, which affects the shaft torque and hence the main engine power consumption, Figure 152.

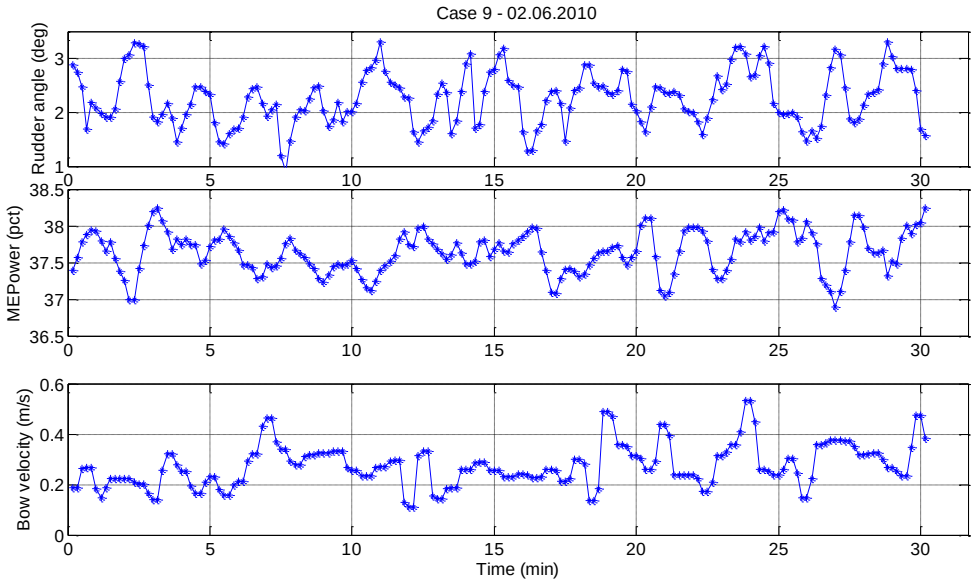

Figure 152 Rudder angle, ME Power pct and relative bow velocity, Case 9.

According to operational analysis the average offset on the rudder during operation is approx. 1° and in this case the constant offset is 2°3 (average). The power consumption is affected by the ship motion caused by the rudder motion and offset combined with the effect of the ships motions (relative bow velocity).

10.3 Filter Effect on Performance Index

In Section 8 a set of filters was established for scatter in the performance indexes. They were

- Trim > -1 m
- Draught > 11 m

After the filtering in this section most of the data with these characteristics are removed. Cases 1 to 6 are subject to fall under these criteria and as seen here the data creates the same scatter in the indexes. Further it is seen that the ship's motions are subject to scatter in indexes as described by Cases 7 and 8. The ship's motions are not sufficiently modelled in the performance models used in this study and therefore another filter based on ship's bow motions (velocity) and rudder angle could be introduced.

- Relative bow motion < 0.1 m/s
- -1 < Rudder angle < 3

The number of data available will of course be reduced but it will also be ensured that the data processed in the model will fit to this.

The data are now processed again and results are compared including the results for the analysis in Section 8.

The performance index values will then be as shown in Figures 153 to 155. Comparisons between models are seen in Tables 46 to 48.

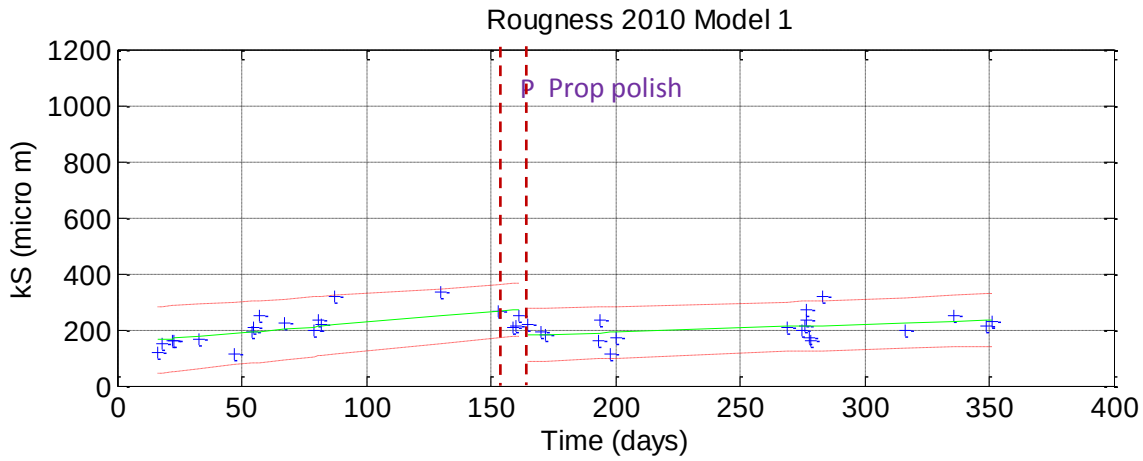

Figure 153 Roughness filtered values 2010.

Model 1	**Before prop clean**	**After prop clean**
RMSE	47.1	43.4
Line slope with 95% conf. bounds	0.7386 (0.2799, 1.197)	0.2947 (-0.05563, 0.6451)
Model 2		
RMSE	185.2	148.6
Line slope with 95% conf. bounds	2.007 (0.2033, 3.812)	0.2983 (-0.9023, 1.499)
Model 3		
RMSE	33.7	52.24
Line slope with 95% conf. bounds	0.8198 (0.4911, 1.148)	0.07472 (-0.3473, 0.4967)
Model 4		
RMSE	62.59	79.02
Line slope with 95% conf. bounds	1.021 (0.4113, 1.631)	0.1968 (-0.4414, 0.8351)
Daily averages		
RMSE	59.21	79.61
Line slope with 95% conf. bounds	0.1434 (-0.1934, 0.4803)	0.2914 (-0.1228, 0.7057)

Table 46 Roughness indexes.

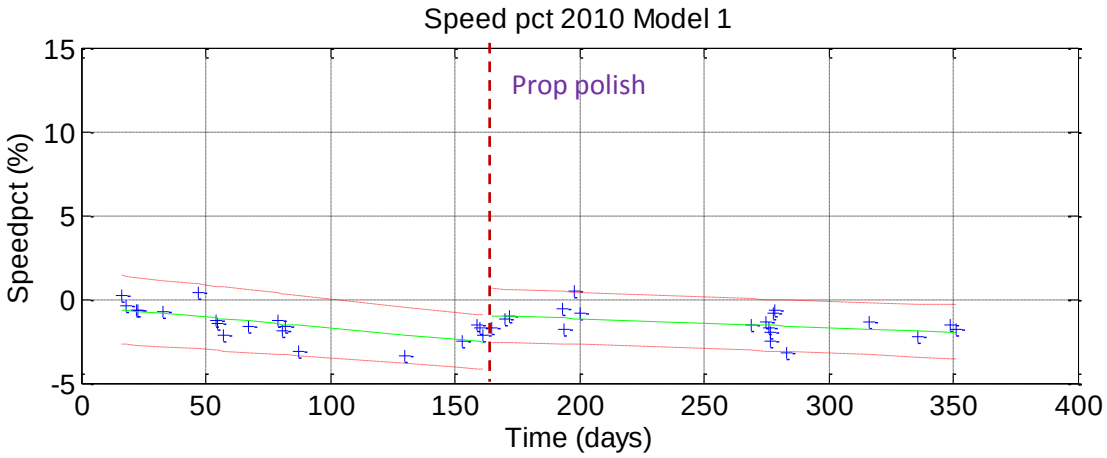

Figure 154 Speed Pct filtered values 2010.

Model 1	**Before prop clean**	**After prop clean**
RMSE	0.7432	0.7636
Line slope with 95% conf. bounds	-0.0053 (-0.01131, 0.000692)	-0.0139(0.02063, 0.005749)
Model 2		
RMSE	1.435	1.648
Line slope with 95% conf. bounds	-0.02165 (-0.0356, -0.00767)	-0.004117 (-0.0174, 0.00910)
Model 3		
RMSE	0.6607	0.9283
Line slope with 95% conf. bounds	-0.01607 (-0.0225, -0.00963)	-0.002431 (-0.00993, 0.00507)
Model 4		
RMSE	0.9005	1.157
Line slope with 95% conf. bounds	-0.01712 (-0.0259, -0.00835)	-0.004048 (-0.0134, 0.00529)
Daily averages		
RMSE	0.993	1.129
Line slope with 95% conf. bounds	-0.0026 (-0.0083, 0.0030)	-0.0045 (-0.0104, 0.0013)

Table 47 Speed pct indexes.

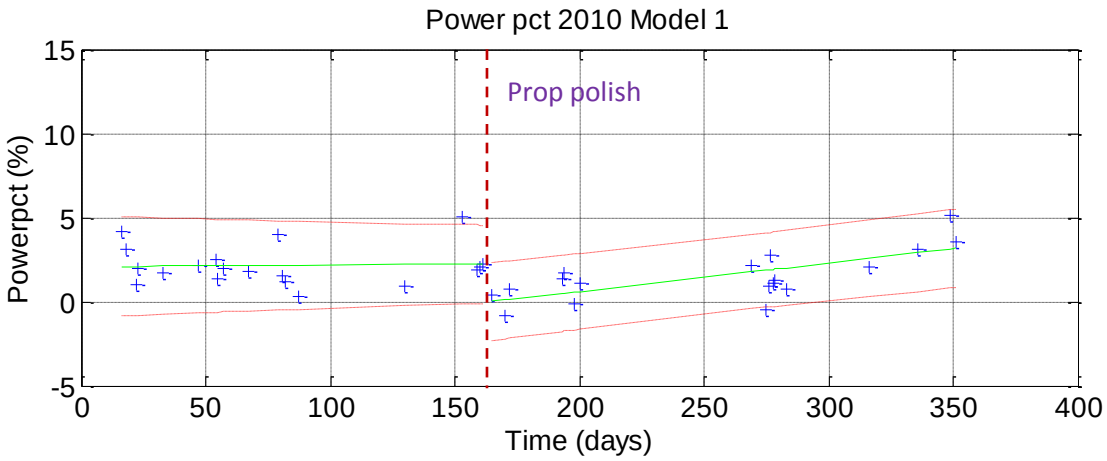

Figure 155 Power pct filtered values 2010.

Model 1	**Before prop clean**	**After prop clean**
RMSE	1.224	1.073
Line slope with 95% conf. bounds	0.0008758 (0.01105, 0.0128)	0.01686 (0.008199, 0.02553)
Model 2		
RMSE	1.059	1.141
Line slope with 95% conf. bounds	0.00814 (-0.002177, 0.01846)	0.01551 (0.006292, 0.02473)
Model 3		
RMSE	1.684	1.412
Line slope with 95% conf. bounds	-0.005318 (-0.02173, 0.01109)	0.01643 (0.005027, 0.02784)
Model 4		
RMSE	1.117	1.455
Line slope with 95% conf. bounds	0.006465 (-0.00442, 0.0173)	0.01477 (0.003022, 0.02652)
Daily averages		
RMSE	1.396	1.356
Line slope with 95% conf. bounds	0.0086 (0.00066, 0.0165)	0.0105 (0.0035, 0.0176)

Table 48 Power pct indexes.

The RMSE values and the accuracy of the slope for a linear regression line are used to estimate how well the different models fit. Based on this estimate, the results are listed in the following with respect to best model performance, Table 49:

Model	**Comments**
1	Overall best performance.
3	For k_S and Speed Pct values the fit is better before the prop clean than Model 1. The same model as used in Section 8.
4	The Cx values for head wind directions are larger than Isherwood values and therefore this model is more sensitive to cases with higher winds or to various load configurations of containers on the deck.
Daily average (Analysis Section 8)	More data points available but also larger scatter in results.
2	This model seems to fail due to large sensitivity in weather direction changes.

Table 49 Performance of models in the system.

The propeller clean is shown most clearly on the Power pct index with a 2% drop in power consumption. The effect of the cleaning seems to last approx. six months - after this period the index values are up at a level as before the propeller clean. The effect of a propeller clean is estimated to last approx. six months, Coast Diving (2011) and is suggested to have a propeller clean interval of maximum five to seven months, MEPC (2011). All though the increase of fouling is varies with the operational profile and the environment, it seems that the estimate of the effect is in accordance with results from this analysis.

It is questionable if the regression line after the propeller clean should be linear as suggested in the above analysis. By implementing data from 2011 it would be possible to see if the trend of the performance index line will follow the one before the propeller clean.

The other indexes also indicate that there has been a propeller clean but not as clearly as indicated by the Power Pct index. The performance index lines show no other degrading of performance due to fouling of the hull which is also in accordance with the hulls surveys performed in 2010 and 2011.

The number of data points is reduced due to the different filters introduced in this work. During 2010 the number of points is reduced to an average of one point per week. The filters are necessary in order to match the constraints in the model and the data quality. By introducing more advanced models, including more data sensors and data with higher sampling rate it will be possible to extend the number of data used in the analysis, see comments in Section 12.

11 Propeller Performance Index

The torque is measured on the propeller shaft measures by a torque meter. The shaft power relates to the torque as

$$P_S = \omega Q \tag{83}$$

The delivered power to the propeller P_D is in the area of $0.98P_S$ due to the power loss over shaft bearings and through the stern tube.

When P_D is known it is possible to find the torque and the thrust coefficient and thus the advance number from the open water propeller diagram.

The following relations between U_S, n and P_S are proposed by Jourdain (1964):

$$U_S = a \cdot n + b \tag{84}$$

$$\frac{P_S}{n^3} = c\frac{U_S}{n} + d \tag{85}$$

The two functions are practically linear over a wide range of operating areas and a relation between U_S, n and P can be outlined as in Figure 156:

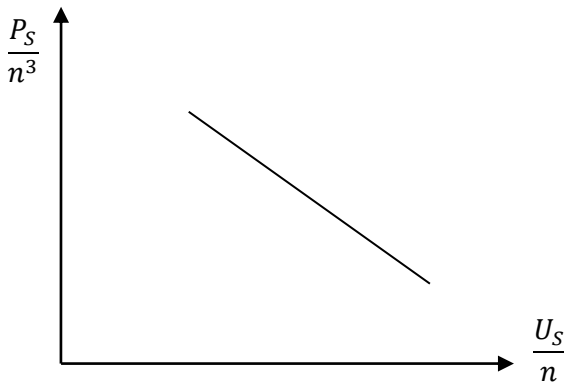

Figure 156 Linear relation on propeller curve.

The slope of the plotted curve will remain the same if the ship is sailing under the same conditions as when the curve was fitted, e.g. in a sea trial. If conditions change the slope will change, i.e. when a change of inflow of water to the propeller occurs this will change the slope. The method is

originally used to indicate if speed is consistent in various runs during a sea trial. Using the knowledge of which effects might cause change in the water flow to the propeller, the slope could be used as a performance index.

Another approach is proposed by Telfer (1964). He also used the linear relationship between speed and power on the propeller curve and defined the relation

$$Q_C = a + bS_a \tag{86}$$

where the torque constant Q_C is defined as

$$Q_C = \frac{100Q}{\rho n^2 D^{3.5} p^{1.5}} \tag{87}$$

where Q is the measured propeller torque, ρ is the sea water density, D is the propeller diameter, n is the propeller revolutions and p is the propeller pitch. S_a is the apparent propeller slip defined as

$$S_a = 1 - \frac{U_S}{np} \tag{88}$$

where U_S is the ship's speed. Here the change in slope can again be used to estimate the performance of the ship and Telfer defined the slope as

$$b = \frac{C - \overline{Q_C}}{1 - \overline{S_a}} \tag{89}$$

where C is the torque constant defined under a 100 % slip condition

$$C = \left(8 + \frac{z^2}{8}\right) \sqrt{\alpha \sqrt[4]{\frac{p}{D}}} \tag{90}$$

where z is the number of propeller blades and α is the propeller disc area coefficient.

The change in slope can be caused by various effects, e.g. change in

- draught and trim
- environmental influence, i.e. wind and waves
- rudder-induced movements of the ship
- manoeuvring conditions, e.g. changes in RPM's or steering
- shallow water operations

and of course

- fouling of hull and propeller

It will be possible to separate the fouling from the other effects by filtering the data, i.e. introducing filtering as in the previous sections and selecting conditions that are alike.

The method is independent of modelling of the ship and the environment and the result can be used also in various logging methods i.e. auto logging or average logging. The result using Telfer's model and the slope b in the Eq. 89 is as seen from Figure 157.

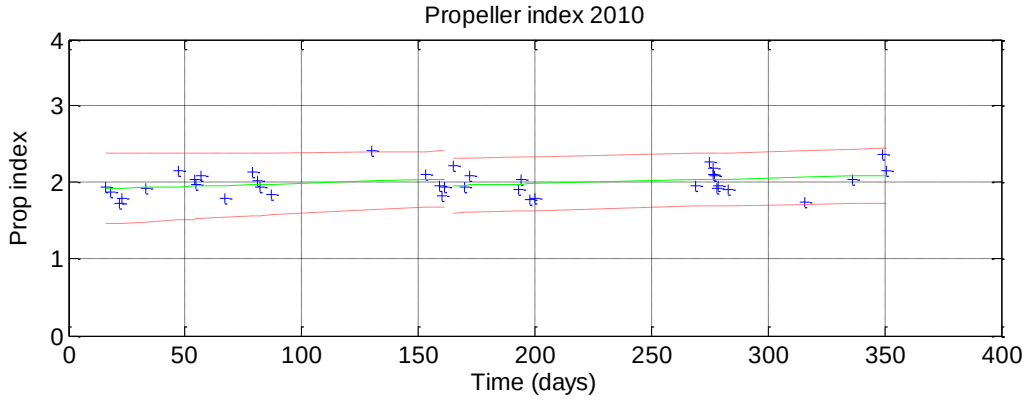

Figure 157 Propeller index 2010 – filtered values.

The trend is as expected. The slope is slightly increasing in value but the propeller cleaning incident is not clear as in analyses using model data. The fouling of the hull of m/v "Clementine Maersk" during the observation period is according to hull surveys not increasing and the method used in this section should be tested on ships where hull and propeller fouling are more dominant. The main focus in this research work has been as described in the previous sections. The analysis in this particular section has been included with the purpose showing that the method proposed are valid to estimate the performance of a ship and can be used where model tests are not available. The method and model should be exposed to more detailed work.

12 Conclusion and Recommendations

12.1 Conclusion

The purpose of the work in this thesis has been to establish a reliable performance system based on auto logged data on board a ship.

A case study during 2010 including a PostPanmax container ship has been used as background for the work.

The work is based on an existing performance system where the data input to the system is from reports based on manual logging and forwarded by the ship's crew. The system is based on daily averages and in this work an analysis of daily averages is included and compared to results achieved by auto-logged data.

Auto-logging of data through an automation system on board the ship is introduced as input to the performance system. A ship's automation system is used to monitor the operational condition and all logged data are assembled in this system. The sampling rate is defined by the user, the constraints in the system and the logging sensors.

A routine handling the data is suggested. In a system which is designed for a large fleet of ships it will not be possible to have manpower to supervise manually each individual ship. It should be possible to extract reports on each ship when necessary. Otherwise boundaries giving alerts of when the ships performance should be examined would have to be determined in the system. It should be possible to handle changes in the data e.g. voluntary changes by the crew or faults in the signals like spikes etc., without giving alert. Therefore routines handling the data before given as input to the system are suggested in this work. A CUSUM algorithm to detect changes in the parameters and routines handling the detected changes are suggested. A routine handling drift in timing of the signals is suggested and implemented in the system.

The existing system is modelled in software based on the bond graph system. The system is based on elements which are connected by bonds. A library of elements with various characteristics has been established and used to compare models or systems with regard to performance. The system has been used to model different ships, e.g. Panmax / PostPanmax container ships and a VLCC. The

models can be based on detailed model tests or general power prediction models. The detailed model test is considered to give the best results, especially for container ships where operating conditions vary during a voyage. For modelling and analysis of performance of a Panmax container ship, see Hansen et al (2010) (Appendix B).

Alternative models have been analysed in order to obtain better results. Two wind resistance models have been compared and a combined wind / wave model has been compared to separate wind / wave models. It was found that the model including the Isherwood wind resistance model and the simple wave model is the best performing model for the particular case study.

The initial performance system has been extended with elements describing the sea water temperature variation, the rudder movement and the influence of water depth on resistance. A wave height estimation element has been included based on wind velocity and vertical bow movements. These elements and their influence have improved the performance of the system and led to less scatter in the performance analysis results.

Constraints in the models have been identified. The models used in this work are based on empirical relations or based on regression analyses of model tests and full-scale trials. In order to achieve valid results the conditions where performance is estimated have to be inside the boundaries of the model. Filters have been determined to establish cases where the ship is in steady state conditions and where these conditions are inside the boundaries of the constraints of the model.

The filters used in this work are listed in Table 50.

Parameter	Limit	Constraint in model
ME Power pct	> 30 %	Power curve from model tests
True wind velocity	< 10 m/s	Hs < 2 m
Water depth	> 60 m	Water depth resistance
Mean draught	> 11m	Power curve from model tests / ship motions
Trim	> -1 m	Power curve from model tests / ship motions
Rudder angles	-1° < RA < 3°	Ship motions
Bow vertical velocity	< 0.1 m/s	Ship motions

Table 50 Filter values

Some of the filters overlap, e.g. constraints in the ship motions model are often connected with low mean draughts and / or large forward trim. As an example on an incident the ship is sailing with a mean draught of 10.8 m and a trim of -1.7 m which causes large rudder movements and induces large scatter in the resulting performance index, see the analysis in Section 8. Even though the detailed model test should give good results in estimating the behaviour of the actual ship, there are some uncertainties in the scaling factors used, Bose et al (2009). Model ship extrapolation and correlation allowances are based on experimental results and there are some uncertainties included in the power prediction based on these. This will specifically be the case when the ship if "off design" conditions i.e. at low draught and large trim conditions where extrapolation will lead to larger uncertainty.

Performance indexes have been defined and indexes have been used to estimate the performance of a ship. Two indexes are related to the logged speed of the ship (Speed Pct and k_S) and one index is related to the measured torque on the propeller shaft (Power Pct). The indexes describe the degrading performance due to fouling of hull and propeller and they are considered to be used as relative indexes, i.e. it is the trend of the index over the observation period that is used to estimate the performance.

Annual hull surveys of m/v “Clementine Maersk” show almost no fouling of the hull. The propeller is cleaned on the occasion of the hull survey. Research shows that the power penalty due to fouled propellers is in the range of 3 – 4 % of most propellers, Mosaad (1986) or up to 5%, Hydrex (2011). The effect of the propeller clean depends on operating conditions. Regular cleaning intervals are proposed by Hydrex (2011) and MEPC (2011). The performance analysis in this work indicates that the effect of the propeller polish is evened out after approximately six months. By examining the trend in the Power Pct index the level of added power consumption reaches the level before the propeller clean after this period. The estimated gain in power is 2 %, the estimated speed increase is 1.5 % and the estimated drop in roughness is 80 µm, Figure 158 immediately after the propeller clean. The results from the Power Pct index show the propeller clean most clearly which is expected as it relates to the torque measurements on the propeller shaft.

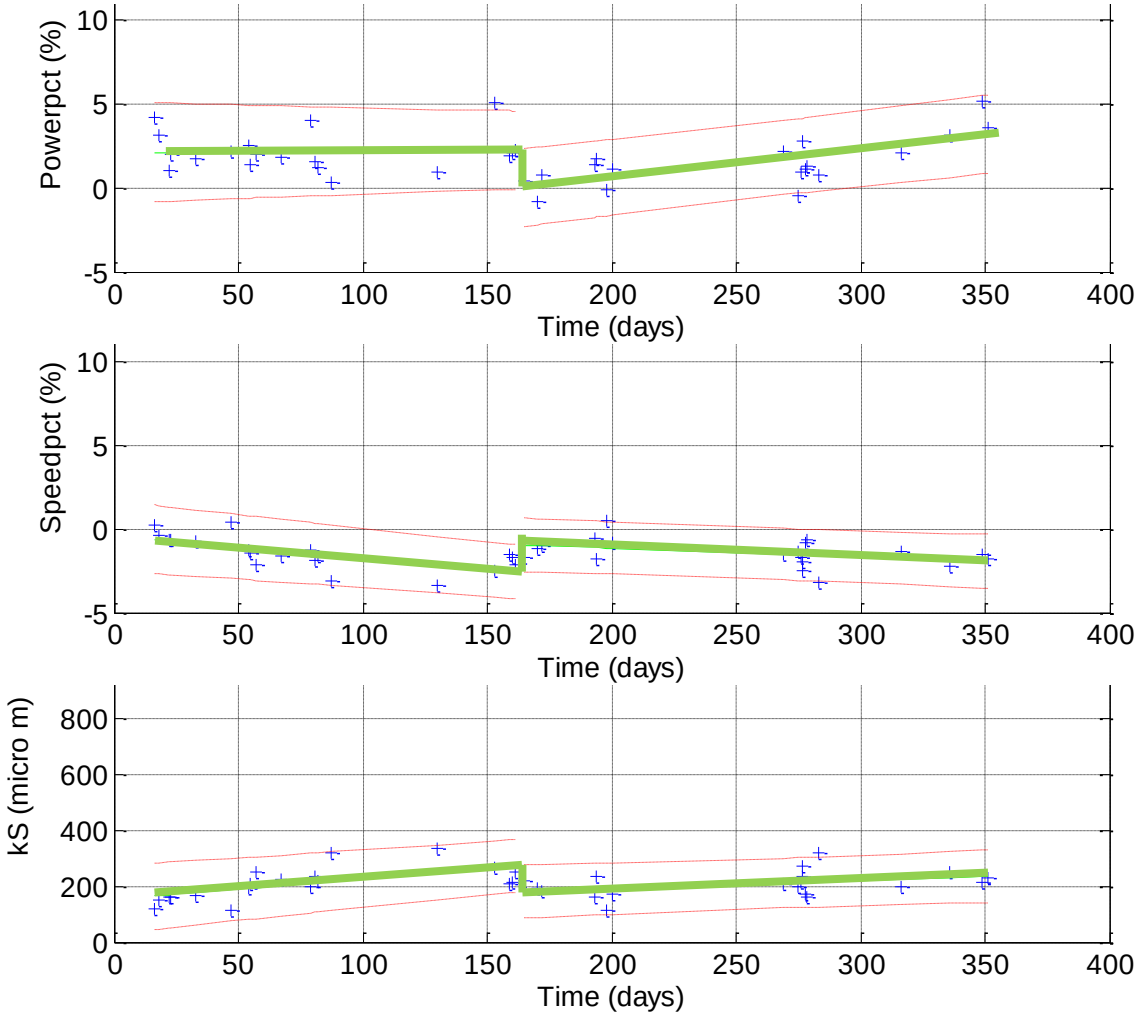

Figure 158 Performance indexes 2010.

By introducing the same filters as used in Table 50 in the propeller performance index, this index is used to estimate the performance of the ship. The results show the same trend in performance as described in the model performance indexes, but with larger scatter in the results. The propeller clean is not clearly indicated by the index but the index can be used as a rough estimate where model tests of the ship are not available.

The results from the developed performance system described in this work show that the system is capable of giving a reliable description of the development of the ship's performance over the observation period. It is capable of identifying the propeller cleaning incident in June 2010 with reasonable accuracy with respect to power, speed and hull and propeller roughness.

12.2 Recommendations for future work

The modelling in this work is partly based on rather simple models as described in ISO 15016 and ITTC guidelines. Due to the simplicity there are also some constraints in these models. The filtering of data suggested in this work ensures that the data used as input to the system is inside the boundaries of the constraints. Using other models and including more signals in the system will extend the number of data which can be used in the performance evaluation. The following suggestions are proposed:

Wave estimation — The present element is based partly on wind velocity and partly on wind direction / bow motions. To be able to include both waves and swell and to give a better estimation of the direction of the incoming wave, the method described by Nielsen (2005) should be implemented. Sensor fusion as proposed by Lajic (2010) should be used to determine the most reliable signal used in the estimations.

Wave resistance — By introducing more accurate wave estimations it is suggested to include another wave resistance model. Several have been suggested in literature, see Section 1.2, and elements with different models should be tested in the system. By introducing more motion signals it will be possible to give a more accurate estimation of the ship's motion during service.

Wind resistance — The exposed areas of the ship which are used for calculating the wind resistance are taken from average load conditions in the ship's cargo manual. By knowledge of the accurate cargo distribution on the weather deck it will be possible to give a better estimate of the wind resistance.

Rudder resistance — The resistance due to motions caused by the rudder is not fully described in the present model. By introducing techniques as described in Section 9.4 the motion of the ship can be modelled.

Water depth — The model describing the effect of sailing in shallow waters should be examined as described in Section 9.3.

Draught & trim — Are the only data given manually by the crew in this system. As long as some of the data are logged manually it is essential to keep a close contact to the crew on board the ship. To establish high awareness in the logging of the data it is imperative to include the ship's crew in the project and to give them feedback on the evaluation of the performance of the ship. There are systems which are able to give information about the dynamic trim during operation e.g. pressure sensors on board m/v "Clementine Maersk" but tests have shown that they are very unstable in measuring the variation in trim.

Thrust measuring — The thrust meter which is installed on board m/v "Clementine Maersk" has proved to be unstable in delivering reliable data to the performance system. By introducing thrust measurements in the performance system it should be possible to monitor the propeller efficiency even more accurately than when using only the torque meter.

Data logging — The auto logged data in this work is logged at a sampling rate of 0.1 Hz. In order to include other sensors and to model the motions of the ship, the sampling rate has to be changed. For normal ship motions a 5 Hz rate will be sufficient, Marin (2011), where smaller ships with faster dynamics would have to sampled at 20 Hz, Fossen et al. (2009).

The data in this study is logged through the ship's automation system. As part of this work, a similar system has been tested on board a VLCC. It has

not been possible to perform all logging through the automation system on board this ship and therefore the ship's VDR has been used as a source. Since all larger ships are equipped with VDRs this study has the potential to introduce auto logging in a wider range of ship.

A third logging project also uses the ship's automation system and the data is stored on board the ship in a database. The database is available through a satellite link which means that database inquiries can be sent from shore to ship when necessary. The configuration of this system is considered to be the way future auto logging should be set up.

Data sensors

In order to improve models it will be necessary to include more signals in the logging process.

Six DOF sensors should be included in the wave estimation and the modelling of the ship motion.

The lateral speed through water is measured through water by the ship's speed log and over ground by the ship's GPS. In order to estimate lateral speed in the ship motions and to estimate the sea current, these signals should be included in the logged data.

The Performance System has potential to become more than a tool for evaluation of the fouling of the hull and propeller. The reliable performance index indicates the performance of the ship and in cases where performance improving retrofits such as rudder bulbs or propeller nozzles is installed, the system would be able to show the effect of these. The system could also be used in evaluating different antifouling products either on one ship or sister ships sailing at the same route.

All operational information is logged in the system and this can be used for various documentation purposes. With reference to Figure 159 a number of solutions are suggested.

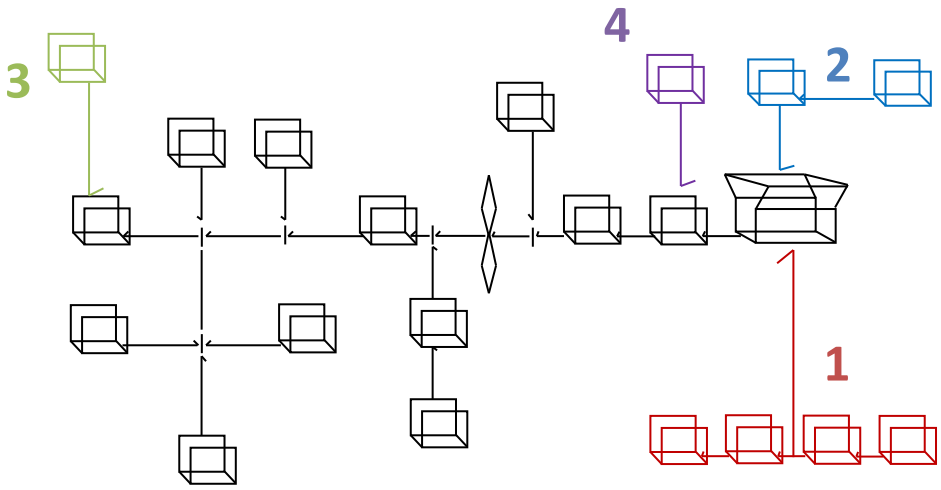

Figure 159 Extended Performance System

1. Auxiliaries consumption and performance. Consumption e.g. fuel, lube and cylinder oil and marine diesel is monitored. Energy consumption to auxiliary machinery, pumps etc. is accounted for and performance of the ship as a complete energy system is accounted for.

2. Emissions and EEOI. By logging of consumption, knowledge of specifications of consumed and the proper model of engine and auxiliaries it will be possible keep an account of all emissions from the ship i.e. SOx, NOx and CO_2. The emissions account could be incorporated in the Energy Efficiency Management Plan (EEMP) as suggested by IMO (2009). Another tool suggested in this plan is the Energy Efficiency Operational Indicator (EEOI). The index is used to monitor CO_2 emissions per amount cargo and per distance sailed, Eq. 89.

$$EEOI = \frac{Fuel \cdot CO_2 conversion\ factor}{Cargo \cdot Distance} \tag{91}$$

The index is used to monitor the CO_2 emissions per voyage or per period defined by the user and can be used as a Key Performance Indicator (KPI) in the Shipping Company.

3. The Performance Index is used to monitor the fouling of hull and propeller with a reliable result. The index can be used as documentation in the Biofouling Management Plan (BMP)

and Record book as suggested by IMO in IMO-MPEC62 (2011). The propeller and hull roughness index k_S could be introduced as reference in the documentation.

4. The Performance System can be introduced as an Energy Optimizing Tool (EOT). A graphical user interface could be implemented in the navigation bridge layout where the navigating officers would be able to gain information about the energy consumption during sailing. Introducing EOT in a long term planning tool such weather routing and / or passage planning systems it will possible to gain information about not only the safe passage but also the least energy consuming and thereby the most economical passage of the ship.

13 Literature list

Aas-Hansen, M. (2010). “Monitoring of hull condition of ships”. MSc Thesis Norwegian University of Science and Technology (NTNU), Department of Marine Technology Trondheim.

Almeida, E., Diamantino, T. C., and de Sousa, O. (2007) “Marine Paints: The particular case of antifouling paints”. Progress in Organic Coatings. 59, pages 2 -20.

Anderson, C. et al. (2003) “The development of foul-release coatings for seagoing vessels”. Journal of Marine Operations and Design, 84, pages 11 – 23.

Aoki, I., Kijima, K., Furukawa, Y. and Nakiri, Y. (2006). “On the Prediction Method for Maneuverability of a Full Scale Ship”. Journal of the Japan Society of Naval Architects and Ocean Engineers, Vol. no. 3, pp. 157-165, 2006.

A. P. Moller-Maersk (2010). ”Maersk Ships Performance System (MSPS)”

Barras, B. (2009). “Ship Squat and Interaction”. Witherby Seamanship Int Ltd. ISBN 13: 978 1 905331 60 4

Blendermann, W. (1994). “Parameter identification of wind loads on ships”. Journal of Wind Engineering and Industrial Aerodynamics, 51, pages 339 – 351.

Blendermann, W. (1997). Messung der Windlast an zwei Containerschiffen in realem Ladezustand im Windkanal. Institut für Schiffbau der Universität Hamburg.

BMT SeaTech. (2009) Safety and performance monitoring (SMART).

Boese, P. (1970) “Eine Einfache Methode zur Berechnung der Widerstandserhöhung eines Schiffes im Seegang”. Institüt für Schiffbau der Universität Hamburg, Bericht Nr. 258.

Bose, N., Malloy, S. (2009). “Reliability and Accuracy of Ship Powering Performance Extrapolation”. First International Symposium on Marine Propulsors, SMP ’09. Trondheim, Norway.

“Mediterranean Pilot” British Admiralty Sailing Directions (2010).Vol.IV, 15th Edition.

Carlton, J. (2007). “Marine Propellers and Propulsion” Butterworth-Heinemann. ISBN 978-07506-8150-6.

Bom, H.J.J., Hout, I.E., Flikkema, M.B. (2008). “Speed-Power Performance of Ships during Trials and in Service”, SNAME 2008. http://www.marin.nl/web/file?uuid=da04b424-81db-4f35-8e94-69bb3e4bdd2d&owner=065ac89a-8ff7-42a7-b3d1-be55fb79ac48.

Broeninck, J.F. (2000). “Introduction to Physical Systems Modelling with Bond Graphs”, University of Twente, Dept EE, Control Laboratory.

Clark, I.C., “Ship Dynamics for Mariners” (2005). Book by The Nautical Institute, ISBN 1 870077 68 7.

Coast Diving Service Inc (2011). http://coastdiving.net/sh_diving1.htm#propeller_polishing

Drinkwater, J.W. (1967). “Measurement of ships performance”. Journal of Scientific Instruments, Vol. 44, pages 702 – 708.

EEMP, Marine Environmental Protection Agency (2011). “Guidance for the development of a ship Energy Efficiency Management Plan”.Annex 17.

Force Technology. (2010) SeaTrend. Performance monitoring of ships in service.

Fossen, Thor I. (1994) “Guidance and Control of Ocean Vehicles”. Wiley and Sons.

Fossen, Thor I. (2002) “Marine Control Systems”. Marine Cybernetics Norway. ISBN 82-92356-00-2.

Fossen, T.I., Perez, T. (2009). ”Kalman Filtering for Positioning and Heading Control of Ships and Offshore Rigs”. IEEE Control Systems Magazine, December 2009.

Friis, A.M., Andersen, P., Jensen, J.J. (2002). ”Ship Design”. Department of Mechanical Engineering, Technical University of Denmark.

Fujiwara T., Ueno, M. and Ikeda, Y. (2001) “An estimation method of wind forces and moments acting on ships”. In Procedings of the Mini Symposium on Prediction of Ship Manoeuvring Performance, pages 83-92.

Fujiwara T., Ueno, M. and Ikeda, Y. (2006) “Cruising performance of a large passenger ship in heavy sea”. In Proceedings of the Sixteenth International Offshore and Polar Engineering Conference, pages 304-311.

Gerritsma, J, and Beukelman, W. (1972) “Anlysis of the resistance increase in waves of a fast cargo ship”. International Shipbuilding Progress, 19, pages 285-293.

Griffiths, G., Bradley, S.E. (1998). ”A correlation speed log for deep waters”. Sea Technology, 39(3), pp. 29-35.

Gustafsson, F. (2000) “Adaptive Filtering and Change Detection”. John Wiley & Sons Ltd. ISBN 0-471-84161-3.

Hansen, S.V., Lützen, M. (2010) “Performance Monitoring and Ship Modelling by the Bond Graph Method”. Proceedings of 11th International Symposium on Practical Design of Ships and Other Floating Structures. Rio de Janeiro, Brazil, 2010. PRADS 2010, PRADS734-744.

Hollenbach, K. U. (1998) “Estimating resistance and propulsion for single-screw and twin-screw ships”. Ship Technology Research 45/2.

Holtrop, J. and Mennen, G. G. (1982) “An approximate power prediction method”. International Shipbuilding Progress, p. 166.

Holtrop, J. (1984) “A statistical re-analysis of resistance and propulsion data”. International Shipbuilding Progress, p. 272.

Hooft, J.P. (1987). “Further considerations on Mathematical Manoeuvring Models”. International Symposium and Seminar on Ship Maneuverability, Prediction and Achievement.

Hydrex (2011). “Underwater Technology” No. 172. http://www.hydrex.be/upload/papers/pdfs/Hydrex_Magazine_172.pdf.

Insel, M. (2008) “Uncertainty in the analysis of speed and powering trials”. Ocean Engineering 35 (2008), 1183-1193.

International Paints (2010) “Fouling Control Explained”. http://www.international-marine.com/foulingcontrol/pages/interactive_presentation.html.

International Paints (2004). “Hull Roughness Penalty Calculator”.

Isherwood, R.M. (1973) “Wind Resistance of Merchant Ships”, Proceedings of Royal Institution of Naval Architects.

ISO 15016. (2002) “Ships and marine technology – Guidelines for the assessment of speed and power performance by analysis of speed trial data”.

ISO 1302 (2010).”Indication of Surface Texture”.

ITTC (1999). “Performance, Propulsion. 1978 ITTC Performance Prediction Method”.

ITTC (2002). “The Specialist Committee on Speed and Powering Trials. Final Report and Recommendations to the 23rd ITTC”. Proceedings of the 23rd ITTC – Volume II.

ITTC (2005_1). “Full Scale Measurements. Speed and Power Trials. Analysis of Speed/Power Trial Data.”

ITTC (2005_2). “The Specialist Committee on Powering Performance Prediction Final Report and Recommendations to the 24th ITTC.”

ITTC (2011). “Proceedings of 26th ITTC – Vo1ume I. The Propulsion Committee Final Report and Recommendations to the 26th ITTC.”

Jensen, J.J., Mansour, A.E and Olsen, A.S. (2004). “Estimation of ship motions using closed form expressions”. Ocean Engineering 31, 61–85.

Jerri, A.J. (1977). “The Shannon Sampling Theorem-Its Various Extensions and Applications: A Tutorial Review”. Proceedings of the IEEE Vol. 65, No. 11 1977.

Journèe, J. M. J. (2003). “Review of the 1979 and 1980 Full-Scale Experiments Onboard Containership m.v. Hollandia”. Report 1349.

Journèe, J. M. J. (2003). “Review of the 1985 Full-Scale Calm Water Performance Tests Onboard m.v. Mighty Servant 3”. Report 1361.

Jourdain, M. (1964). “Speed Trials”. Bull. ATMA, p. 493.

Kijima, K., Katsuno, T., Nakiri, Y., and Fukuwara, Y. (1990) “On the maneuvering performance of a ship with the parameter of loading condition”. Journal of the Society of Naval Architects of Japan, Vol. 1990, number 168.

King, M.J. (1982). “The Measurement of Ship Hull Roughness”. Second International Conference on Metrology and Properties of Engineering Surfaces, Leicester Polytechnic, Leicester, Gt. Britain, April 14–16, 1982

Kreitner, J. (1939). “Heave, Pitch and Resistance of Ships in a Seaway”. 8th session of the Institution of Naval Architects, 1939.

Kwon, Y.J. (2008) “Speed loss due to added resistance in wind and waves”. The Naval Architect, March 2008, pages 14-16.

Lackenby, H. (1963)"The Effect of Shallow Water on Ship Speed", Shipbuilder, 70, No. 672.

Lajic, Z. (2010) “Fault-Tolerant Onboard Monitoring and Decision Support Systems”. PhD Thesis. DCAMM Special Report No. S121. DTU Mechanical Engineering.

Larsen, N.P.L. (2008) ”Dæmpning af rullebevægelse og fremdrivningsoptimering”. MSc Thesis, DTU.

Litton Marine Systems (1998). “SRD-500 Dual axis Doppler Speed Log. Operation Manual.”

Litton Marine Systems (1998). “Navigation Echosounder LAZ 5000. Manual”

Lützen, M. (2001) “Ship collision damage”. Phd thesis, Technical University of Denmark, Department of Naval Architecture and Offshore Engineering.

Marin (2008) “Ship Service Performance Analysis Method”. SPA-JIP project.

Marin (2011) “Motion Monitoring”. http://www.marin.nl/web/Research-Topics/Offshore-operations/Motion-monitoring.htm.

MEPC, Marine Environmental Protection Agency (2011). “Prevention of air pollution from ships. Example of a Ship Energy Efficient Management Plan”. IMO MEPC 62nd session.

Marorka. (2006). “Energy Analysis. S Series. Analysis of energy consumption and results from computer modelling”. Marorka report M0601.

Molland & Turnock. (2007) “Marine rudders and control surfaces”, Butterworth & Heinemann.

Mosaad, M.A.A-R. (1986) “Marine Propeller Roughness Penalties”. Phd Thesis. Newcastle University, U.K.

Mosteller, F. and Tukey, J.W. (1977), “Data Analysis and Regression”. Addison-Wesley Pub. Co.

Munk, T. (2006) “Fuel Conservation through Managing Hull Resistance”. Motorship Propulsion Conference, Copenhagen.

Wärtsila, Muntean, T. (2008). “Ship propulsion train efficiency sensing”. Wärtsila Technical magazine “In detail” 2008, p.p. 34 – 38.

Nielsen, J.K. et al. (2006).”SeaSense – Real-time Onboard Decision Support”, WMTC.

Nielsen, U.D. (2005) “Estimation of directional wave spectra from measured ship responses”. PhD Thesis. Technical University of Denmark, Department of Mechanical Engineering, Coastal, Maritime and Structural Engineering

NOAA's WAVEWATCH III global model http://polar.ncep.noaa.gov/waves/

Pedersen, B.P. (2009) “Prediction of Full-Scale Propulsion Power using Artificial Neural Networks”. COMPIT '09, 8th International Conference on Computer and IT Applications in the Maritime Industries, pages: 537-550.

Pérez Arribas, F. (2007) “Some methods to obtain the added resistance of a ship advancing in waves”. Ocean Engineering, Volume 34, Issue 7, Pages 946-955.

PNA, “Principles of Naval Architecture Vol III” (1988). The Society of Naval Architects and Marine Engineers, ISBN 0-939773-02-3.

Salby, Murry L. (1996). “Fundamentals of Atmospheric Physics”. Academic Press, 1996, Elsevier Science.

Schultz, M.P. (2007) “Effects of coating roughness and biofouling on ship resistance and powering”. Biofouling, 23(7), pages 331 – 341.

Siemens (2000). “Simar Drive Synchro, Shaft Motor”, Manual.

SICK/Maihak (2005). “Maihak Shaft Power Meter. Manual”

“Ship Performance”. RINA, North East Coast Joint Branch RINA/IMarE, 04/1993.

Sperry Marine Inc. (1995) “Rudder Servo Unit RCW10-440”, Manual.

Steen, Sverre, Faltinsen, O.M. (1998) “Added Resistance of a Ship Moving in Small Sea States”. Practical Design of Ships and Mobile Units, p 521.

Telfer, E.V., “Some Ship Generalized Power Diagram Developments and Related Considerations”. Ingenieurs Navales Societe, Belge, April 1964.

TNO (2010). “Geïntegreerde Energie Systemen (GES)”, http://www.tno.nl.

Townsin, R.L., Kwon, Y.J., Baree, M.S., and Kim, D.Y. (1993) “Estimating the influence of weather on ships performance”. Royal Institute of Naval Architects.

Townsin, R.L., Byrne,D., Svensen, T.E., and Milne, A. (1986) “Fuel Economy Due to Improvements in Ships Hull Condition 1976 – 1986”. International Shipbuilding Progress, 33(383).

Townsin, R.L. (2003). “The Ship Hull Fouling Penalty”. Biofouling, 2003 Vo l 19 (Supplement), pp 9–15.

Tx Marine, Hamburg (2010). “EVOThrust. Propulsion efficiency measurement system”.

Vugt, H.V. (2005) “Dynamisch ondiepwater effect op een schip”, TNO.

Yelland, M.J., Moat, B.I., Pascal, R.W., Berry, D.I. (2002). “CFD Model Estimates of the Airflow Distortion over Research Ships and the Impact on Momentum Flux Measurements” Journal of Atmospheric and Oceanic Technology, Volume 19, 2002.

Yoon, H. K., Rhee, K. P. (2003). “ Identification of hydrodynamic coefficients in ship maneuvering equations of motion by Estimation-Before-Modeling technique”. OCEAN ENGINEERING — 2003, Volume 30, Issue 18, pp. 2379-2404.

Young Meteorological Instruments (2000). “Model 06206. Marine Wind Tracker. Manual”

14 Appendix A

Modelling and logging of data from a VLCC

Figure A1 VLCC used in the modelling

A VLCC, Figure A1 is modeled in GES as shown on Figure A2. According to the operational profile the ship is generally sailing in two conditions – one loaded and one ballast condition. The GES model is therefore modeled with reference to the two conditions; see Power curves, Figure A3.

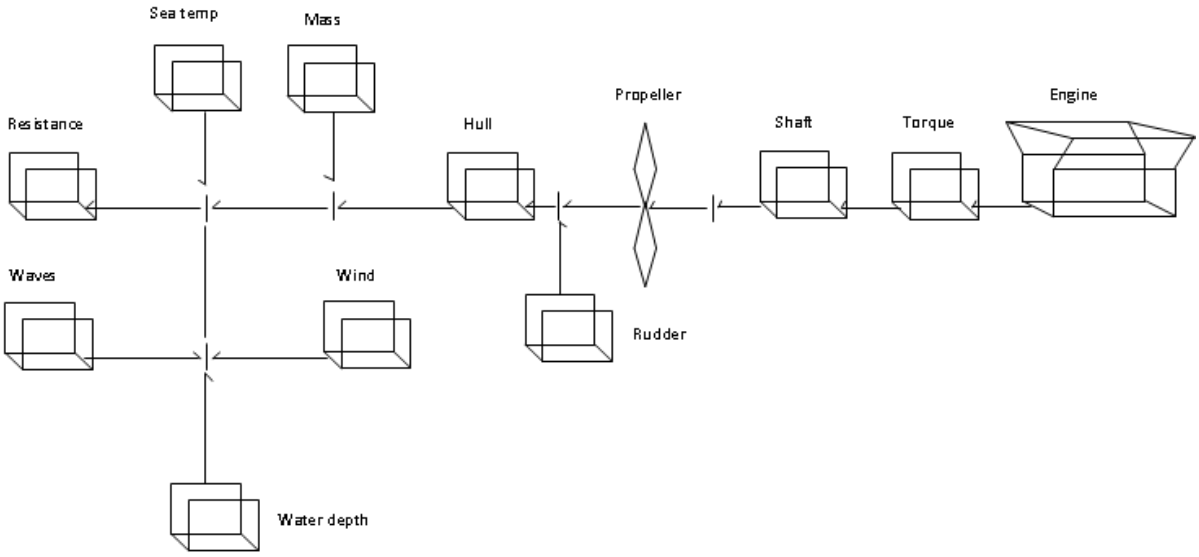

Figure A2 The GES VLCC model

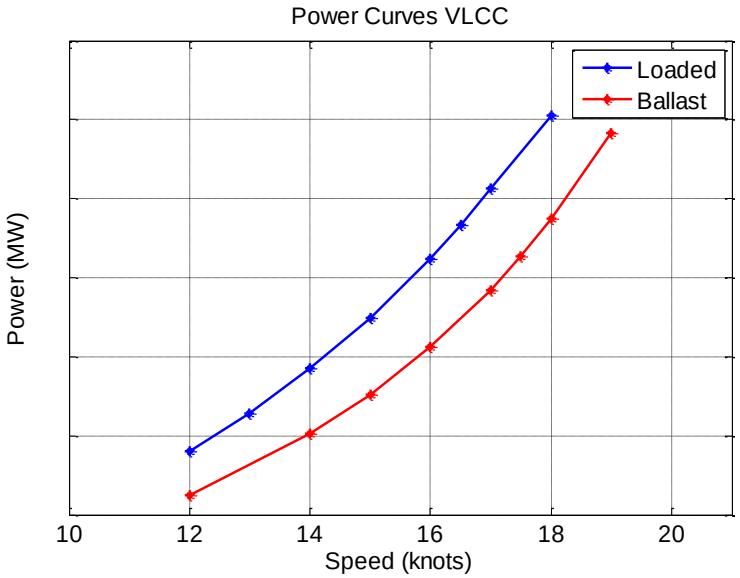

Figure A3 VLCC Speed - Power curves

The data is logged from the ship's Voyage Data Recorder (VDR) and from the ship's automation system (FleetMaster). Draught and seawater temperature data are logged in the MSPS (Performance) system.

Data handling and logging interval is as in Table 50.

A short set of data are subtracted from the series and tested in the GES model to verify the model elements. An example of model speed vs. logged speed can be seen on Figure A4.

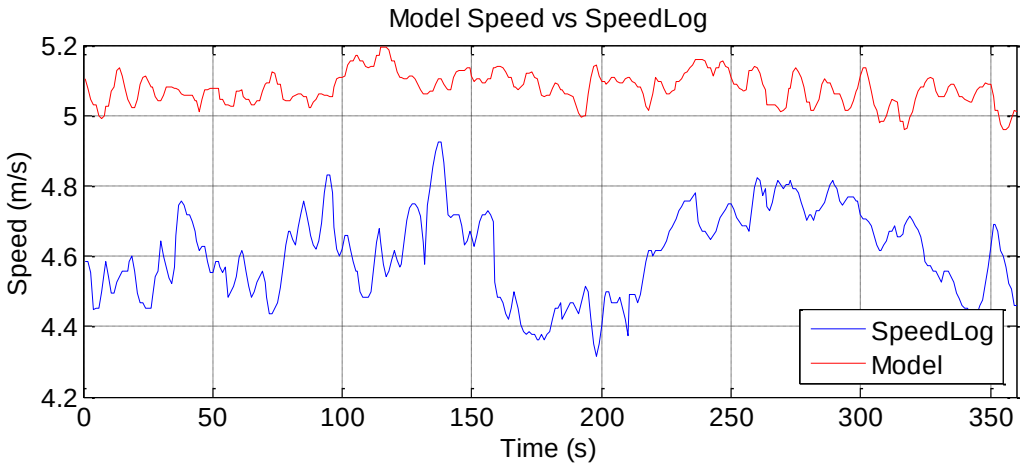

Figure A4 Model peed vs. VLCC logged speed

GES Parameter	Logging interval	Initial step	Conversion
Ship Time	1 s	Remove spikes and outliers Consolidate data to uniform time stamp	Logging interval
Latitude	1 s		
Longitude	1 s		
Sea water temperature	24 hrs		
Water depth	1 s		
Relative wind speed	1 s		10 min average
Relative wind direction	1 s		10 min average
Draught mean	24 hrs		
Draught fore	24 hrs		
Draught aft	24 hrs		
Heading	1 s		
Speed ground	1 s		
Speed log	1 s		
ME power	1 s		
Shaft torque	1 s		
ME RPM	1 s		

Table A1 Logged parameters from VLCC

The model has been set up to the data format given by the logging devices and performance indexes are k_S, Speed Pct and Power Pct.

The performance analysis is made from the set of data logged through 2011. The number of logged parameters is restricted compared to those logged on board m/v “Clementine Maersk” and therefore the used model has fewer elements.

It is not possible to perform a full analysis for the ship as there is a large gap in between the logged periods. The data for the ballast voyages are omitted in order to avoid too large scatter in the results.

The first data set had some errors in the timestamp (not synchronized data from VDR and FleetMaster). This was later adjusted and the final set of data was received late August 2011. There still were some unclear issues with the timing of the signals. The FleetMaster data timestamp is in local (ship) time and the time is controlled by the ship's Master Clock on board. The local time is controlled by the ship's crew i.e. during sailing through time zones the time is adjusted accordingly. The timing of the signals from the VDR is UTC which means that there are an offset between the two timestamps when the ship is out of a UTC time zone. The offset is adjusted by using the Local Time Offset value from the GPS. This offset value is adjusted – also by the crew – independently of the Master Clock timing. This could mean that the offset value is not always following the local time setting on board the ship.

The ship had a hull survey and a propeller cleaning in August 2011 and this incident has not been included in the analysis as the last received data are from late July 2011.The data is filtered according to the coarse filter as suggested in Table 8, section 8. It has not been possible to use the water depth as filter as there were too few incidents where the water depth was logged.

The ship had a hull and propeller inspection in August 2011 and results with regards to fouling on hull are as

MARINE FOULING CONDITION

Type (1) Acorn Barnacle (2) Tubeworm (3) Gooseneck (4) Algae
(5) Slime (6) Mussels (7) Calcareous / Others

Severity (A) Light (B) Moderate (C) Heavy

LOCATION	TYPE	% AREA			SEVERITY	LENGTH / HEIGHT
		Bow	Mid	Stern		
Port	3 4	10% 40%	5% 60%	10% 30%	B	Up to 20mm
Starboard	3 4	10% 40%	5% 60%	10% 30%	B	Up to 20mm
Flat Bottom	1 & 3	(1) 10% & (3) 5%			A	Up to 10mm
Rudder	1 & 4	(1) 15% & (4) 60%			A-B	Up to 20mm
Gratings	1	(Port) 80% (Stb'd) 5%			C A	Up to 30mm
Propeller	4 & 7	(4) 40% & (7) 70%			B	
Bow Thruster/s	NA					

Figure A5 Hull and propeller condition VLCC August 2011

The ship is normally sailing during two conditions – loaded and ballast. In the two operating conditions there is large difference in between draughts (10 – 23 m) and especially the sides of the ships is exposed to light which increases the fouling rate. Figure A6 shows fouling on sides and on flat bottom.

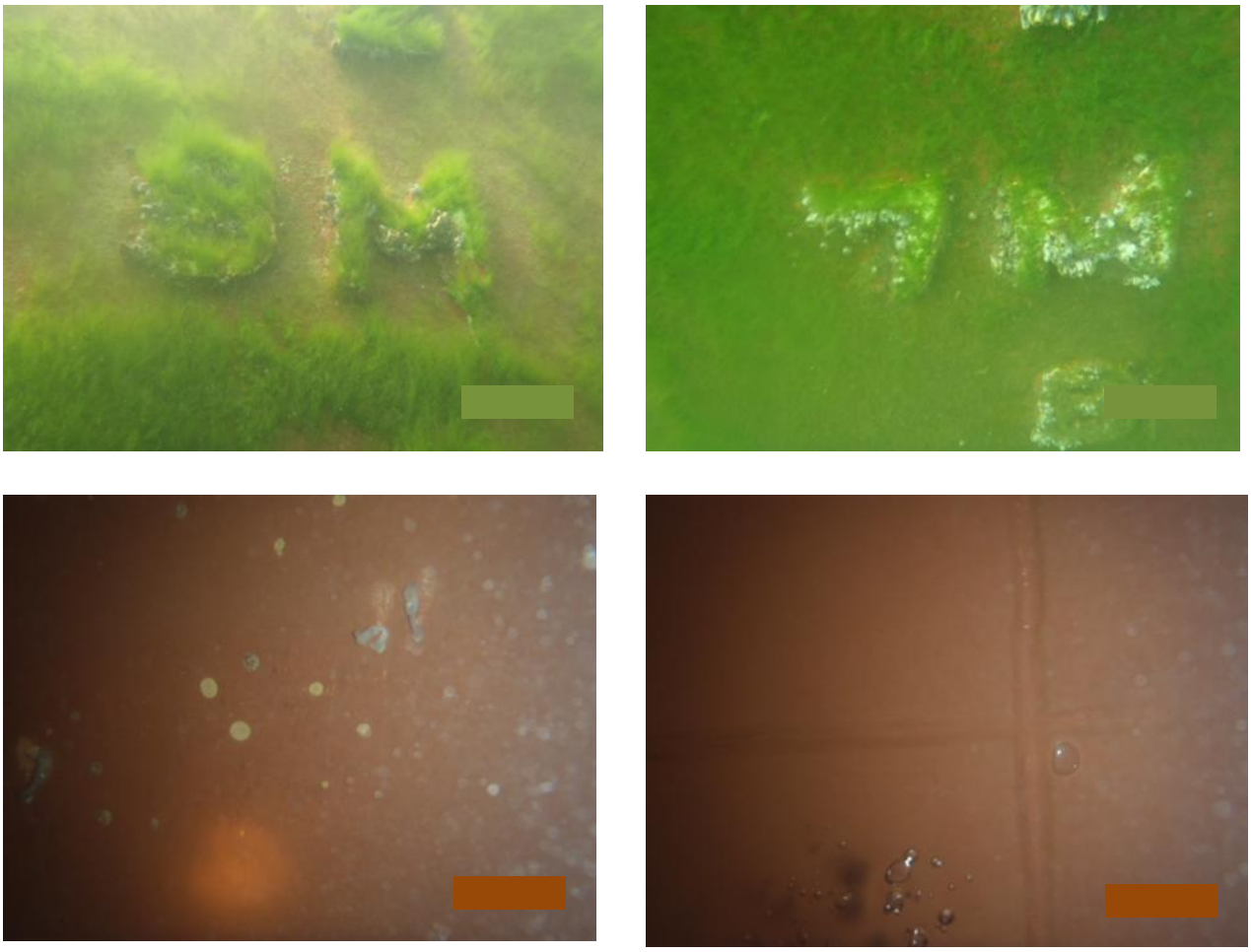

Figure A6

Top pictures: Hull fouling on vertical sides starboard and port. Bottom pictures: Hull fouling on flat bottom

The performance indexes are now calculated from the received data and the models are evaluated on estimated RMSE and line slope uncertainty, Figures A7 – A9.

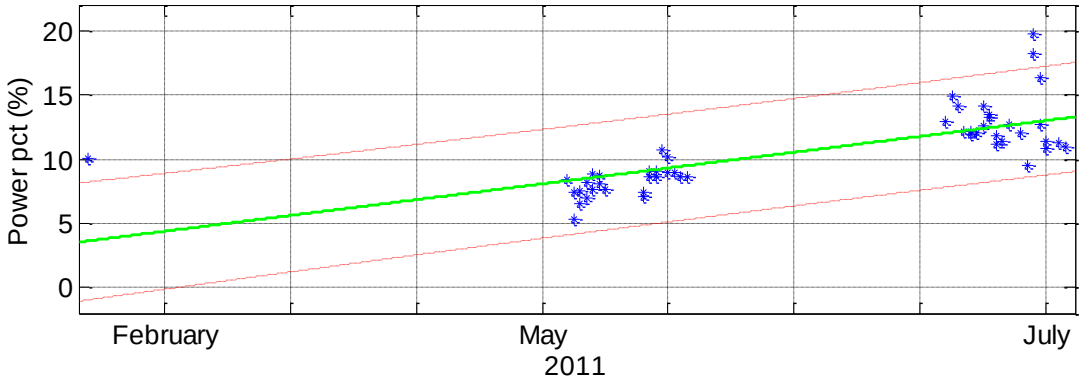

Power Pct	**Value**
RMSE	2.059
Line slope with 95% conf. bounds	0.06156 (0.04478, 0.07835)

Figure A7 Power Pct

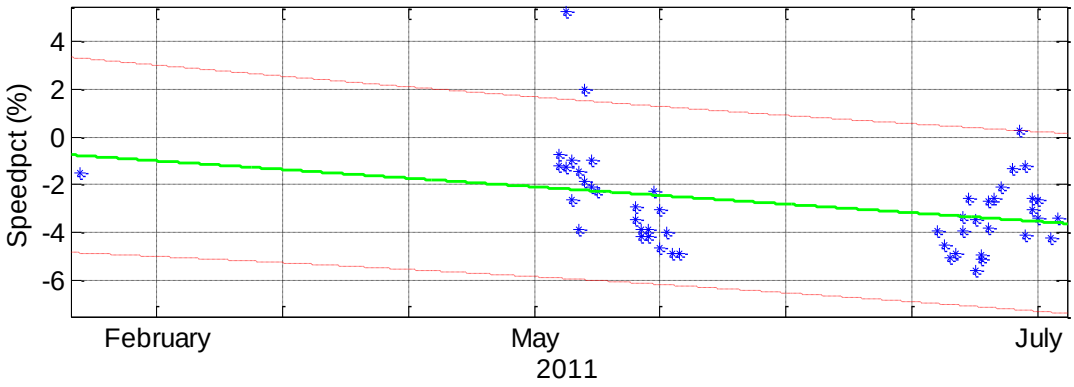

Speed Pct	**Value**
RMSE	1.834
Line slope with 95% conf. bounds	-0.01819 (-0.03315, -0.003239)

Figure A8 Speed Pct

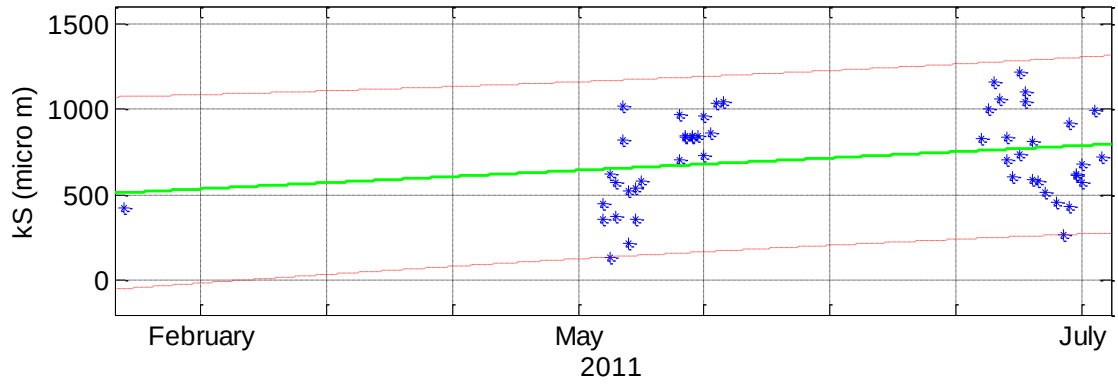

kS	Value
RMSE	251.2
Line slope with 95% conf. bounds	1.809 (-0.2389, 3.857)

Figure A9 Roughness

The calculated indexes are based on daily averages as described for m/v "Clementine Maersk", Section 8. There is only one valid data set for early 2011 and the main data sets are from May and July 2011.

Comments to the index values:

The Power pct is increasing during the logging period. The increase in Power pct has a value of 10 % over the period. There is a drop in Speed pct of 3 % over the period. The hull roughness is increasing with app 300 micro m over the period. All values are more scattered than the Clementine results in Section 8, especially the Roughness values.

The results indicate that the development of the grade of fouling is rather high compared to the one identified in the Clementine case and underwater surveys shows a higher degree of fouling especially on the vertical sides of the hull. More data would be needed to give a better estimation of the performance of the ship.

15 Appendix B

Performance Monitoring and Ship Modelling by the Bond Graph Method

Søren Vinther Hansen[1)], Marie Lützen [2)]

[1)] Department of Mechanical Engineering, Technical University of Denmark
Denmark
[2)] Faculty of Engineering, Southern University of Denmark
Denmark

Abstract

The propulsive performance of a ship in service tends to deteriorate over time, mainly due to fouling of hull and propeller. The added resistance due to fouling will lead to increased fuel consumption of the ship and thus increased CO_2 emissions to the environment and the operation costs for the shipowner will grow. In order to take appropriate action to reduce emissions of CO_2 in a global perspective and to obtain optimum operation and planning of cost savings, it is therefore important to monitor the ships propulsive performance during service.
Performance analyses of a panmax container ship are presented in this paper. The ship is modelled by the bond graph method. The added resistance due to fouling is calculated by use of the Holtrop resistance model. The added roughness to hull and propeller is used as performance index. Results indicate that the modelled system can be used as a performance monitoring system by using real time data from a ship in service. A discussion of the uncertainties in the evaluation is included.

Keywords

Ships; performance monitoring; data logging; ship modelling; added resistance; bond graph method

Introduction

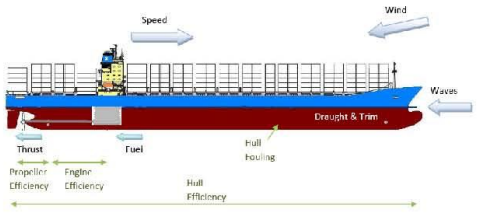

Fig. 1: The performance parameters

The basic purpose of a propulsive performance system on board a vessel is to provide feedback of how the vessel performs during a voyage or a period in a vessels life, Fig. 1. By use of a performance system the goal of making the most efficient voyage may be achieved. It not only indicates how the vessel performs at the moment of measurement, but also, on the basis of data collected over a period, monitors the condition of the vessel while in service. The overall purpose will normally be to gain information on how to make the most economical or environmentally efficient voyage.

An evaluation of the vessels performance must comprise a comparison of two or more conditions. As the sailing conditions, e.g. the environmental and loading conditions, might be of great importance during the time of operation, a performance index taking this into account must be used. A suggestion is to compare the present condition with a model condition defined by some given standard circumstances.

The index of performance is defined by the performance system and is dictated by the purpose. Monitoring data during a period can be used to estimate the amount of fouling on the vessel for deciding intervals of hull and propeller cleanings or dry-docking intervals. The engine efficiency due to wear and tear can be estimated, and finally the monitored data can be used for estimating the most efficient way of operating the vessel, optimal engine settings, navigation and loading conditions of the vessel.

Various indexes can be chosen, e.g.:

- Added resistance of hull and propeller
- Propulsive efficiency
- Loss in speed
- Increased fuel consumption

Ship Model

The propulsive system of a container ship is modelled by the bond graph method (Breedveld, 2003). This method is well suited for modelling of physical systems and describes the energy exchange between elements in the system. By application of the General Energy System (GES) (TNO, 2010) software, developed by the Netherlands Organization for Applied Scientific Research (TNO) and based on the bond graph method, a model is developed of the propulsive system of a panmax container ship.

The Bond Graph Method

The bond graph method was developed in 1960 by H. Paynter, MIT and is used to describe dynamic systems (Breedveld, 2003).

The power flow between two interacting systems results

in interdependence between the energetic states of the two systems, as it bonds the two systems together in one. Consequently, the basic symbol of the bond graph notation is a line called a bond. It depicts the exchange of power between the two systems or subsystems or elements at each end of the bond.

In the method a special notation is used to show the relation between the two systems A and B, Fig. 2.

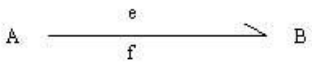

Fig. 2: Bond graph notation

The half arrow indicates the direction of the power flow (from system A to system B), and the effort (e) and the flow (f) are the variables which give the power when multiplied. As an example this could be an engine where the effort is the torque and the flow is the revolutions or the shaft speed and the power is the two variables multiplied.

The bond graphs represent the energetic coupling between the elements. This implies interaction between the systems and therefore output from one system will be input to the other and vice versa. This can be illustrated by a block diagram, Fig. 3.

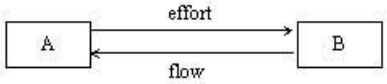

Fig. 3: Effort and flow

Because energetic interaction is a function of two variables, there are two possible choices for the input and output of each element (or subsystem) when a system shall be described in terms of mathematical operations on numbers (i.e. signals). In these choices one variable is assigned to the role of cause (or input) and the other to the role of effect (or output), so this choice is referred to as causality assignment. To represent this choice on a bond graph a causal stroke is added at one end of the bond, Fig. 4.

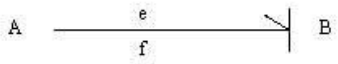

Fig. 4: Causal element

This graphical symbol means that the system nearest the causal stroke has effort impressed on it as input and produces flow as output. Necessarily, the system at the other end of the bond has flow imposed on it as input and produces effort as output.

To connect more elements to a flow, two types of junctions can be used, Fig. 5. The 1–junction where the flow is common and the sum of efforts equals zero and the 0-junction where the effort is common and the sum of flow equals zero.

Fig. 5: Junctions

The Physical Model

The ship is modelled with principal dimensions and data from model tests. The propeller model is based on the propeller characteristics for the vessel, where the parameters include the propeller shaft speed (n), the propeller diameter (D) and the sea water density (ρ).

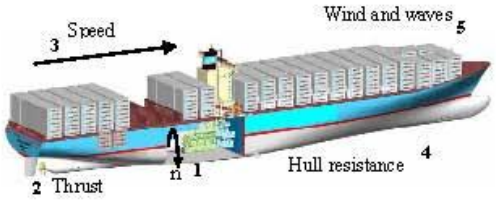

Fig. 6: The ship model

From the propeller characteristics the advance number of the propeller (J) is found by

$$J = \frac{U_a}{n \cdot D} \tag{1}$$

the torque coefficient (k_Q) by

$$k_Q = \frac{Q}{\rho \cdot n^2 \cdot D^5} \tag{2}$$

and the thrust coefficient (k_T) by

$$k_T = \frac{T}{\rho \cdot n^2 \cdot D^4} \tag{3}$$

The hull model is based on the hull wake fraction (w) and the thrust deduction factor (t) found by model tests. The ships speed (Us) is found by

$$U_S = \frac{U_a}{1 - w} \tag{4}$$

and the resistance (R) can finally be found by

$$R = (1 - t)T \tag{5}$$

The combined wind/wave model is based on the model of Townsin/Kwon (Townsin, 1993, Kwon 2008), where included parameters are the wind speed on the Beaufort scale (BN), the relative wind direction (W_D), the Froude no (Fn), the block coefficient (C_B) and the displacement volume (∇). The speed loss of the vessel (ΔU_S) can be determined from

$$\Delta U_S = A \cdot \mu \cdot \alpha \tag{6}$$

where A is

$$A = 0.7BN + \frac{BN^{6.5}}{2.2\nabla^{2/3}} \quad (7)$$

and μ (W_D) is the wind direction coefficient and $\alpha(C_B, load\ condition, F_n)$ is the ship coefficient.

The Holtrop (Holtrop/Mennen 1982, Holtrop 1984) model is used to find the total resistance (R_{TOTAL}), where included parameters are the ships draught (d), the block coefficient (C_B), the displacement volume (∇), the sea water temperature (T_W) and the hull wet surface (S):

$$R_{TOTAL} = R_F(1+k) + R_{APP} + R_W + R_B + R_{TR} + R_A \quad (16)$$

The resistance components are:

R_F	frictional resistance according to the ITTC-1957 friction formula
$1+k$	hull form factor, based upon a regression equation and expressed as a function of aft body form, breadth, draught, length of run, displacement and prismatic coefficient
R_{APP}	appendage resistance
R_W	wave resistance
R_B	additional pressure resistance of bulbous bow near the water surface
R_{TR}	additional pressure resistance due to transom immersion
R_A	model-ship correlation resistance or resistance to express hull roughness

To be able to use the Holtrop model in other conditions than the service condition, a service condition multiplication factor (F) is used. This factor is found by the relation between the wet surface area at actual draught (S) and the wet surface area at design draught (S_D).

The model-ship correlation resistance (R_A) can be expressed by

$$R_A = \tfrac{1}{2}\rho U_S^2 S C_A \quad (17)$$

where the correlation allowance coefficient (C_A) can be used to express larger hull roughness than standard. In this case C_A can be expressed by

$$C_A = (0.105 k_S^{1/3} - 0.005579) / L^{1/3} \quad (18)$$

where L is the ships length and k_S is the roughness factor. The standard value for the factor, k_S, is $150\ \mu m$. This factor is used as performance index in the present analysis. An increasing value of k_S over time indicates added resistance due to fouling of hull and propeller. An initial condition is used to establish the model of the ship which acts as reference over the observed time.

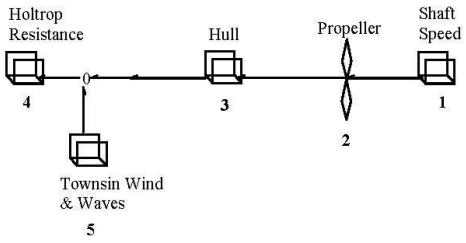

Fig. 7: The ship model in GES

The ship, Fig. 6, is modelled in GES, Fig. 7, and the relations are

1. A shaft speed, n, is given from the diesel engine to the propeller. The propeller torque, Q, is measured on the shaft and used to find the torque coefficient k_Q
2. Knowing k_Q and the propeller curves, k_T and J are found, which again leads to the propeller thrust, T, and the speed of advance, U_a
3. By means of the wake fraction, w, and U_a the ships speed U_s is found
4. By use of the thrust deduction coefficient, t, and the propeller thrust, the resistance R is found. The resistance consists of resistance from hull and appendages (rudder and stabilisers)
5. Further, environmental conditions add to the resistance, i.e. resistance from wind, waves and variation in sea temperature

The ship is modelled in GES, Fig. 7. Numbers (1) to (5) refer to those in Fig. 6. The ships speed is found by iteration in the causal element (3). The wind/wave model is connected to the system by a 0-connection. This affects the system by a speed loss (dU_S), i.e. the flow at the wind/wave module takes a negative value ($f\_gate(0) = -dU_s$.)

Data Logging

The data used for the performance system is logged on board and regularly sent ashore for further analyses. An example of logged data is given in Table 1. Some data will be manually logged by the crew, others will be collected using sensors and a data logger. Which parameters will be automatically logged depends on the installed systems on board. It is possible to log all data automatically, but normally the loading and the sea state will be described by the crew and typed manually into the system.

In the present analyses the loading condition, information about waves, the fuel oil consumption as well as the stabiliser position are described manually. All data, both

manually and automatically collected, are continuously logged during service and stored in one-hour log files (time series) on board.

Table 1: Examples of data logged on board a ship.

	Logged data
Loading conditions	Draught – trim Loading – wind area Position of point of gravity
Operational conditions	Heading Speed through water (speed log) Speed over ground (GPS) Rudder angle Stabilisers in/out Bow vertical movements Engine shaft torque Engine shaft trust Engine RPM ME fuel consumption ME power Shaft engine power Position – Latitude/longitude
Environmental conditions	Wind speed and direction Wave height and direction Water depth Sea water temperature Sea water density Air temperature Air pressure

Filtering of Data

The data available is stored in two formats. Format 1 is one-hour peak log files and besides the data and intervals listed in Table 2, they also give statistical information for the one-hour logging period, e.g. the running mean, min/max and the RMSE value.
Format 2 is time series files which contain data and intervals as listed in Table 2.

Table 2: Data logged in one-hour time series files

Variable	Logging	Format 1 Interval	Format 2 Interval
Time	Sensor	1hour	Continuous
Speed log	Sensor	1 hour	Continuous
RPM	Sensor	1 hour	Continuous
Sea water temp	Manual	1 hour	1 hour
Wind direction, relative	Sensor	1 hour	Continuous
Wind speed, relative	Sensor	1 hour	Continuous
Draught mean	Manual	1hour	1hour
Draught forward	Manual	1 hour	1 hour
Draught aft	Manual	1 hour	1 hour
Water depth	Manual	1 hour	1 hour

Not all data in the files will be used for the analysis. The data is selected on the basis of the following criteria:

1. The data is filtered to observations where there is no lack of data (no reports of missing data)
2. Only reports where the ship is at sea are included
3. The wave and wind model used in the model is sensitive to periods with high winds and seas (limit 1, Table 4) (Townsin, 1993, Kwon 2008)
4. The logged speed, the RPM's and the torque (power) measurement should be stable. The dynamics of the ship while sailing is poorly described in this model, and incidents where the ship is manoeuvring are to be avoided (limits 2 and 3, Table 3)
5. The Holtrop resistance model is sensitive to cases deviating from design condition and speed. The logged speed should not be too low and incidents with large trim and mean draughts too far away from design should be avoided (limits 4, 5 and 6, Table 3) (Holtrop/Mennen 1982, Holtrop 1984)
6. Sailing in areas with shallow waters increases the resistance and these incidents should be avoided (limit 7, Table 3)

Large rudder movements and the use of fin stabilisers will lead to added resistance. In the present analysis the rudder movements are not logged and therefore not included. The use of fin stabilisers is not considered. Although the crew indicates by manual input if they are in use, the movements are not logged and therefore not considered in this analysis.

Table 3: Filtering limits

Data	Filter	Limit no.
True wind speed	< 10 m/s	1
RPM	RMSE < 0.2	2
Logged speed	RMSE < 0.1 speed > 10 m/s	3 4
Mean draught	10.5 m < dm < 13.3 m	5
Trim	-0.5 m < trim < 0.5 m	6
Water depth	depth > $\frac{4.44}{C_B^{1.3}} \cdot dm$	7

Results

Validation of Model

The data is collected on board a panmax container ship in the period from January 2007 to December 2007. The main particulars of the ship are shown in Table 4.

Table 4: Main particulars

Length between particulars	277.6	m
Breadth moulded	32.22	m
Design draught moulded	12.20	m
Engine type	Diesel	-
Number and type of propellers	1 fixed	-
Available engine power at MCR	58,344	kW
Propeller rotation rate	102	RPM

The hull roughness factor k_S is used as performance index. The default value is 150 µm, which is used as initial value. The factor k_S is then optimised by the Newton Raphson method with reference to the ships logged speed. To avoid negative values the roughness data is filtered to a low pass filter with limits 0 to 4.0×10^{-3} m and a frequency of 0.01 Hz, Fig. 8.

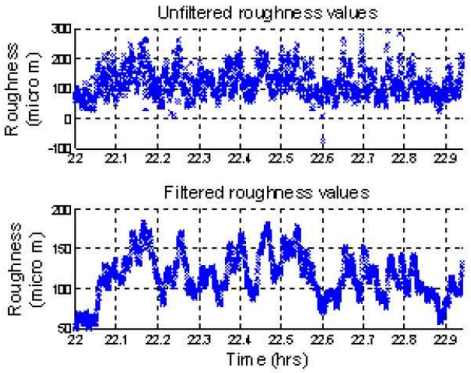

Fig. 8: Roughness values for the initial model

The optimisation is performed in a condition with mean draught 11.95 m, trim 0.1 m and service multiplication factor F = 0.9789. This results in a mean roughness factor of 117 µm, Fig. 8. With this factor the data is now run through the model again, and the ships logged speed compared to the model speed, Fig. 9.

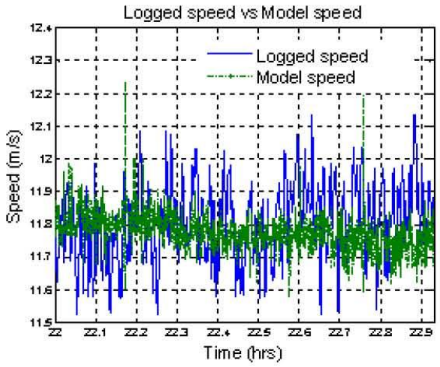

Fig. 9: Comparison of logged and model speed

Statistical values from model and logged speed are shown in Table 5.

Table 5: Statistical values

	Mean	Std. deviation
Model speed	11.78 m/s	0.0749
Logged speed	11.81 m/s	0.1158

An initial model of the ship is now established. This model having a roughness factor of 117 µm is used to determine the effects of development of roughness over time.

Roughness Analysis

To analyse the performance of the ship, the roughness factor is examined over a period of 325 days. One-hour peak log files are filtered as in Table 3 and used for the analysis. Linear regression is used to describe the development in roughness, Fig. 10.

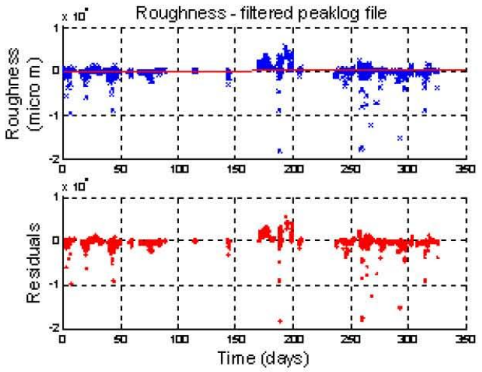

Fig. 10: Roughness values, peak log files

The diagrams in Fig. 10 show a large variation in the roughness factor values, which also affects the residuals plot. The peaks are unnatural for a slow degrading performance. The peaks and the negative values can be explained by poor data quality of the manual input data, see *Discussion of Results*.

To establish a more accurate development in roughness a number of time series are chosen for further analysis.

Every day the ship also sends reports to shore with performance data. The reports are manually generated and contain performance data averaged over the reporting period, which is normally 24 hours. The information from the daily reports is used to verify the manual input in the log files, see *Discussion of Results*.

Data log information of the draught, seawater temperature and water depth information are compared to data given in the daily reports. Incidents are omitted if information in the two reports not are identical.

Reports from the beginning and from the end of the period are used to establish the development in roughness. The time interval is the same 325 days as used for the peak log files.
For every time series data file a mean roughness factor is calculated and the results are given in Fig. 11. Linear regression is used to describe the development in roughness.

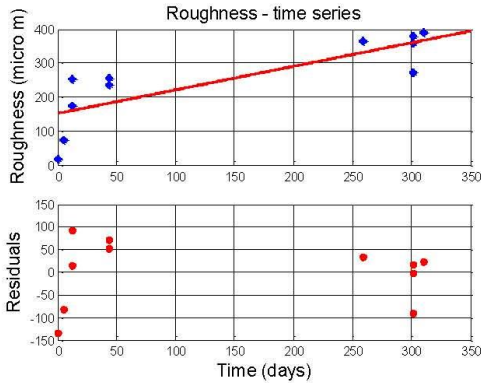

Fig. 11: Roughness values time series

A comparison between the results the peak log files and the time series files are shown in Table 6. Fig. 12 compares the development in roughness found by the linear regression in the two steps. The time series roughness start value is lower than the peak log and the slope is steeper, see *Discussion of Results*.

Table 6: Comparison of roughness results

Roughness analysis	Linear regression line	Residuals std. deviation
Peak log files	f(x) = 0.2362x + 228	1384.1
Time series	f(x) = 0.6929x + 152	71.6

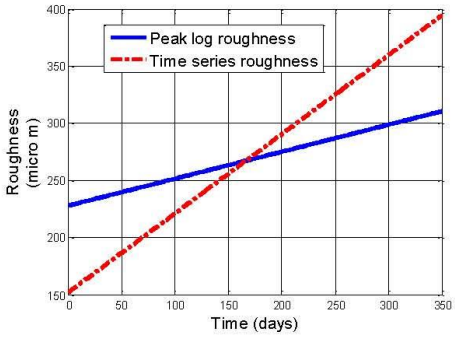

Fig. 12: Development in roughness

Roughness Influence on Ships Performance

The effect of the roughness development on the ships performance is now examined. The linear regression for the time series is used for analysing the development of roughness. The effect is shown on the time series for the initial model (Case 1) and after one year (Case 2), Table 7.

Table 7: Roughness influence on performance

	Case 1	Case 2	Difference %
Roughness	117 µm	370 µm	216
Resistance	$1.363 \cdot 10^3$kN	$1.498 \cdot 10^3$kN	10
Speed	11.80 m/s	11.37 m/s	3.6
Power	$21.33 \cdot 10^3$kW	$23.04 \cdot 10^3$kW	8

The results indicate an added resistance of *10 %* over the period. This leads to an increased power consumption of *8%* at initial speed and draught. If the power is kept constant the ship will experience a speed loss of *3.6 %*.

Discussion of Results

Good data quality is of great importance to evaluation of a ships performance. The data used for this analysis has been logged both manually and automatically. The data quality is discussed in the following paragraphs.

Logged Data, Sensors

The raw data logged by sensors on board the ship is used without filtering.

Shaft speed (RPM) is measured continuously on the shaft along with the torque. Once calibrated the measurement is considered to be reliable (accuracy < 0.1%) (Kyma, 2010).

Wind direction and speed are measured by an anemometer placed on top of the navigation bridge. The placement of the anemometer is not analysed with regard to disturbance or disruption in wind direction and speed measurement with regard to various relative wind directions. The raw data is used in the wind/wave model, which leads to unreasonable peak values in ships speed when peaks in wind speed measurements are taken into account.

Ships speed through water is measured by the speed log, which is of an Acoustic Correlation log type. Once calibrated, the measurement is considered to be reliable (accuracy < 0.1 knots or 0.5 % whichever is greater) (Consilium, 2010).

Logged Data, Manual Input

The manually logged data is draught information, sea water temperature and water depth information.

It is the intention that this information is updated by the crew when conditions change.

Reporting reliable manually logged data requires great awareness by the ships crew. Reporting performance data to shore every day is part of this shipowner's policy and has been for many years. The ships crews are introduced to the performance system when they start working on board the ship and the reporting is incorporated as a daily routine. The ship has been equipped with a data logging system where the manual input is to be taken care of as an additional system. A comparison of the daily reports with the peak log files for identical dates shows that there is

- Large differences in the data reported in the two systems
- Non-consistent update of peak log files when sailing from port
- Non-consistent update of sea water temperature
- Non-consistent update of water depth

Reliable performance calculations are strongly dependent on correct logging of the load condition of the ship.

Ship Model

The resistance model is made by Holtrop (Holtrop/Mennen 1982, Holtrop 1984) based on regression models from model tests. The model is generally used for design draught and conditions and does not take into account off-design conditions and large trim variations. To use the model in other draught conditions a service condition multiplication factor is applied. The effect of the bulbous bow being submerged or being above water is not considered in this model.

The wave/wind model is based on Townsin/Kwon (Townsin, 1993, Kwon 2008). It is a combined model where the input is the wind speed and direction. The model is sensitive to high wind and sea conditions and gives best results for head wind and seas. An average wind area is used as reference in this model and variations in load conditions are not considered.

The hull model is based on fixed values of wake fraction and thrust deduction factor. Variations in speed and load condition are not taken into consideration.

The shaft and the diesel engine are not modelled in this analysis. A shaft model would enable the model to be compared to torque measurements on board the ship. A diesel engine model would make it possible to model the fuel consumption and the emissions from the engine.

The Roughness Factor as Performance Index

The performance index used in this analysis indicates an increase of roughness on the hull over the observed period. Increasing roughness leads to added resistance and thus increased power consumption. The increase in power consumption might also be caused by other factors than fouling on the hull. In this system it is not possible to separate the degrading performance to fouling on hull and/or propeller or a decrease in engine efficiency due to wear and tear. The index gives an overall view of the ships performance during service. The development in roughness is also strongly dependent on the type of antifouling paint used on the ship (International, 2010) as treatment of the hull in between dry-docking. Operational conditions also influence the development of hull roughness. If the ship is sailing in tropical waters hull roughness will increase faster than in cold water. Long time at anchor or in port will also lead to a faster increase in hull roughness.

Improvements of the System

In this analysis the bond graph method has been used for performance evaluation of a ship. The system has potential for development into a more accurate performance evaluation tool by improving:

The resistance model. Results from model tests should be implemented to substitute the Holtrop model. Varying draught and trim conditions are taken into consideration, and also rudder and stabiliser models should be included in the resistance model. A model including data from model tests and rudder movements along with model of fuel consumption, diesel engine and shaft motor have been developed, Fig. 13.

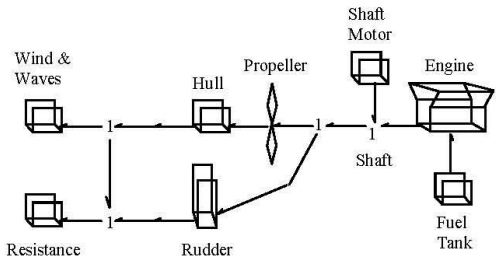

Fig. 13; Advanced Ship Model in GES

Filtering of data. Raw data from wind sensors should be filtered with a proper filter to exclude peak values. (Yelland et al 2002)

The wave model. Estimating the sea state manually is a difficult task on board. A model using roll, pitch and heave measurements from motion sensors as input should be implemented in the system. (Nielsen 2006, Nielsen 2007, Ito et al 2010)

The wind speed. The impact of the wind on the ship in various load conditions should be analysed. Various relative wind directions should be included in the analysis. (Moat et al 2006, Moat et al 2005)

Shallow waters. A model for cancelling the effect of added resistance in shallow waters should be implemented in the system. A model including the Lackenby correction has been developed. (Lackenby 1963)

Logging of data. As long as some of the data are logged manually it is essential to keep a close contact to the crew on board the ship. To establish high awareness in the logging of the data it is imperative to include the ships crew in the project and to give them feedback on the evaluation of the performance of the ship. Using automatic logging of data missing update of data might be avoided. Systems for identification of faulty sensors have been developed. (Lajic et al 2009, Lajic and Nielsen 2009, Lajic and Nielsen 2010)

Conclusion

A ships propulsive system has been modelled by the bond graph method. An initial model of a panmax container vessel has been established based on real time data logged on board during service. The roughness factor in the Holtrop resistance model has been used as performance index. The increase of hull roughness has been used to describe the degrading of performance over time. The results have been applied to an initial condition to show the effect of degradation of performance over time. The results show that the bond graph method can be used as a performance monitoring system. It is also shown that the quality of data used in the performance calculations is of great importance to the reliability of the system.

Acknowledgements

The authors wish to thank Chief Specialist Jakob Buus Petersen, A.P.Moeller-Maersk and Professor Jørgen Juncher Jensen, DTU for valuable comments and discussions. Also a special thank to the developer of GES, Hans v.Vugt for valuable assistance and discussions during the development of models in GES.

References

Breedveld, Peter (2003), "Bond Graphs". Geoplex Summer School, 2003.

Consilium (2010). "SAL T2 Log System Manual". Manual for the log type on board the container vessel.

Holtrop, J, and Mennen, GGJ (1982). "An approximate power prediction method", International Shipbuilding Progress, Vol. 29, 1982.

Holtrop, J (1984). "A statistical re-analysis of resistance and propulsion data", International Shipbuilding Progress, Vol. 31, 1984.

International Marine Coatings (2010). "Hull Roughness Penalty Calculator", http://www.international-marine.com/ supportadvice/Pages / ProductLiterature.aspx

Kwon, YJ (2008). "Speed loss due to added resistance in wind and waves", The Naval Architect, March 2008.

Kyma, Norway (2010). "Kyma Performance Monitoring", http://www.kyma.no.

Lackenby, H, (1963) "The Effect of Shallow Water on Ship Speed", Shipbuilder, 70, No. 672, 1963.

Lajic, Z., M. Blanke, and U.D. Nielsen (2009). "Fault Detection for Shipboard Monitoring - Volterra Kernel and Hammerstein Model Approaches", Proceedings of 7th IFAC Symposium on Fault Detection, Supervision and Safety of Technical Processes, Barcelona, Spain.

Lajic, Z. and U.D. Nielsen (2009). "Fault Detection for Shipboard Monitoring and Decision Support Systems", Proceedings of OMAE'09, Honolulu, HI, USA.

Lajic, Z. , U.D. Nielsen and M. Blanke (2010)."Fault isolation and quality Assessment for Shipboard monitoring", Proceedings of OMAE 2010, Shanghai, China.

Moat, BI, Yelland, AJ, Molland, AF (2006). "Quantifying the Airflow Distortion over Merchant Ships. Part II: Application of the Model Results" Journal of Atmospheric and Oceanic Technology **23**:3, 351-360.

Moat, BI, Yelland, AJ, Molland, AF (2005). "An overview of the airflow distortion at anemometer sites on Ships". International Journal Climatology, **25,** 997–1006.

Nielsen, UJ (2006). "Estimations of on-site directional wave spectra from measured ship responses", Marine Structures 19, 33–69 (2006).

Nielsen, UJ (2006). "Introducing two hyperparameters in Bayesian estimation of wave spectra", Probabilistic Engineering Mechanics 23, 84–94 (2008).

Ito, Y and Nielsen, UJ and Jensen, JJ (2010). " Estimation of Fatigue Damage from Full-scale Measurements of Hull Girder Stresses", The 11th International Symposium on Practical Design of Ships and Other Floating Structures (2010).

Townsin, RL et al (1993). "Estimating the influence of weather on ships performance", RINA transactions and annual report (1993).

TNO (2010). "Geïntegreerde Energie Systemen (GES)", http://www.tno.nl.

Yelland, AJ, Moat, BI, Pascal, RW and Berry, DI (2002). "CFD Model Estimates of the Airflow Distortion over Research Ships and the Impact on Momentum Flux Measurements" Journal of Atmospheric and Oceanic Technology 19:10, 1477-1499

16 Appendix C

Assuming linear regression can be used in estimating the trend of the performance, a set of values describing the goodness of fit are generated for each model. The RMSE values are used to indicate the scatter in the results.

$$RMSE = \sqrt{\frac{\sum(y_i - \hat{y}_i)^2}{n-1}} \quad \text{(C1)}$$

where y_i is the value of the dependent variable for observation *i*, $\hat{y}_i$ is estimated value of the dependent variable for observation *i* and n is the number of observations.

The line slope with 95 % confidence bounds describes the goodness of fit of the slope of the regression line. The line can be expressed as:

$$y = a + bx \quad \text{(C2)}$$

where a is the intercept and b is the slope of the line. The slope can be expressed by, Mosteller et al (1977):

$$b = \frac{\sum x_i y_i - \frac{(\sum x_i \sum y_i)}{n}}{\sum {x_i}^2 - \frac{(\sum x_i)^2}{n}} \quad \text{(C3)}$$

The value of the slope is affected by uncertainty given by the uncertainty in y values only, as the x values can be considered as known independent values. The standard deviation of the slope can therefore be expressed as:

$$\sigma = \frac{S_e}{\sqrt{\sum {x_i}^2 - \frac{(\sum x_i)^2}{n}}} \quad \text{(C4)}$$

where S_e is an estimate of the standard deviation of the residuals, which is identical to Eq. C1.

17 Appendix D further model descriptions

17.1 Aerodynamic Force R_{XA}

Under service conditions the ship's performance is affected by the forces of the wind as in Eq.14.

The density of air is varying with the temperature, pressure and humidity of the air. The variation is given by Salby (1996):

$$\rho_A = \frac{p_d(T)}{R_d T} + \frac{p_v(T)}{R_v T} \quad \text{(D1)}$$

where ρ_A is the air density, p_d is the partial pressure of dry air, p_v is the water vapour partial pressure, R_d is the specific gas constant for dry air, R_v is the specific gas constant for water vapour and T is the temperature.

The wind is measured by an anemometer placed on the mast in the forward section and/or in the mast on top of the navigation bridge of the ship.

The wind force coefficient can be found by using a wind resistance model. Two different wind models have been evaluated in this work. One of the models is based on the method of Isherwood (1973), which is based on empirical formulas for calculation of the wind force coefficients.

The wind force coefficients are found by analysing a number of wind tunnel tests on various ship types. The tests were performed in the 1970's and the ship types were mainly tankers and general cargo ships. The data was analysed by multiple regression techniques and was fitted to an equation for C_X:

$$C_X = A_0 + A_1 \frac{2(A_L + A_{SS})}{LOA^2} + A_2 \frac{2A_T}{B^2} + A_3 \frac{LOA}{B} + A_4 \frac{S}{LOA} + A_5 \frac{C}{LOA} + A_6 M \quad \text{(D2)}$$

where A_0 to A_6 is a set of constants derived from tests tabulated in Isherwood (1973), LOA is length overall, B is breadth, A_L is lateral projected wind area, A_{SS} is lateral projected area of superstructure and deck cargo, A_T is transverse projected wind area, S is length of perimeter of lateral projection (excluding waterline and slender bodies), C is distance from bow to the centre of lateral projected area and M is number of distinct groups of masts or king posts, Figure D1.

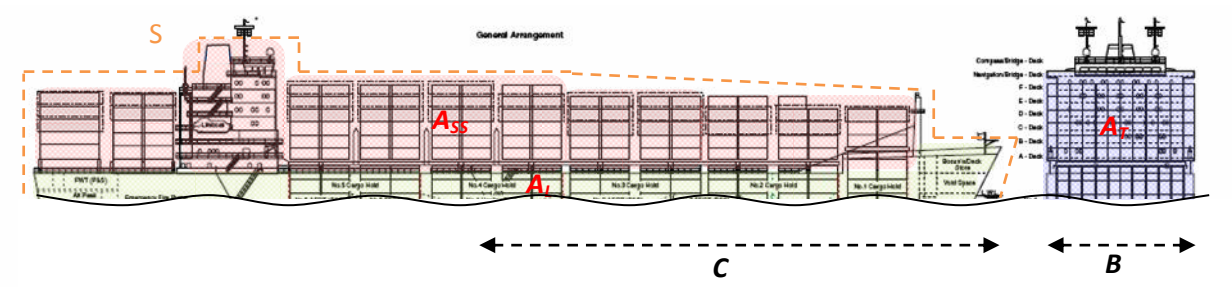

Figure D1 Wind force parameters on the ship.

The lateral projected areas are estimated from a profile of the ship with an approximated amount of containers loaded on the weather deck, Figure D2.

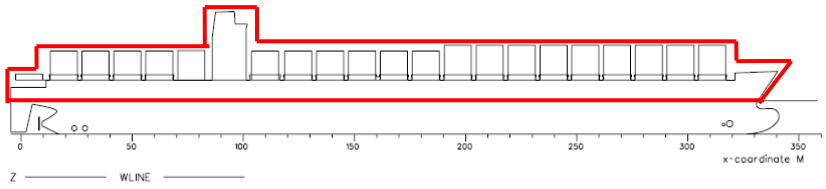

Figure D2 Lateral projected area.

The container configuration on the weather deck is unknown. An estimate of the areas is made from a standard load condition. C is estimated from this condition. The C_X values with regard to variation in relative wind direction are shown later in Figure 10.

To compensate for the velocity gradient over the exposed surface of the ship, the calculation of the wind load is based on a mean square wind

$$U_{RW}^2 = \frac{1}{h}\int_0^h u_{RW}^2\, dz \qquad \text{(D3)}$$

where h is the height from the water level to the top of the superstructure and u_{RW} is the relative wind speed measured at height z.

The wind forces acting on the ship also affect the yaw and the heeling moment. To counteract these, the ship is given an incident angle α relative to the direction of travel producing a lifting

hydrodynamic force. This will result in an increased drag on the ship in the longitudinal direction. The effect will be described in the section referring to rudder and drag resistance.

The transverse area of the ship is found from a profile plan. The area is defined by the profile of the accommodation and/or the container deck cargo. In the present model the area is kept constant and a full container deck load is assumed, Figure D3.

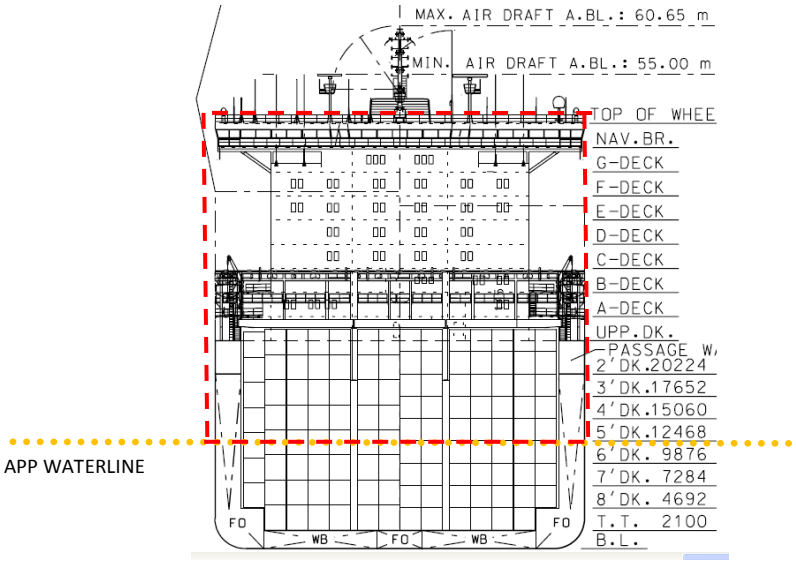

Figure D3 Transverse projected area.

A second model is based on the work of Fujiwara et al. (2001), (2006) and also employs wind tunnel tests with a large number of ship models. The wind coefficient C_X is defined as

$$C_X = F'_{LF} + F'_{XLI} + F'_{ALF} = C_{LF}cos\beta_{RW} + C_{XLI}(sin\beta_{RW} - ½sin\beta_{RW}cos^2\beta_{RW})sin\beta_{RW}cos\beta_{RW} + C_{ALF}sin\beta_{RW}cos^3\beta_{RW} \quad (D4)$$

The longitudinal flow coefficient CLF is given as

$$C_{LF}^{0°\leq\beta_{RW}\leq90°} = \beta_{\beta10} + \beta_{\beta11}\frac{A_L}{LOA\cdot B} + \beta_{\beta12}\frac{C}{LOA} \quad (D5)$$

$$C_{LF}^{90°\leq\beta_{RW}\leq180°} = \beta_{\beta20} + \beta_{\beta21}\frac{B}{LOA} + \beta_{\beta22}\frac{H_C}{LOA} + \beta_{\beta23}\frac{A_{SS}}{LOA^2} + \beta_{\beta24}\frac{A_F}{B^2} \quad (D6)$$

The lift and drag induced coefficient C_{XLI} is given as

$$C_{XLI}^{0°\le\beta_{RW}\le90°} = \beta_{\delta10} + \beta_{\delta11}\frac{A_L}{LOA\cdot H_{BR}} + \beta_{\delta12}\frac{A_T}{B\cdot H_{BR}} \quad \text{(D7)}$$

$$C_{XLI}^{90°\le\beta_{RW}\le180°} = \beta_{\delta20} + \beta_{\delta21}\frac{A_L}{LOA\cdot H_{BR}} + \beta_{\delta22}\frac{A_T}{A_L} + \beta_{\delta23}\frac{B}{LOA} + \beta_{\delta24}\frac{A_T}{B\cdot H_{BR}} \quad \text{(D8)}$$

The coefficient C_{ALF} is given as

$$C_{ALF}^{0°\le\beta_{RW}\le90°} = \beta_{\varepsilon10} + \beta_{\varepsilon11}\frac{A_{SS}}{A_L} + \beta_{\varepsilon12}\frac{B}{LOA} \quad \text{(D9)}$$

$$C_{ALF}^{90°\le\beta_{RW}\le180°} = \beta_{\varepsilon20} + \beta_{\varepsilon21}\frac{A_{SS}}{A_L} \quad \text{(D10)}$$

where H_{BR} is the height of the bridge deck and the non-dimensional parameters β_β, β_δ and β_ε are tabulated in Fujiwara et al. (2001). The dynamic pressure of the wind is given as

$$q = q_T + q_S + 2\sqrt{q_T q_S}\cos(\beta_{TW} + \alpha) \quad \text{(D11)}$$

where β_{TW} is the true wind direction and α is the drift angle. q_T and q_S are expressed by

$$q_T = \tfrac{1}{2}\rho_A U_{TW}'^2 \quad \text{(D12)}$$

$$q_S = \tfrac{1}{2}\rho_A U_S^2 \quad \text{(D13)}$$

where U_{TW}' is the wind velocity at height z_a using the standard height z_{Al}, which is the point 10 m above sea level.

U_{TW}' is given by

$$U_{TW}' = U_T\left(\frac{z_a}{z_{Al}}\right)^{\gamma_a} \quad \text{(D14)}$$

where γ_a is given by

$$\gamma_a = \frac{1}{-0.2U_T + 12.0} \quad \text{(D15)}$$

A set of C_X values generated for a PostPanmax container ship based on the two models is shown in Figure D4 (0° is head winds).

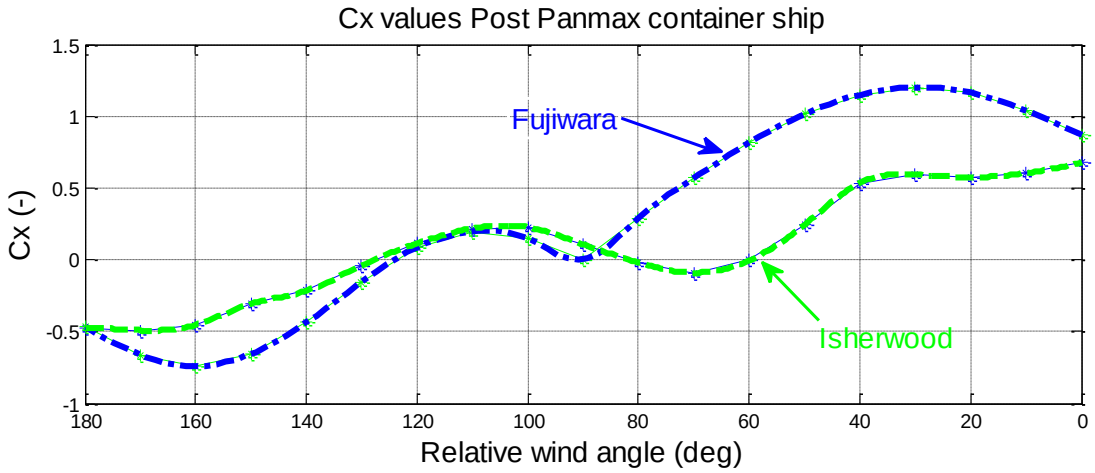

Figure D4 Cx values from two wind models.

The C_X values are more or less consistent in the areas with aft relative winds. From beam to head relative winds the Fujiwara model generates considerably larger C_X values.

17.2 Hydrodynamically Induced Force R_{XH}

The hydrodynamic force F_{XH} is given by

$$F_{XH} = ½\rho_W C_T S U_S^2 \qquad \text{(D16)}$$

where C_T is the resistance coefficient, S is the hull wetted surface area and U_S is the ship's speed.

The resistance coefficient is found from model tests. In the resistance test, measurements are made of the force required to pull the model through the water at a constant speed. The results are extrapolated from model to ship values and the resistance coefficient is found by ITTC (1999):

$$C_T = C_F + C_R + C_A \qquad \text{(D17)}$$

where C_R is the residuary coefficient, C_F is the frictional coefficient and C_A is the allowance coefficient. C_F is found by the following relation, ITTC (1999):

$$C_F = \frac{0.075}{[log_{10}(Re)-2]^2} \quad \text{(D18)}$$

where the Reynolds number is calculated by

$$Re = \frac{U_S L}{\upsilon} \quad \text{(D19)}$$

where L represents the wetted length of the ship and v is the kinematic viscosity of sea water. C_R is found by model tests for a number of draught and trim conditions, see the section "Modelling" in this thesis.

C_A allows for the resistance of deck houses, bilge keels, hull roughness and steering loss and can be expressed in accordance with ITTC (1999):

$$C_A = \left[105\sqrt[3]{\frac{k_S}{L}}\right] 10^{-3} \quad \text{(D20)}$$

where L is the wetted length of the ship and k_S is an expression for the hull roughness.

One of the performance indexes is based on the increased use of power during service. The effective power, P_E, is dependent on draught, trim and speed. The relation between P_E and F_{XH} is expressed as

$$P_E = F_{XH} U_S \quad \text{(D21)}$$

The shaft power P_S is found by the relation

$$P_S = Q\omega \quad \text{(D22)}$$

where Q is the propeller shaft torque and ω is the propeller shaft revolutions.

The propeller thrust force F_{XP} is defined by the propeller model. The propeller characteristics are obtained by model tests, Figure D5. The advance number, J, is found by

$$J = \frac{U_a}{nD} \quad \text{(D23)}$$

where n is the propeller revolutions, D is the propeller diameter and U_a is the advance speed

$$U_a = (1 - w) U_S \quad \text{(D24)}$$

where w is the wake fraction. This fraction is also dependent on draught, trim and speed and found by the same method as P_E. The thrust force, F_{XP}, is found by the relation

$$F_{XH} = (1 - t)F_{XP} \tag{D25}$$

where t is the thrust deduction factor. This factor is found by linear interpolation by using draught and speed as input arguments.

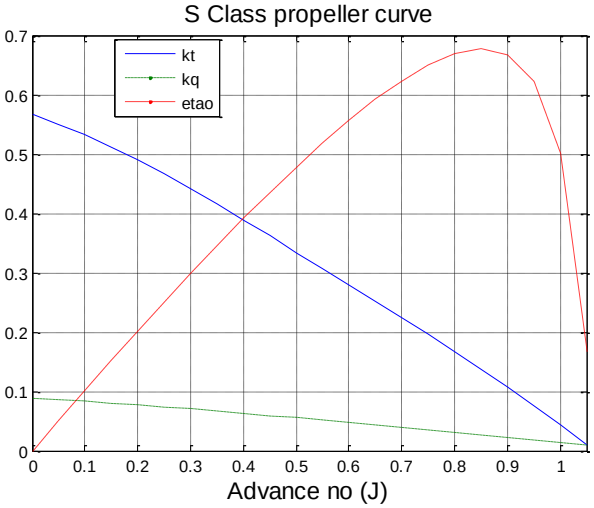

Figure D5 Propeller characteristics, example: a PostPanmax (S Class) container ship.

17.3 Closed Form expressions

The RAOs for heave and pitch can be found by using closed-form expressions, Jensen et al. (2003):

$$\Phi_3 = \mu F_T \tag{D26}$$

$$\Phi_5 = \mu G_T \tag{D27}$$

μ is given as

$$\mu = \left(\sqrt{(1 - 2kT\alpha^2)^2 + \left(\frac{A_{hyd}^2}{kB\alpha^2}\right)^2} \right)^{-1} \tag{D28}$$

where T is the ship's mean draught.

A_{hyd} is given as

$$A_{hyd} = 2sin(½kB\alpha^2)e^{-kT\alpha^2} \quad \text{(D29)}$$

and α is given as

$$\alpha = 1 - Fn\sqrt{kL}cos\beta \quad \text{(D30)}$$

Fn is given as

$$Fn = \frac{U_S}{gL} \quad \text{(D31)}$$

Forcing functions F_T and G_T are determined by

$$F_T = \kappa f \frac{2}{k_e L} sin\left(\frac{k_e L}{2}\right) \quad \text{(D32)}$$

$$G_T = \kappa f \frac{24}{(k_e L)^2 L}\left(sin\left(\frac{k_e L}{2}\right) - \frac{k_e L}{2} cos\left(\frac{k_e L}{2}\right)\right) \quad \text{(D33)}$$

where the Smith factor κ is given by

$$\kappa = e^{-kT} \quad \text{(D34)}$$

k_e is given by

$$k_e = |kcos\beta| \quad \text{(D35)}$$

and f is defined as

$$f = \sqrt{(1 - kT)^2 \left(\frac{A_{hyd}^2}{kB\alpha^3}\right)^2} \quad \text{(D36)}$$

Ship's breadth in calculations is given by

$$B = B_0 C_B \quad \text{(D37)}$$

where B_0 is maximum breadth and C_B is the block coefficient.